

Tooling technology for bulk forming of micro components

Eriksen, Rasmus Solmer; Hansen, Hans Nørgaard; Bissacco, Giuliano; Arentoft, Mogens

Publication date:
2010

Document Version
Publisher's PDF, also known as Version of record

[Link back to DTU Orbit](#)

Citation (APA):
Eriksen, R. S., Hansen, H. N., Bissacco, G., & Arentoft, M. (2010). Tooling technology for bulk forming of micro components. Kgs. Lyngby, Denmark: Technical University of Denmark (DTU).

DTU Library

Technical Information Center of Denmark

General rights

Copyright and moral rights for the publications made accessible in the public portal are retained by the authors and/or other copyright owners and it is a condition of accessing publications that users recognise and abide by the legal requirements associated with these rights.

- Users may download and print one copy of any publication from the public portal for the purpose of private study or research.
- You may not further distribute the material or use it for any profit-making activity or commercial gain
- You may freely distribute the URL identifying the publication in the public portal

If you believe that this document breaches copyright please contact us providing details, and we will remove access to the work immediately and investigate your claim.

Tooling technology for bulk forming of micro components

- theoretical and practical aspects of micro forming technology

Rasmus Solmer Eriksen

Ph.D. Thesis

Department of Mechanical Engineering
Technical University of Denmark

2010

Tooling technology for bulk forming of micro components
- theoretical and practical aspects of micro bulk forming technology

Copyright ©2010 by Rasmus Solmer Eriksen
Department of Mechanical Engineering
Technical University of Denmark
ISBN: 978-87-89502-91-5

Preface

This thesis is submitted as a partial fulfilment of the requirements towards earning the Ph.D. degree at the Technical University of Denmark, Department of Mechanical Engineering. The work have been carried out in the period from October 2006 to March 2010 at section of Micro and Nano Manufacturing under the supervision of Prof. Hans Nørgaard Hansen. One month was spend as a visiting research scholar at the Lehrstuhl für Fertigungstechnologie, Universität Erlangen-Nürnberg, Germany under the supervision of Prof. Dr.-Ing. habil. Ulf Engel and Dipl.-Ing. Stephan Weidel.

I would like to thank all contributors for their inspiration and contribution to my work, both affiliate researchers at DTU and external partners. In particular, I would like to thank Prof. Hans Nørgaard Hansen, Dr. Mogens Arentoft and Nikolas Paldan for their numerous tangible contributions, inspirational discussions and constant encouragement during my times as a doctoral student. Prof. Dr.-Ing. habil. Ulf Engel and Dipl.-Ing. Stephan Weidel is thanked for the hospitality at the Lehrstuhl für Fertigungstechnologie and for facilitation of the research visit.

The work have been funded through DTU's Ph.D. scholarships, being national government grants. Parts of the activities have been co-financing through the European Commission funded FP6 project MASMICRO, no. 500095-2 and by the national Innovation Consortium MIKROMETAL, no. 66334. granted through by the Danish Ministry for Science Technology. Financial support for the external research stay have been received by the German Research Foundation, through Lehrstuhl für Fertigungstechnologie, Universität Erlangen-Nürnberg, Germany. The financial support, making this project possible, is greatly acknowledged.

Lyngby, May 2010

Rasmus Solmer Eriksen

Abstract (English)

The aim of the current study was to advance state of the art within tool design for the micro bulk forming process. The micro bulk forming process is a topic of researched within mechanical manufacturing engineering and complications in tool design is one of the key barrier for industrialization of this process as preferred method for bulk fabrication of militarized metallic components.

A number of micro forming tools were manufactured using conventional and dedicated micro tool manufacturing processes all based on electric discharge machining. Studies of the electric discharge machining process have been conducted with the aim of establishing a method for estimation of electrode wear for different tooling materials.

Micro metrological methods based on direct- and replication techniques were developed for measurement of the manufactured tools and forged micro specimens. A round-robin manufacturing and measurement experiment have been conducted, involving micro size artifacts designed to mimic a punch and die geometry for the micro bulk forming process. Further, a comparative study of different suitable measurement technologies for assessment of micro specimens is conducted.

An thorough investigation of the influence of tool surface topography on the friction during forming is conducted. Through the application of the double cup extrusion test, in the macro and micro scale the process conditions related to friction is studied. A simulative friction test, using a novel Micro Tribology Tester, is conducted to provide a secondary set of result for the micro case.

Empirical knowledge and developed methods for manufacturing of tool system for the micro bulk forming process is described. Examples of process chains for tool manufacturing are given. A number of tools are manufactured utilizing different manufacturing methods and the results are described. Finally recommendations for tool manufacture, alignment strategies and material are considered.

A range of dedicated equipment designed for the micro bulk forming process is demonstrated. These include micro billet cropping equipment, a micro press system and examples of a handling and transfer system.

The work is concluded with a number of advanced micro bulk forming experiments using conventional and amorphous material. An small potentiometer axle, a gear wheel for a drug delivery system and a dental component is manufactured by application of the micro bulk forming process. Examples of tool design for application at ambient and elevated temperatures are given and the results are discussed.

It is shown that the micro bulk forming process can be applied as manufacturing method for miniaturized micro components. However, the process suffers from the physical limitations known from conventional metal forming processes and a subset of adjacent

size effects. The design and manufacturing of tools for the micro bulk forming process can be realized through a compounded design strategy involving knowledge of the forming process, tool manufacturing process, surface tribology, micro metrology and framework considerations. Complications were found within forming tribology, relating to the achievable low surface roughness of the forming tools. Also, high values of friction was seen, leading to complications during forming and ejection for the specimens.

Resumé (Dansk)

Målet med den nærværende Ph.D. afhandling er at undersøge mulighederne og bidrage til udviklingen inden for værktøjsteknologi til flydning af mikro-metalliske emner. Koldflydning af metalliske mikroemner er et forskningsområde inden for mekaniske fremstillings processer, hvor komplikationer under fremstillingen af de krævede højpræcisionsværktøjer i millimeter størrelser, udgør en barriere der hindrer et industrielt gennembrud af denne fremstillingsproces.

Et antal værktøjer er blevet fremstillet ved hjælp af almindelige og dedikerede mikrobearbejdnings processer, fortrinsvist baseret på gnist-bearbejdning. I forbindelse med gnist-bearbejdningen er der blevet udført målinger på processen men henblik på at bestemme elektrode-slid under bearbejdningen i forskellige materialer, men henblik på opnåelse af højest mulig geometrisk nøjagtighed af det færdige emne.

Igennem projektet er der blevet udviklet metoder til metrologisk opmåling af de fremstillede værktøjsgeometrier og de fremstillede koldflydte komponenter. Metoderne baserer sig på både direkte og indirekte opmåling. En række institutioner og virksomheder har deltaget i et forsøg med fremstilling og efterfølgende rundsending af nogle forsimplede stempel og kerne emner, men henblik på opmåling og sammenligning af den opnåede geometriske kvalitet.

Endeligt er der blevet udført en undersøgelse af indflydelsen af værktøjets overfalde-ruhed på friktionen under mikro-koldflydning. Friktionen under formning af emnet er blevet målt ved brug af den konventionelle dobbelte kop-presning metode, både i makro og mikro størrelses-skala. For at forbedre datagrundlaget er der yderligere blevet udført en trække translations friktions-tests i mikro størrelse ved hjælp af et nyudviklet mikrofriktions apparat.

De erfaringer og metoder der er blevet opsamlet og udviklet gennem del-projekter omhandlende værktøjsdesign er blevet omhyggeligt beskrevet. Der gives praktiske eksempler på kombinationer af processer til fremstilling af formgivningsværktøjer i mikrostørrelse af høj kvalitet. Slutteligt gives generelle retningslinjer for god praksis inden for fremstilling af værktøjer til koldflydning af mikrokomponenter, baseret på den erfaring der er blevet opnået igennem Ph.D. projektet.

Der er blevet udviklet et antal specielle maskiner og apparater til understøttelse af teknologien til fremstilling af mikro komponenter ved hjælp af koldflydning. Eksempler på udviklede maskiner inkluderer: en maskine til klipning af udgangsemner fra stang, et dedikeret fleksibelt presse system designet til mikro-koldflydning samt et system til håndtering og opsamling af mikro-emner.

Rapporten afsluttes med eksempler på formgivning af avancerede emner ved hjælp af kold- og varmflydning. Der anvendes almindelige krystallinske og amorfe materialer. Værktøjer til fremstilling af en lille potentiometer aksel, et miniature tandhjul til et

medicinsk apparat samt et implantat tiltænkt dentalt formål bliver formgivet ved hjælp af mikro-smedning. Der gives eksempler på værktøjsteknologi til mikroformgivning af metalliske materialer i kold og varm tilstand og resultaterne diskuteres.

Konklusionen viser at det er muligt at mikro-koldflydnings-teknologi kan tænkes anvendt som produktionsmetode for mikro-metalliske komponenter under hensyntagen til de fysiske begrænsninger af denne proces. Processen kompliceres yderligere i mikro-skala, hvor en række størrelseseffekter tilgår. Værktøjer til mikro formgivning kan realiseres under hensyntagen til flere aspekter af processen, deriblandt formgivningsprocessen, værktøjsfremstilling og processering, overflade topografi, mikro-metrologi og rammebetingelserne for processen. Der blev mødt flere udfordringer under projektet med at opnå tilstrækkelig fine værktøjsoverfald og lav friktion.

Acknowledgments

First of all, I would like to thank Professor Hans Nørgaard Hansen and Dr. Mogens Arentoft for their joint cooperation in making it possible for me to embark on the Ph.D. studies at the Technical University of Denmark, Department of Mechanical Engineering. Your professionalism, experience, personal insights and support during the past four years have been worth a lot to me.

I would like to thank peers and fellow students from the Micro/Nano Manufacturing research group for actively contributing to an active and attractive research environment. Professor Niels Bay, Dr. Guido Tosello and fellow Ph.D. student Stefania Gasparin is especially thanked for a rewarding and fruitful cooperation.

My colleges at IPU - division of technology development, Nikolas Aulin Paldan, Johan Gregersen, Jesper Mørkhøj, Jørgen Dai Jensen, Klaus Schütt Hansen and Peter Torben Tang is acknowledged for their collaboration and encouragement during my time as a doctoral student. In particular Nikolas Aulin Paldan must be acknowledged for the numerous tangible contributions, inspirational discussions over lunch, dark humor and never failing good mood.

I am grateful for all the support I have receive from the technical staff at the department og Mechanical Engineering. I would like to thank Lars Peter Holmbæk, Jakob Rasmussen and Rene Sobiecki for the time you have spend on my projects and the vast experiences you have shared. A special thanks should go to the people of the workshop in building 427 and their foreman Jan Frank Pedersen for magically transforming my obscure technical drawings into high quality parts.

The present and former students at the Department of Mechanical Engineering: Martin Hedgaard, Matteo Calaon, Jakob Viggo Holstein, Christopher Hansson, Jacob Duus Dolris, Tomaso Gastaldi and Stefan Geisler is thanked for their contribution and for having in trust in me as an advisor on their projects.

Prof. Dr.-Ing. habil. Ulf Engel and Dipl.-Ing. Stephan Weidel is thanked for the hospitality at the Lehrstuhl für Fertigungstechnologie, Erlangen, Germany. Your huge effort in facilitating my research at you wonderful institute, and making me fee at home, surpassed any expectation.

I would like to thank my family - you all have a share in making this work possible. I am grateful to my parents, Dorthé and

Frode Eriksen, for your heroical efforts during refurbishment of my fantastic flat and for the enormous amount of loving support you have given over the years. My sister Sidel is thanked for the numerous evening dinners and talks of life and friendship. Mikkel, my younger brother, is thanked for his always kind interest in my technical projects and for not being the one to follow precious advice from those who know better.

Special loving thoughts and gratitude should to go my girlfriend Sheau Lin Foo Midjord for the time we have spend together. You are indeed a fantastic girl and your love, cool attitude and sweet smile enrich my life.

What a journey it has been - I am grateful to all of you.

Contents

Contents	ix
List of Figures	xiii
List of Tables	xix
1 Thesis structure and guide to the reader	1
1.1 Thesis research statement	1
1.2 Structure of the work	1
1.3 Guideline for reading	2
2 Background and objectives	5
2.1 Introduction	5
2.2 Applications of micro components	6
2.3 Cost and production series challenges	8
2.4 Micro factories	10
2.5 Impact and outlook	12
3 The Micro bulk forming process	15
3.1 Bulk forming at the macro scale	15
3.2 Micro Bulk forming	16
3.3 Size effect in micro bulk forming	17
3.4 Materials in micro forming	19
3.5 Warm forging of micro components	23
3.6 Handling and ejection system	25
3.7 Prefab or net-shaping	26
4 Micro metrology	29
4.1 Introduction	29
4.2 Challenges in Micro Metrology	30
4.3 Measuring uncertainty	32
4.4 Replica technique	34
4.5 Verification of the shrinkage of replica - an example of uncertainty evaluation	36
4.6 Micro manufacturing and geometric dimensioning and tolerancing	42
4.7 Micro EDM-benchmark test	44
4.8 Measurement of complex 3D structures.	57
5 Tribology in microforming	67
5.1 Friction in Metal Forming	68
5.2 Micro tribology and Micro friction	70
5.3 Tests for Evaluation of Tribological Behavior	72
5.4 Macro scale double cup extrusion tests	77
5.5 Micro size friction experiments	91

5.6	Micro tribology tester friction experiments	99
6	Tooling for the micro bulk forming process	111
6.1	Introduction to tool design	111
6.2	Micro tooling characteristic and challenges	112
6.3	Geometrical limitations and tolerancing	114
6.4	Micro bulk forming analysis	116
6.5	Tooling elements and properties	117
6.6	Tooling materials for micro bulk forming tools	120
6.7	Micro tooling manufacturing processes	122
6.8	Micro forming tool for micro axle application	129
6.9	Alignment tolerances within micro bulk forming	137
6.10	Conclusion	140
7	Micro bulk forming framework	143
7.1	Billet preparation	143
7.2	Press and system design for micro forming	150
7.3	Handling, ejection and transfer of components	161
7.4	Conclusion	171
8	Results of advanced micro forming experiments	173
8.1	Micro forming of axle for a potentiometer application	173
8.2	Comparative micro forming operation of Gear-wheel component.	177
8.3	Micro forming of dental implant in medical grade pure titanium	193
8.4	Tooling design	195
8.5	Conclusion to advanced micro forming experiments	210
9	Conclusion	213
9.1	Summary	213
9.2	Suggestions for future work	215
	Author Publications	217
	References	219
	Appendix	225
A	Flow curves of popular cold forging materials	227
B	RAP EDM die deflection	229
C	RAP polishing procedure - mirror finish	231
D	RAP polishing procedure - functional finish	243
E	Tiesler Size chapter	255
F	Mechanical properties of common BMG materials	259
G	Tool system for forming of Dental implant	263
H	Macro DCE-results	267

Nomenclature

λ	Scaling factor
λ_F	Failure rate
μ	dynamic coefficient of friction, Columb model
τ	Shear stress
τ_0	Critical shear stress
d_G	Mean grain size
f_s	Shear friction force
K	Hall-Petch constant
k	Shear stress of work piece material
m	Friction factor
n	Material strain hardening exponent
p	Compressive normal stress at interface
T_l	Lower tolerance
T_u	Upper Tolerance
AFM	Atomic Force Microscope
ASTMs	American Society for Testing and Materials
CAD	Computer Aided Design
CAM	Computer Aided Machining
CMM	Coordinate Measuring Machine
DLC	diamond-like carbon
ECAP	Equal Channel Angular Pressing
ECM	ElectroChemical Machining
EDM	Electric discharge machining
EFAB	Electrochemical FABrication
GPS	Geometrical product specification
GUM	Guide to the expression of Uncertainty in Measurement

CONTENTS

HRC	Hard Rockwell C
IFM	InfiniteFocus Microscope, by Alicona GmbH
LIGA	German: Lithographie, Galvanoformung, Abformung
MEMS	Micro Electro-Mechanical Systems
MPE	Maximal permissible error
MTT	Micro Tribology Tester
MZPL	peak-to-valley deviation
PDF	probability density function
RAP	Robot Assisted Polishing
SEM	Scanning Electron Microscope
SPM	Scanning Probe Microscope
TIR	Total Indicated Run
UTS	Ultimate tensile strength
XRD	x-ray diffraction analysis

List of Figures

2.1	Example of a dental implant, a so-called a <i>abutment</i> , that technically qualify as a micro components	7
2.2	Medium complex geometry forged micro part (left and middle) and the machined component (right)	8
2.3	Cost factors involved in cutting of a micro component with medium advanced geometry and a production batch size of 300.000 pc.	9
2.4	Cost estimation of forming of a batch of 300.000 pc batch of micro components	10
3.1	Basic cold forging procedures [12].	16
3.2	Overview of dominant size effects in micro bulk forming.	19
3.3	Yield stress for Mg60Cu30Y10 bulk amorphous alloy.	21
3.4	Comparison of component formed in BMG Mg60Cu30Y10 (a) and in an annealed aluminum EN AW-6060	22
3.5	Tooling system for warm forging of Titanium	24
3.6	Example of a transfer system and with different gripper technologies for a micro bulk forming system.	25
4.1	Photograph of the Alicona Infinte Focus Microscope, based on the confocal microscopy principe, uses focus variations to build build a 3D model of the measurements.	31
4.2	Clip from the Struers Repliset datasheet.	35
4.3	Example of quality control of a die with replica	35
4.4	Calibration data and step gauge photo	36
4.5	3D representation for the acquired data from the Alicona IFM.	38
4.6	Sketch showing the recommended procedure for characterication of step height using ISO 5436-1 [13].	39
4.7	Measurement procedure for single step height used in the experiment.	39
4.8	Photo of the silicone replica of the step gauge. The Repliset compound GF1 from Struers was utilized.	40
4.9	Illustration of product development cycle for a conventional macro scale micro product.	43
4.10	Illustration of the proportions between measurement uncertainty and the allowable tolerance of a geometrical feature of a mechanical component [14]	43
4.11	Optional caption for list of figures	45
4.12	Technical drawing of EDM benchmark punch	46
4.13	Technical drawing of EDM benchmark die	46
4.14	47
4.15	Orientation of the measurement coordinate system for CMM measurements.	48
4.16	FH1 punch measurements, taken from Tables 4.5 and 4.4 ,Zeiss OMC values corrected for systematic error.	50
4.17	FH2 punch measurements, taken from Tables 4.5 and 4.4 ,Zeiss OMC values corrected for systematic error.	51

LIST OF FIGURES

4.18	FH3 punch measurements, taken from Tables 4.5 and 4.4 ,Zeiss OMC values corrected for systematic error.	52
4.19	FH4 punch measurements, taken from Tables 4.5 and 4.4 ,Zeiss OMC values corrected for systematic error.	52
4.20	FH5 punch measurements, taken from Tables 4.5 and 4.4 ,Zeiss OMC values corrected for systematic error.	53
4.21	DTU punch measurements, taken from Tables 4.5 and 4.4 ,Zeiss OMC values corrected for systematic error.	53
4.22	TEK punch measurements, taken from Tables 4.5 and 4.4 ,Zeiss OMC values corrected for systematic error.	54
4.23	Plot of the individual measurement deviation from nominal value. The order is sorted according to average deviation (last bar in the plot).	55
4.24	95% confidence interval for the variability of the face width of the punch geometry.	55
4.25	Calculation of the face flatness. Please not the rather uncertainty contribution originating from the measurement machine.	56
4.26	Micro gear for drug delivery system. The gear wheel is currently manufactured in Stainless AISI 316 using powder pressing.	57
4.27	Classification of measurement equipment. Definition of 2D, 2½D and 3D according to reference. [15]	58
4.28	Working principle of the 3 Shape D700 scanner. Image taken from promotion pamphlet.	59
4.29	Comparison between scanned geometry and CAD generated STL file. The color coated deviations are specified in millimeters.	60
4.30	SEM image of the gear wheel component in ALU 6060	61
4.31	Color coated model showing the deviation from the solid CAD model. Data acquired on the Alicona Infinte Focus microscope.	63
4.32	Illustration of the difference between intended and achieved geometry for the gear wheel tooth. The specimen was scanned on an Alicona Infinte Focus instrument.	64
5.1	Various tribological experiments suggested by Da Vinci [16]	67
5.2	Illustration of the relation between the Coulomb- and constant- and Wanheim-Bay models friction behavior.	69
5.3	Illustration of the influence of the open- an closed lubricant pocket theory when scaling the process to micro size [17].	71
5.4	(a) 3D simulation of pre-form for a micro axle. (b) Photo of the formed component where unwanted reverse forming have occurred during ejection from the forming die	72
5.5	Metal flow in the ring compression test. (a) Low friction. (b) High friction [18]. The position of the Neutral plane, geometrically dependent on friction, will determine if the internal diameter of the ring will grow or shrink.	73
5.6	Illustration of the Double Cup Extrusion test.	74
5.7	Calibration curves for DCE-test of C8C material with moderate strain hardening tendency $n = 0,20$. The curves were generated through a number of simulations using the DEFORM commercial FEM code. The simulations were conducted assuming a plastic material deformation model and a 10.000 nodes grid.	75
5.8	Simulative tests with global plastic deformation by upsetting [19].	76

5.9	Photographs of the RAP polishing machine (a) and the general purpose robotic arm carrying out the movement of the polishing substrate (b). . . .	78
5.10	Close up pictures of the active elements engaged in the polishing process in the RAP machine.	79
5.11	Technical drawing of the die for DCE-test.	80
5.12	Measured roughness values of the three manufacture dies. The confidence interval indicated is with 95% taken from the uncertainty estimation of the roughness stylus profilometer.	81
5.13	Visual representation of the RAP-1 die surface.	82
5.14	Profiles of the die finished with the RAP 2 -functional surface. (b) is extracted along the longitudinal direction of the profile, while (c) is taken in the transversal direction.	84
5.15	3D and profiles of roughness surface from the die finished with the wire EDM process. (b) is extracted along the longitudinal direction of the profile, while (c) is taken in the transversal direction.	85
5.16	Drawing of the punch and ejector geometry in accordance with the general guidelines outlined by ICFG [20].	86
5.17	Tool system for double can extrusion [12]	87
5.18	Sketch of the cup-height measurement setup	88
5.19	Results of the macro size double cup test. The indicated confidence interval is with 95 % coverage factor	89
5.20	Results of the macro size double cup test, allowing the disregard of one outlier measurement pr. reduction height batch.	90
5.21	The punch geometry for the upper and lower punch.	92
5.22	Results of the upsetting test of 1 and 2 mm CuZn15 α -copper alloy.	92
5.23	Example of surface topography after wire-EDM processing. This case is a surface scan of the 2-F die replica.	94
5.24	Comparison of predicted and measured punch load during double cup forming.	95
5.25	Sectional sketch of the die set utilized for the micro DCE-test (a) and a photograph of the tool system mounted on the general purpose testing machine (b).	96
5.26	Results of the 1 mm DCE test plotted on top of the reference values from the numerical simulation.	96
5.27	2mm results from the DCE-test. Confidence intervals are 95% coverage.	97
5.28	Punch load during micro DCE-test for 1mm specimens. Plot of three representative single samples.	98
5.29	Punch load for 2mm DCE-test. Plot of three representative single samples	98
5.30	Sectional sketch of the working principle of the Micro Tribology Tester Figure (a). Figure (b) show the one-sided 3D model of the test, where the workpiece is marked blue and the tool is semi-transparent.	100
5.31	Outline of the mechanical design and control system for Micro Tribology Tester.	101
5.32	a) Close view of the testing equipment; b) Center tools made of high performance cold work steel Vanadis 6; c) Cylindrical test workpiece before and after the test; d) Friction force transducer [21].	102
5.33	Microscope images of the tool inserts for the MTT apparatus.	103
5.34	Micrographs of the tool surfaces after forming.	104
5.35	Plot of friction- and normal force measurements for a tool featuring a fine surface finish, $R_a=0,01 \mu\text{m}$	105
5.36	Plot of friction- and normal force measurements for a tool featuring a rough surface finish, $R_a=1,8 \mu\text{m}$	105

LIST OF FIGURES

5.37	Plot of friction measurements for the \varnothing 1mm specimens.	106
5.38	Plot of friction measurements for the \varnothing 2mm specimens.	107
5.39	Bar plot of the ultimate friction coefficient, measured at the end of the translational movement.	107
6.1	Parameters influencing the design of tools for micro bulk forming.	113
6.2	Contributors to deviation for nominal geometrical dimensions in micro bulk forming	115
6.3	Typical processing sequence for a macro scale bulk forming tool	118
6.4	Typical processing sequence for a macro scale bulk forming tool	119
6.5	Die geometry to be manufactured. The die is a pre-forming die for a two step forming process for manufacturing of a micro axle for a potentiometer. . . .	124
6.6	Principle of electroforming (left) and a turned geometry in aluminium to be used as stencil for electroforming.	124
6.7	Micro bulk forming die to be manufactured using electroplating.	125
6.8	Photograph of the Sarix SX-200-HPM 3D Micro EDM machine (a) and a closeup image of the active components involved in the central spark erosion process line (b)	126
6.9	Photograph of micro forming dies manufactured using electroplating and EDM processes. The black colored die in the center has been coated with DLC coating.	127
6.10	Silicone replica of forming dies manufactured by electroforming and by EDM.	128
6.11	Technical drawing of the axle component. The general tolerances are $\pm 20\mu m$ on most geometrical elements	129
6.12	Simulation of suggested forming procedure of axle component.	130
6.13	Micro-EDM tool path for machining of die for cardan-shaft.	131
6.14	Photograph of the manufactured forging dies for micro bulk forming of the cardan axle component. The brass bushing in the background is used for alignment of the two dies during forming.	131
6.15	A photograph of the manufactured die geometry and profile line (a) and the extracted profile along the line (b)	132
6.16	Micro-EDM tool path for machining of die for cardan-shaft.	133
6.17	3D representation of the surface roughness measurements. The three numbered lines indicate the position extracted roughness profiles.	134
6.18	Formed cardan-shaft specimen. The shape of the forged readily recognizable. A profiled cross section can be seen in the plot (b).	135
6.19	Micro-EDM tool path for machining of die for cardan-shaft.	136
6.20	Suggested die geometry for the final forging step of the new three step forging procedure.	137
6.21	Typical tolerance chain for the micro bulk forming process.	137
6.22	Rigid fixation of tool elements through high precision support elements. . .	138
6.23	Suggested die geometry for the final forging step of the new three step forging procedure.	139
6.24	Illustration of self-alignment between tool elements through floating tool elements.	140
6.25	Illustration hybrid alignment approach. Alignment of the upper and lower die is ensured through relative alignment of the two tool holders. The holders are self guiding through the conical surfaces [22].	140
6.26	An adjustable punch fixture allows for alignment of punch and die through an adjustment screw	141

7.1	Schematic of a shear with axial load to improve shear quality [18].	144
7.2	Test equipment for cropping of micro billets [23].	145
7.3	Required shear stress (τ) as a function of axial stress (σ_N).	146
7.4	FE-simulation of high speed cropping process. Temperatures up to 87 °C can be noted.	146
7.5	Results of the three different cropping experiments. (a) is the end surface achieved when cutting with an enclosing blade. (b) is cropped with the addition of hydrostatic pressure and (c) is cropped under high speed with the blade speed exceeding 10 m/s.	147
7.6	Prototype cropping machine for cropping of micro billet under hydrostatic pressure.	148
7.7	Results of the a trial run of the cropping machine with brass material. A total of 50 specimens were produced and weight on a high precision scale. The cropped length could then calculated.	148
7.8	Histogram of the cropped billet lengths after disregarding a 26 % subset of outlier observations. Punctuated blue lines indicate the upper and lower bound of a 2 % volume conformance zone.	149
7.9	micro forming press with force transducers for process control	154
7.10	FEM-simulation of the frame stiffness under full 50 kN load. Maximum deflection of the frame is around 60 μm total.	155
7.11	Illustration from the C5K press CAD model with indications of vital elements and components.	157
7.12	Photograph of the functional C5K press with tool system.	159
7.13	Control screen of the C5K press system software. The interface features a number of control options and realtime plotting of process values.	160
7.14	Control system for the C5K press. The the left the three position safety handle can be noted.	160
7.15	Gravitation, electrostatic, van der Waals and surface tension forces. Attraction between a sphere and a plane [24].	161
7.16	Mock-up type test transfer rig [25].	163
7.17	Example of transfer sequence of a two stage micro bulk forming process. . .	165
7.18	FE-simulations of dynamic pre-stressing system for micro bulk forming. . .	167
7.19	Force interaction of the piezo driven pre-stress system.	168
7.20	Working curve of a ceramic piezo actuator. The product of the exerted force and the stroke length is constant.	169
7.21	Illustration of piezo based tool pre-stressing system	169
7.22	Photograph of the dynamic piezo pre-stressing system (a) and a closeup of the small forming die with a overlaid human hair (b)	170
8.1	Technical drawing of the potentiometer axle component.	174
8.2	Technical drawing of the pre-form component (a) and a photograph of the micro formed specimen, in a soft aluminium alloy, at different extrusion lengths (b).	175
8.3	Photographed aluminum axle component - from preform to final component. 176	
8.4	Machine brass axle component (a) and the micro bulk formed aluminium axle realized in this work (b).	176
8.5	Technical drawing of the gear wheel component. Tolerances are ranging between $\pm 20\text{-}50 \mu\text{m}$	178
8.6	Simulation of the gear wheel extrusion process.	179
8.7	Technical drawing of gear wheel extrusion die.	179

LIST OF FIGURES

8.8	CAD model of the extrusion tool elements. General tolerances are $\pm 50 \mu\text{m}$.	180
8.9	Photograph the extrusion tool parts (a). In this image the die and the tool holder ring is mounted in the aligning fixture. The container die can be noted on the side. The photo to the right (b) shows a billet pressed half-way through the extrusion die.	180
8.10	Plots of the press load over three successive extrusion experiments (a). (b) is a photo showing the result of a number of successive extrusions.	181
8.11	Example of transfer sequence of a two stage micro bulk forming process [26].	182
8.12	CAD model of the closed die forging tool system (a) and a photograph of the constructed tool system (b). The bulk metallic glass billet, colored gray, can be noticed inside the die in figure (a).	184
8.13	Micrographs of the $\text{Mg}_{60}\text{Cu}_{30}\text{Y}_{10}$ specimens. The cut billet is shown in (a), where the chip originating from the wire-EDM cutting is visible to the right. Figure (b) is an imperfect forming experiment due to under-heating. (c) and (d) show a good example of a the formed gear wheel geometry.	185
8.14	Load stroke curve of three successive forming of the gear wheel component in the $\text{Mg}_{60}\text{Cu}_{30}\text{Y}_{10}$ metallic glass.	186
8.15	Thermal behaviour of $\text{Mg}_{61}\text{Cu}_{28}\text{Gd}_{11}$ BMG material. (a) plots experimental values for crystallization of the material. As the crystalline material is at a lower energy state, the exothermal response of the crystallization is a sign of when crystallization happens. Figure (b) show that super cooled forming window and the time to crystallization [26].	187
8.16	Load stroke curve of forming with different process parameters.	188
8.17	Microscope images of the formed gear wheel specimens, $\text{Mg}_{61}\text{Cu}_{28}\text{Gd}_{11}$. (a) is a top-down image while (b) is acquired from the side.	188
8.18	Plot showing the expected crystallization time and viscosity of the Vitreloy 1B BMG as a function of temperature [27].	189
8.19	SEM images of the gear wheel formed at 450°C with only manual down-pressing of the punch.	190
8.20	Load-stroke curve of gear wheel forming experiment of the Vitreloy 1B alloy tempered at 430°C .	190
8.21	SEM micrographs of the gear wheel specimen formed at 430°C .	191
8.22	SEM images of the unintended back-ward rim formed on the Vitreloy 1B specimen moulded at 430°C is shown in ?? and ?. The images (c) and (d) show the results of the manual pressing of the Vitreloy 1B alloys at 450°C .	192
8.23	Figure (a) and (b) is a machined gear wheel from the extruded aluminium profile. Figures (c) and (d) show the gear wheel obtained through forming of the $\text{Mg}_{60}\text{Cu}_{30}\text{Y}_{10}$ low temperature BMG.	193
8.24	3D drawing of the Saddle component with markers denoting the features of the component.	194
8.25	Stress-strain curve for $\text{O}4$ mm upsetting of Titanium alloy specimens G1,G2 and G4 at ambient- and elevated temperature.	195
8.26	Tool stress analysis at different levels of friction and stroke length. (a) is the die geometry for the first forming step and (b) is the second forming step.	197
8.27	Illustration of the two-step forging process. In (a), showing the first step, the hex-geometry is extruded. In the second step, (b), the conical head is pressed onto the billet and the skirt is vertically extruded as flash.	198
8.28	Sectional drawings of tool system for warm forging of titanium. (a) show the preform extrusion of the hex geometry and (b) depict the sectional drawing of the second forming step.	199

8.29	Results of forming process simulations and calculations of tool stress resistance for the first (a) and second (b) forming step.	200
8.30	Simulated load of the two forming operations with different friction factors.	201
8.31	Simulation on the forming filling during heading of the abutment component. The green and blue dots donate areas of die contact.	202
8.32	Micrograph image of the first forming.	202
8.33	Load-stroke curve for commencing trial of first forging operation.	203
8.34	Micrographs of three successive forming experiment of the first forming operation. The specimen in (a) is the first specimen to be formed and the (c) is the last.	204
8.35	Load-stroke curves of the three consecutive warm forming experiment utilizing the pure G4 titanium alloy.	205
8.36	Copper coated titanium billets. The copper coating have been applied through electro plating as earlier described. The estimated layer thickness is around 10 μm	205
8.37	Measured forming load during the execution of the first step of the forming process with the copper coated specimens.	206
8.38	First specimen to leave the second forming step. A clear misalignment between the upper and lower forming die is noticeable.	206
8.39	Component formed after alignment of the upper and lower forming die. The component length is short measured and the material is flashed out at the skirt prematurely.	207
8.40	Aluminium component formed after polishing of the upper forming die. The polishing removed much of the side cut in the conical die.	208
8.41	Silicone replica of the second forming step upper and lower forming die.	208
8.42	Plot of two successive forming operations.	209
A.1	Stress strain curves for various cold forging materials [28].	228

List of Tables

4.1	Corresponding values of measured values from the step gauge and calculated values according to the procedure outlined in the previous section. All values are in microns.	40
4.2	Step height measurements of silicone replica and uncertainty figures. All values are in microns.	41
4.3	Roughness measurements of calibrated step gauge and replica	41
4.4	Punch measurement values from the Zeiss F-25 CMM, Fraunhofer-IPK,Berlin. All values in millimeter.	48
4.5	Punch measurement values from the Zeiss OMC CMM, DTU-CGM,Lyngby. All values are in millimeters without systematic error correction.	49
4.6	Measurements of die geometry, optical CMM DeMeet 220. The measurement uncertainty, U95, was estimated to $\pm 2\mu\text{m}$	55
4.7	Process characteristics from the manufacturing process of the punch geometry	56
5.1	Indication of the number of DCE-test to be conducted.	87

LIST OF TABLES

5.2	Indication of the number of DCE-test to be conducted.	93
5.3	Achieved surface roughness parameters of the manufactured dies.	94
5.4	Surface roughness parameters of the manufactured tool inserts for the MTT. Measured values are based on five repeated roughness measurements. The values marked CI(95%) are confidence intervals with 95% coverage for the five measurements, corresponding to the double standard deviation.	102
6.1	Typical processability of metals and advanced ceramic material for micro tooling.	121
6.2	Measured surface roughness values of the cardan-shaft forming die. Profiles acquired as marked in Figure 6.17.	134
7.1	Diameter measurement values take with a ZEISS UPMC 850 CARAT CMM at DTU-MEK having a resolution of $0,1\mu\text{m}$. Measurements are not corrected. <i>Average</i> values are the average of the three preceding measurements and Δ <i>initial</i> is the difference between the initial averaged diameter and the averaged diameter values measured following the excitation of the piezo actuators.	171
H.1	Measurement results of the Macro size DCE-test	267

Chapter 1

Thesis structure and guide to the reader

1.1 Thesis research statement

Micro bulk forming is a technology facing a number of technological challenges, before it can be applied as an industrial mass production process. Some of the fundamental challenges, specifically relating to the physical aspects of geometrical scaling the metal forming process, have been established at present time.

The aim of this project has been to investigate on the challenges in tool design for the micro bulk forming. Through research, design, simulation and realization of a number of practical micro bulk forming processes examples, the work seeks to increase the knowledge of tool design for the micro bulk forming process. Reflections on performance and concepts for the different tool designs will be provided through the thesis. Elaborate investigations and experiments have been conducted in areas of special importance for the micro tool design process. These include:

- Tooling process chain and tool process characterization
- Design of tool-, handling and press systems
- Micro Metrology
- Tribology and friction in micro forming
- Novel approaches in relation to micro forming tool design
- Forming of advanced and amorphous materials

1.2 Structure of the work

The structure of the thesis reflects the research question presented in the previous section. The thesis is divided into a total of seven chapters (Chapter 2-8), covering the main subjects related to the tool manufacturing and design for the micro bulk forming process.

Background and objectives (chapter 2) This introductory chapter introduces the current trends with micro manufacturing technologies. A cost analysis example is undertaken, demonstrating the cost effectiveness of the bulk forming process. Impact and outlook implications for the future is given.

The Micro bulk forming process (chapter 3) This chapter describes general aspects relating to the micro bulk forming process. Special emphasis is given to the conditions met when forming at micro scale. The chapter touches on size effects, workpiece and tool materials, tooling for elevated temperatures and transfer- and handling systems.

Micro metrology (chapter 4) Micro metrology is a field of great importance for micro tooling. The need for characterization of tool geometry and surface characteristics is critical. Methods for micro measurements and different measurement equipment is treated.

Tribology in micro forming (chapter 5) Tribology has all ready been identified as one of the key challenges to overcome within micro forming of metals. The chapter holds several experiments seeking to establish a connection between surface roughness characteristics and friction during micro bulk forming. The tests consist of two double cup extrusion tests, one in the macro scale and one in the micro scale, plus a supplementary test conducted on a novel micro tribology tester device.

Tooling for the micro bulk forming process (chapter 6) Chapter 6 is the process of designing a tool for micro forming. General characteristics and challenges within micro tooling is described. Tool manufacturing processes are outlined and strategies for alignment, surface coating and tool design is given.

Micro bulk forming framework (chapter 7) The chapter on micro bulk forming framework describes important aspects of the framework surrounding the central forming tools. Examples of component handling systems and billet preparations systems are given. A design for a micro press, realized over the course of this projects, is presented.

Results of advanced micro forming experiments (chapter 8) Chapter 8 holds results of the micro bulk forming experiments conducted. An aluminium axle is formed in a soft aluminium alloy. A micro gear wheel is formed in a number of different metallic glasses in their amorphous state using closed die forming. Finally, a titanium dental implant component is formed utilizing a two step forming procedure at elevated temperatures.

Furthermore, chapter one holds a general introduction to bulk forming processes, specialties related to micro bulk forming and some of the motivational aspects of why the application of these processes are relevant. Chapter one is concluded with a section touching on the impact and outlook of the micro forming technology and the work of this thesis.

1.3 Guideline for reading

A few introductory remarks should be given to aid the reader in working his/her way through the thesis.

Students, peers and associates who have contributed actively in the work described in this thesis, is acknowledges in the acknowledgment section of this thesis. The acknowledgment section also hold references to related publications co-authored during the project.

Graphics, data or concepts that have been adopted from previous work, or in any other way which is not a direct results of the work of present work of the author, is references in square parentheses []. For figures the citations are placed in the figure caption. For text describing concepts, results, ideas of others, inline references are placed in the body text right after the description.

Chapter 2

Background and objectives

2.1 Introduction

In the 1960's scientist discovered that a large number of microscopic transistors can be integrated on a small piece on semiconductor substrate. Using photolithography, the desired circuit design can be printed onto a small semiconductor substrate, instead of building an electronic circuit from discreet elements. This allowed for cost effective integration of complex electronic systems with low power consumption and high clock speed. Both analogue and digital systems could now be integrated onto the same piece of semiconductor material. Thousands of such integrated circuits could be placed on a silicone wafer, making bulk production possible. The introduction of integrated circuits paved the way for a range of new application within a wide spread areas. Technological leaps have been made within almost every trade or industry due to the introduction of electronic micro technology and computers have become the central element within all but every professional trade. Ultimately, the introduction of micro technology is responsible for the transition from the former industrialized world to the modern information society.

In recent years, researchers have predicted that not only electrical devices, but also mechanical devices, may be miniaturized and batch-fabricated, promising the same benefits to the mechanical world as integrated circuit technology has given to the world of electronics. Where electronics has provided computation power, interfacing and intelligence, micromechanics can provide the sensors and actuators which interface to the outside world. Today micromechanical devices are the key components in a wide range of products such as automobile airbags, ink-jet printers, blood pressure monitors, and display systems. It is predicted that in the future these devices will be as common as integrated electronics are today.

The term Micro Electro-Mechanical Systems, MEMS in short, was introduced in the 1980s to describe advanced mechanical systems on a chip. There are thousands of MEMS process with a famous few like the German named LIGA process (Lithographie, Galvanoformung, Abformung) and the Electrochemical fabrication (EFAB). However, the majority of MEMS process are a combination of three basic building blocks, the ability to deposit thin films of material on a substrate, to apply a patterned mask on top of the films by photolithographic imaging, and to etch the films selectively to the mask. Most of these manufacturing technologies have been adopted from the world of micro electronics

and is suited for fabrication of 2D and $2\frac{1}{2}$ D structures. Typical length scales for MEMS component ranges from 1 to 100 micrometers, where the typical device is between 20 micrometers and 1 millimeter along the major length scale. By combination of MEMS manufacturing with the silicon technology, the intelligence, sensors and actuators can be combined on the same substrate. An example of clever integration of an electrical system with a MEMS device is the MEMS microphone found in the bulk of mobile phones today. By integration of the amplifier circuit with a pressure-sensitive diaphragm, etched directly into the silicone chip, the microphone MEMS can be mounted as a normal surface mounted component - eliminating the manual work routine of placing the a microphone onto the circuit board [29].

2.2 Applications of micro components

A range of components exists in the micro length scale, between the conventional macro size and the length scale of the MEMS technology. Typical dimensions in micro scale ranges from a few millimeters to about 100 microns in contour dimensions. Examples of components that fall into this category are miniaturized connectors for the electronic industry, dental implants, screws and pins for mobile phones and elements for hearing aids. Today the bulk of these components are produced in conventional polymer- or metallic materials. However, the production of micro sized components cannot simply be realized by a simple scaling of existing processes. Scaling or *size effects* come into play and the paradigm of the manufacturing processes shifts [30,31,32]. Within polymer injection moulding processes the flow characteristics of the material change and boundary effects occur when the part size enters the micro domain [33]. However, with the use of a dedicated micro injection moulding machine, featuring separate melt plastification and melt injection feed screws, in combination with a high die closure pressure, it is possible to realize high precision polymer micro components. Indeed millions of micro sized polymer components are annually produced world wide and can be found in applications within the electronics industry, hearing aids and medical equipment.

Due to the limited mechanical strength of polymer materials, polymer micro components are generally limited to application requiring low to moderate strength of the constituent micro parts. Further, it is not unusual to see the application of conductive metallic inserts in combination with a polymer based support structure. This construction imposes some secondary challenges related to alignment and handling of the hybrid polymer and metal component.

For applications requiring high mechanical strength, bio comparability, high wear resistance or ability to conduct electricity the choice of metallic material is obvious. Examples of component geometries include small springs with various geometries, gear wheels and ranges of screws, bolts and pins. The electronic industry is a large-scale consumer of miniaturized headers, connectors, gate connection leads and wire bonding technology.

A substantial part of these micro mechanical elements are currently manufactured using mechanical punch and bending operation processes or chemical etching. Both of these processes are wasteful and chemical etching further contains some environmental issues to be dealt with. For 3D metallic micro components the predominant manufacturing methods are currently based on cutting processes. High precision turning and milling processes are commonly applied to mass produce miniaturized metallic components [34,35].

Cutting processes are costly in terms of operator costs, material waste and cycle time and thus not well suited for bulk production. Further, the application of the processes in micro scale requires careful planning of tool paths and specialized handling of the small workpiece [36,37]. Figure 2.1 is a photograph of a collection of micro sized components to be used in a dental implant. These elements are currently manufactured in Grade 1 pure Titanium using conventional turning and milling processes.



Figure 2.1: Example of a dental implant, a so-called a *abutment*, that technically qualify as a micro components

Bulk forming technology holds the promise of delivering precision components in large quantities at high production rates with remarkable accuracy. However, the application of cold forming technology at micro size is complicated by several size effects, preventing forming technology from being used at micro scale. In the current work we will look at some of the theoretical and practical aspects of the micro bulk forming process.

Some of the early research on basic micro forming *size effects* have been done at the research group at Lehrstuhl für Fertigungstechnologie at University Erlangen-Nürnberg in Germany [38,39]. Later, several research collaborative have revolved around the subject, such at the EU framework 6 funded *Masmicro* and the *4M* network of excellence.

The current work is part of a national Danish collaborative initiative by the name *MikroMetal*, where a number of Danish public body research organizations and industrial partners have worked together to explore theoretical and practical aspects of micro forming technology.

2.3 Cost and production series challenges

The continuing trend towards miniaturization and more densely integrated products with complex functionality have imposed new challenges on manufacturing technology. The demand for small components with medium geometrical complexity and high precision has constantly risen since the beginning of the 1990's. This trend is confirmed in market analysis of micro systems worldwide, reaching a turnover of 52 billion USD in 2009 and with an annual growth rate of 16%. The current growth areas for MEMS and Micro systems technology is the areas of consumer electronics and medical and life sciences [40].

With the growing trend of micro technology in mind, we turn the attention to an example of the potential in utilizing the bulk forming process for fabrication of a batch of 300.000 metallic micro components with medium complex geometry. An illustration of the intended component to be formed is shown in Figure 2.2 The calculation takes



Figure 2.2: Medium complex geometry forged micro part (left and middle) and the machined component (right)

offset in the same figures as in the paper of Arentoft et al. where a conservative standpoint is adopted [41]. The analysis compares the estimated production costs of a batch of specimens manufactured with conventional cutting process and a similar batch manufactured using micro bulk forming. For bulk forming process the analysis assumes that the components can be net-shaped and that the resulting components can be regarded as functional identical to result for the cutting process. The pie charts in Figure 2.3 and 2.4 illustrates the elements contributing to the unified cost of production of the individual micro component. *Production cost* encompasses energy costs, labor, maintenance cost and lease of production space. The chart also take account of the relative cost addition of machinery and tools, material costs and spillage of the individual production methods. The total cost of one produced specimen is more than double in the case of production with cutting process when compared against the bulk forming equivalent.

It is clear from the relative cost distribution of the two processes that the cutting process is both wasteful and labor intensive. Even when considering the reutilization of waste material, the material cost of the cutting process remains a substantial factor of the overall cost of manufacturing. In the case of micro forming, where precious materials are commonly used, the burden of material cost will be even more pronounced.

For the bulk forming process, the dominant contributor to the cost balance chart is the cost of machine and tools. This is primarily due to the substantial development cost and limited lifetime of the forming tooling system. Also the preparation of the required

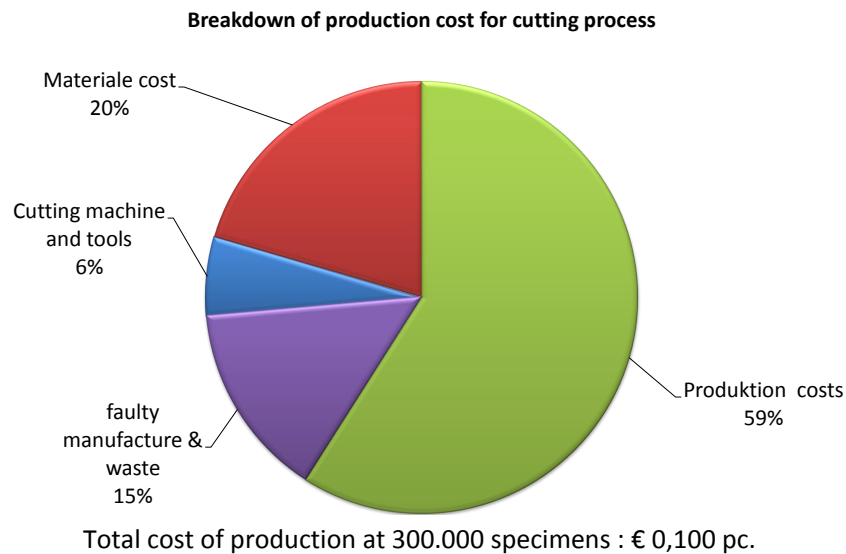


Figure 2.3: Cost factors involved in cutting of a micro component with medium advanced geometry and a production batch size of 300.000 pc.

preform billet takes up 9% of the collective cost of production.

Concluding on the production cost analysis, the applicability of the cutting and forming processes as production methods can be decided. The cutting process is versatile by nature and can easily be adopted to different component geometries. The penalty for the increased flexibility is longer cycle times, more material waste and increased labor costs. For the bulk forming process, the major contributors to the cost is related to the design, setting-up and commencing of the process, whereas running cost are modest. The flexibility of the forming process is low due the need of process re-design and tool manufacturing involved. Thus, for a bulk production scenario, the forming process is advantageous in terms of costs and production volume whereas the cutting process are to be chosen when flexibility is important and production volumes are low. The point of cost break even between cutting and forming processes happens at production volumes between 300.000 and 800.000 pieces pr. year, [41].

The potential cost saving, the low material waste and the small cycle times are among the properties that make the micro bulk forming process aspire as preferred for production of large quantities of metallic micro components. However, the application of the micro bulk forming is not straightforward and a number of challenges is still to be overcome before this process can be fully industrialized. The major challenges in micro forming fall into one of four broad categories: workpiece material, tooling, equipment, and process control. The work of the present Ph.D. thesis revolves around the subject of micro tooling. However, due to the close bonds between the constituent elements of the micro forming process, influence of the contiguous process elements will also be treated.

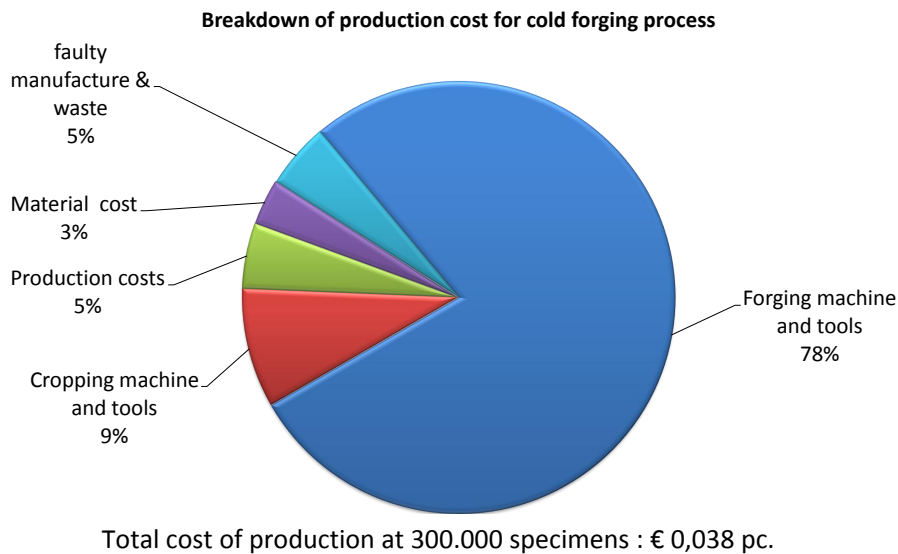


Figure 2.4: Cost estimation of forming of a batch of 300.000 pc batch of micro components

2.4 Micro factories

Once the drivers and production methods of a typical micro component is understood, the concept of micro factories is not difficult to envision. Owing to the small size of the component envelope, a scaling of the production equipment seems straight forward. By realizing desktop size manufacturing machines, a new world of flexible production equipment could begin. In traditional manufacturing the processes are clearly separated and the produced specimens are constantly relocated between the different production stations. Within the subject of LEAN manufacturing and production analysis, shop floor optimization have long been an area of study.

By realizing a number of small flexible desktop process stations, the opportunity to dynamically redesign the concatenated process chain, to suit the need of the specimen in question, becomes feasible. This means that the elements of the production chain can easily be rearranged to suit the actual need of the production chain, rather than moving the produced specimens from one process station to the next. Apart from saving costs, this approach opens new opportunities to lease, upgrade or exchange elements of the production chain, realizing a truly flexible and modular micro production platform [34, 42, 43].

Research groups worldwide are working to advance the basic foundation that is going to make micro factories realizable. Especially Japan is active in this arena, but initiatives have also been started by U.S. public and military bodies and within the European Union research framework. At present time some of the key drivers in realization of the micro factory vision have been identified [44]:

Higher speed: Higher accelerations can be achieved because of reduced inertia. Spindles of machine tools can reach extremely high rotational speeds because of the relaxed restrictions on DN value on bearings.

Precision Freedom of configuration and proportion in machine design will increase. With flexibility in design, the structural framework stiffness and resonant frequency can be increased, whereby machines will be more robust against external vibration and thermal deformation. Positioning accuracy can be improved.

Productivity Productivity can be increased by the dense and highly parallel allocation of machinery. In a production line, transfer distances can be shorter and material-handling equipment will be lighter.

Piece-by-piece process Unlike a batch process, a piece-by-piece operation can decrease the statistical likelihood of faults, so the yield will be improved.

Shortened ramp-up In conjunction with piece-by-piece operation, one can proceed to mass production immediately after setting up the machinery for small-quantity production by just parallelizing a number of machines, without needing to re-design and create new machine paradigms for mass production.

User-oriented machine design Modular design of machines can be realized, and the machines can be reconfigured with ease. Operators can design and configure their machines by themselves.

Due to the appealing potential of the micro technology, strong voices in research society have predicted that a revolution within science and engineering; through the application of micro mechanical systems, is imminent. However, in spite of the promising potential, there is still some important challenges to overcome before the commendable vision of flexible micro factory production system can be realized.

Some of the most dominant issues to be solved are the following:

- Realization of scaled micro manufacturing processes
 - Tooling technology
 - Precision and tolerancing
 - Tribology and wear
 - Environmental influence
 - Size effects
- Process integration
 - Interface design
 - Alignment precision
 - Transfer of specimens
 - Concatenated process chain effects
- Assembly and packaging

- Flexibility for variety of models
- Pick and place accuracy and control
- Integration of component and fixture
- Quality assurance and inspection
 - Micro metrology
 - Inspection systems

In the present work we will directly look at some of these challenges, while others will be mentioned briefly. However, it has been a priority during the work with this thesis, to leave the reader with a general impression of some of the possibilities and challenges encountered when applying the micro bulk forming process. A second priority has been to touch on some the more general aspects of application of micro manufacturing methods at present time and further to identify ways realizing the micro bulk forming process as a part of a micro factory manufacturing system.

2.5 Impact and outlook

The present work will seek to advance the state of the art within theoretical and practical aspects of the micro bulk forming tooling technology. Upon completion, the reader should have a good overview of the present state of the field and the advances contributed through this work. The guidelines and observations made throughout the following aim to be as universal applicable within micro forming as possible. Further, through repeated utilization of industrial component geometries as objects of study, a certain degree real-world relevance and applicability is assured. Tool designs and components are, where relevant, based on present standard tooling elements, thereby saving cost and accommodating the professional reader, who is already familiar with conventional forming tooling technology.

With the current thesis in hand, a person skilled in forming tooling technology should be able to readily identify a suitable route for design and realization of a new micro forming operation. By taking advantage of the theoretical and empirical knowledge that has been gathered throughout the present work, the development cycle of the micro bulk forming process of a new forming scenario could be shortened. Researchers embarking on new studies within metal forming technologies in the micro size range, could benefit from the more generalized observations of this work in areas such as micro metrology, tribology or tool alignment strategies for high precision tooling elements.

Parts of this work have been adopted by an industrial partner wanting to explore the opportunity to produce advanced micro components by means of the bulk forming process. It is the hope of the author that the industry can benefit from the knowledge gained in this project through their development process. Further, the more general findings from this work have been accepted for publication in a professional book dealing broadly with the state of the art within micro manufacturing [1].

As the projected number of applications of micro and nano technologies grow in the future, so will the need to mass manufacture these elements. Polymer injection moulding, LIGA technology and hot embossing processes have already proved capable realizing

micro sized component is great number. However, many future micro applications require micro mechanical elements with high strength or wear resistance. For this purpose, metallic micro components is anticipated to play an important role.

Chapter 3

The Micro bulk forming process

Forming of metals is a well established process, dating back more than a thousand years. During the early colonization in Europe, the village blacksmith formed horseshoes, fittings and weapons using hammer, anvil and forge. The concept of plastically deforming metals into the shape desirable makes good use of the material and will often enhance the performance of the material [45]. In the ancient Asian, cultures the forging of the Samurai sword was considered to be a black art. By forging steel alloys with different carbon content into a sword blade, it was possible to combine the ductility of the low carbon steel with the hardness of the high carbon steel, into a blade which was both flexible and sharp. The subsequent heat treatment of the sword blade included addition of a mixture of water and clay to the cutting edge of the blade in order to lower the cooling gradient in this area during quenching. Only by mastering the craftsmanship of forming, the literacy of materials and the empirical knowledge of the hardening and quenching procedures, the Samurai sword maker was able to make the ultimate weapon [46, 47].

3.1 Bulk forming at the macro scale

Today cold forging is applied extensively within industrial manufacturing of metallic components worldwide. Especially within the automotive industry, huge tonnages of rack, axles and other transmission component are manufactured through utilization of bulk forming technology. Components leave the bulk forming operation either as prefabricated preforms, that subsequently undergo machining, or as net shaped components which are finished after the forming process.

A typical forming scenario consist of multiple forming stages and comes in a range of variants. Each of the forming variants can however be classified into one the eight basic bulk forming operations depicted in Figure 3.1.

The industrial popularity of the bulk forming process still rely on the underlying theory of material flow and behavior; something that has not changed since the early days of forging. Even with the employment of numerical simulations and modern computer aided design systems, a well functioning bulk forming system requires extensive knowledge of strain hardening of the material, flow behavior as well as friction and lubrication conditions (tribology). These parameters generally dictate the forming limits of the bulk forming process and thereby also the achievable geometry of the workpiece. A medium

3. THE MICRO BULK FORMING PROCESS

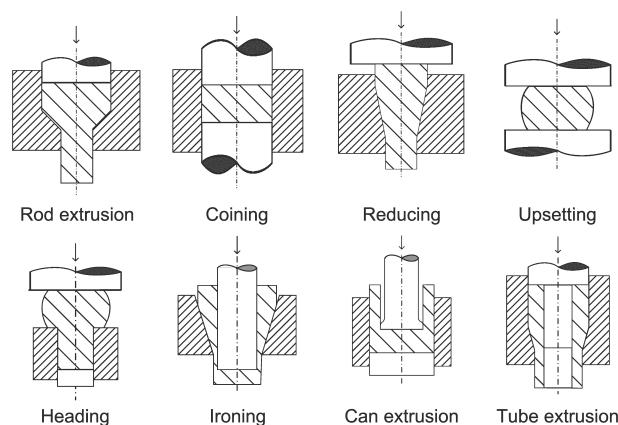


Figure 3.1: Basic cold forging procedures [12].

advanced bulk forming process often consists of 3-5 consecutive forming steps, either mounted in the same press frame or realized as individual operations. This means that a typical bulk forming process actually is a process chain of several forming operations, each carefully designed and analyzed to arrive at the best possible end result.

A well designed bulk forming process is capable of fabricating specimens at a fast pace with good accuracy and little to none material waste. These properties have contributed towards the popularity of the modern forging processes, making them the process of choice for mass manufacture of metallic components.

However, the design and operations of a bulk forming process is not a simple task. The startup cost associated with analysis, design, development and manufacture of tools are high. It is not unusual that the cost to arrive at the first successfully formed component can exceed millions of Euros. Further, the design and operation of a bulk forming process usually requires specialist knowledge of material flow, tribology, tool- design and manufacture.

3.2 Micro Bulk forming

Micro bulk forming is utilization of the bulk forming process to form micro components. A micro component is often defined as a component with two or more dimensions below the millimeter scale [39]. The definition can be widened to include macro sized component with functional features that themselves qualify as a micro component.

Compared to more traditional micro manufacturing processes, like turning and milling, bulk forming holds the potential of producing high quality components, faster and with no or only little material waste. Even though some of the incentives for wanting to realize the bulk forming process at micro scale seems identical to those of the macro scale, most of these properties are aggravated at micro scale.

Production speed is important, as the lifespan of the consumer products, possibly featuring micro components, is generally short, when compared to a larger product; a cell phone model is replaced before a car model. Considering material waste, micro

components are often manufactured in more precious metals such as Palladium, Titanium or Silver, meaning that material have dominant influence on the cost of manufacturing.

Finally, the required high precision of the finished micro component is both the driver and a barrier to the predicted breakthrough within micro manufacturing. Being able to mass produce micro component at low cost and with accuracy, advanced mechanical systems can be packed into small volumes. This opens the door to a new range of applications within several industries, including the consumer-, dental-, medical- and IT markets. Among the applications that have been proposed is a spine-repair kit. Using the repair kit, a person who have suffered a fracture of the spin can have a section of the spinal column replaced with a mechanical system of micro components.

A number of effects have reported during the effort of scaling the bulk forming processes to micro size. These effects can be treated as deviations from the linear continuum theory when entering the micro domain. The effects often constrains the achievable geometries in the forming process and is commonly dubbed *Size effects*.

3.3 Size effect in micro bulk forming

By decreasing the size of the components in small mechanical systems, the weight and volume of the device can be reduced without sacrificing functionality. Often the micro component technology is the enabler of such new miniaturized products.

Today micro components are a central part of the mechanical systems in consumer products like hearing aids, computer drives or mobile phones. The medical sector is another important application for micro components. Here the micro components are used as parts of dental implants, in knee implants or as elements in drug delivery systems. These applications often require low failure rate in combination with high functionality; giving raise to strict quality and tolerance requirements. It is not uncommon to see 100 % manual inspection rate requirements for these types components, something that is incompatible with mass production at low cost.

Size effect is a term for the deviation from the linear continuum theory, when the scale is reduced to micro- or nano scale. That is, when scale is reduced to the micro level, some of the rules change and a new set of theories have to be applied. Or put it in another way, when the size on the component is within orders of magnitude of the physical elements of the process, e.g. material grain size, the linear theory of the macro domain breaks down [38].

Contributors to the size effects can be attributed to three categories of effects; the shape, density and structural effects [48]. Shape effects are closely related to the surface to volume ratio of the component. Consider a dice with a scalable side length of λ . Now, the volume of the dice scales with the third power λ^3 , whereas the surface area scales with the second power λ^2 . Generally speaking, this means that a small component will have a higher surface to volume ratio, by λ , when compared to its larger equivalent. The surface to volume ratio is an important parameter when considering an ejection operation or a handling situation where friction is a factor of the component surface area and the component mechanical strength is related to material volume. Following, designing an ejector system to de-mould a micro component from the forming die is

3. THE MICRO BULK FORMING PROCESS

challenging, due to the risk of collapse or reverse forming during ejection. Further, small components are prone to the sticking effect, where adhesive forces between the gripper and the component outweigh gravitational forces. These adhesive forces primarily consist of surface tensions, Van der Waals, and electrostatic forces and can be the limiting factor of a handling system for micro components.

The second effect contributing to the size effect is the group of micro structural effects. This group of effects is made up of physical elements which either experience a physical length limitation, where it is not practiced to scale the micro-geometry or where secondary scaling effects come into play. Surface roughness is an example of a quantity that, in practice, is not fully scalable. The roughness topography of a forming tool is often an inherit property of the manufacturing process and is only scalable within a certain window. This results in a relatively higher roughness when the component is scaled down. Manufacturing tolerance is another important property prone to the size effect. High precision tooling machines are costly with an, approximately, exponential correlation between achievable precision and machine cost. However, the machine precision is independent of workpiece size and is strictly bound to the precision of the tooling machine itself. However, when the overall size of the component is reduced to the millimeter scale, it is seldom acceptable to inherit the tolerance band of the macro scale, which is normally within a few orders of magnitude of a millimeter.

Density type of effects relate to the in-homogeneity of materials at small scale. If we consider the average grain size of a material to be of the order of $40\ \mu\text{m}$, a macro size component would contain millions of grains, meaning that the material could modeled as homogeneous. Going to the micro domain, a $500\ \mu\text{m}$ feature would only contain about 12 grains over the cross-section, giving the properties of the individual grains substantial influences on the forming process. This can lead to in-homogeneity in shape, micro-hardness and spring-back during bending and forming for thin foils.

For micro forming two distinct effects of flow stress influence related to the relative grain size have been reported [17, 38].

The apparent yield strength of the material will decrease with decreasing specimen size. This behavior is explained by adopting a laminar surface layered model, wherein each grain is associated with a layer according to its relative distance to the boundary surface of the specimen [49]. With the assumption that grains located on the surface experiences fewer constraints, when compared to grains in the middle of the specimen volume, the local flow behavior must be dependent on the position of the individual grain in the specimen. Now, dislocations induced by the forming process are able to sum up over grain boundaries inside the workpiece volume, but not for grains near a free surface. Thus, lower local strain hardening will occur close to the billet surface. This implies that a micro billet, with a high surface to volume ratio, overall will appear as having lower material yield strength. Further, the more dominant influence of the individual grain size, order and orientation at micro scale will lead to increased scatter of the apparent flow stress of the material [38]. These effects are generally only present in the case of unrestricted material flow, such as in air bending or open die forging. In the case of closed die forming the effects of decreasing flow stress and increased scatter will be minor due the restricted material flow and the influence will often be concealed by the increasing influence of friction.

Figure 3.2 depicts prominent scaling effects affecting the micro forming process; the

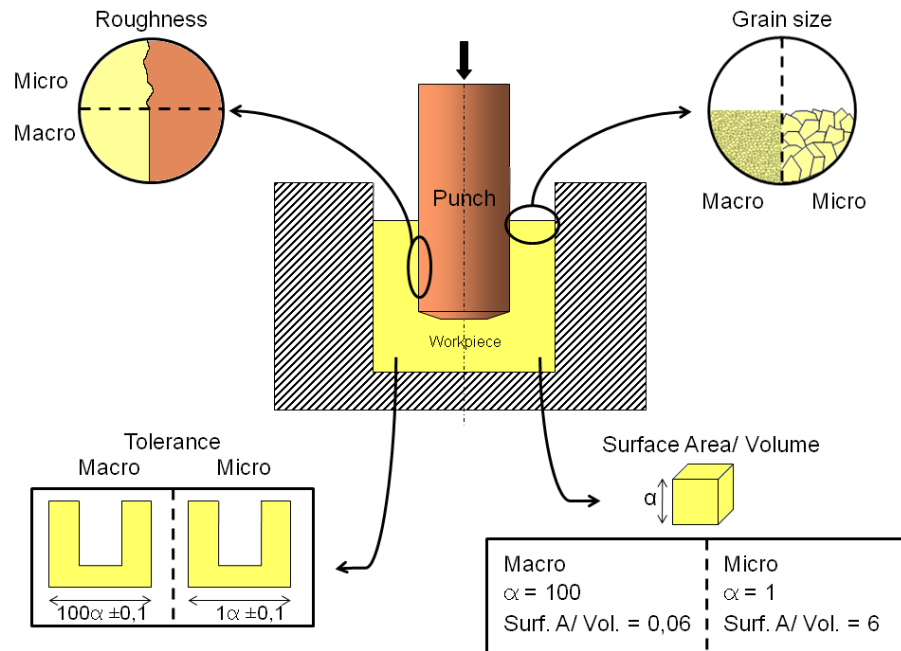


Figure 3.2: Overview of dominant size effects in micro bulk forming.

Overview of dominant size effects in micro bulk forming. The influence of roughness scaling, grain size scaling, tolerance scaling the nonlinear scaling for surface to volume ratio.

bound roughness characteristics, the fixed tolerances inherited of the tool manufacturing process, the grain size determined by the physics of metallurgy and the geometrical nonlinearity of the surface/volume ratio.

3.4 Materials in micro forming

Material knowledge is central for the bulk forming process, which fundamentally relies on differences in flow stress between two materials. These two materials are often termed "work piece material" and "tooling material", relating to their respective functional purpose in the bulk forming process. Properties like cost, flow-stress, ductility and strain hardening are important for the forming material whereas the yield strength, machinability and ductility are performance parameters for the tool material. In order to accurately analyze and simulate the forming process, work piece material data is needed. These data can be acquired by performing an upsetting test, where the mechanical strain/stress curve of the material can be acquired. This can be done by using length and force transducers connected to a data acquisition device. The resulting data can be fed into a numerical finite element program and the forming process can be simulated. The selection of work piece material is normally a trade-off between requirements set by the component application and formability performance. Materials with a high strength is generally desirable, leading to lower mass and a more compact design, however these materials are often difficult to form in a bulk forming process. On the other hand, a soft material is easier to extrude or form but the strength of the finished component is often

not interesting for high performance applications. The choice of work piece material further influences tool life expectancy, forming temperature, the choice of lubricant, coating and the number of forming operations required.

Polycrystalline metals for bulk forming

The predominant work piece materials for cold forging are Steel, Aluminium, Copper and Zinc as well as alloys of these. Generally, a material is sought to have as low yield strength as possible and a high formability, while still being able to fulfilling the strength requirements of the finished product. For the case of most metals suitable for plastic forming this translates to a low number of alloying elements. For steel, the presence of C, Si, Cr, Cu, Mn and Ni have particular influence on the yield strength of the Fe-C alloys. Typically, a material with increased yield strength, due to alloying elements, will simultaneously suffer a reduction of the attainable formability [12].

Cold forged components with high strength can be attained by using low-alloyed steels with moderate strain hardening characteristics behavior or by the subsequent application of thermal hardening processes.

Aluminium in the pure state can readily be forged. This is also the case for low alloyed ageing and non ageing types of alloys. Due to the low yield strength and the high ductility, aluminium is often used in a test specimen when commencing a new cold forging tool.

The formability of Cu and low alloys is comparable to that of aluminium. Good formability is also attained for the CuZn-alloys belonging to the family of α -brasses (Zn<37%) [12].

Forging of precious metals have become cost effective in micro forming due to the limited material consumption and waste in this process. Further, Magnesium and Titanium are interesting given their bio comparability and ability to conduct osseointegration and osteoconductivity with living bone and tissue. Both of these materials can be formed at elevated temperature with a typical formability comparable to that of stainless steel [50,51].

Recent advances in material research and the increased interest in micro manufacturing have lead to exploration of ultra fine grained and nano crystalline materials. One process of realizing fine grained materials is through severe plastic deformation processes. With these processes, like the classical equal channel angular pressing (ECAP), it is possible to divide grains in a coarse grained material into so-called sub-grains. Under certain metallographic conditions, these sub-grains qualify for being treated a individual grains. The structural changes result in an changed mechanical and physical properties of the metals such as a 3-4 fold increase in yield strength, hardness and high cycle fatigue life [52]. The influence of grain size effects in micro forming is well established [17]. Application of ultra fine grain materials will eliminate or lessen the grain size related density effects. However, the correlation between grain structure and material properties is not yet fully understood and remains a research area.

Amorphous metals

Amorphous metals are a new range of non-crystalline materials with interesting properties for manufacturing of metallic micro components. The amorphous structure of the materials is generally realized by combining at least three alloying metallic elements of considerable different atom sizes. The melted metal alloys undergo rapid cooling when transitioning from the liquid to the solid phase. During the rapid cooling the alloy is frozen in the amorphous state, prohibiting the metallic atoms to combine into the well known lattice structure characterizing conventional metals. The required critical process cooling rate limits the achievable forms in which amorphous metals can be realized, typically thin ribbons, foils and wires. However recent development has allowed for casting of amorphous metals with dimensions exceeding one millimeter, these are known as bulk metallic glasses (BMG). Bulk metallic glasses are interesting for forming micro components because this material is not subject to the grain size forming limitations, dislocations and sliding planes, of normal crystalline materials. This allows the BMG material to be formed in the micrometer scale with good result.

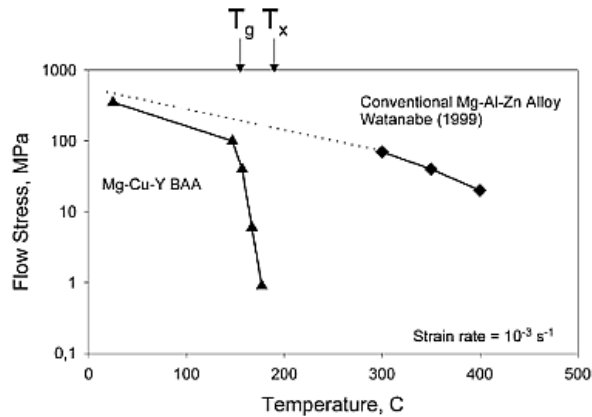


Figure 3.3: Yield stress for Mg60Cu30Y10 bulk amorphous alloy.

The forming of bulk metallic glasses takes place between the glass transition temperature T_g and the crystallization temperature T_x . At T_g the BMG becomes a super cooled viscous liquid exhibiting decreasing flow stress with increasing temperature. A second dependent parameter of the forming temperature is the crystallization time t_{cryst} where the amorphous structure is lost and the material crystallises. There is a time/flow stress tradeoff when selecting the forming temperature; higher temperature results in low flow stress and low viscosity but limited forming time due to the decreasing crystallization time. On the other hand, a lower forming temperature results in increased flow stress and viscosity of the BMG, resulting in increased tool loads and longer process time. The window of amorphous processing time is lengthened. Further, BMG materials are very strain rate dependent and fast processing results in high flow stresses. It has been claimed that BMG above the glass transition temperature behaves like asphalt on a summers day, since the viscosity of both BMG and asphalt is strongly dependent on temperature and strain rate.

Figure 3.3 depicts the flow stress dependency of Mg60Cu30Y10 bulk amorphous alloy in comparison a conventional crystalline magnesium-aluminum alloy.

3. THE MICRO BULK FORMING PROCESS

In the temperature range above T_g , a BMG is a thick liquid. For liquids, the stress required for flow is related to the temperature and strain rate. The following equation has been developed to describe the high temperature flow behavior of several BMG. The term in curly brackets is the dynamic viscosity, usually denoted η having units Pa·s

$$\sigma = 3\dot{\epsilon} \left\{ B \exp\left(\frac{H}{RT}\right) \left[1 - \exp\left(\frac{D}{(\dot{\epsilon}C \exp(H^*/RT))^\beta}\right) \right] \right\} \quad (3.1)$$

,where $\dot{\epsilon}$ is true strain rate, B, H, D, C, H^* and β are material constants, R is the gas constant and T is the absolute temperature.

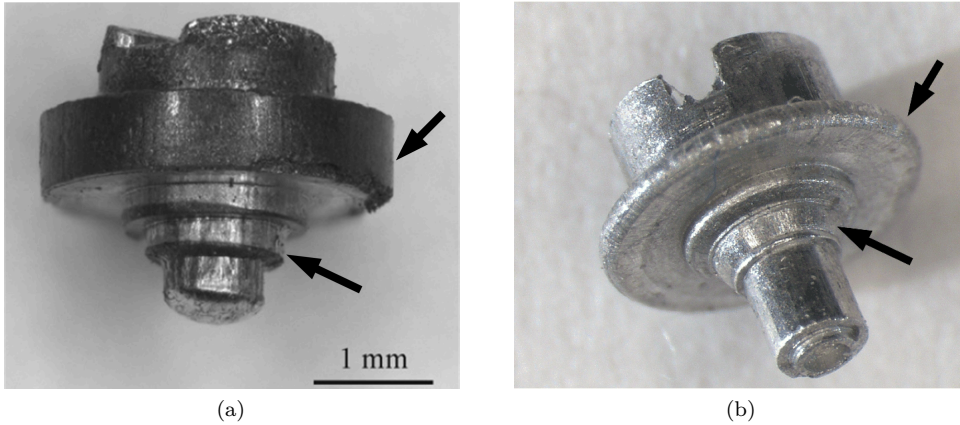


Figure 3.4: Side by side comparison of a potentiometer axle for a hearing aid bulk formed in an annealed aluminum EN AW-6060 (a) and in BMG Mg60Cu30Y10 (b) [26].

Figure 3.4 depicts a micro component formed by bulk forming in BMG and a soft aluminum alloy. By comparison it is observed that there is better form filling in the case of the BMG material (a) even though the forming process is not fully completed. As marked by the arrows, the outer rim of the component is subject to rounding in the case of the aluminum material whereas the BMG case exhibits sharp edges. The forming of BMG material is not trivial and remain a research topic [26,27]. Some of the issues yet to be solved relate to fracture strength and high temperature tool development. Low temperature BMG, with a glass transition temperature below 200°C are brittle with fracture strength as low as 500 MPa and may easily fracture during ejection or use. Zirconium and Iron based BMGs are formed at between 360 and 600 $^\circ\text{C}$ and have a higher yield and fracture strength, but here the design of the tooling setup becomes challenging due to the elevated temperature.

Tool Materials

The most dominant tool steels for bulk forming tools are powder metallurgical steels with high toughness, hardness and metallurgical homogeneity. Due to the high surface pressures involved in bulk forming, a tool material hardness of more than 50 HRC is normally required. The tool steels used to be cut in their soft state and subsequently heat treated to their maximum hardness and ultimately polished or surface treated. However, modern tooling machines can directly cut hardened steel allowing for better tolerances of the finished tool by avoiding the inevitable geometrical deflections during

heat treatment. In micro bulk forming the geometrical tolerances of the tool are very narrow and deflections of the tool during heat treatment often exceed the total allowable tolerance deviation of the tool. Thus tooling materials for micro bulk forming needs to be hardened already from bulk and will be machines in their hard state using grinding, hard micro milling or electro discharge machining. Owing to the small size of the tools, it is cost effective to use known prefab elements such as standard industrial punch needles or bushings as starting point for a bulk forming tool. These ISO standardized machine elements are cost effective, easy to source and have the mechanical properties required. Hard metal, ceramics or solid Tungsten carbide materials are another option for tooling materials. The cost of these materials is often much higher than traditional tool steel. However, since the amount of material used for a micro bulk forming die is small, the solid Tungsten carbide can be economically viable a tool material. The benefits of using Tungsten Carbide as tool material is the increased hardness of 62-70 HRC and a very low elasticity. The drawback of using Tungsten carbide as tool material is the limited options for machining, normally limited to electro discharge machining, and the low tensile fracture strength of the material (as low as 400 MPa). Especially tensile hub stress is unwanted for Hard Metal dies due to the risk of crack initiation. With a correct dimensioned pre-stress system, in the form of conical stress-rings, it is possible to superimpose compressive stresses onto the hard metal forming die. By superposition, the stress rings counteracts the tensile stresses arising from the forming process, thereby eliminating any effective tensile stresses on the hard metal die. The outer ring in a pre-stressing system is often designed in a material with good tensile strength and is only hardened moderately in order to retain a degree of ductility.

3.5 Warm forging of micro components

Micro components are often manufactured using special or lightweight metals such as alloys of Palladium, Titanium or Magnesium. The choice of material is often given by the end-application, where the environment of use can be humid, corrosive or have special demands for strength or bio-compatibility. Also new age materials, such as bulk metallic Glasses are expected to find wide use within micro bulk forming. With some of these advanced materials it can be beneficial to utilize warm forging, where the central forming tool elements are operating at elevated temperature. The main benefits of warm forging is a decreased tooling load, increased ductility of the work piece material and elimination of heat treatment process prior and post to forging. For some materials, such as bulk metallic glasses or high grade Titanium, warm forging is required in order to have acceptable lifetime on the tooling solution. Warm forging is defined as forging at elevated temperatures above ambient temperature and below the material re-crystallization temperature, typically in the range 100-400 °C. The use of warm forming tools requires an advanced tooling setup with good thermal isolation, heat shields and possible external cooling. It is essential to control the temperature gradient between the warm forging tool elements and the cold framework elements, in order to minimize thermal deflections with the following misalignment and possible tool damage. Apart from a more complicated tool design, other drawback of utilizing warm forging include higher friction, limited availability of lubricants and surface oxidation of tool and workpiece. Figure 3.5a depicts a prototype tool system for warm forging of a dental implant in Titanium.

3. THE MICRO BULK FORMING PROCESS

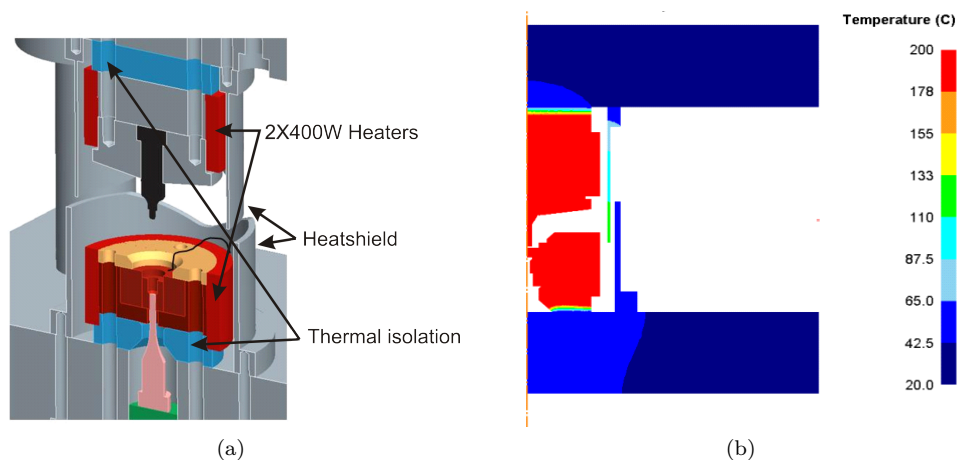


Figure 3.5: Tool system designed for warm forging of a dental Titanium implant. Figure (a) shown a CAD model of the tool and Figure (b) depicts the steady-state thermal analysis simulation results.

Figure 3.5b show a steady state thermal analysis of a tool system for micro forming at elevated temperatures. The system consists of a central heated core including die, punch, ejector supporting structure elements and resistance heater cartridges. The framework die set is thermally isolated from the warm core by a calcium silicate based ceramic material with a thermal conductivity of 0.4 W/mK. Heat shields with an optical reflective finish is placed around the upper and lower heated tooling elements. These heat shields prohibit heat transfer to the frame by radiation and functions as a simple safety measure for touch of the warm tool parts. Figure 3.5b illustrates the steady state temperature distribution of the tool system when heated to 200 °C. It can be observed that the tool frame is kept cold with only an insignificant temperature gradient over the supporting tool frame. This keeps the thermal deflections to an acceptable level. In an industrial setup, it is usually necessary to apply external cooling system as known from injection moulding machines for thermoplastics. The elevated temperature in warm forging imposes some additional design challenges on the tooling parts located in the heated zone of the tool. For an open die forging scenario, the primary adjoining factors to handle are more challenging tribological conditions. The tribological conditions can be controlled by applying suitable coatings on the punch and die and by carefully matching the workpiece material and the lubricant. The section on tribology later in the chapter touches more on these challenges. Further, periodically cleaning of punch and die might be needed to remove residues of lubricant and work piece material pickup. In the case of closed die forming the challenging tribological conditions remain and are further aggravate by oxidation and lubricant entrapment issues. When tempering punch and die at temperatures near the recrystallization point, oxides will form on the surface of these parts. The oxide layer, having a high friction coefficient, will give raise to a narrowing of tool clearances and increased friction between the tool pieces and between tool and workpiece. This can lead to tool breakdown and should be avoided. Further, pickup due to lubricant breakdown and lubricant entrapment is more dominant at elevated temperatures. Most lubricants are unfit for warm forging because the base liquid components become volatile, leaving solid lubricant residues in the forming die and on the workpiece surface. However, by careful application of the right coatings in

combination with the right type and amount of lubricant, it is possible to realize a micro bulk forming process at elevated temperature.

3.6 Handling and ejection system

Today, most industrial machines handling micro components are based on conventional circular vibrating screeners. These screeners are cross-vibrating vessels that are able to align a specific component geometry according by means of a custom-build mechanical gate. The gate system allows only components that are correctly aligned to pass through. Depending on the component geometry, material and the specially crafted design of the gate system, the mean failure rate of a vibrating screen system is usually around $\lambda_F=10^{-2}$ to $\lambda_F=10^{-6}$ pieces, meaning that between every hundred to every million component will jam the system and an operator has to inspect the system. Further, the vibrating screeners are bulky, noisy and inflexible, making them unsuitable as handling system for a multistage micro manufacturing machine. The sticking of matter is another issues that influences handling of micro components. With the increased surface to volume ratio for these small components, the Van der Waals forces will cause sticking of the components. Primarily the components will tend to stick to each other, requiring a handling strategy capable of both handling and separation. For this reason handling concepts of micro components have been studied intensively in later times [34, 53]. The use of robots cells, advanced gripper systems and self assembly systems have been proposed, but none have been widely employed within micro manufacturing because of the unfavorable combination of cost, complexity and speed of these systems.

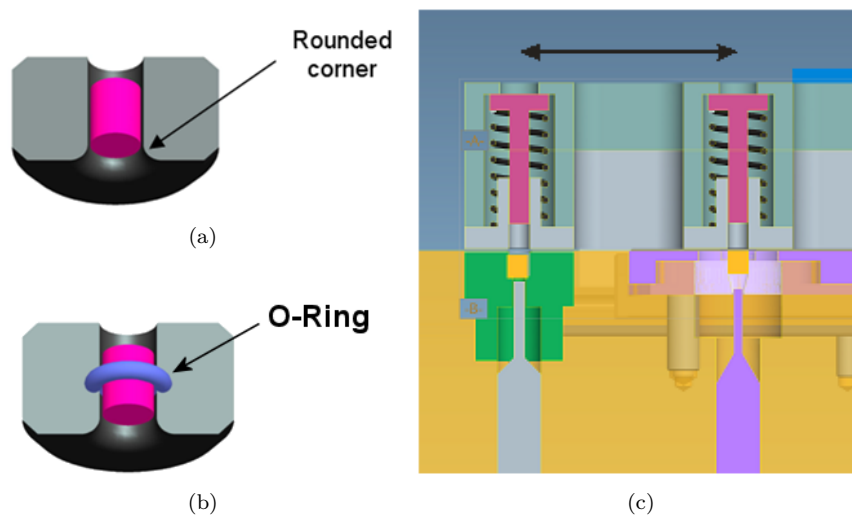


Figure 3.6: Example of a transfer system and with different gripper technologies for a micro bulk forming system. Figures (a) and (b) show different methods for clamping the component in the transfer system. Figure (c) depict an example of a transfer system.

Figure 3.6 depicts a handling system for the micro bulk forming process. A cut-out of the transfer system is illustrated in Figure 3.6c, where the components, drawn in yellow, can be ejected into the container fixture, moved laterally to the next station and reinserted into the succeeding forming die. This system is capable of transferring components

at high speed and is simple to monitor for failure. The holder for the component is a precision container used to hold and transport the components from one forming station to the next. For the container depicted in Figure 3.6a, the component is held in place by a combination of friction forces and surface tension forces (Van der Waals forces). In order for the surface tension forces to overcome the gravitational forces and keep the component in the container, a specific clearance in the order of micrometers between the component and the container wall must be realized. Furthermore, wear of the container, production tolerances and lubrication quantity must be under control. Another concept for keeping the component in place in the transfer container is show in Figure 3.6b. In this design an O-ring is placed inside the container die where it primarily functions as a friction gate. Further, the O-ring also has a centering function because the rubber O-ring will absorb minor alignment errors and self-center the component in the container. The proposed transfer system is only capable of handling rotationally symmetric components, but can be further developed to include freeform workpieces geometries.

3.7 Prefab or net-shaping

The desire to easily realize high quality net or near-net shaped forged parts have been a subject of discussed for a long time in the cold forging community. Today most forged parts are formed with a certain machining allowance. The part then undergo several subsequent machining process after forming. Net shaped parts are parts that geometrically conform to specifications after forming, allowing subsequent machining processes to be skipped. Near-net shaping is the case where the finish forged specimen only undergo light machining, such as a simple cutting operation or turn off a end-facet.

The current minimum dimensional error in macro sized cold forging is $\pm 20\text{-}50\mu\text{m}$, while the error in machining has been reduced to less than $\pm 1\mu\text{m}$ in later times. For forging to compete with machining process, the accuracy of the formed parts should be within $\pm 10\mu\text{m}$ over the lifespan of the wearing forming tool. In order to achieve this amount of accuracy, a number of process variables must be known with a high degree of accuracy. The following list include some of the groups of factors influencing the quality of a near-net shaped forged component:

- Tool variables
- Material variables
- FE simulation variables
- Process variables
- Environmental variables
- Human and information variables

Tool variables have the most direct and thus dominant influence the quality of the forged component. Especially manufacturing tolerances, tool material and overall design of the tool system directly impact the achievable precision of the forged part.

Material variables are variations in dimensions and physical properties of the work piece material. These might be due to variations in the material itself or results of variations in the preceding processes, such as heat treatment.

Accuracy of the simulations conducted during the design phase will have an impact on the quality of the forged specimen. Good accuracy FE simulation of forging processes include the influences from process and environmental variables. Examples of the variables might be the temperature of billet and die during forming and accuracy of the press system. Only by accurately knowing and modeling the influence of all major parameters within the groups above, can a near-net shaped forging process be realized. Integrated simulations of this kind is challenging to set up and execute and require expert knowledge [54].

Tool system for net shaping requires advanced material, such a cemented tungsten carbide, in combination with high accuracy die manufacturing processes. Often the die is surface coated to increase the hardness and reduce the risk of tool fracture under the high internal pressures. A pre-stressing system is applied as an integrate part of the tool design to limit the influence of elastic deflection.

Net-shaping in micro bulk forming

Within micro bulk forming, the option of relying on subsequent machining is not economically or practically viable. The cost of handling, positioning and clamping a pre-formed micro component prior to machining will in most cases exceed the savings gained by utilization of the forging process. Further, as the amounts of bulk material in a typical micro component is rather limited, the relative cost of the material waste by utilizing cutting processes will often be manageable. Last, the design an operation of a cutting processes is more flexible and the clamping of the unformed bulk material, delivered in rods and square blocks, is straightforward.

For the reasons mentioned above, it is hard to imagine a micro bulk forming scenario not including net-shaped components. Thus, any micro bulk forming process must be designed to ultimately achieve specimens with the quality requirements of the end application. This enforces strict demand on the precision of the forming tools; elasticity of die, tool frame and press. Further, the geometric tolerance band of micro components is often reduced considerably, ultimately demanding tooling tolerances in the sub micrometer range.

A number of techniques can be applied to better the precision of formed micro parts. In a multi-step forging process it is possible to insert a calibration step, where the final envelope dimensions of the component is being adjusted utilizing a high precision die. Also, by keeping the overall length scale of the die and tooling system low, the elastic deflections can be limited. Further, the application of cemented tungsten carbide tools and adjustable tool pre-stressing systems can lead to better accuracies. Last the integration of high precision sensor, such as force or length transducers, make it possible to dynamically counteract minor process variations. Examples of these techniques will be seen in the following chapters.

Conclusion

A discussion of the micro bulk forming process characteristics have been given. The influence of size effects have been outlined and the implications for micro tooling discusses. The formability of different work piece materials have been shown, focusing on application in the micro scale. A preliminary introduction to amorphous materials forming was given, including an example of a formed micro component. A preliminary introduction to warm forging a micro scale was given and an examples of a tool design was shown. An introduction to setup and handling challenges in the micro bulk forming process was given. The analysis was illustrated with examples of gripper and handling concepts. The chapters was concluded with section dealing with net shaping and a discussion on the possibilities of subsequent machining.

Chapter 4

Micro metrology

Metrology or '*the science of measurement, embracing both experimental and theoretical determinations at any level of uncertainty in any field of science and technology*' as defined by the International Bureau of Weights and Measures (Bureau international des poids et mesures in French), is an increasingly important element of all aspects of modern science and technology. Metrology is a very broad field that can be dated back to the antiquity. Generally metrology can be roughly subminiaturized into three categories

- Fundamental metrology, is the science of fundamental processes and laws governing them in physics.
- Applied metrology
- Regulatory metrology
- Legal metrology

As the world economy have evolved into a global marked place, making it possible to source products from virtually any business on the marked, so have the global trade of information, products, sub-components and parts. This have risen the requirements for specification, standardization and the need for a common foundation of reference systems for specifying the properties of mechanical artifacts.

One role of metrology is to establish a common framework of reference for specification, fabrication and assessment of mechanical elements.

4.1 Introduction

Micro metrology will here be limited to applied metrological assessment of micro components, including dimensional, roughness and uncertainty determination in the micro regime.

The geometry of mechanical components are popularly divided into three subcategories according to increasing geometrical complexity:

- 2D components are flat and do only change geometry in a plane. A typical example of a 2D component geometry is the cut-out of a sheet metal part before forming.
- $2\frac{1}{2}$ D components are generally flat components with some small scale variation of the geometry in the height direction (z axis). An example could be a lab-on-a-chip system, where a small channel is carved into a flat substrate.
- 3D components are full three dimensional geometrical components, where often the length of the three dimensions are comparable.

The same subdivision is often found when defining the capability of various manufacturing and measurement technologies.

A micro component can be defined as a component with two or more dimensions below the millimeter scale. A relaxation of this definition is the case where a large component exhibits functional features that themselves qualify as a micro component according to the above definition.

When considering micro components, micro manufacturing technologies or micro metrology, this geometrical subdivision continues to be valid, only at a different length scale. Instead of measuring millimeters, we are measuring at the micro- or nano-meter scale. Some metrological approaches can readily be scaled to micro length scale, keeping validity and sufficient dynamic range to satisfactorily quantify elements in the micro scale. This is in the main true for the 2D and $2\frac{1}{2}$ D metrological instruments, such as contact roughness measurements devices and the various microscope technologies.

Full 3D metrological assessment in the micro scale is challenging. Both manual measuring techniques, such as vernier caliper or dial gauge, as well as semiautomatic measuring techniques, such as conventional tactile 3D coordinate measuring machine (CMM), are impacted by the size effects. In a 2D scenario, the scale of the measuring volume of the instrument is only scaled by the scaling factor λ squared (λ^2) whereas for the 3D case all three axes are scaled down, meaning the measuring volume scales as λ^3 . The reduced measuring volume introduces practical as well as metrological challenges on the assessment and quality assurance of micro components.

4.2 Challenges in Micro Metrology

When considering the challenges involved with micro metrology, we will firstly go over practical and physical challenges and later look at implications for uncertainty and tolerance setting. We put emphasis on 3D components around the millimeter scale.

Many of the physical challenges met in micro metrology has to do with realizing a measuring instrument itself with sufficient precision and mechanical stability. It is a well known rule of thumb that the precision a manufacturing process or a measuring device has to exceed the required accuracy quality of the measurement or artefact in question by at least one order of magnitude. Measuring ball styluses for tactile CMM come standard down to 0.5 mm in diameter, setting the lower limit of the achievable measuring rounding at about 0.3 mm ($d = 0,6$ mm), leaving a 0,1mm gap for movement of the stylus. The small stylus is fragile and can only tolerate a low touch force during measurement. The low touch force gives rise to an increased uncertainty as a decreasing

force result in increased stick-slip effects between the workpiece and the stylus. Further, the physical downsizing of ball stylus leads to an increased uncertainty in the probe form and a lower stiffness of the probing shaft, as the probe becomes a micro-element itself [15].

Alternative probes exist, where the probe or stylus is replaced with an active probing element. This shifts the CMM into a touchless approach and a measuring machine working under this principle is commonly denoted Scanning Probe Microscope (SPM). One example is where the stylus is replaced with a light fiber with a ball or cylinder shaped termination. By analyzing the amount of light reflected from the fiber end and using this information to reposition the scanning head (CMM probe) it is possible to trace the probe along any geometry with high accuracy [55]. A thorough exposition of various CMM probe concepts can be found in the paper by Weckenmann et Al [55].

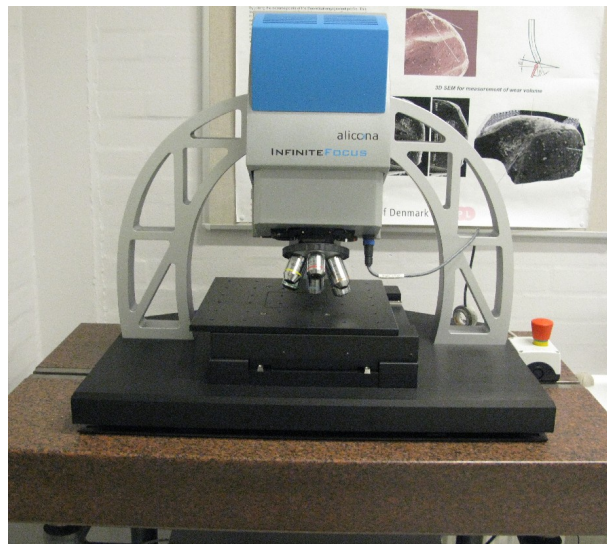


Figure 4.1: Photograph of the Alicona Infinte Focus Microscope, based on the confocal microscopy principle, uses focus variations to build build a 3D model of the measurements.

Another variant of the SPM is the Atomic Force Microscope (AFM). The AFM uses a cantilever with a sharp tip, with a round radius in the order of nanometers, to measure a number of microscale forces, including mechanical contact force, van der Waals forces, capillary forces and magnetic forces, etc. The bending of the cantilever is usually detected by shining a laser beam onto the cantilever and detecting the deflected light using a photodiode.

There is a number of different approaches that can be utilized to measure 2D and $2\frac{1}{2}$ D micro and nano-size components, including the Scanning Electron Microscope (SEM) , Light optical microscope and SPM. However, when it comes to full 3D geometries, even simple shapes, like a bore with a high aspect ratio, there is no good alternative when a normal CMM have to give up at a length scale around 1 mm [15].

A list of general micro metrological assessments are listed in the following [15].

- Distance as defined between two surfaces oriented in the same direction. Example distance between two lines of a line grating or two planes in a microstructure.
- Width as defined by the distance between two opposing surfaces. Example width of a channel.
- Height as defined by the distance between two surfaces of same orientation but placed in a vertical direction. Example: depth of microfluidic channel.
- Geometry (or form) as defined by the distance between the surface of the object and a pre-defined reference. Example: flatness of wafer.
- Texture and roughness defined as geometries of surface structures whose dimensions are small compared to the object under investigation. This poses a particular challenge for micro or nano sized objects because the surface becomes dominant with respect to object volume.
- Thickness of layers
- Aspect ratio as defined by the depth of a structure divided by its width.

For geometrical assessment or validation of 3D artifacts below the millimeter scale, several non standardized techniques can be utilized. In section 4.4 we will have a look at one of these techniques.

4.3 Measuring uncertainty

Uncertainty is a quality parameter describing the quality of a measurement. The uncertainty of measurement (U) is a parameter, associated with the result of a measurement, that characterizes the dispersion of the values that could reasonably be attributed to the measurand [56]. Depending on the measured parameter, the magnitude of the measurement uncertainty on the outgoing parameter of the experiment can partially or totally overrule the influence of the ingoing parameters in the experiment, thereby masking the influence and invalidating the experiment. It is therefore crucial to evaluate the uncertainty of the equipment and the procedures employed.

The first step in an uncertainty estimation analysis is to identify the sources of uncertainty. Once the individual sources of uncertainty have been defined, the combined uncertainty of the procedure can be calculated by calculating the quadratic sum of the individual standard uncertainty contributions, each scaled by a weighing factor. The standard uncertainty represents the standard deviation of the measured, due to the influence of the evaluated particular source of uncertainty.

The standard uncertainty is generally subdivided into Type A and Type B evaluation.

The Type A evaluation of standard uncertainty can be applied when a certain number of observation of the same measurement setup exists. When applying the observed measurement values with an a priori statistical knowledge of the class of probability density function applicable to the values. If assuming normal distribution of a measurement

values, the standard uncertainty is equal to the standard deviation of the sampled values as given by equation 4.1.

$$\sigma = \sqrt{\frac{1}{n-1} \sum_{i=1}^n (y_i - \bar{y})^2} \quad (4.1)$$

, where n is the number of measurements, \bar{y} is the average of n measurements and y is the measurand.

The Type B standard uncertainty evaluation is based solely on a priori knowledge of the probability density function of a measured variable. Together with a scientific judgement of variability of the measured in question, the standard uncertainty contribution can be estimated without the need for actual observations. Values belonging to this category may be derived from previous measurement data, experience with or general knowledge of the behavior and properties of relevant materials and instruments, manufacturer's specifications, data provided in calibration certificate, etc. Type B standard is obtained from an assumed probability density function based on the degree of belief that the event will occur [56].

Uncertainty contributors in measurement can be classified as follows [56]:

- Workpiece
- Equipment:
 - Measurement equipment
 - Measurement set-up.
 - Software and calculations
- Procedure:
 - Measuring procedure
 - Metrologist.
 - Definitions of characteristics
- Environment
- Reference element

Once all uncertainty sources have been determined and their respective standard uncertainty contribution calculated, the combined standard uncertainty of the measurement as a whole can be found. For **uncorrelated** input quantities, the combined standard uncertainty $u_c(y)$ is calculated as in Equation 4.2.

$$u_c(y) = \sqrt{\sum_1^n \left(\frac{\partial f}{\partial x_i} \right)^2 u^2(x_i)} \quad (4.2)$$

, where n is the number of uncertainty contributors, f is the model function of the measurement and $u(x_i)$ is the standard uncertainty of the i -th uncertainty contributor.

Finally, the expanded uncertainty U can be obtained by multiplication with the chosen coverage factor k . The coverage factor is chosen on basis of the desired level of confidence. A popular choice for coverage factor is $k = 2$ equaling an approximate level of confidence of 95%.

The outlined framework for uncertainty assessment will be applied throughout the present work.

4.4 Replica technique

Metrological assessment of 3D micro structures is not straight forward, as discussed in the previous section. Considering a deep hole with a micro sized diameter as a case, direct characterization of the internal dimensional and surface roughness is virtually impossible. A method of inverting the internal geometry to a more accessible external geometry is through utilization of the replica technique. This method has been used extensively throughout the course of this project.

The replica technique is a very versatile technique for non destructive metrological and metallographic assessment purposes. The process works by application of a two component mixture using a pistol onto the specimen surface or simply by flooding the features that is to be replicated. Because the viscosity of the replica medium is very low, it is possible to replicate features with length-scales down to $0.1 \mu\text{m}$. After a curing time the replica medium can be pulled off the target area. Evidently the replica will inverse the geometry in question. However, this behavior is often beneficial because it makes it possible to measure deep holes, steep cavities and complicated internal geometries.

The main component of the replica medium is usually silicone or acrylic, each having their advantages. Acrylic based replica medium suffers about 0,5-1% volume shrinkage, a property which will cause distortion of the replica geometry and lead to increased measurement uncertainty. The cured acrylic replica has a high density and is inelastic, thereby allowing for measurement using a contact instrument, such as the CMM. For the silicone replica medium this is almost the other way around. The cured silicone is very elastic, elastic enough to allow for replica for inverse geometries and undercuts. The soft silicone based replica can only be quantified using optical measurement methods, unless special coatings are applied. Further, the silicone medium does not shrink considerably and can even tolerate geometrical distortion whereupon it will return to its original shape within minutes.

An example of the data sheet of a commercial silicone based replica medium is reproduced in Figure 4.2.

If we consider the example of a micro forming die, where the important geometry is internal, often consisting of a small hole with a high depth to width aspect ratio, it is virtually impossible to access the internal geometry without cutting the die open. With the silicone replica technique it is possible to take a cast of internal geometry. The result is a geometrically sound inverse copy of the internal geometry that can be characterized using a microscope or non contact scanner. This is why the replica technique is classified as a non destructive testing method.

TECHNICAL DATA	RepliSet
Viscosity of uncured compound	Very low (F-types) Low (T-types)
Detail reproduction	Down to 0.1 μm
Shrinkage	Negligible
Tear strength	15-20 kN/m ²
Hardness	30 Shore A
Temperature range for the surface to be examined	-10°C to + 180°C (14°F to + 356°F)
Life span of the finished replica	Practically indefinite

Figure 4.2: Clip from the Struers Repliset datasheet.

The following illustrates an application example of the use of the replica technique. The micro cold forming die in Figure 4.3a is used as the first of a two step forming process in which a small brass axle was formed. The die features a complex internal micro geometry with a number of strict ISO GPS tolerance specifications. The internal conical-shape of the die makes it virtually impossible to characterize the internal geometry using a conventional stylus type instrument.

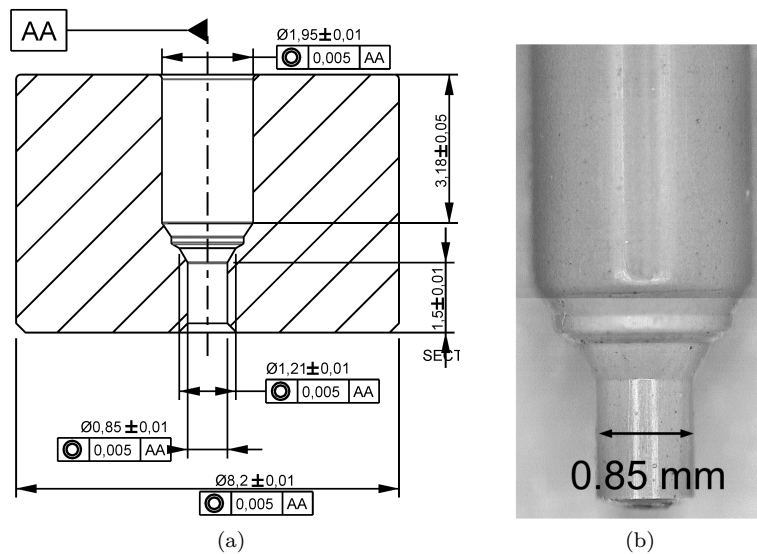


Figure 4.3: Example of quality control of a die with a complex internal geometry and strict tolerance requirements. A part of the technical drawing is reproduced in (a) and a photograph of a replica of the machined die is shown in (b)

When comparing the replica and the machine drawing in Figure 4.3b the similitude is apparent. With this geometrically negative replica it is a simple task to validate the different diameters. Also the critical roundings with short arc-lengths around the mid section of the die is now easy accessible for microscope analysis.

The replicate technique has for a long time been utilized for replication of low aspect ratio structures such as threads, gratings, surface roughness or even finger prints.

4.5 Verification of the shrinkage of replica - an example of uncertainty evaluation

The shrinkage of the Struers replica compound is indicated as 'negligible' in the data sheet, Figure 4.2. This vague specification might be practically valid for roughness replication and for geometry reproduction at macro scale. At micro scale however, even a minor shrinkage will give rise to an increased uncertainty of the geometric assessment, when using the replica technique. A linear percentage-wise dimensional shrinkage is presumed, something that have been acknowledged in literature [57,58]. In the following an evaluation of the increase in dimensional measurement uncertainty will be undertaken. Using a calibrated step gauge and the commercial Repliset compound GF1 from Struers (order number 40900078), we will evaluate the increase in measurement uncertainty due to the intermediated silicone replication step.

The Alicona InfiniteFocus confocal Microscope (IFM) will be used as measurement instrument and a certified 1 mm step gauge as the calibrated workpiece. This instrument features a vertical resolution of down to 20 nm and a lateral resolution of down to 400 nm.

An illustration of the data from the calibration certificate and a photograph of the step gauge is depicted in Figure 4.4.

alicona	Alicona IFM Calibration Tool Standard for calibration and testing of the IFM system and other optical instruments	Alicona Imaging GmbH Testlastraße 8 8074 Grambach Tel.: 0043 316 4000 700 www.alicona.com
	Calibration Mark: 20ALICONA08 Serial Number: 002110407208	Made in Austria
Measurement Results For details please refer to the calibration certificate		
Height Step	Grid Spacings	Circle Diameters
Height: 1001.86µm Uncertainty: 0.1µm	Grid 2x: 119.854µm Grid 5x: 49.939µm Grid 10x: 23.963µm Uncertainty: 480nm (2x), 200nm (5-10x)	Circle 2x: 2000.80µm Circle 5x: 999.97µm Circle 10x: 499.92µm Circle 20x: 249.96µm Circle 50x: 99.94µm Circle 100x: 49.90µm Uncertainty: 2µm (2x), 1µm (5-100x)

(a)

(b)

Figure 4.4: Data from the calibration certificate (a) and a photograph of the step gauge (b)

Uncertainty estimation of measurement

Principles for uncertainty evaluation using a calibrated workpiece is outlined the ISO 15530 part 3 standard [59]. Following the procedure, three terms will be contributing to the combined uncertainty, denoted U .

The combined uncertainty in this case can then be estimated using 4.3.

$$U_{cal,step} = k \times \sqrt{u_{cal}^2 + u_p^2 + u_w^2} + |b| \quad (4.3)$$

,where k is the coverage factor, $U_{cal,step}$ the combined uncertainty, u_{cal} is the inherited standard uncertainty of the calibrated artifact, u_p the standard uncertainty of the measurement procedure, u_w is the standard uncertainty arising from influences of the workpiece and b donates the systematic error during evaluation.

4.5. Verification of the shrinkage of replica - an example of uncertainty evaluation

The procedure above is designed for CMM measurements in a production environment and does not include the standard uncertainty contribution arising from the finite resolution of the measuring instrument, in this case the IFM. According to the revised version of *Guide to the expression of Uncertainty in Measurement* (GUM) the standard uncertainty arising from a digital instrument with finite resolution can be expressed using the rectangular probability density function (PDF) with a width of δx with variance $u^2 = (\delta x)^2/12$. Thus, the standard uncertainty arising from the limited resolution of the IFM can be expressed as in 4.4. However it is expected that the contribution from this term will only have minor influence on the mean combined uncertainty of the measurement.

$$u_{res} = \frac{\delta x}{2\sqrt{3}} \approx 0.29\delta x \quad (4.4)$$

, where u_{res} is the standard uncertainty contribution from the finite resolution and δx is the distance between two quantization levels.

Further the standard uncertainty estimator of the mean value of n measurements u_p expresses as the ISO 15530-3 as the standard deviation as in 4.6.

$$u_{p(N)} = \sqrt{\frac{1}{n-1} \sum_{i=1}^n (y_i - \bar{y})^2} \quad (4.5)$$

, where n is the number of measurements, y_i it the measured value of the i -th measurement and \bar{y} is the mean of all n measurements.

Equation 4.6 implies a normal distribution PDF of the mean measurement value. This assumption can be further defined in the present case, as we are considering n repetitions of the *same measurement and the same workpiece*. According to the revised GUM (section C.3.8) will a the probability distribution of a continuous random variable follow the t-distribution or Student's distribution [56]. Applying this assumption; the experimental standard deviation of n observations can be expressed as:

$$u_{p(t)} = \frac{\sigma}{\sqrt{n}} \quad (4.6)$$

, where σ is the standard deviation and n is the number of observations.

The u_w term captures the influences arising from the manufacturing process of the workpieces as well as variations related to thermal expansion and elastic deformation. In this case the term is restricted to capturing thermal stability of the workpiece within a temperature variation window. In the following we assume a temperature variation $\delta T = 5,5$ K and a coefficient of thermal expansion of $\alpha_{silicone} = 4,68[10^{-6}K^{-1}]$ and $\alpha_{steel} = 11[10^{-6}K^{-1}]$ for the silicone and steel workpiece respectively. The influence of thermal stability in the current experiment is expected to be very small. Thus, the calculation of the thermal stability of the two material should be interpellated as indicative.

With these figures at hand we proceed to estimate the uncertainty contribution due to thermal expansion using equation 4.7.

$$u_w = \delta T \times u_\alpha \times l \quad (4.7)$$

, where δT donates temperature deviations in kelvin, u_α is the coefficient of thermal expansion and l is the length in meters.

When employing the influence of the finite resolution of the IFM and the modified estimation of the standard uncertainty of measurement procedure u_p , the combined uncertainty of the mean height measurement of the step gauge is expressed as in 4.8.

$$U_{cal,step} = k \times \sqrt{u_{cal}^2 + u_{p,t}^2 + u_w^2 + u_{res}^2} + |b| \quad (4.8)$$

Using the new expression for $U_{cal,step}$ we will continue to evaluate the combined uncertainty of the calibrated workpiece and the silicone replica respectively.

Step height measurement procedure

Having finalized the uncertainty budget for the measurement, we proceed to the actual evaluation. The step gauge is placed in the microscope and the upper an lower scanning position is set. A 10X magnification lens was chosen and the vertical resolution (Z-axis) was set to 500 nm.

When the scan is completed and the data is saved to disk, the analysis of the data can commence. A 3D representation of the acquired data is reproduced in Figure 4.5. Recognizing the implicit assumption in the uncertainty budget above, that each of the measurements should be independent (zero covariance), we perform the height measurement in a number of line-profiles going across the step gauge.

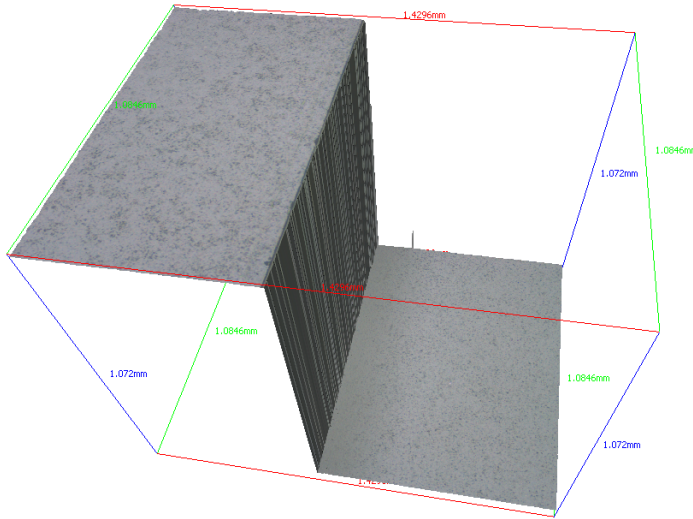


Figure 4.5: 3D representation for the acquired data from the Alicona IFM.

The ISO standard 5436 part 1 specifies a procedure for measuring a step height with a quantified approach using nine length bands [13]. The procedure works by approximating the line segments A,B and C in Figure 4.6 using the least square method while limiting

4.5. Verification of the shrinkage of replica - an example of uncertainty evaluation

the evaluation length to $2/3 W$ for A and B and $1/3 W$ for the C length. This procedure is only applicable across a double step structure with a width greater than $3W$, thus not suitable for application in the present case.

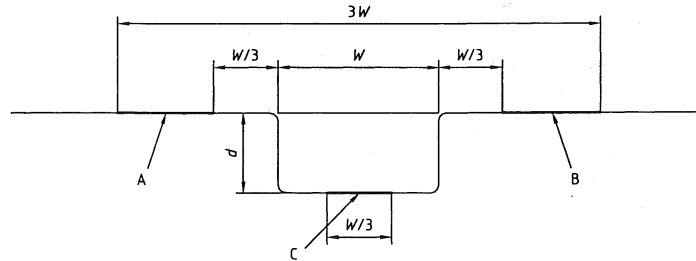


Figure 4.6: Sketch showing the recommended procedure for characterization of step height using ISO 5436-1 [13].

Inspired by the procedure described in ISO 5436-1, we specify a procedure for measurement of a single step profile. A sketch of the proposed single step measurement procedure is shown in Figure 4.7. The width clearance scale around the step has been inherited from the ISO 5436-1. Due to the unspecified lateral scaling in the case of the single step gauge, a specified minimum of the aspect ratio between the step height d and the width W have been set as a requirement. Like in the case of the ISO 5436-1 procedure outlined in Figure 4.6 we employ the least square method for straight line approximation.

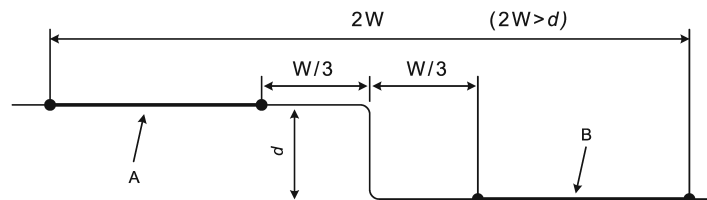


Figure 4.7: Measurement procedure for single step height used in the experiment.

The proposed method is readily implementable in the software for the Alicona IFM simply by choosing a double step height analysis and setting the boundary points of the line approximation as indicated with dotted circles in Figure 4.7.

Measurements results of step height and uncertainty

Having specified the uncertainty framework and the measurement procedure for step height evaluation, we proceed to the results of the analysis.

The step heights and the factors of standard uncertainty are shown in Table 4.1. The main contributors to the combined uncertainty comes from the terms relating to the standard uncertainty for the measurement procedure $u_{p(t)}$ and the term donating the systematic error b .

4. MICRO METROLOGY

calibrated workpiece measurement- and uncertainty values [μm]				
n	value	mean	stdev	$u_{p(t)}$
1	1001,4	1001,4	0,7648	0,3420
2	1001,4	u_{cal}	u_w	b
3	1002,3	0,05	0,0604	0,46
4	1001,7	u_{res}	k	$U_{cal,step}$
5	1000,2	0,1443	2	1,22

Table 4.1: Corresponding values of measured values from the step gauge and calculated values according to the procedure outlined in the previous section. All values are in microns.

We expected that $u_{p(t)}$ term will increase when measuring the replica step. The finite replication resolution and various inclusions of the silicone compound will increase $u_{p(t)}$ due to a higher roughness of the sample.



Figure 4.8: Photo of the silicone replica of the step gauge. The Repliset compound GF1 from Struers was utilized.

The values of the step height measurements of the silicone replica is printed in Table 4.2. Like in the case of the calibrated step gauge, the main contributions to the combined uncertainty can be attributed to the terms $u_{p(t)}$ and b . Please note that the combined uncertainty number, $U_{replica,step}$, was not calculated for the replica step due to the lack of a second source calibration data for systematic error evaluation b

4.5. Verification of the shrinkage of replica - an example of uncertainty evaluation

Replica measurement- and uncertainty values [μm]				
n	value	mean	stdev	$u_{p(t)}$
1	1001,2	1000,31	0,8200	0,3667
2	1000,3	u_{cal}	u_w	
3	999,85	0,05	0,0257	
4	1001,0	u_{res}	k	
5	999,21	0,1443	2	

Table 4.2: Step height measurements of silicone replica and uncertainty figures. All values are in microns.

When comparing the values of the calibrated steel step against the silicone replica, a decrease of the mean step height value can be observed. Further, a minor increase in the standard deviation is observed, impacting the value for $u_{p(t)}$.

Assuming that the difference in the mean height between the two cases can be attributed to shrinkage of the silicone compound alone, we can estimate the linear length shrinkage in percent using the formula 4.9.

$$\alpha_{silicone}[\%] = 100 \left(\frac{\overline{h_{rep}} - \overline{h_{cal}}}{\overline{h_{cal}}} \right) \quad (4.9)$$

, where $\overline{h_{rep}}$ and $\overline{h_{cal}}$ is the mean step height of the replica and the calibrated step gauge respectively [57].

Talking the numbers from Tables 4.1 and 4.2 we arrive at a shrinkage value of:

$$\alpha_{silicone} = -0,109\% \quad (4.10)$$

Finally the roughness parameter of the two surfaces were evaluated using the Alicona IFM software. These values are not calibrated and are intended for quantitative rather than absolute evaluation. Evaluating on the roughness parameters in Table 4.3 we

	Step gauge	Replica
R_a	0,071	0,370
R_z	0,354	1,594

Table 4.3: Roughness measurements of calibrated step gauge and replica

notice an increase of surface roughness for the silicone replica. The roughness values R_a , expressing the arithmetic average of absolute values is increased. This is likely due to bubble inclusions during the replica process. The roughness values in this scale only add an negligible amount of uncertainty to the height measurement of the step.

Concluding on the shrinkage value found for the silicone replica compound, we see that the value is small but finite. In a scenario where the replica technique is used to reproduce the width of a 1 mm width channel, the shrinkage will give rise to a width measurement error of about 1 μm . This is acceptable in many cases, because other uncertainty contributors will be greater in magnitude.

4.6 Micro manufacturing and geometric dimensioning and tolerancing

In the following we turn our attention to an analysis of a simplified micro manufacturing and measurement scenario. A series of tools-like artifacts is manufactured at different facilities. The specimens are subsequently measured and the results are compared. The analysis serves the purpose of establishing typical tolerances met in micro manufacturing today.

The typical knowledge base of a product follows a top-down approach where the level of knowledge and details increase almost linearly during the product development cycle. In the initial phase the designer is faced with choices primarily relating to function, shape and esthetic appearance of the product. In order to do radical innovation, this phase is often decoupled from the actual industry, location and production facility where the product in question is later going to be produced.

In the next phase an engineer or a designer with material and production knowledge takes ideas, functional sketches and shapes and turns them into technical drawings. The materials are selected and the individual parts are typically modeled using a Computer Aided Design suite (CAD). Once the product assembly, material choices and functional requirements are fulfilled, the designer sets the geometric dimensioning and tolerancing. The ISO Geometrical product specification is an abstract standardized hierarchical framework for specifying geometry and production tolerances for virtually any shape. The framework consists of global, general and complementary standards, meaning that a global standard will also have validity to a complementary standard, but not vice versa. One of the principles of the GPS system is the abstraction from the metrological verification procedure, this is denoted the principle of duality, a part of the global standard. Further, the abstract nature of the GPS standard involves not specifying the manufacturing method, but only the desired nominal shape and allowable deviations. Once the technical drawings for the product are finalized, they are handed over to manufacturing and production. Here a production engineer will make the choice of production method and specify the sequence of manufacturing processes (process chain). The complete product development cycle can be visualized as the top-down approach depicted left in Figure 4.9. In the case of a micro size product, or any other product with close bounds between design, geometry, technology and manufacturing, the development cycle is often changed. Owing to the strong interaction between the micro processes by which the product is realized and the product designed, these processes influence the design process from the very beginning of the design process. The design cycle can be illustrated by the pyramid to the right in Figure 4.9.

When working in the micro scale, the designer has to be aware of the physical limitations of the material, the achievable tolerances of the micro manufacturing process as well as other technical aspects of the production and application of the micro product. Efforts are going on to reinvent the GPS system to capture this radical change in the workflow of a typical product design cycle [60].

Size effect in tolerancing

One of the dominant influences of the size effect in the micro scale is the inherent desire to let the length scale of the tolerancing follow the scale of the component. Popularly said, the application of tolerancing is linked to the length scale of the product rather than being an independent geometrical element. This scaling of tolerancing is one of

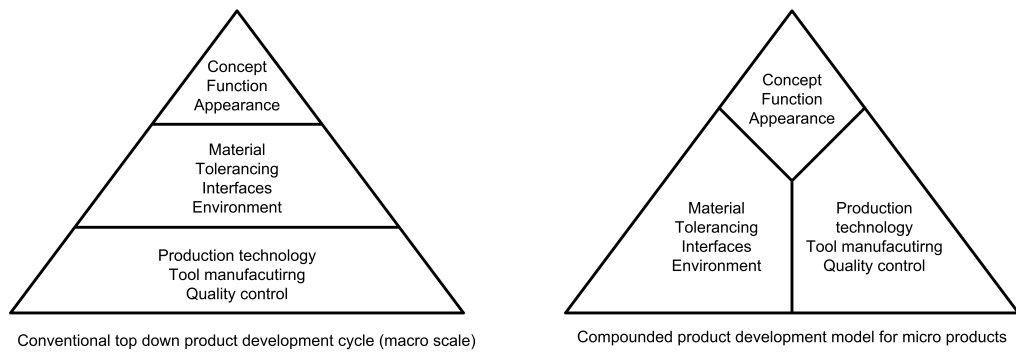


Figure 4.9: Illustration of product development cycle for a conventional macro scale micro product.

Illustration of a typical product development cycle for a conventional macro scale product (left) and a complicated micro product (right). The growing width of the triangle illustrates the knowledge level of the product and product development cycle is timely referenced vertically.

the key challenges in all micro technology and is a key element to realizing functional products and technologies.

Strong efforts are currently going into developing micro manufacturing technologies with the required precision and some technologies are inherited from the medical and electronics industries. However, where the actual scaling of product size only have minor impact on the design costs of a product, this is not the case for precision in manufacturing and assembly.

There is an almost exponential relation between manufacturing precision and cost, potentially making the micro component too costly for the consumer marked. Figure 4.10 illustrates how the conformance zone of a critical component dimension is prone to size effect. In order to successfully mass manufacture micro components the production process must be able to reproduce geometry with high precision.

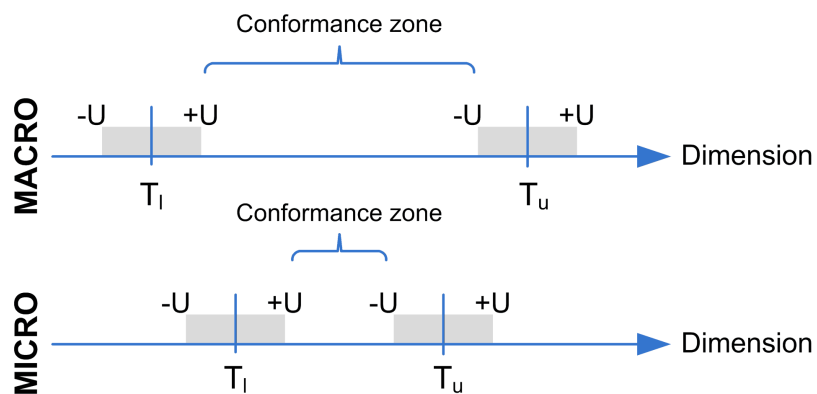


Figure 4.10: Illustration of the proportions between measurement uncertainty and the allowable tolerance of a geometrical feature of a mechanical component [14]

On top of the cost issues related to manufacturing of a micro geometry come the quality assurance and metrological challenges. At present time several companies are struggling to source micro components with the required precision and quality. It is not uncommon to see manual inspection of the geometrical and functional properties of a micro component in combination with a required inspections rate of 100%. Needless to say, this solution is not viable in terms of cost and manpower in the long term.

In the following we will consider the Electric discharge machining (EDM) process as a micro tool manufacturing technology. The tools produced will be quality controlled using 3D metrological methods as a round-robin style experiment.

4.7 Micro EDM-benchmark test

In the following we will direct our attention towards metrology and manufacturing technologies within the micro scale. The analysis is setting out to investigate the '**as delivered performance**' of both a manufacturing process suitable for micro tool production and the subsequent performance of a metrological characterization. The EDM benchmark test was conducted as a sub-activity under the Masmicro project with participation from DTU, IPU and 34 other partners. The Masmicro project was launched in July 2004 and concluded in September 2008. Masmicro was a research Integrated Project for the Integration of Manufacturing Systems for Mass-manufacture of Miniature/Micro-Products, supported by the European Commission under the Framework Programme 6 (FP6).

Several partners involved in micro tool manufacture were invited to participate in the round robin style tool manufacturing experiment, where each partner would manufacture a simple punch- and die- geometry in the millimeter scale. The partners initially taking part in the group were University of Strathclyde - UK, Pascoe Engineering LTD - UK Fraunhofer-Institut für Produktionsanlagen und Konstruktionstechnik IPK in Berlin, Fundacion Tekniker - ES and IPU -DK. The specifications of the experiment were established at a workshop at the University of Strathclyde on May 17, 2006. The workshop was set to discuss experience gained about the EDM process for tool manufacturing at micro scale and the research partners were invited to share research results and experiences gained during the research project.

Before concluding the workshop, the partners agreed on the goals for the experiment and the final geometry of the artifacts to be produced. It was decided to manufacture two simple cubic structures, an internal and an external, with a net volume of 1 mm^3 , as depicted in Figure 4.11.

It was decided on to aim for a *best effort delivered* strategy for the manufacturing process. This choice was in favor of a more traditional as-intended geometry approach with geometric dimensioning and tolerancing. The best effort approach was chosen in order to allow for individual influence of the different manufacturing technologies and the experience of the operator. By comparing the achieved precision of the benchmark geometry, where the operator has been given the freedom of setting the process parameters, the experiment will convey the *as delivered* performance of the manufacturing processes, rather than evaluating the results as a boolean compliance, non-compliance variable. Further the empiric selection of process parameters can be made an object of study itself.

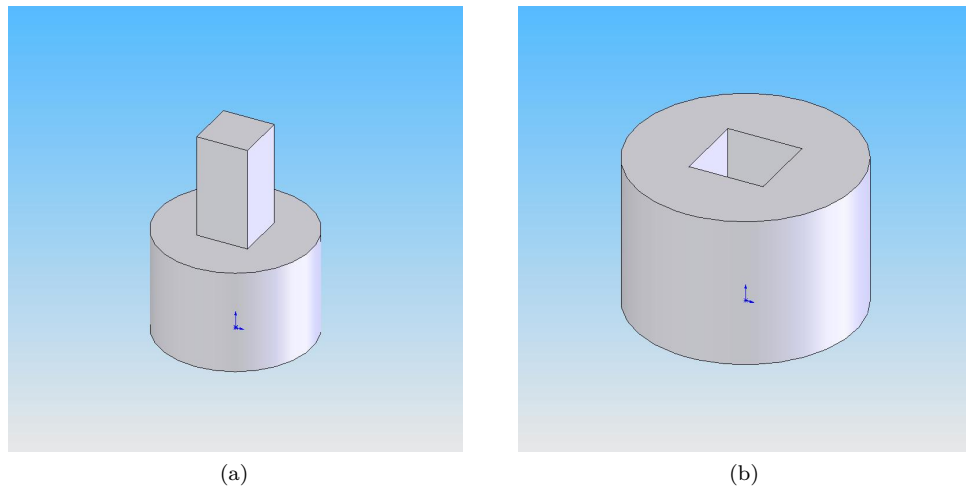


Figure 4.11: Punch (a) and die (b) geometry

In order to guide the operator of the machine tool in selecting the process parameters, a list of geometrical priorities were compiled.

1. reach dimensional accuracy as closely as possible
2. minimum surface roughness
3. minimum inner and outer corner radii and best reachable contouring accuracy between punch and die radii
4. best reachable centre accuracy of structures compared to outer contour of punch or die
5. machining time, approximate costs

The last item on the list is to be understood as a reminder that the manufacturing process should not take a disproportionate amount of time.

A $\text{Ø}3$ mm rod of ultra fine grained cemented tungsten carbide was chosen as bulk material for the EDM benchmark test. Ultra fine grained tungsten carbide is well suited for micro tool manufacturing because of its excellent compression strength. Further, fine-grain or ultrafine structures tend to have better erosion and wear performance.

A machine drawing of the punch and die geometries is depicted in figures 4.12 and 4.13 respectively. The design is meant to be simple yet challenging to bring to perfection. For the punch geometry in Figure 4.12, challenges primary related to meeting the strict geometrical tolerances and obtaining a low surface roughness. The die structure, depicted in Figure 4.13 is challenging to manufacture because of its internal geometry. When starting from a blank, a start hole will have to be drilled using an ED-drilling process. This center hole will form the reference feature for the subsequent wire-EDM process. The use of two cascaded processes will mean that the positioning precision of the internal

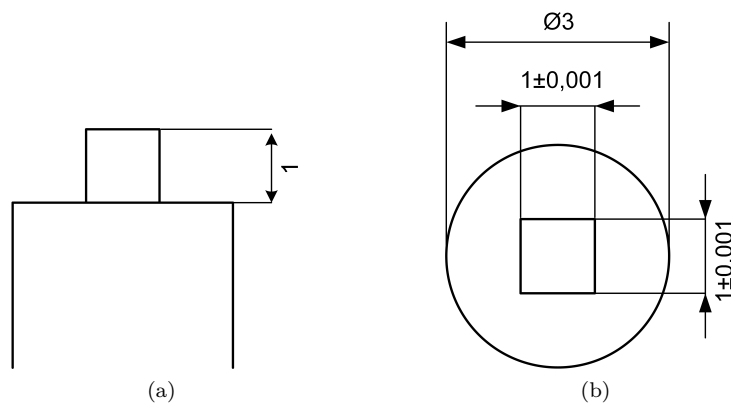


Figure 4.12: Technical drawing of EDM benchmark punch geometry. Figure (a) is a side view and (b) is the top view. Note the narrow tolerance of $\pm 1\mu\text{m}$

geometry will be negatively impacted. Further, the diameter of the wire will be the limiting factor of the minimum achievable internal corner radii.

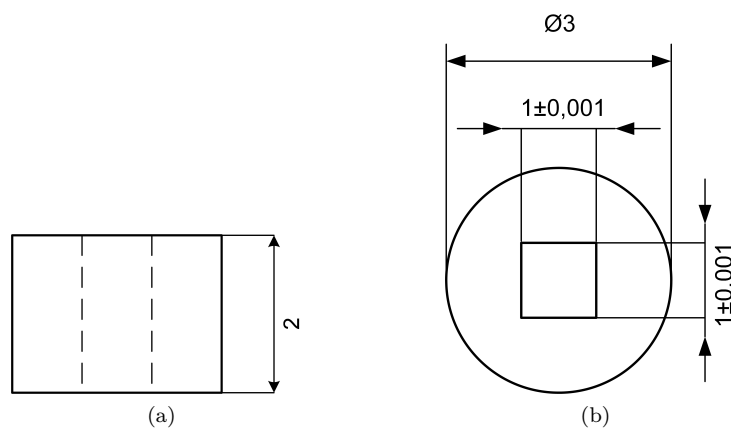


Figure 4.13: Technical drawing of EDM benchmark die geometry. Figure (a) is a side view and (b) is the test piece seen from the top.

Procedure for tactile measurement.

In order to allow for comparison of measurements between the different metrology labs, the need for a specified measurement procedure is evident. The procedure should be simple to understand, yet capture the desired geometrical form accurately.

In many cases it is standard practice in CMM measurement to first establish a frame of reference for the measurement. This could be in form of a datum plane, a line or an edge. This virtual measurement reference is aligned to the geometry of the work piece by a number of pilot measurements. By including some extra measurements during the alignment of the reference feature, it is possible to get a valuable estimate of the

uncertainty related to the referencing. However, the measurement procedure is often a tradeoff between complexity and actually capturing the measurement values in question.

For a simple geometry, like the one treated in this case, the choice was made to discard an explicit reference feature for the tactile measurements. The reasons for this choice were twofold. Since we are measuring a width quantity, defined as the distance between two opposing faces, with a ball tip stylus, a small tilt or rotation angle of the specimen will only have minor influence on the measurement error. Further, the accuracy of the measurement will be higher since only two of three axis of the CMM will be moved during the width measurement procedure.

The proposed measurement procedure, illustrated in Figure 4.14, consists of a total of 16 tactile measurements, translating to 8 equivalent width measurements. These width measurements are distributed as four measurements on each of the perpendicular faces on the head of the punch geometry.

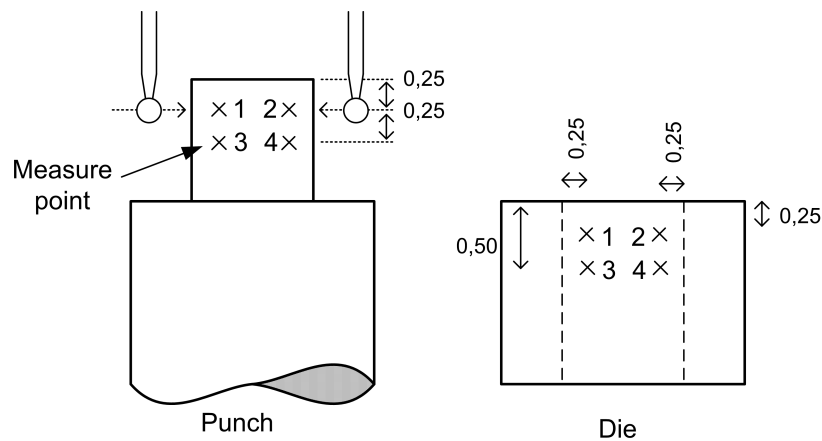


Figure 4.14

The four measurements on each face will allow for flatness assessment of the faces. Further, four width measurements on each face will allow for tolerance estimation of the manufacturing process.

Results of CMM measurements and uncertainty estimation

In order to interpret the measurements data from the tactile CMM measurements, a reference coordinate system must be applied. The measurement values will be identified using the following naming protocol:

(punch name N) (parallel plane of face) (position number)

The names of the individual EDM benchmark pieces are abbreviated as follows:

FH Fraunhofer-Institut für Produktionsanlagen und Konstruktionstechnik IPK, DE

TEK Fundacion Tekniker - ES

DTU IPU & Technical University of Denmark, DK

The orientation of the measurement coordinate system can be seen from Figure 4.15 and the measurement position number is indicated on the sketch of the point position in Figure 4.14.

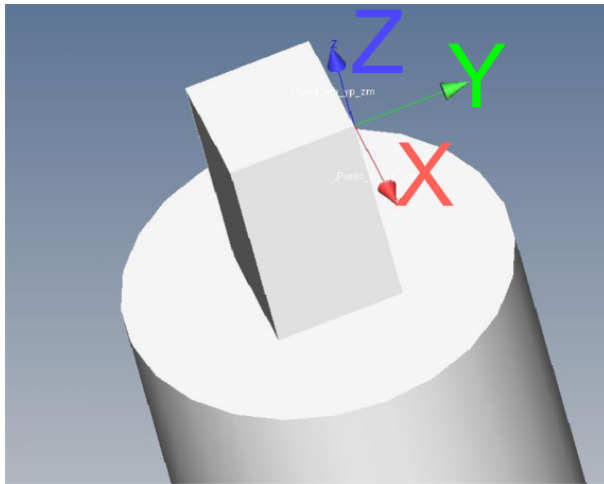


Figure 4.15: Orientation of the measurement coordinate system for CMM measurements.

Of the initial partners involved in the EDM benchmark test, three partners successfully delivered a specimen for the experiment. FH delivered 5 different punch geometries, manufactured with different machine settings and wires. The specimen was machined on a traditional wire EDM machine. FH did not deliver any die geometry and report difficulty achieving the die geometry. DTU delivered one die and punch geometry machine in a Sarix SX-200 Micro EDM machine. TEK delivered one punch geometry, machined using a traditional wire edit machine using 0,25 mm wire.

Punch	zy 1	zy 2	zy 3	zy 4	zx 1	zx 2	zx 3	zx 4
FH1	1,00166	1,00189	1,00153	1,00148	0,99959	0,99933	1,00117	1,00071
FH2	1,00434	1,00422	1,00420	1,00407	1,00010	0,99976	1,00017	0,99999
FH3	0,99946	0,99987	1,00018	0,99998	1,00044	0,99971	1,00020	1,00074
FH4	1,00086	1,00062	1,00039	1,00025	1,00072	1,00063	1,00057	1,00089
FH5	0,99949	0,99943	0,99997	0,99961	1,00152	1,00115	1,00186	1,00160
TEK	1,00322	1,00339	1,00258	1,00215	0,99514	0,99467	0,99487	0,99476
DTU	1,00560	1,00657	1,00575	1,00573	1,00732	1,00730	1,00718	1,00649

Table 4.4: Punch measurement values from the Zeiss F-25 CMM, Fraunhofer-IPK, Berlin. All values in millimeter.

The measurements at FH were conducted on a Zeiss F-25 CMM. The F-25 is a dedicated micro 3D CMM machine. The machine exhibiting an expanded combined uncertainty of the tactile machine length measurements, in accordance with the ISO standard 10360-2, $\pm(0,25 + L/666)\mu\text{m}^1$ MPE under certain environmental conditions. This high-accuracy measurement capability has been verified by several sources [61,62].

An uncertainty estimation for the measurements conducted at FH was not given by the metrologist. However, due to the high degree of similarity between the ISO 10360-2 calibration standard and the measurement procedure in this experiment, the MPE values for combined uncertainty from the Zeiss F-25 CMM will serve as the a proxy for an uncertainty estimation in this case.

Inserting into the MPE formula for the combined uncertainty, we arrive at a value of $U_{95} = (0,25 + 1/666) = 0,252\mu\text{m}$.

Punch	zy 1	zy 2	zx 1	zx 2
FH1	0,9999	0,9998	1,0001	0,9996
FH2	1,0022	1,0018	0,9963	0,9958
FH3	0,9981	0,9967	0,9988	0,9986
FH4	1,0001	1,0007	0,9999	0,9971
FH5	0,9986	0,9984	1,0000	0,9988
TEK	1,0004	1,0006	0,9928	0,9918
DTU	1,0023	1,0013	1,0065	1,0063

Table 4.5: Punch measurement values from the Zeiss OMC CMM, DTU-CGM,Lyngby. All values are in millimeters without systematic error correction.

The measurements at DTU were conducted on a Zeiss OMC 850 CMM. The Zeiss OMC 850 CMM is specified with a MPE of $\pm(3 + L/300)\mu\text{m}^2$.The expanded combined uncertainty, U95, was stated by the metrologist to a values of $\pm 1,87\mu\text{m}$. This uncertainty is based on the variance of a series of similar width measurements conducted on a certified gauge block. Moreover, the measurements from the Zeiss OMC 850 CMM have been corrected for a systematic error of $b = 1,36\mu\text{m}$ in the measures given in Figure 4.16 and forward, according to the procedure outline in the ISO 15530-3 standard.

The width measurements on the OMC CMM were conducted with the minimum possible probe size, featuring a ball diameter of 0,8 mm. The probe ball diameter limited the reachable measuring points on the external punch geometry, only allowing for measuring of points 1 & 2 out of the four points specified in Figure 4.14.

The results of the uncorrected measurements are reproduced in Table 4.5.

We now turn our attention to the measurement results obtained from the two CMM machines. It is clear that while the Zeiss F-25 is a dedicated micro machine, the Zeiss OMC 850 is a CMM machine intended for macro size metrology. The goal of the following comparative analysis will be to access the validity of the uncertainty estimate for the two CMM machines. Secondly the analysis will seek to establish a guideline for the required precision required in order to access typical tolerance-bands encountered in micro tool manufacturing.

¹(*: L is expressed in mm).

²(*: L is expressed in mm).

For a simple geometry, like the one applied in this experiment, a manufacturing accuracy of a modern wire spark cut machine should be in the order of $2\ \mu\text{m}$ to $5\ \mu\text{m}$, for dual-wire and dedicate micro EDM machines down to $1\ \mu\text{m}$ to $2\ \mu\text{m}$.

When noticing the width measurements in Figure 4.16, an overlap between respective measurement uncertainty spans is observed. However, it is readily noted that the uncertainty estimation of the width measurement on the Zeiss OMC 850 machine is of the same order of magnitude as the anticipated tolerance variation of the manufacturing process. This makes the OMC 850 CMM unfit for evaluation of this high precision manufacturing process since the tolerance variation of the manufacturing process is concealed inside the uncertainty span of the measurement. A rule of thumb within metrology requires the measurement method to be superior in precision by a factor of 5-10, in order to be applicable for assessment of a manufacturing process or product.

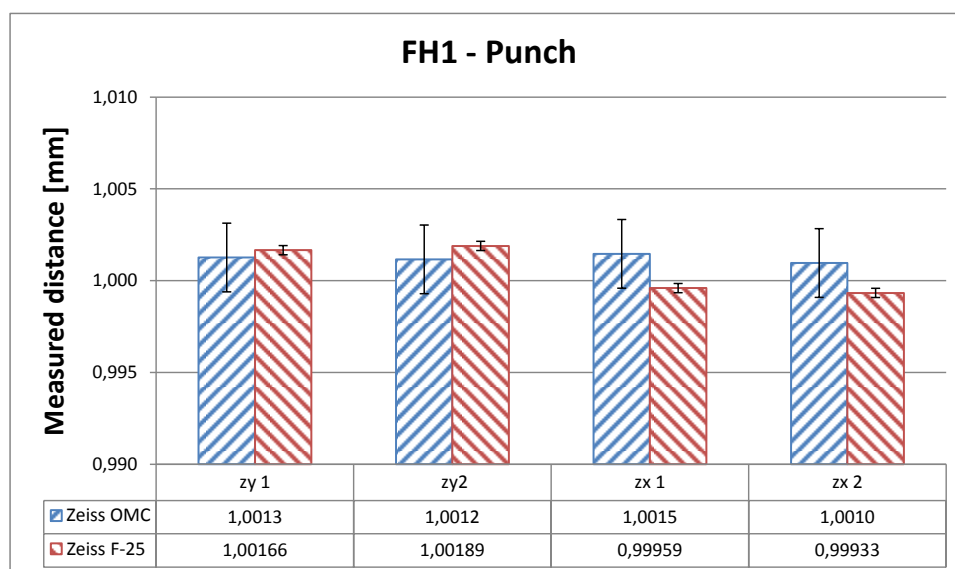


Figure 4.16: FH1 punch measurements, taken from Tables 4.5 and 4.4 ,Zeiss OMC values corrected for systematic error.

The FH 2 punch, Figure 4.17, shows an increase in width deviation between the perpendicular faces of the dice. This deviation is more than $4\ \mu\text{m}$ in both cases. Further, for the width measurements ZX 1 and ZX 2, an increase in the disagreement between the two measurement sets is observed.

The punches named FH3 and FH4 get close to the nominal value of the specified width. In both cases the deviation is within $\pm 1\ \mu\text{m}$. The measurements are depicted in the bar diagrams in Figure 4.18 and 4.19.

For the FH5 punch in Figure 4.20, an increased deviation is noted between the two dice faces. The variation within each side with is low. In this case there is relatively good agreement between the measurements of the F-25 and the OMC 850 CMM. The width measurements for the punch geometry manufactured at Fundacion Tekniker in Spain is represented by the bar-plot in Figure 4.22. The punch geometry shows a relatively large

width difference between the faces of the dice. The width variation is more than $6\mu m$ between the faces. A tolerance gap of this kind would not be acceptable for a closed-die micro forming tool. However, the width variation within the two faces are less than a micron.

The punch manufactured at Technical University of Denmark is exceeding the nominal width for all measurements with an average of $5 - 7\mu m$. When compared to the TEK punch, the DTU punch shows less width variation between the two faces. For one measurement (zy 2) there is a $4\mu m$ deviation between the width measured by the F-25 and the OMC 850 CMM. A plot of the measure values can be seen in Figure 4.21.

The following comparative analysis of the manufacturing process will take offset in the measurement data acquired F-25 CMM. When doing comparative analysis, especially when subtracting the average or calculating numerical derivatives, it is important to remember to account for the uncertainty affiliated with each of the ingoing measurements. If this is not done, misleading conclusions can be drawn.

Figure 4.23 displays a graph of the deviation from nominal of each of the 8 width measurements conducted on each of the punch geometries. Also a calculation of the average absolute deviation from nominal width have been plotted. As the order have been sorted with respect to the average absolute deviation, it is clear to see that the FH3 geometry gets closes to the nominal width. Further, the nature of the deviations can be studied. The TEK punch is both over- and under nominal width by several microns whereas the DTU specimen is constantly over-shooting.

An constant offset from nominal width can simply be corrected by changing the process parameters of the EDM-process, whereas as variability between two specimens, or faces

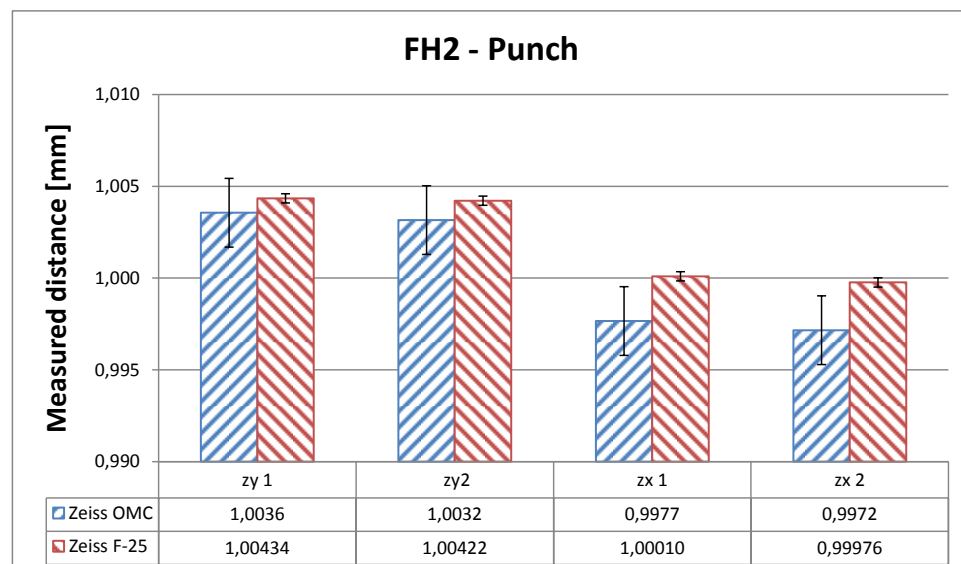


Figure 4.17: FH2 punch measurements, taken from Tables 4.5 and 4.4 ,Zeiss OMC values corrected for systematic error.

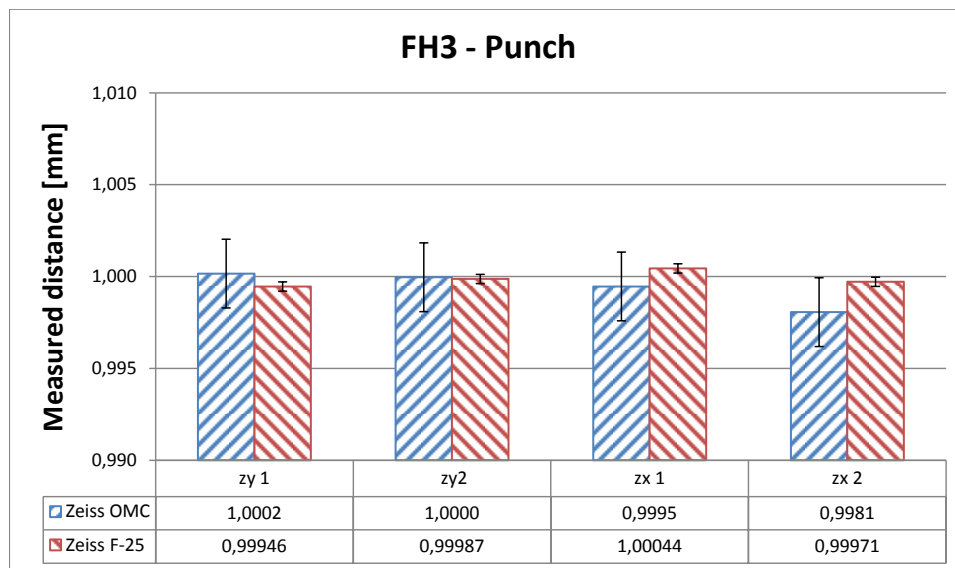


Figure 4.18: FH3 punch measurements, taken from Tables 4.5 and 4.4 ,Zeiss OMC values corrected for systematic error.

in this case, is bound to the precision of the machine and process itself. Or put in another way, an error on the accuracy of the manufacturing machine can be corrected, whereas the precision of the machine is dependent on the machine quality. In order to capture the repetition accuracy of the process, the standard deviation of the complete set of measurements for each geometry have been calculated. The resulting

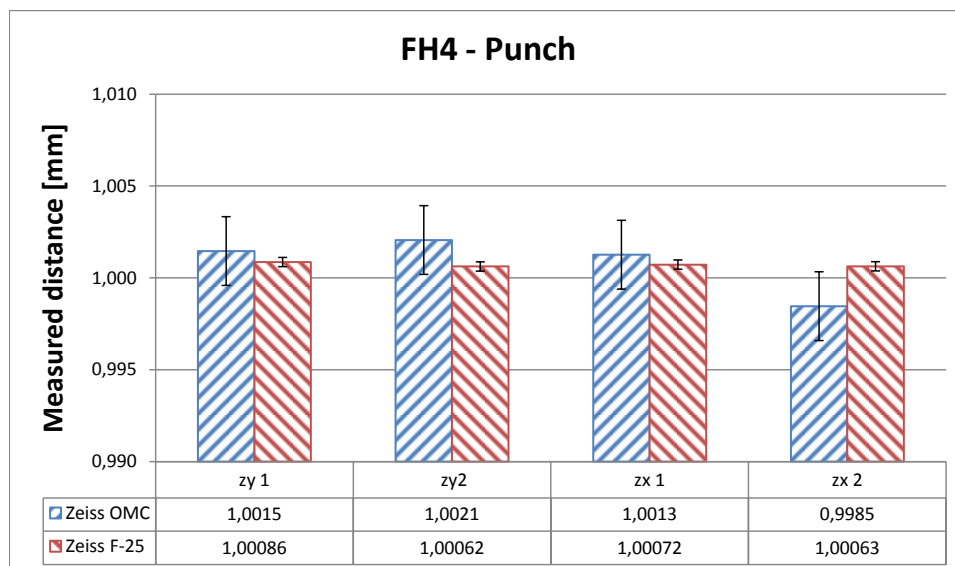


Figure 4.19: FH4 punch measurements, taken from Tables 4.5 and 4.4 ,Zeiss OMC values corrected for systematic error.

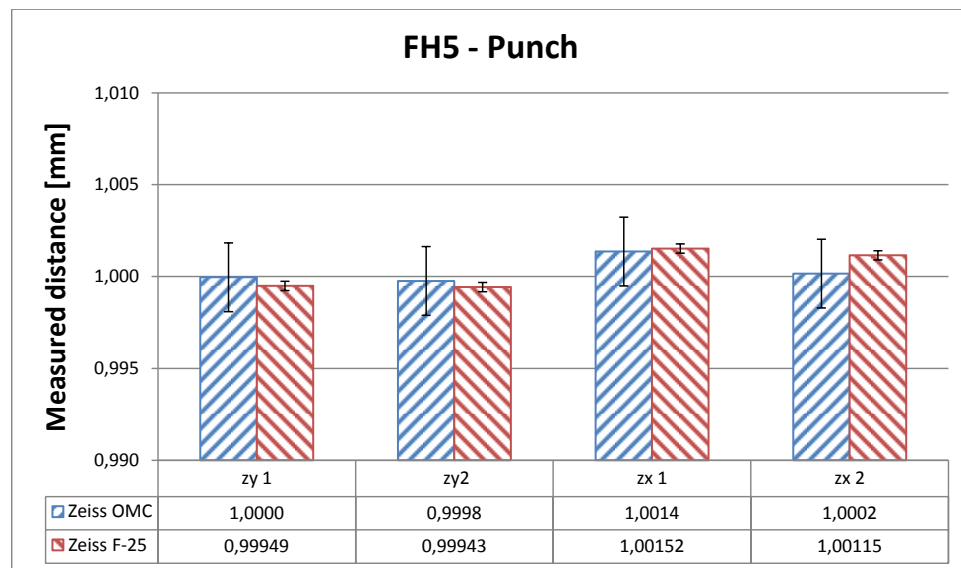


Figure 4.20: FH5 punch measurements, taken from Tables 4.5 and 4.4 ,Zeiss OMC values corrected for systematic error.

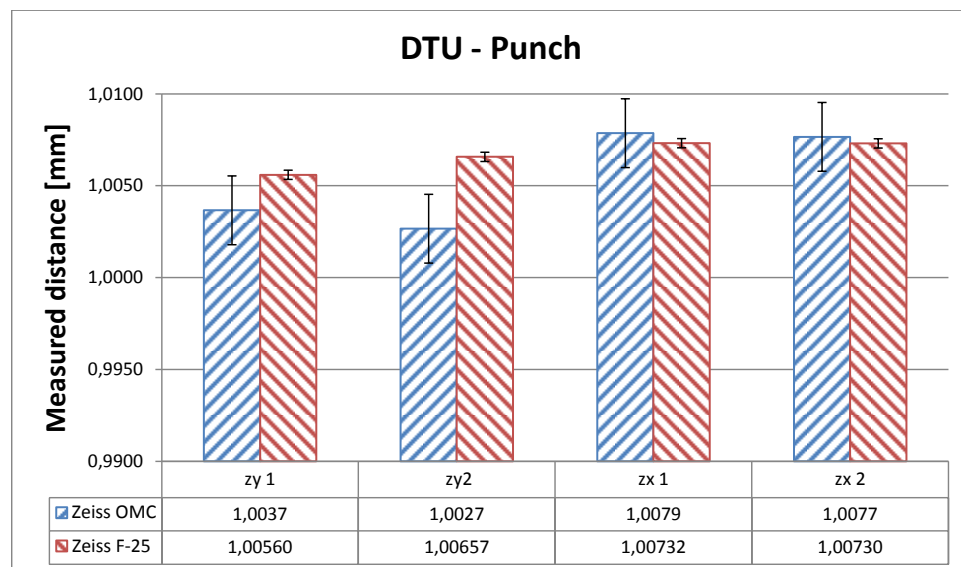


Figure 4.21: DTU punch measurements, taken from Tables 4.5 and 4.4 ,Zeiss OMC values corrected for systematic error.

values were multiplied with a coverage factor of 2 to get to an approximate 95% confidence interval. The result is graphed in Figure 4.24. Finally, the parallelism between the two facets will be treated. In this analysis one of the parallel facets will be treated as having an ideal flatness, attributing any deviations to waviness of the opposing face. Now the results are treated as flatness measurement according to the ISO standard 12781-1. According to ISO 12781-2 a large number of sample point should be acquired

to ensure robustness and a validity of a flatness analysis. This criteria is not fully met in the present case as the number of sample point is only four. Thus, the following results must only be interpreted as indicative. The flatness is given as peak-to-valley deviation (MZPL) which is equivalent to Total Indicated Run (TIR) by ASTM terms . A plot of the punch flatness estimation is shown in Figure 4.25.

Measurement of die geometry

DTU was the only partner successfully capable of manufacturing the die geometry. The reason for this is likely to be found in the resources and effort necessary to achieve an internal geometry of this size. A modern dual-wire wire-EDM machine is capable of achieving internal geometries of high precision and with small corner radii. The die geometry at DTU was manufactured on a dedicated micro-EDM machine capable of machining blind-hole internal geometries with fine tolerances and small corner radii.

The die geometry was not measured in the Zeiss F-25 CMM, even though this would be possible. The operator reported that the risk of damage to the probe was present and he was not comfortable measuring such small internal geometries.

The die was then measured on a DeMeet 220 CMM, using the optical measuring system. The optical measurement system functions fundamentally different than the point oriented CMM approach; Two lines are approximated to the contrast edge of the images. Thus, the optical method is only capable of evaluating 'geometrical extremities' residing on or close to the edge of an object. Because the optical method is different by nature, a further comparative study with the results from the F-25 and OMC 850 will be omitted.

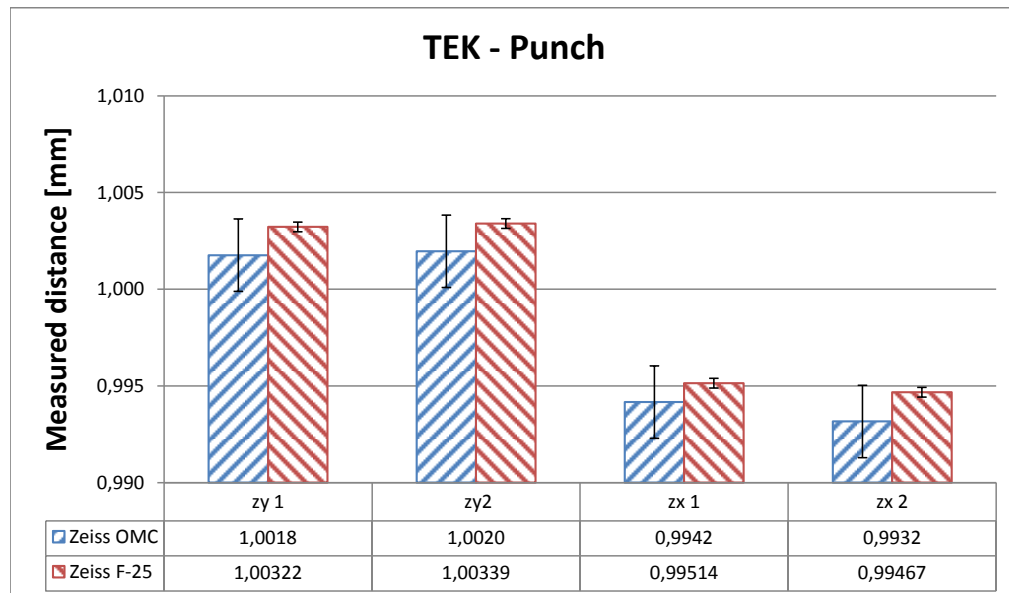


Figure 4.22: TEK punch measurements, taken from Tables 4.5 and 4.4 ,Zeiss OMC values corrected for systematic error.

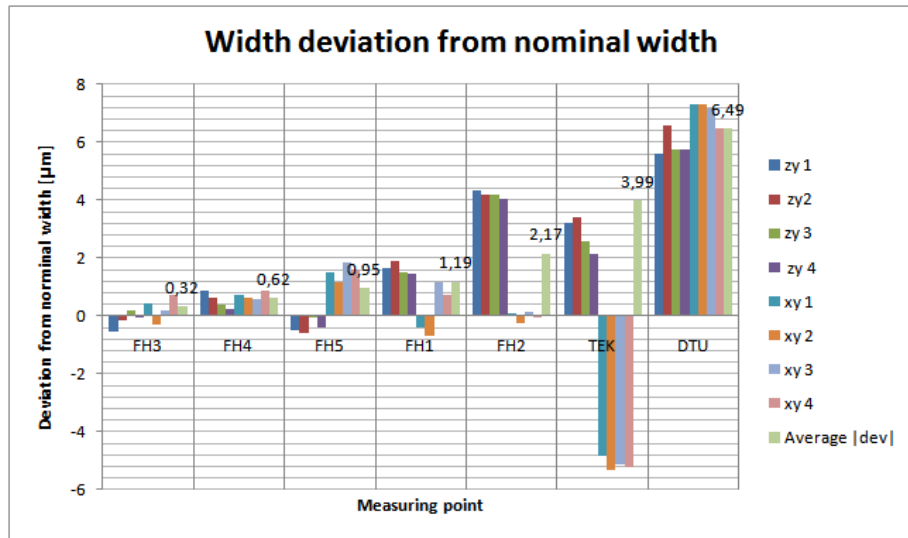


Figure 4.23: Plot of the individual measurement deviation from nominal value. The order is sorted according to average deviation (last bar in the plot).

Die	zy	zx
DTU	1,0239	1,0231

Table 4.6: Measurements of die geometry, optical CMM DeMeet 220. The measurement uncertainty, U95, was estimated to $\pm 2\mu\text{m}$.

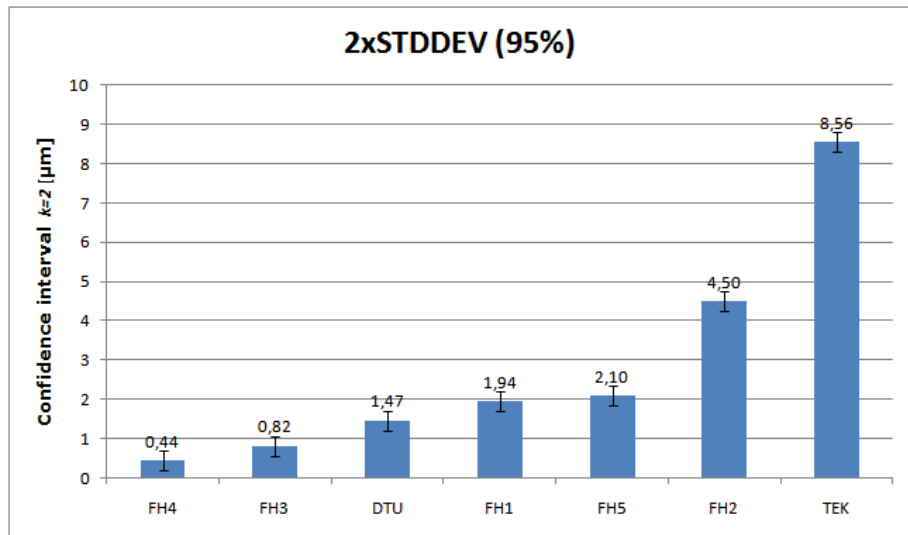


Figure 4.24: 95% confidence interval for the variability of the face width of the punch geometry.

95% confidence interval for the variability of the face width of the punch geometry. The results are sorted according to value. Error bars donate the estimated measurement uncertainty of the Zeiss F-25 CMM.

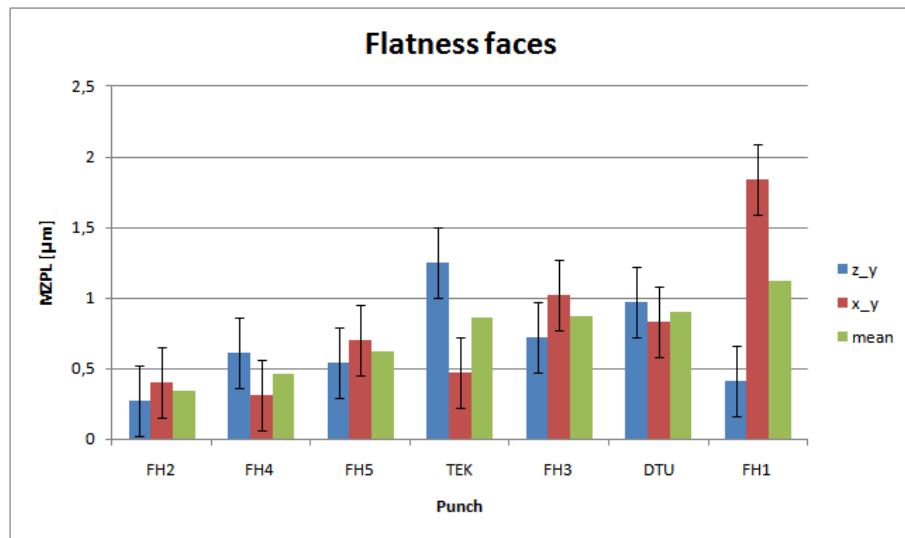


Figure 4.25: Calculation of the face flatness. Please not the rather uncertainty contribution originating from the measurement machine.

The width of the die geometry is too large by more than $20 \mu m$, as noted from the values in Table 4.6. However, the relative deviation between the two widths are within a micron. No depth measurements were conducted on the die geometry.

The various machine parameter reported for the experiment specimens is summarized in Table 4.7. Ideally a closer comparison between the achieved manufacturing precision and the various machine settings should be conducted. However, due to the diverse nature of the electric discharge machines used in this experiment and the uncomplete data set manufacturing data, this will be left for future work.

punch	wire size	number of cuts	notes
FH1	0,250	3	
FH2	0,100	5	I&A Schurl
FH3	0,250	6	
FH4	0,050	4	W-technology SP05
FH5	0,160	5	
DTU	0,3 and 0,1	-	Sarix SX-200 machine
TEK	NA	NA	

Table 4.7: Process characteristics from the manufacturing process of the punch geometry

Conclusion on the EDM-benchmark round robin-test

A total of eight micro tool inserts was machined using wire-EDM and μ -EDM processes by three different organizations. This resulted in seven punch-like geometries and one die geometry, with an external and internal dice geometry and an edge length of 1 mm. The tool inserts were manufactured in ultra fine grained cemented tungsten carbide.

The width distances was subsequently measured using a dedicated micro CMM as well as a conventional CMM. Only the high precision CMM was able to deliver the required performance to conduct the measurements with sufficiently small uncertainty.

One punch geometry, FH3, was within $\pm 1 \mu\text{m}$ for the width measurement on the tool head. This tool was machined with a standard 0,250 mm wire with six cuts. The punch tool that came in second closest to the specified width, the FH4 punch, was manufactured with a dedicated micro-cut wire with a diameter of $50 \mu\text{m}$. The two specimens were also the ones to exhibit the smallest variance between the two perpendicular facets, closely followed by the punch geometry DTU with an average variability of $1,47 \mu$ for the 95% confidence interval. The DTU punch showed the largest tolerance deviation with a average deviation of $6,47 \mu\text{m}$ from the specified width of 1 mm.

Rounding up, we can conclude that with some consideration and a number of attempts, it is possible to manufacture simple micro tools with external geometries and high precision using the wire-edm process. A high accuracy measuring machine is required to access the resulting geometry and verify tolerance conformance. Only one specimen with internal geometry was successfully manufactured. In this case the measurement with CMM failed due to the complexity of the measurement procedure on the CMM. The die geometry was measured using an optical microscope method and the results showed a width exceeding the specification by approximate $20 \mu\text{m}$.

4.8 Measurement of complex 3D structures.

Until now we have looked at relative simple measuring tasks and geometries. This might be beneficial when outlining basic metrological aspects and for a round-robin manufacturing geometry. However, applicable mechanical components often have more complicated geometries with several different classes of requirements for tolerance and surface finish, also within the same component.

To finalize the analysis of micro metrology we will now look at a small gear wheel currently being utilized in a drug-delivery system. The gear component is currently being manufactured using a powder metallurgical process. The gear wheel is manufactured in AISI 316 stainless steel.

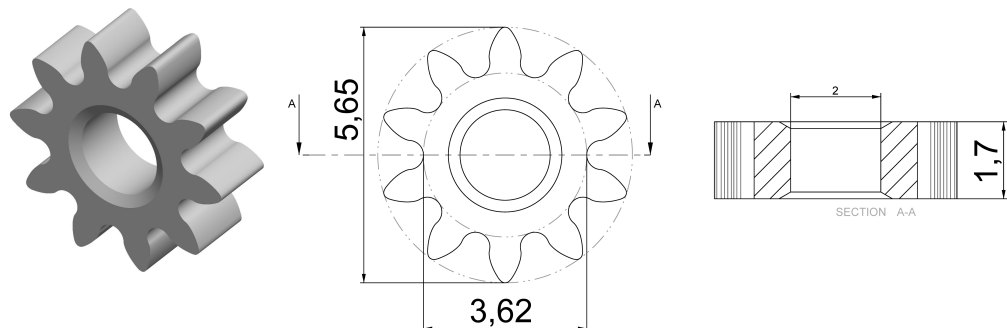


Figure 4.26: Micro gear for drug delivery system. The gear wheel is currently manufactured in Stainless AISI 316 using powder pressing.

4. MICRO METROLOGY

The general tolerance requirements are ranging from 30-100 microns, with a narrow tolerance band of maximum $30 \mu m$ for the tooth-to-tooth tangential composite deviation. The total tangential composite deviations is specified to a maximum of $60 \mu m$ with an option to inherit unused tolerance deviation for the roundness error of the center hole. The allowable roundness error for the center hole is specified to $30 \mu m$.

Verifying that the tolerance constraints for the gear wheel geometry have been met is as a challenging task. Often only a subset of the tolerance specifications can be inspected with one instrument. For example the surface roughness could be checked with a roughness stylus instrument and the hole with plug gauge respectively. In the micro domain, the choices of metrological instruments are even more restricted due to the maximum possible size of the stylus head and the strict tolerance demands. Sometimes it is possible to utilize an instrument intended for surface roughness analysis to access geometrical elements, as these elements are small enough to reside inside the measuring range of the roughness instrument. However, at present no versatile 'whole-in-one' solution for full dimensional characterization in the nanometer scale exists [15]. Figure 4.27 suggests some common measuring technologies for characterization of 2D, $2\frac{1}{2}D$ and 3D geometries going from micro to nano-scale.

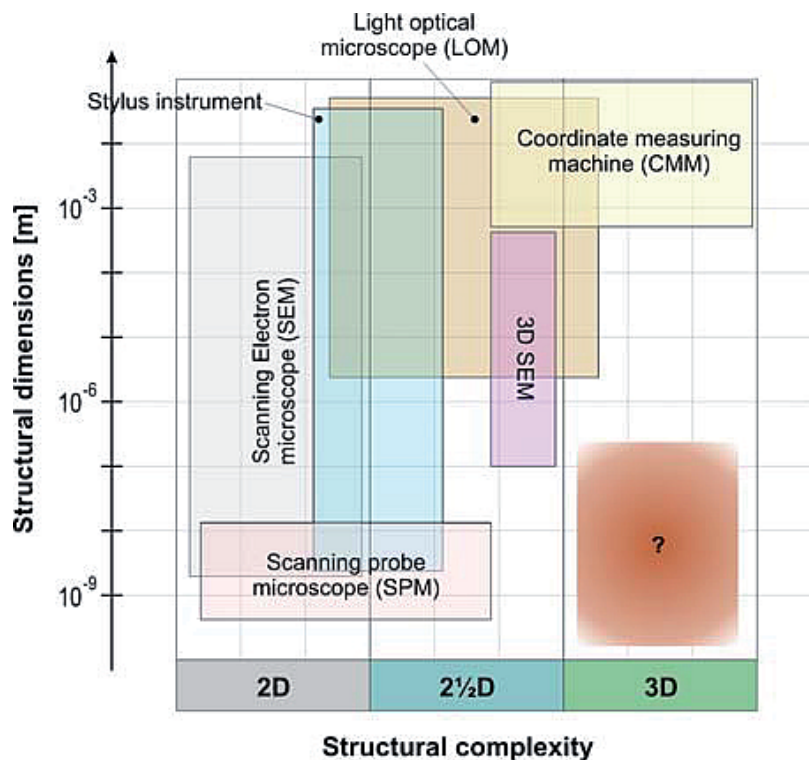


Figure 4.27: Classification of measurement equipment. Definition of 2D, $2\frac{1}{2}D$ and 3D according to reference. [15]

There is a true need for a good instrument for characterization of 3D objects in the micro and nanometer scale. Some work is going on within x-ray tomography, but a present

time the resolution of this technology is within hundreds of microns. Further, due to the density coupled attenuation of the x-ray radiation, this technology is generally only suitable for components in polymer and lightweight metals.

In the following the gear wheel geometry is used as a representable artefact for validation using two different method capable of characterizing near 3D geometries with micrometer accuracy.

3D scanning with the 3 Shape D700 scanner

The 3 Shape scanner built for characterization of dental components. The scanner features a laser source in combination with two cameras and a pan-, tilt- rotate stage. By combining the amount of laser light received by the two cameras with the current position of the stage on which the scanning objects sits, the scanner is capable of building a 3D model of the object in question. This technology is dubbed laser surface interferometry and relies on the detection of the phase difference between several areas on the surface in question. The accuracy of surface interferometry is largest in the Z-direction; the beam direction, explaining the need for a rotational stage to conduct 3D scanning.

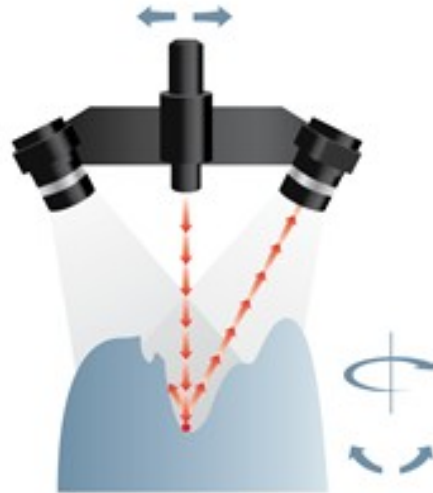


Figure 4.28: Working principle of the 3 Shape D700 scanner. Image taken from promotion pamphlet.

The accuracy of a general scanning on the 3 Shape D700 scanner is specified to 20 microns. The scanner works best with surfaces having a diffuse scattering characteristic at the wavelengths of the laser, meaning that shiny metallic components will result in poor scanning results. This problem can be solved by spraying the component surface with a dedicated thin layer of white powder-based varnish. This powder assures diffuse scattering of the laser light while only altering the surface geometry to a minor degree with an estimated film thickness in the range of a few microns. However, since the application of the powder-varnish is done with a spray can by hand, the added

measurement uncertainty from this additional process step is largely dependent on the skill of the operator.

Once the scanned has have been acquired, the results can be compared against a solid CAD model. This is done by importing a STL type geometry file into the scanning software and aligning the two data-sets, either manually or by means of a minimum square distance type algorithm. Once the two imported geometries from the CAD model and the point cloud from the scanner have been aligned, the distance between the two can be calculated. The result is shown as color coated images. Figure 4.29 depicts an actual scanning of the gear wheel geometry. The external geometry of the component was extruded in Aluminium alloy 6060 as a toothed rod. Subsequently the individual gear wheels where parted off and the internal center hole was drilled on a lathe. The component was sprayed with white powder-varnish and placed in the 3 shape D700 scanner.

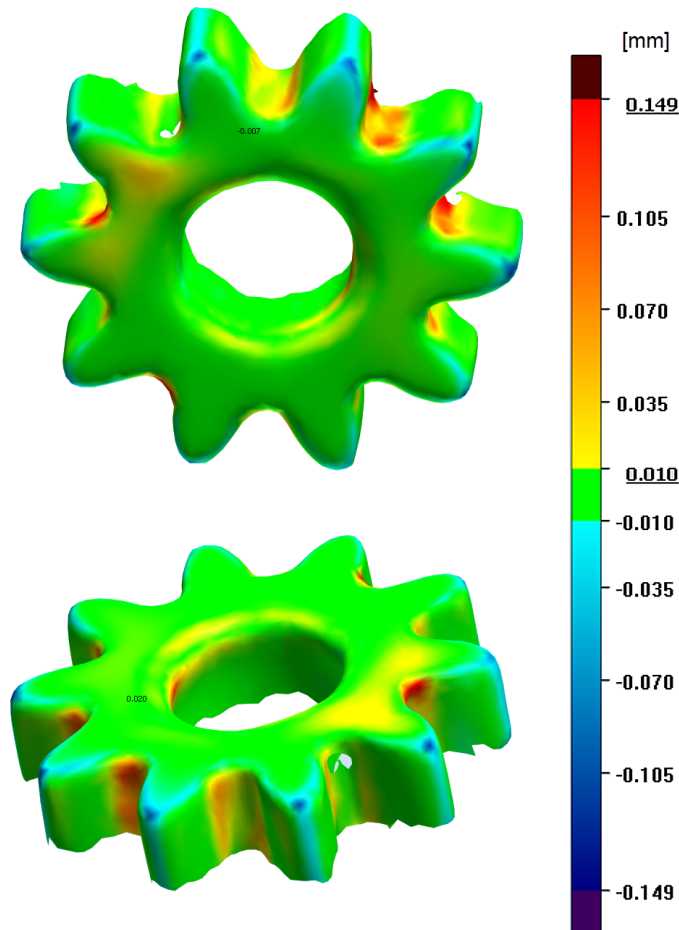


Figure 4.29: Comparison between scanned geometry and CAD generated STL file. The color coated deviations are specified in millimeters.

The overall deviations are marked as ranging $\pm 149\mu\text{m}$. Generally the valleys of the toothed rim is exceeding the specifications, whereas the tips of the rim is short measured. The excess measure at the tooth valleys can be explained by clogging of the powder-vernish in this region, leading to an artificial thickening of the component surface at this region. Further, the short measure of the tooth tip could be traced to a slight radius reduction of tooth tip during manufacturing of the die. The radius reduction was done in order to be able to utilize a more cost effective machining strategy and a thick wire on the wire-EDM machine. The radius reduction of the tip diameter translates to a reduction of the overall tip diameter of the gear wheel of $-8,72\ \mu\text{m}$ or $-4,36\ \mu\text{m}$ at each tooth. When comparing the short measure of the tip of the gear wheel to the specified accuracy of the scanner and the specified deviation of about $-10\ \mu\text{m}$ in Figure 4.29, it is unlikely that tip reduction ratio alone is enough to trigger the blue-coloring of the tooth tips in the figure.

Returning to the general quality assessment of the scanning and the comparison analysis in Figure 4.29, an undesirable rounding of the component edges is noted. For these type of components it is generally desirable to have sharp and defined edges, even though for bulk forming the grain size effect can limit the achievable corner radii. Optical triangulation laser scanners, as the 3 shape D700 scanner, are prone to errors at surface discontinuities and sharp features. The rounded tips of the gear wheel, shown as spotted dark blue points in Figure 4.29, can be attributed to scanning errors due to the sharp tip of the gear wheel tooth edge rather than a physical deviation in the physical gear wheel. The hypothesis that the tooth edge geometry is indeed sharp can be verified in the SEM image Figure 4.30 further ahead.

Now, in order to assess the accuracy of the 3 Shape scanning we a second image source as reference. A SEM image of the extruded gear wheel component is show in Figure 4.30.

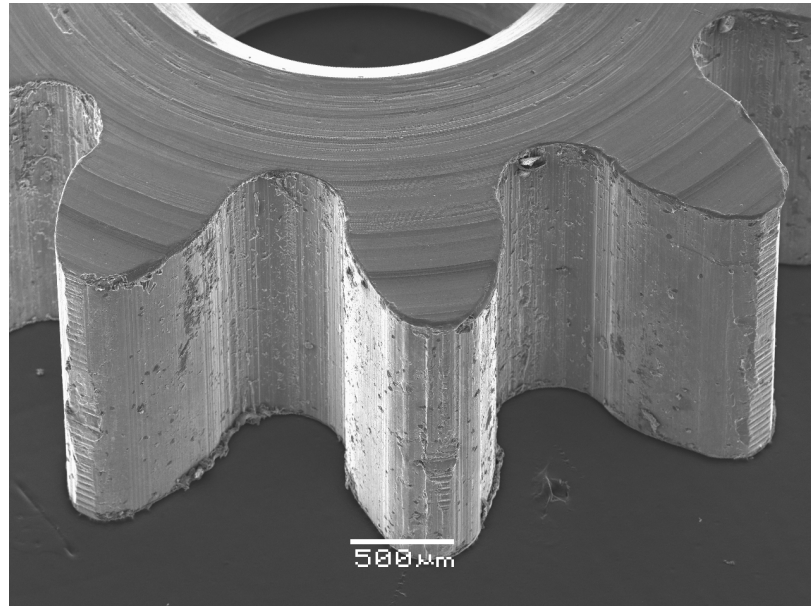


Figure 4.30: SEM image of the gear wheel component in ALU 6060

When comparing the SEM image with the CAD comparison image from Figure 4.29, it becomes apparent that the rounding of the corners is indeed a scanning defect of the optical triangulation surface scanning.

A slight under-filling of tooth geometry can be detected on the SEM image, implying that the indicated short measure of the tooth tip indicated in Figure 4.29 might in fact be valid. While the SEM images is suitable for getting a visual impression of the specimen geometry, it is less applicable for metrological validation. As seen in Figure 4.30, the presence of a scaler bar implies that the image is dimensionally sound. This is true to a certain extent and the method is precise enough for estimation of simple width or length measures. However, the SEM does only output a 2D monochrome image where the pixel intensity represents the amount of second electron scattering in the specimen. A 3D SEM method exists, but this technology is still unmaturred at present time. As the SEM instrument does not achieve to produce a full characterization of the 3D object, it will only be utilized for reference in this analysis.

3D scanning with the Alicona InfinteFocus microscope

As second source of qualifying complex 3D geometries, we now seek to qualify the gear wheel geometry with an Alicona InfinteFocus focus variation microscope. This microscope is capable of building a 3D model of the object in question with sub nanometer accuracy in the Z-direction and and a resolution around one micron in the lateral directions. The software package for the microscope system features the possibility to import CAD model via a STL type file. Like in the case of the 3 shape scanner, the STL model and the point cloud from the scanner can be aligned and color indicators showing the distance deviations can be superimposed onto the model. In this case, the resolution of the focus variation microscope was set to one micrometer in all directions (X,Y & Z) and a lense with 10X magnifications was used. The 3D model was acquired without the use of stitching, meaning that the image represents the total field of view of the microscope. Also, because the focus variation technique works without tilting the specimen, only surfaces with angles of 30° or more between the Z-direction and the surface plane can be captured. This usually means that a gap in the point cloud will occur between two plateaus separated by a vertical facet. The scanner software holds a feature to concatenate different scanned surfaces into one model. This feature could for example be a number of scans of the same part with different orientation and inclination. However, this operation involves human judgement interaction and it thus does not provide an entirely predictive and objective result. Figure 4.31 represents the point cloud of a scanning of the gear wheel geometry. The color coating is applied according to the calculated deviation from the CAD model.

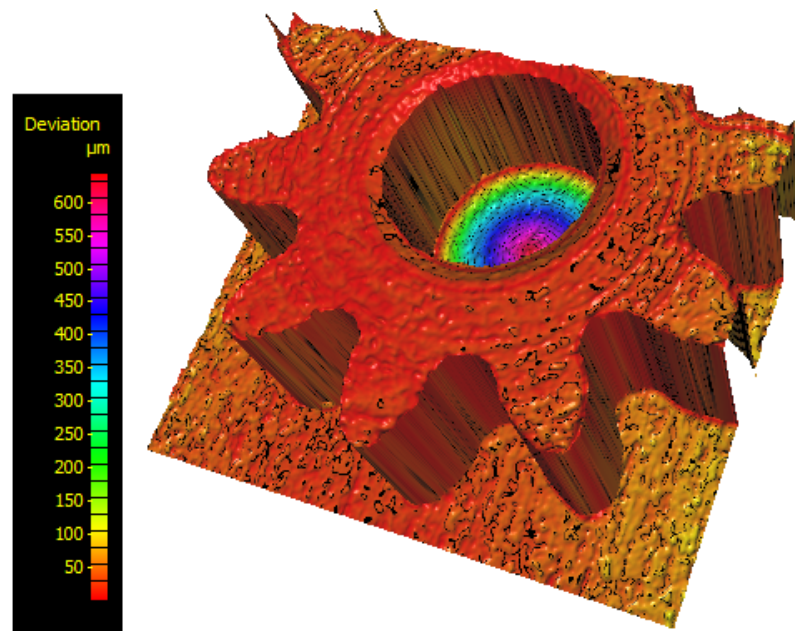


Figure 4.31: Color coated model showing the deviation from the solid CAD model. Data acquired on the Alicona Infinite Focus microscope.

The indistinct and blurry edge profile is readily perceivable. Further, some spikes are present in the point cloud near the vertical surfaces. Another thing to notice is the change of the color highlighting towards the sides of the image. As the specimen was placed on a flat-ground surface, the change in deviation must be attributed to optical curvature distortion in the lens system. This means that the 3D point cloud will only feature the required accuracy near the center of the microscope focal plane. This further implies that the focus variation microscope technique is not well suited for inspection of specimens where the specimen dimension is comparable to the image plane size.

We now crop the data set and limit the analysis to only include one of the gear wheel teeth. The data set illustrated in Figure 4.32 again shows the difference between the scanned geometry and geometry imported from the CAD model.

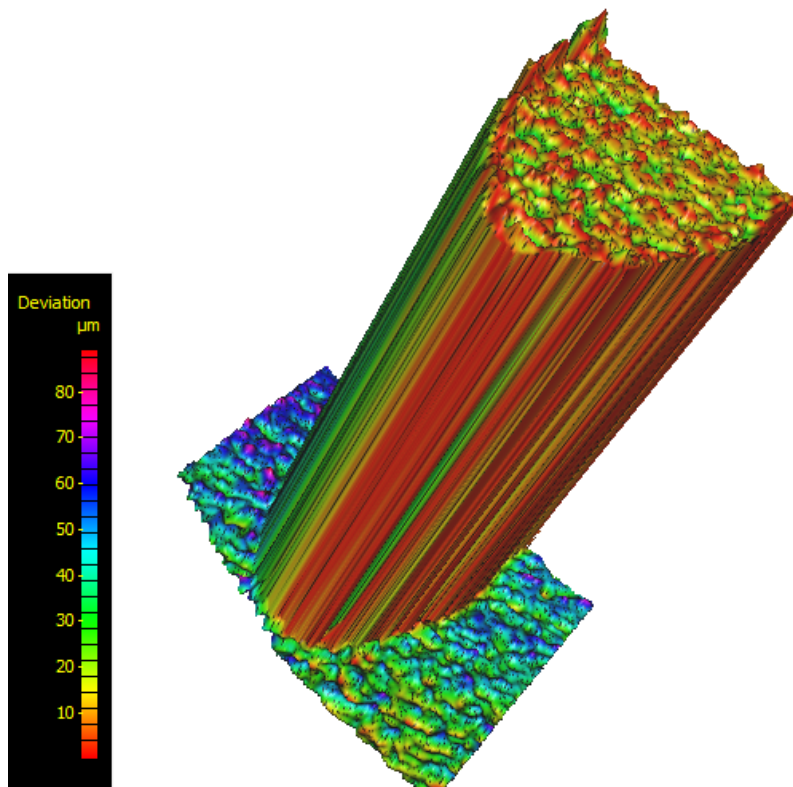


Figure 4.32: Illustration of the difference between intended and achieved geometry for the gear wheel tooth. The specimen was scanned on an Alicona Infinte Focus instrument.

Also in this case is the limited vertical (height) resolution of the scanning instrument evident, whereas the vertical surfaces of the component is somewhat blurry. The deviation from the intended tooth geometry varies in the range between 0 - 30 μm for the envelope of the gear tooth. The measured tolerance deviations is comparable to the specified tooth-to-tooth tangential tolerance deviation of maximum 30 μm as specified in Section 4.8. This means that the Alicona InfinteFocus focus variation microscope is probably unfit or marginal to qualify the gear wheel geometry with the required accuracy due to vertical measurement uncertainty. No distortion of the deviation measurement is seen near the rim of the image field, as it was the case in Figure 4.31.

Conclusion

In the past section we have studied the science and craft of inspecting a 3 dimensional artefact with a size near the limit between the macro- micro- size domain. The empirical experiment sought to touch on some of the typical challenges encountered when seeking to validate geometric tolerance compliance. A gear wheel component was chosen as a representable geometry for the family of components with medium complex geometry and an overall size in the millimeter range. Further, tolerance requirements of 30-60 μm is typical for these types of specimens.

Rather than going through each tolerance requirement individually as usually done in the macro scale, we have sought to find a method of inspecting the overall geometry with as few instruments as possible. This approach is in line with a typical production scenario, where only limited resources are available for quality control of the produced specimens. Further, it is always desirable to be able to achieve inspection ratios of 100% for product critical parts.

According to literature, no universal 3D measurement equipment exists for full characterization of micro size specimens. However, we have applied some of the instrument techniques often used to inspect these types of geometries, namely a spatial laser scanner, a scanning electron microscope and a focus variation microscope.

It was found that the Laser scanning technique was generally fast and produces reliable results. However, the uncertainty of $20\ \mu\text{m}$ is often comparable to the tolerance requirements of the component itself. Also, the application of a special varnish for shiny surfaces will further reduce the achievable precision of the method.

The Alicona focus variation microscope produced reliable results within a smaller spatial range. The method is however not capable of accurately tracing steep edges and suffers from minor distortions over the image field.

None of the selected methods were able to fully characterize the gear wheel geometry and validate compliance against the given tolerance band. This was expected and is in line with what was found in literature. The laser scanner were able to generate the most profound model of the gear wheel geometry, with some rounding of the geometry discontinuities. This rounding was not found when comparing with the SEM image of the same geometry and must be an inherit effect of the scanning technology. The focus variation microscope was able to fully characterizes part of the geometry and a successful comparison to the CAD model was accomplished. However, the variance associated with the focus variation microscope indicated that this method was marginal or unfit for qualification of the required $0 - 30\ \mu\text{m}$ range.

To conclude on the measurement example in this section, a few points can be stated. Simple features of a component can be readily verified with the focus variation microscope, while this is not true for the specimens with complex geometries.

By combining several scanning techniques or taking several scanning views with the same technology, a basis can be established for a accurate but not exact evaluation of the micro component geometry.

Chapter 5

Tribology in microforming

The word tribology is originally derived from the Greek verb $\tau\rho\iota\beta\omega$ - tribo, meaning "I rub". In engineering and science the word is covering effects occurring between surfaces in relative motion. These effects include well known elements such as friction, lubrication and wear.

Tribological effects are important in many modern applications, naming medicine, cosmetics and design of bearing systems out of many.

One of the first known scientist to embark on the study of tribological effects was Leonardo da Vinci (1452-1519) who discovered two fundamental laws of friction: That friction is constant for two objects with the same weight but with different contact surface area. Further, he also discovered that the friction would double when the weight of the movable element would double. Figure 5.1 illustrates some of the experimental setups suggested by Leonardo da Vinci in his sketchbook. Later studies of tribology were conducted by Charles-Augustin de Coulomb (1736-1806), giving name to the Coulomb friction model.

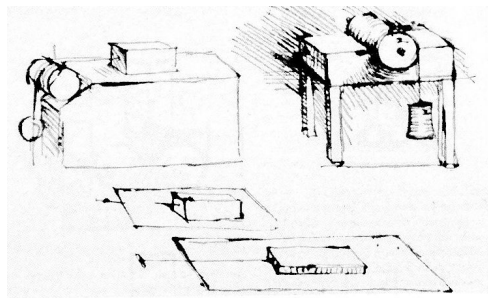


Figure 5.1: Various tribological experiments suggested by Da Vinci [16]

Although the science of tribology has been studied intensively and can be dated back to the early Renaissance, it remains a subject of great empirical influence. The fundamental laws of friction, lubrication and wear are very complex and as of today no governing rules have been established that connects these quantities in an explicit way. Some general statements can be made of the interdependent of surface roughness, lubrication choice, surface wear and friction, but by and large tribological effects remain an empirical trade.

In literature, a large number of experiments have been conducted in order to uncover the nature of tribological conditions. Most often in these experiments friction and wear

becomes the outgoing parameters of study, while surface topography and lubrication conditions constitute the ingoing variables to be optimized. This observations also holds for tribology in metal forming where there is a quest for lowering friction and wear through deliberate design of tool surfaces and application of advanced lubricants.

5.1 Friction in Metal Forming

The friction conditions at the tool-material interfaces greatly influence the material flow, formation of surfaces and stresses acting on the tool system. Further, high friction normally also leads to higher energy requirements and have impact the achievable lifetime of the forming tools.

The frictional conditions of metal forming can be categorized into three lubrication scenarios [63]:

Dry In dry condition no lubricant is applied in the interfaces between the work piece material and the forming tools. Dry lubrication condition includes cases where oxide layers or solid surface coatings might act as intermediate- or separation layer between die and material. In general very high friction is seen for dry lubrication conditions, making it suitable for a limited number of forming operations where high friction is desirable. Application of dry lubrication condition can be found in hot rolling of slabs or for nonlubricated hot extrusion of aluminium alloys.

Boundary lubrication is the case where a thin solid film with a strong physical or chemical adhesion prohibits direct contact between die and work piece material. The film often consists of organic matter but may also be solid surface coating such as cobber, zinc, etc. Typical values of coefficient of friction in this regime is $\mu = 0,1-0,3$.

Mixed-layer lubrication is the most common lubrication condition in metal forming. In this case the interface between the die and work piece material is often modeled as a hybrid of dry lubrication condition and hydrodynamic lubrication with pressurized lubricant pockets. Boundary lubrication does not lend itself to reliable analysis. As a consequence hereof, most of the knowledge of metal forming lubrication is empirical. Expected values of coefficient of friction in the mixed-layer case is $\mu = 0,03-0,1$.

Hydrodynamic or full-film lubrication conditions exists when a thick layer of lubricant is present between the forming die and the work piece material. In this case the friction is dictated by the viscosity of the lubricant and the velocity of the forming operation. The viscosity of most newtonian fluids decrease rapidly with increasing temperature, meaning that hydrodynamic lubrication conditions only can exist within a limited temperature window. However, the full-film regime also includes MoS₂ and graphite based lubricants which are stable at elevated temperatures. Values of friction in the case of full-film lubrication is very low, typically $\mu < 0,03$

Several friction models have been proposed during the years of research but in metal forming two predominant models are applied:

The Coulomb friction model is the classical model incorporating the observations of early friction research. In the Coulomb model the friction shear stress f_s is expressed as:

$$f_s = \mu p \quad (5.1)$$

, where μ is the *dynamic coefficient of friction* and p is the compressive normal stress at the interface.

The Coulomb friction model is readily applicable in cases with small to moderate normal pressures, such as sheet metal forming or bending operations. For high normal pressures, the shear friction from the Coulomb model can exceed the shear stress of the work piece material. The behavior is not physical and therefore a friction model incorporating the shear stress of the work piece material is introduced.

The *constant friction model* the *sticking friction model* or *Tresca friction model* is expressed as follows:

$$f_s = mk \quad (5.2)$$

where k is the shear strength of the work piece material and m is the friction factor belonging to the interval $0 \leq m \leq 1$. In the constant friction model, the friction factor m dictates the amount of stiction occurring at the interface between die and work piece. For $m = 0$ no stiction is present and the material flows without frictional drag. When $m = 1$ the friction stress is equal to the force required to achieve shearing of the work piece material.

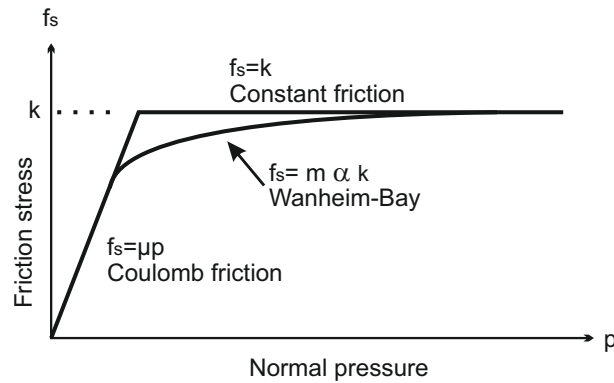


Figure 5.2: Illustration of the relation between the Coulomb- and constant- and Wanheim-Bay models friction behavior.

The rough transition between the Coulomb and the constant friction models is not physical, meaning that in reality an intermediate regime exists where predictions from the Coulomb friction model is approaching that of the constant friction model. The Wanheim-Bay model incorporates the intermediate regime through the introduction of the function α_{RC} . The α_{RC} -function models the influence of the ration between the apparent and the real area of contact through a special slip-line theory and a simplified repeated triangular model of the surface topography. The relation between the Coulomb, constant and Wanheim-Bay friction models are illustrated in Figure 5.2.

$$f_s = f \alpha k \quad (5.3)$$

The Wanheim-Bay friction model has later been extended to incorporate the flattening of the surface asperities during forming [64].

Even though the more advanced friction models have been proven to more accurately model friction behavior in some metal forming operations, the Coulomb friction model is still the dominating model of choice in sheet metal forming. The constant friction model is de facto standard in bulk metal forming, with exception of special cases.

The following list outlines typical values of the friction factor m to be expected in various bulk forming operations [18]:

- $m = 0,05$ to $0,15$ in cold forming of steel, aluminium or copper, using phosphate-soap lubricant or oil based lubricants.
- $m = 0,2$ to $0,4$ in hot forming of steel, aluminium or copper utilizing graphite based lubricants.
- $m = 0,1$ to $0,3$ in hot forming of titanium and other high-temperature alloys using glass based lubricants.
- $m = 0,7$ to $1,0$ for dry condition in rolling application or extrusion of aluminium

More information of recommended choice of lubricants and lubrication procedure can be found in literature [18, 65].

5.2 Micro tribology and Micro friction

Micro tribology is the subcategory of tribology dealing with interaction of surfaces of micro sized components. As mentioned in the earlier section on size effects, the laws of friction and lubrication are impacted by size effects when the process is scaled. The main reason for this shall be found in the underlying surface roughness, or surface asperities, which only scales to a certain extent. This means that the relative surface roughness of a micro component will be higher compared with macro size. However, the main parameter of interest in bulk forming is friction. Friction is dependent on surface load, lubrication and surface characteristics; including surface roughness. Amontons law of friction dictates a linear dependence between load and friction force: $F_f = \mu N$, where F_f donates the friction force and μ is the friction coefficient and N the load measured in newton. It can be noted that the friction force is independent of contact area, something that was later proven by the Bowden and Tabor adhesion theory of friction. Here the friction force F_f is expressed at the product of the effective shear stress, donated $\bar{\tau}$, and the sum of the asperities areas in contact: $F_f = \bar{\tau} \sum A_{asp}$. In bulk forming, the friction factor m is often established on basis of conducted experiments and there is seldom an explicit formulation for this quantity. The double cup extrusion test (DCE-test) is a recognized way of establishing the friction coefficient experimentally. A number of micro scaled DCE-tests have been carried out by Tiesler and it was found that the measured friction coefficient depends on the scale of the experiment [17]. It was further found that the friction coefficient would increase by a factor of 20 when the experiment was scaled by a factor of 8, going from a cup diameter of $4mm$ to $0.5mm$. According to Tiesler, this is due to the fact that for micro scale surfaces, more surface asperities reside close to the

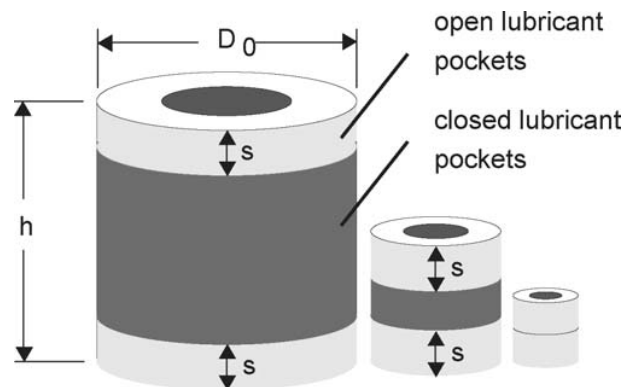


Figure 5.3: Illustration of the influence of the open- and closed lubricant pocket theory when scaling the process to micro size [17].

boundaries of the workpiece where they are less likely to form lubricant pockets under hydrostatic pressure. This influences the surface contact area, leading to an increase in friction force, as observed from the Bowden and Tabor adhesion theory of friction. Figure 5.3 illustrates the reduction of the pressurized closed lubricant pocket area of the double cup test, as the scale of the experiment is reduced. More studies of friction behavior when downsizing can be found in references [31, 66].

The influence of the increase in friction coefficient, when working in the micro size domain, brings about challenges for handling and ejection of the bulk formed micro components. Recapitulating on the increase of the surface to volume ratio, by the scaling factor λ , it is clear that the relative surface contact area of a micro component is large. This leads to increased friction, according to Tiesler and the Bowden and Tabor adhesion theory of friction. Further, the relative material volume of a micro component is decreased, thereby lowering the overall mechanical strength of the workpiece. These two opposing effects, the increased friction and lowered structural strength of the component, signify that attaining low friction is a key challenge in micro bulk forming.

Figure 5.4a illustrates a simulation of a pre-form for component to be manufactured by micro bulk forming. In this case the lower pin extrusion with a diameter of about 0,5 mm must be able to withstand the total friction force during ejection. If the friction force is greater than the yield strength of the component the pin will collapse and reverse forming will occur. The picture in Figure 5.4b visualizes an example of reverse forming of the component. This component is the realization of the simulation illustrated in Figure 5.4a, where the forward rod extrusion has collapsed during ejection. The problem was later resolved by a reduction of the press load, change of lubricant and polishing of the forming die. The use and application of lubricants for micro bulk forming is at present time not very well researched. In conventional bulk forming phosphate coated and soap lubrication has been the lubricant of choice for several decades. Unfortunately this lubricant is unsuitable for micro bulk forming due to the chemical properties of the lubricant layer, only allowing down scaling to a very limited extent.

In the example discussed above and other micro bulk forming experiment at ambient temperature, the use of a commercial silicone paste showed good results in this project.

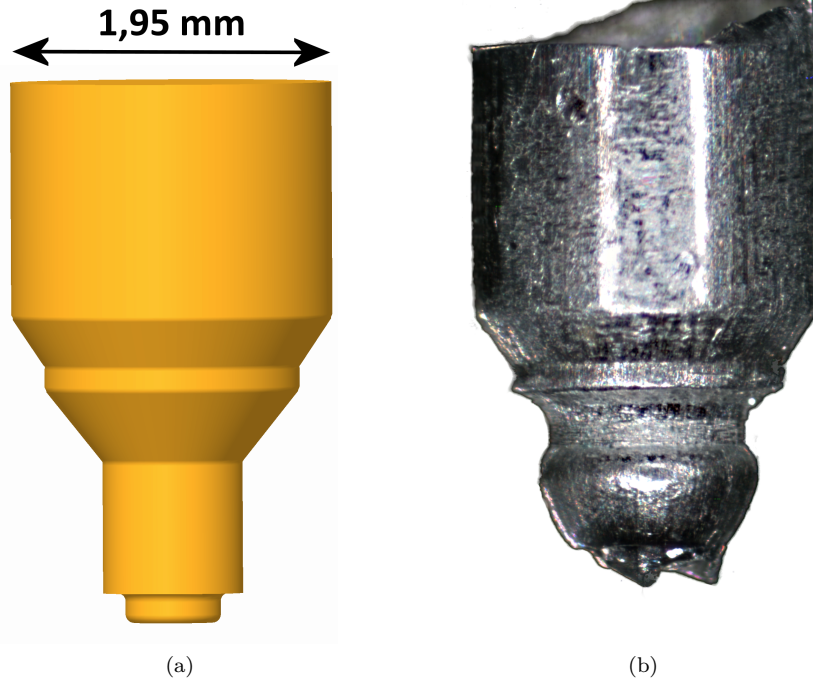


Figure 5.4: (a) 3D simulation of pre-form for a micro axle. (b) Photo of the formed component where unwanted reverse forming have occurred during ejection from the forming die

However, the application and removal of the lubricant as well as unintended confinement of lubricant in the forming die has been identified as challenges. For warm forging and forming of bulk metallic glasses a commercial sprayable lubricant based on Molybdenum disulfide (MoS_2) was utilized. This lubrication approach worked fairly well and is suitable for forming at elevated temperatures. A drawback of utilizing a MoS_2 based graphite lubricant is the undesirable integration with the workpiece surface. This will leave a dark-colored, rough surface which is difficult to clean and is generally unsuitable for use in any advanced or medical applications.

5.3 Tests for Evaluation of Tribological Behavior

In many forming operations the performance of the lubricant is the most dominant influencing factor on friction. In order to qualify lubricants a number of friction tests have been proposed to measure the influence of surface topography and lubrication on friction. According to Bay [19] these large numbers of suggested forming tribology tests can be divided into two main categories:

- Simulative tests
- Process tests

where process tests are characterized as tests applying typical metal forming operations without changing the basic process kinematics, whereas simulative tests are tests modeling the tribological conditions in metal forming processes with the attempt to study friction and/or lubrication in a specially controlled way [19].

Process tests

Two of the most commonly encountered process tests for accessing tribological effects in bulk forming processes are the *Ring Compression Test* and the *Double Cup Extrusion test*. The ring test is the simplest test of the two and involves upsetting of a ring shaped specimen between two planes. The friction between the press planes and the ring specimen is quantified through measurement of the decrease of the internal diameter of the ring. Figure 5.5 illustrates the case of low and high friction in the ring test. In case of

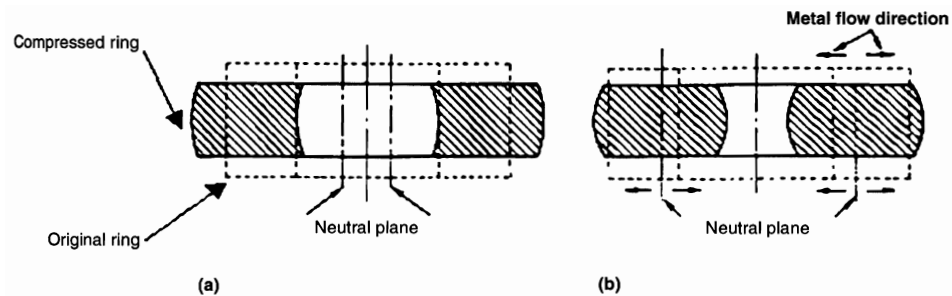


Figure 5.5: Metal flow in the ring compression test. (a) Low friction. (b) High friction [18]. The position of the Neutral plane, geometrically dependent on friction, will determine if the internal diameter of the ring will grow or shrink.

low friction (a), the material will flow radially outwards, thereby increasing the diameter of the outer and inner diameter. When high friction is present, the ring material will 'stick' to the face of the upsetting plane causing the material flow to change and the ring will bulge. The buckling of the ring leads to a decrease of the internal diameter of the ring. By calculating the percentage reduction of the internal ring diameter and holding this value against theoretical calibration curves, friction parameters can be estimated with good accuracy.

The ring compression test holds a number of characteristics making the test simpler to execute than other tribological process tests. The test is independent of the flow stress of the work piece material, meaning that the same theoretical calibration curves can be regarded as universal across several materials, as long as the aspect ratio of the ring specimens are kept constant. It further means that the load on the press utilized for compression must not be calculated prior to the experiment. Note however that the ring compression test is not insensitive to different strain hardening behaviour, expressed as the material model exponents n , meaning that often tailored calibration curves are obtained using finite element simulations prior to the ring test. Typical surface expansion ratios of the ring compression test is about 100%, making it suitable for friction assessment of light to medium deformation operations. This is also the reason that ring test is recommended as friction test for sheet forming operations.

The Double Cup Extrusion test (DCE-test) is an alternative test for quantifying frictional

behavior in metal forming processes exhibiting medium to severe plastic deformation. The test was proposed by R. Geiger and later advanced by Altan [67]. The double cup extrusion test works as outlined by the sketch in Figure 5.6. Through simultaneous forming of a backward can extrusion and a forward can extrusion, the DCE-test is able to quantify the friction along the die container wall.

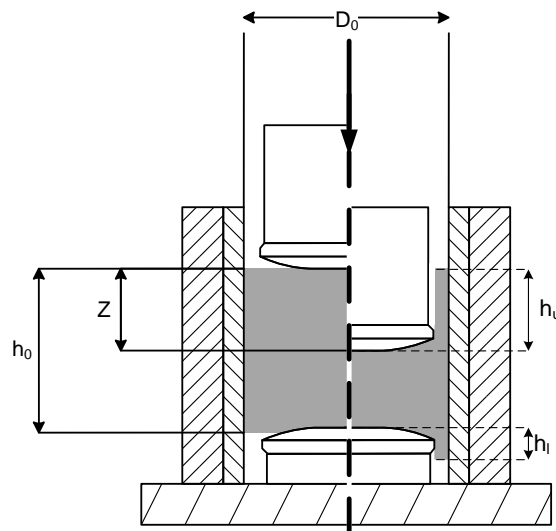


Figure 5.6: Illustration of the Double Cup Extrusion test.

The friction is measured through the relative cup height ratio h_u/h_f , as this ratio is greatly influenced by the friction along the container wall. The two limiting cases are: for infinite friction the material is only able to flow backward, giving rise to the forming of a backward can only - in which case the cup height ratio will be large. In the case of low friction, the forward- and backward cans will be equal in height, thus giving rise to a cup height ratio of one.

As in the case of the ring compression test, the cup height ratio from the DCE-test will have to be compared against theoretical calibration curves to arrive at a friction factor. However, the calibration curves for the DCE-test are sensitive to the material strain hardening exponent n , meaning that each calibration curve must be tailored to the work piece material in question. The calibration curves for the DCE-test are normally constructed through a series of finite element analysis, where the simulation parameters are chosen to replicate the forming process as accurately as possible. Figure 5.7 shows a calibration curve extracted from FEM simulations of the DCE-test of a low alloyed steel cold forging steel (C8C or Ma8). Depending on the nominal area reduction during forming and the work piece material parameters, surface expansions up to 500% surface expansion ratio and surface pressures up to 2000 MPa can be noted. Owing to the process values, the process conditions of the DCE-test are better at mimicking typical cold forging processes conditions when compared to the ring compression test [18].

Equation 5.4 expresses the areal reduction ratio of the double cup extrusion test. By altering the relative diameter of the billet and the punches, the pressure at the container wall can be adjusted. A high reduction ratio gives rise to high pressures along

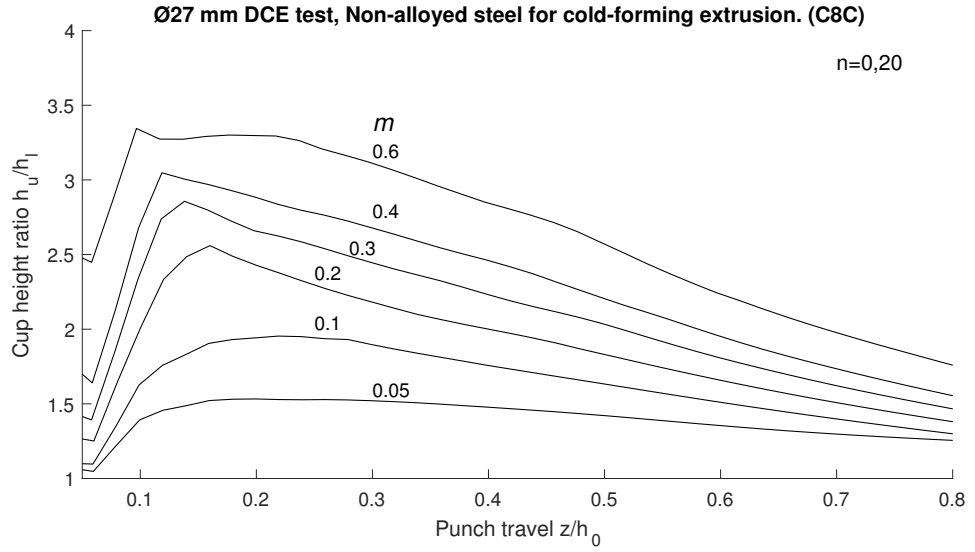


Figure 5.7: Calibration curves for DCE-test of C8C material with moderate strain hardening tendency $n = 0, 20$. The curves were generated through a number of simulations using the DEFORM commercial FEM code. The simulations were conducted assuming a plastic material deformation model and a 10.000 nodes grid.

the container wall and greater surface expansion.

$$r = \left(\frac{D_i}{D_o} \right)^2 \quad (5.4)$$

, where D_i and D_o is the diameter of the punch and billet respectively.

Sensitivity of the DCE-test towards the influence of friction is generally increased with reduced reduction ratio and reduction of the strain hardening exponent of the workpiece material (n -value). As such, the choice of reduction ratio represents a trade-off between high surface expansion and surface pressures and the sensitivity of the DCE-test towards frictional influence [68].

The relative punch travel is given by equation 5.5.

$$\frac{z}{h_0} = \frac{h_0 - (h_{tot} - h_u - h_l)}{h_0} \quad (5.5)$$

From the ring compression test and the double cup extrusion test, which may be categorized as process tests, we will now turn the attention to some general concepts for simulative tests of frictional behavior.

Simulative tests

The group of simulative tests are types of test that target specific parameters in a forging process. These types of test do not necessarily mimic the actual conditions of the forming process, but often focuses on a single parameter to be evaluated. Simulative tests often allow a wider window of evaluation for the process parameters, meaning that higher pressures, longer stroke lengths or easier visual access can be provided.

A number of concepts for simulative tests for evaluation of friction and lubrication behavior is shown in Figure 5.8 [19]. These tests each have characteristics making them suitable for evaluation of certain processes and process parameters. As an example the G1 process is extensively applied in the form of a strip drawing test, where the interaction between material, surfaces, lubrication and friction on the pick-up or galling of the workpiece can be easily evaluated over long drawing lengths.

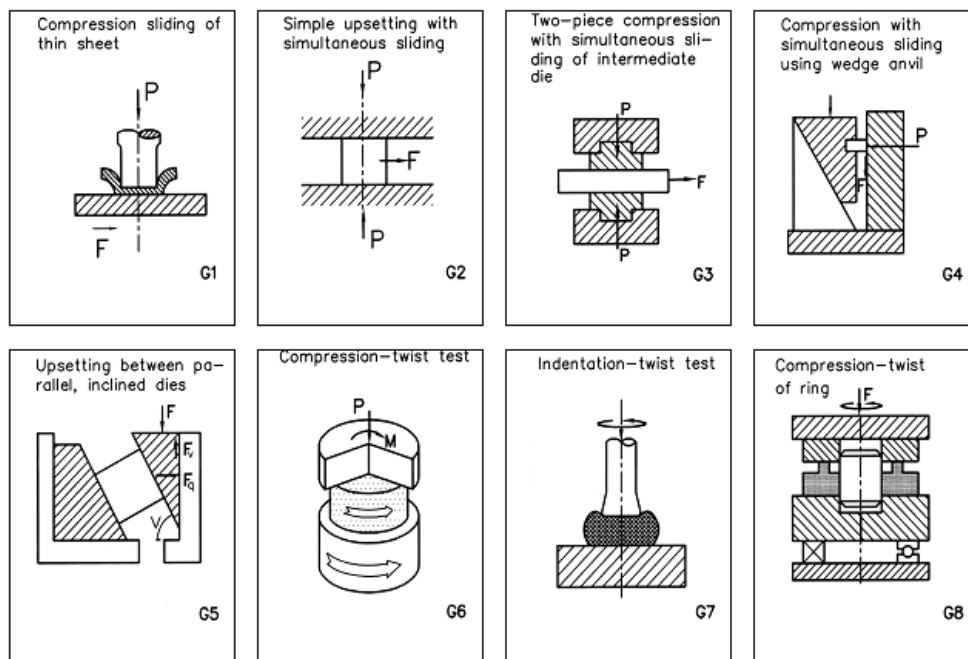


Figure 5.8: Simulative tests with global plastic deformation by upsetting [19].

Later in this chapter, a number of micro friction tests are conducted on a special equipment applying the methodology G3 from Figure 5.8. In the G3 test, two pieces of a work piece material is compressed on each side of a tool element. By continued application of compression force, while transversely pulling the rigid tool element, the friction shear stress can be determined. By applying enough compression force the work piece material can be upset against the tool surface thereby imitating the surface interaction commonly encountered in metal forming processes.

5.4 Macro scale double cup extrusion tests

In order to investigate the influence of the surface roughness on the friction parameter, a number of double cup extrusion tests were carried out at macro scale. The purpose of the investigation was to study whether the structure of the tool surface had any significant influence of the friction during forming.

A preliminary small scale investigation was planned, including the manufacture of three dies with different surface finish. Two of the dies would be polished on a novel robot assisted polishing machine whereas the forming surface of the third die would be machined using wire-EDM technology.

State of the art within polishing

The polishing and lapping processes are among the oldest manufacturing processes known and are still widely used today. Polishing normally takes place as a finalization procedure, giving the manufactured component the desired surface finish. Depending on the application, polishing of surfaces is important to satisfy optical or roughness or functional demands on the surface in question. Lapping and polishing is today used in as different applications as tool manufacturing, alignment of reading heads for hard drives, semiconductor manufacturing and fine tuning for optical components.

Despite the wide employment of the technology no good predictive process models exist within literature [69]. Several papers have discussed general guidelines and provided technological overviews [?, 70, 71], but no general applicable models have been suggested. The abrasion/wear-based Preston's equation (5.6) is generally able to predict the polishing process accurately, but is often referred to as the starting point for new or alternative process models.

$$MRR = K_p P_0 V \quad (5.6)$$

, where MRR is the material removal rate, P_0 is the down pressure, V is the relative velocity between the polishing substrate and the workpiece, and K_p is a constant representing the effect of other remaining parameters,

A typical polishing process consists of an interaction of four basic elements. Some authors refer to the polishing system as a *three-body abrasive processes*, typically counting the polishing paste as one element. The work piece is the part that is going to be polished. Depending on the surface- material, micro characteristics and general topography and the desired surface finish after polishing, a certain amount of material needs to be removed. This is achieved by applying a polishing paste on top of the workpiece. The polishing paste consists of a carrier fluid with embedded granular particles. Finally, the lap is the moving part that excites the polishing process. The lap can either be a rigid part or a plate with a pad attached. The four basic parts of a typical polishing system each have several degrees of freedom, making it an extremely complex system to describe mathematically [72]. Some general observations regarding granule-size versus material removal rate can be stated when looking at the basic kinematics of the system, observations that have been experimentally verified [73]. The polishing and lapping process is often accomplished as a manual operation, even in industrial environments with a large numbers of blanks to be polished. The operator carries out the polishing procedure while visually determining when to change paste or conclude the operation.

This visual inspection is subjective to some extent and differs among the different operators.

In conclusion on the small review above, there seems to be a need for a new polishing tool that can reduce the large degree of freedom in the polishing process, eliminate subjective inspection methods and tame the unpredictable outcome of the manually operated polishing operations.

Polishing by Strecon RAP

The Strecon Robot Assisted Polishing (RAP) is a prototype machine intended for predictable and repeatable polishing of macro size rotational symmetric specimens with simple geometry. Compared to traditional manual polishing, the RAP machine offers the possibility to polish specimens with a high degree of predictability and repeatability. Where the manual polishing involves a degree of randomness, the machine assisted polishing is executed explicitly according to the loaded polishing program.

In short, the RAP machine consists of a rotational stage, as known from turning lathes, and a generic 3-axis robot arm. A stage, for application of sinusoidal vibrations and polishing pressure, is mounted on the tip of the robotic arm, see Figure 5.9. Through a

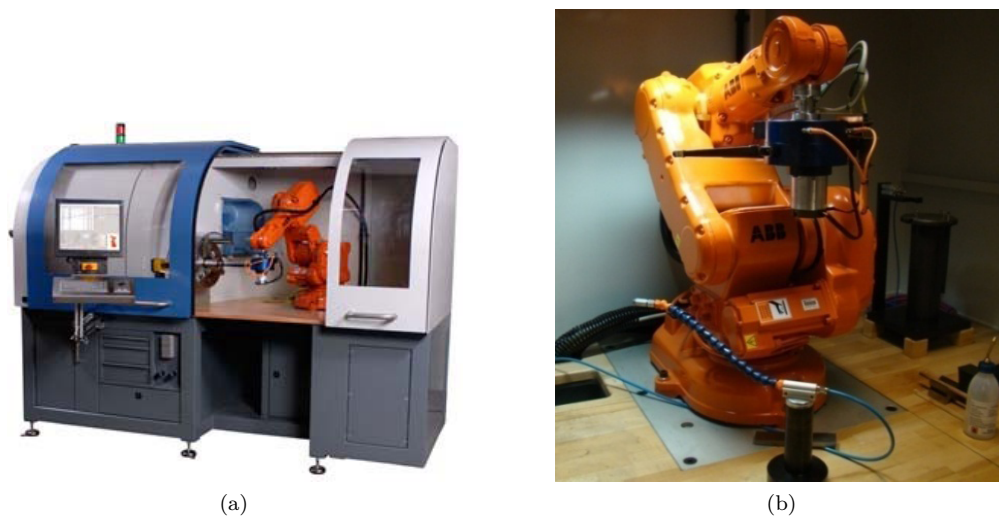


Figure 5.9: Photographs of the RAP polishing machine (a) and the general purpose robotic arm carrying out the movement of the polishing substrate (b).

simple CAM interface, the user specifies the envelope geometry, rotational speed of the specimen, the pressure applied between the polishing substrate and the specimen and the frequency of vibration of the polishing arm. The user further has to mount the right polishing tool and paste, according to the chosen polishing sequence.

The machine then executes the polishing program, one sequence at a time. The operator then changes the tool, applies the right polishing paste and cleans polishing debris from the specimen in-between every polishing step. The operator also visually inspects the

achieved polishing result and makes adjustments on the fly. Two of the elements of the three body polishing system in the RAP are shown in Figure 5.10.

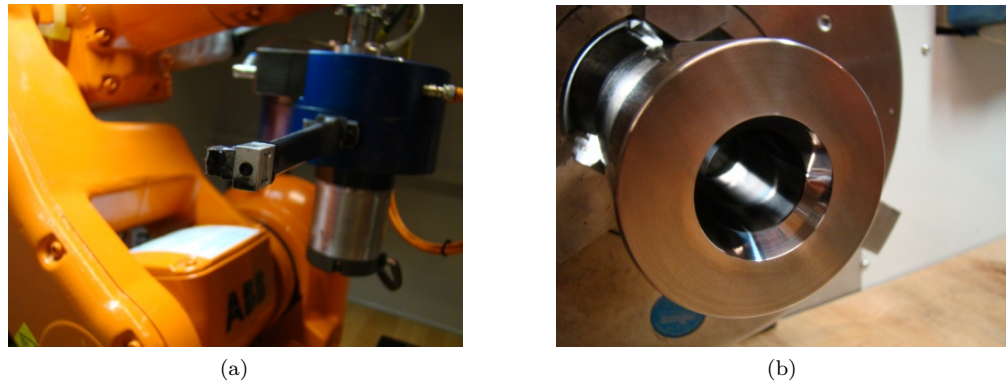


Figure 5.10: Close up pictures of the active elements engaged in the polishing process in the RAP machine.

Close up pictures of the active elements engaged in the polishing process in the RAP machine. (a) shows the tip of the polishing tool, in this case mounted with a plexiglass substrate. (b) is the workpiece to be polished. Note the internal lighting for easy visual assessment of the polishing result.

All known polishing substrates can be utilized in the RAP polishing process, including ceramic polishing, stones, hard wood, plexiglass and cloth. The polishing substrate is paired with a polishing compound containing abrasive particles.

An added benefit of polishing by the RAP machine is the possibility of tailoring surface characteristics of the specimen. Groves for storage of lubrication can be created through a rough grinding of the surface followed by selective polishing. By the application of a robot assisted polishing technique, a homogenous surface structuring can be guaranteed.

Polishing of dies for double cup extrusion test

A drawing of the final geometry of the die for the macro sized double cup extrusion test is shown in Figure 5.11. The tapered outer envelope of the die is made to facilitate later press fitting in a strip-wound container manufactured by Strecon A/S.

In order to arrive at three different internal surface roughnesses, the three different dies are manufactured in different ways. All dies are cut to approximate dimensions and the tempered to a hardness of HRC 61. The respective dies follow the manufacturing procedure outlined below.

RAP 1 - blank polished The die is first press fitted in the strip-wound container and ground to the specified internal diameter. The die is then ejected from the strip-wound container and polished in the RAP machine according to the procedure outlined in **Appendix C**. This polishing procedure was designed to achieve as smooth a surface finish as possible.

RAP 2 - functional surface As in the case above, the die is pressed in the container, ground to nominal diameter, ejected from the container and polished in the RAP

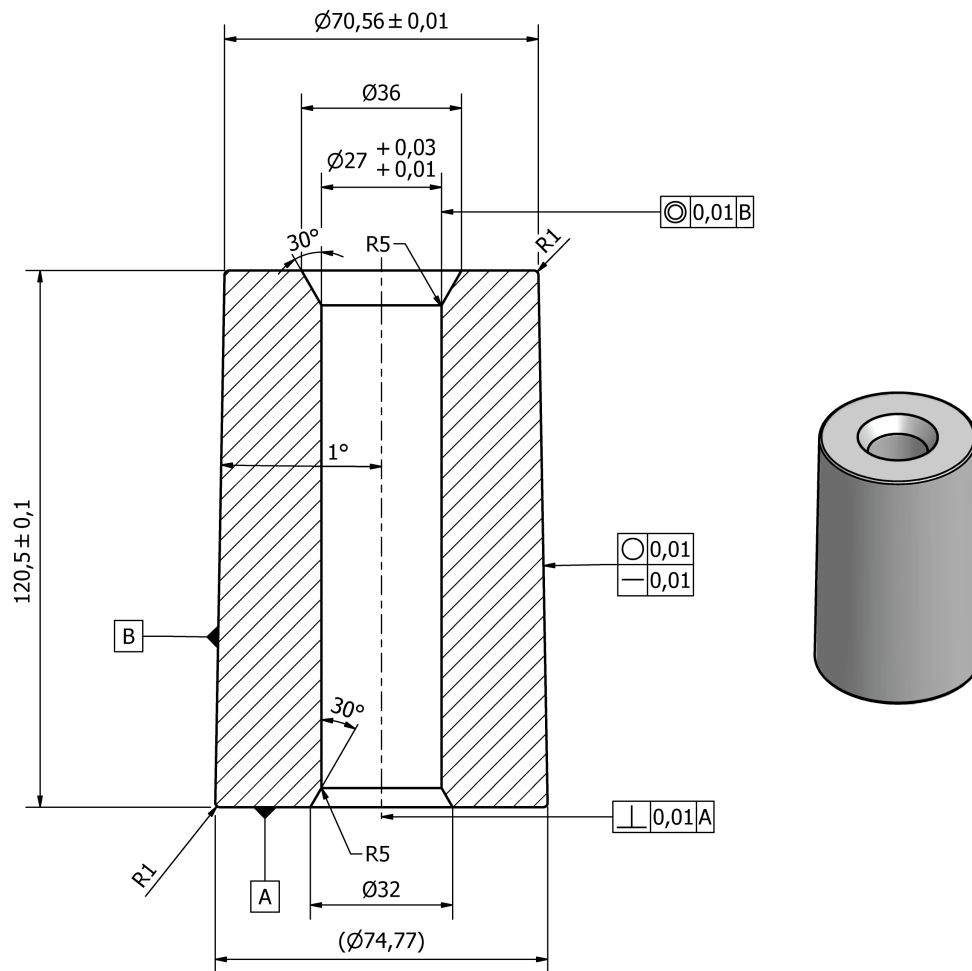


Figure 5.11: Technical drawing of the die for DCE-test.

Technical drawing of the die for DCE-test. The material is specified to Vanadis 4E, a High carbon-chromium tool steel equivalent to AISI D2, and the tool is hardened to HRC 61.

machine as outlined in **Appendix D**. In this case, the polishing time with the rougher polishing stones is shortened, meaning not all grooves from the grinding operation are fully removed. The intended effect of the polishing is that the residual grooves could create a helpful reservoir for lubricant entrapment.

EDM - micro blast The die is cut using a conventional wire cutting machine. The internal diameter is cut in a slightly conical shape in order to account for the uneven elastic deflection of the die, due to the difference in stiffness between top and bottom, when it is later press fitted in the stress-container. The number of wire passes was set to four, thereby realizing a surface roughness of $R_a = 0,12 \mu m$. The die is then micro blasted with two different types of boron nitride abrasive particles, a popular finishing treatment following EDM machining. The die manufactured using EDM will serve as reference surface in the DCE-test. The details are reproduced

in Appendix B.

Characterization of the die surfaces

The internal surfaces of the manufactured dies were characterized using a stylus roughness profilometer from Taylor Hobson. The equipment features a standard uncertainty of $\pm u_{equip,stylus,rough} = 0,026\mu m$ for the average roughness (R_a) and $u_{equip,stylus,rough} = 0,087\mu m$ for the average maximum height of the profile. The uncertainty of the measurement equipment was estimated using a calibrated roughness artefact with a R_a value of $0,606\mu m$. The roughness value of the calibrated roughness artefact is considerably higher than expected for the measurement of the tool specimen surface, which is expected to be at least one order of magnitude lower. It is therefore suggested that the roughness measurements will serve as indicative measures of the relative roughness between the manufactured specimens, rather than an exact absolute measure of the roughness values.

The 3D roughness measurements were acquired with an acquisition length of $400\mu m$ and $200\mu m$ in the X- and Y direction respectively. The spacing between the data points was $1\mu m$ and $2\mu m$ for the X and Y coordinates respectively, giving rise to a total of 4000 data points pr. specimen.

The roughness parameters of the three specimens are visualized in Figure 5.12. The measurements are taken as the average of three profile measurements and the confidence interval is based on 95% coverage of the estimated uncertainty of the roughness profilometer. Though the specification of roughness parameters is widely used, the simple

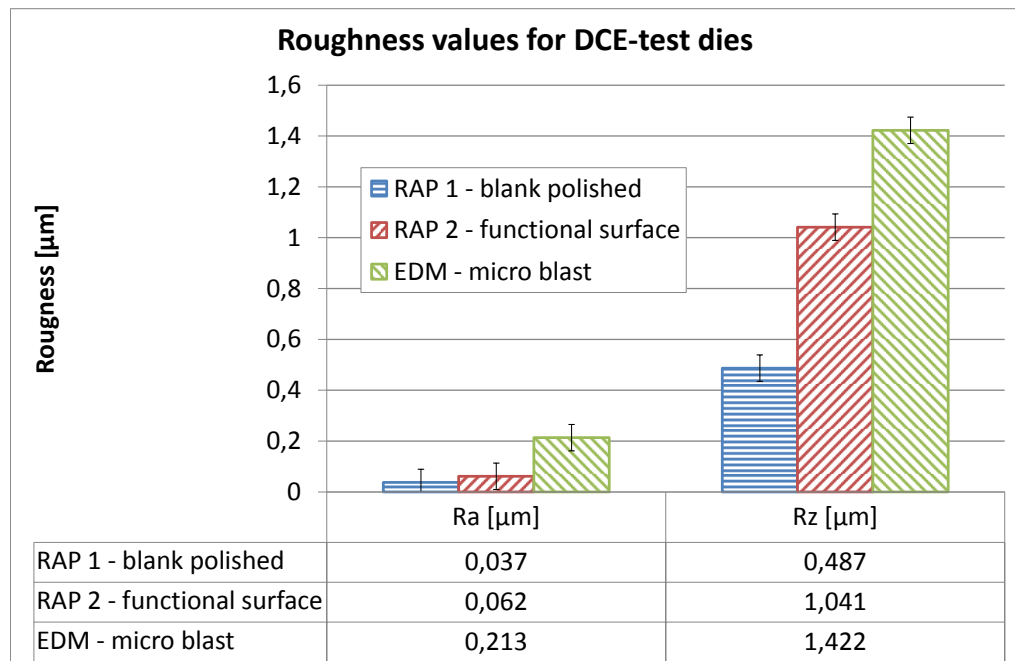
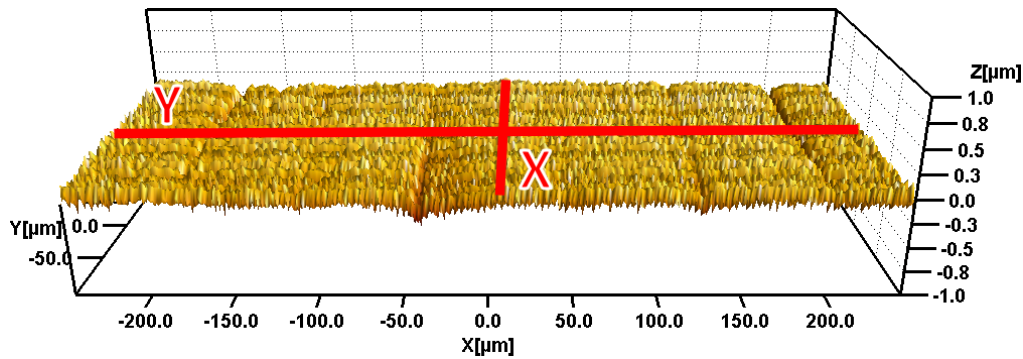
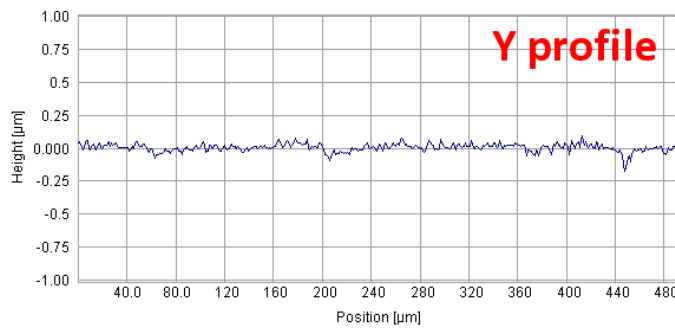


Figure 5.12: Measured roughness values of the three manufacture dies. The confidence interval indicated is with 95% taken from the uncertainty estimation of the roughness stylus profilometer.

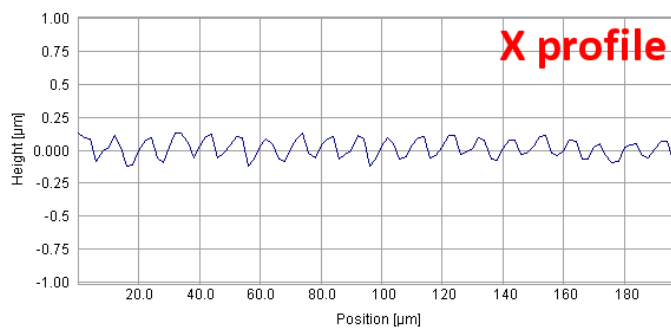
representation of a few parameters describing the surface characteristics is not adequate in the case of functional and tailored surfaces. In order to visually observe the course of the surface envelope, a number of 3D plots and 2D profiles have been produced. The 3D and 2D plots for the *RAP 1-blank* surface is shown in Figure 5.13. In order to filter out the geometrical distortions of the roughness profiles that are due to the curviness and alignment of the specimen, the measurement values have been corrected using a global polynomial filter of second order.



(a)



(b)



(c)

Figure 5.13: Visual representation of the RAP-1 die surface.

Visual representation of the RAP-1 die surface. The surface has been globally corrected using a polynomial filter of first order. The profile plotted in (b) is extracted along the longitudinal direction of the profile, while (c) is taken in the transversal direction.

It can be noted that the surface is very flat with no major valleys or peaks. The roughness of the profile plots 5.13b and 5.13c seems to be distinct, but this can be attributed to the measurement and filtering methods used.

Figure 5.14 shows the 3D and 2D profile plots for the die *RAP2 - functional* polished die. Here a deep indentation is observed with a depth of about $1\mu\text{m}$. This indentation is a remainder from the grinding operation that purposely has been left during the polishing operation. The indentation is intended to serve as a pressurized lubricant buffer. The indentation is repeated with a periode on about 1 mm in the Y-direction, as can be noted from the detailed roughness profiles in Appendix D. Apart from the indentation, the remaining surface roughness is comparable to the that of the *RAP 1- blank* die.

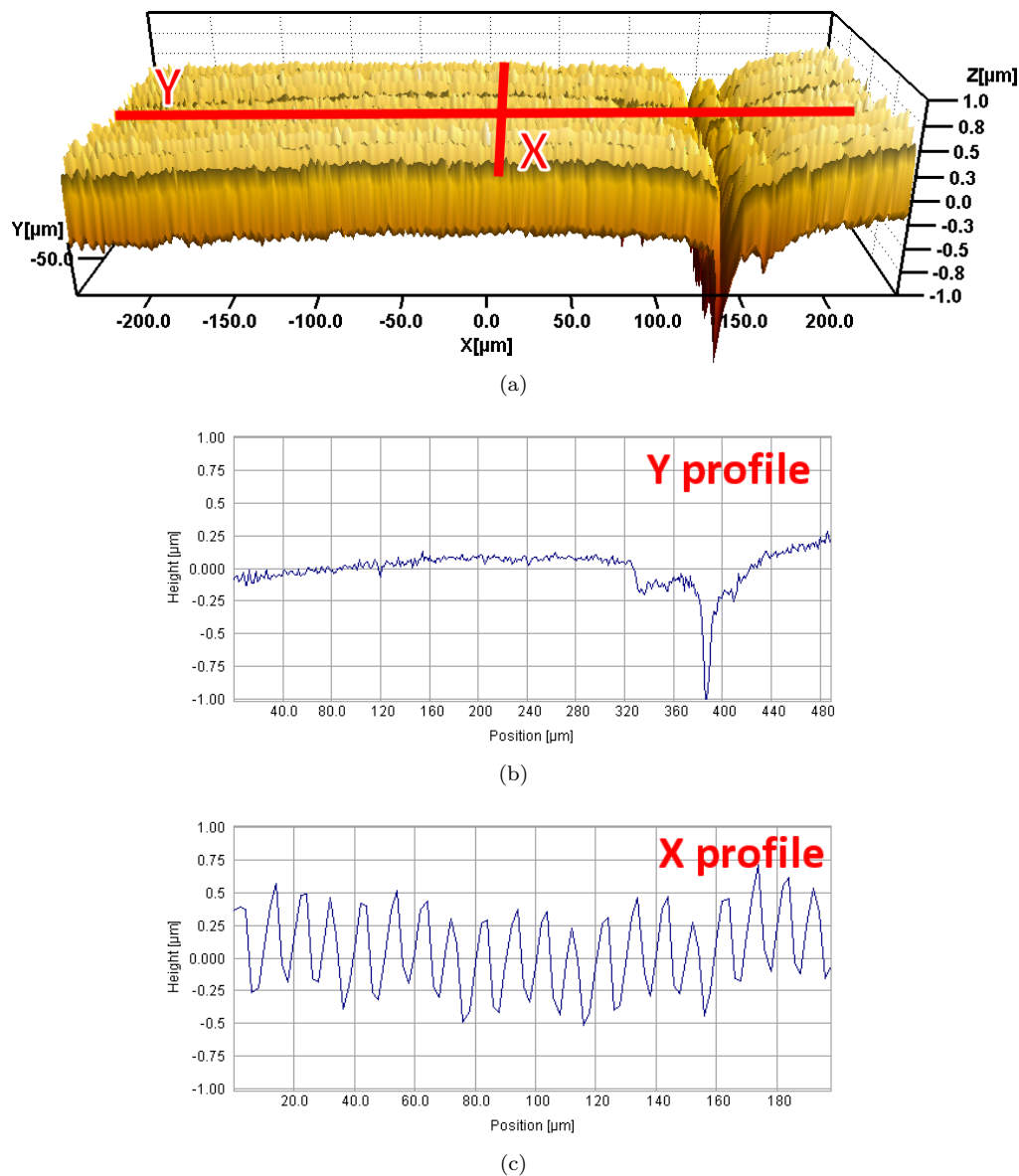


Figure 5.14: Profiles of the die finished with the RAP 2 -functional surface. (b) is extracted along the longitudinal direction of the profile, while (c) is taken in the transversal direction.

The third die, *EDM - micro blast*, exhibits a higher roughness compared to the polished dies. The surface topography is randomly distributed due to the electro discharge machining process.

Concluding on the surface characteristics of the three dies for the DCE-test; three distinct surface characteristics have been successfully created. The first die features a surface with a flat envelope and a fine surface finish. The second die surface features marks or

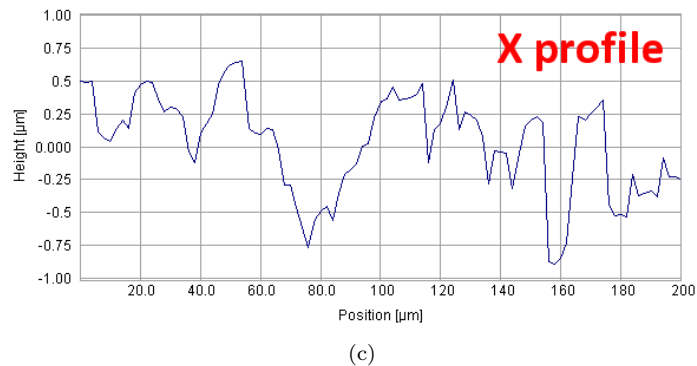
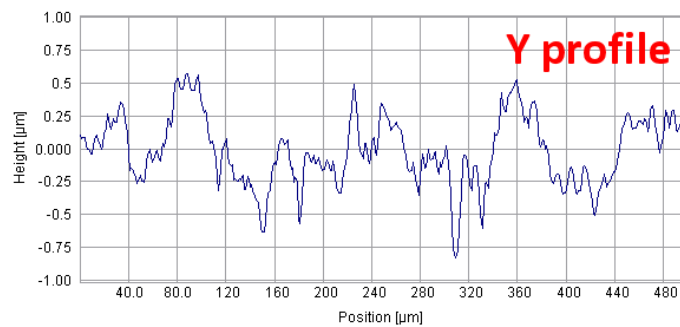
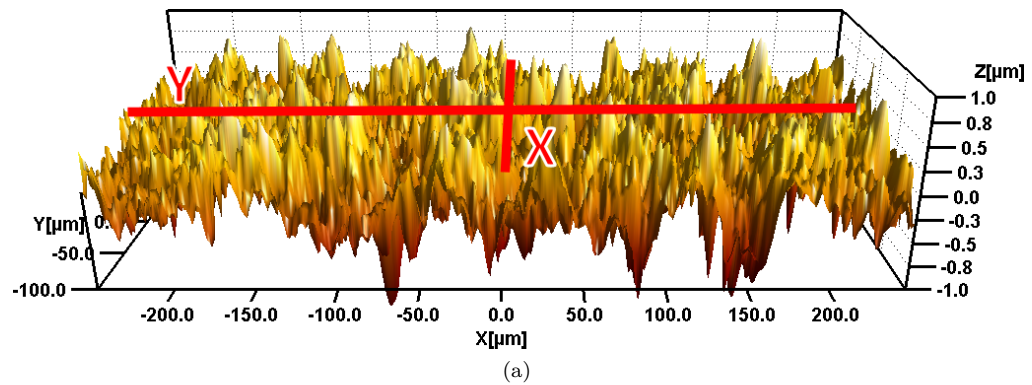


Figure 5.15: 3D and profiles of roughness surface from the die finished with the wire EDM process. (b) is extracted along the longitudinal direction of the profile, while (c) is taken in the transversal direction.

indentation for active entrapment of lubricant and the third surface features a random distribution and relative high roughness.

Experimental setup

Before testing the frictional behavior of the individual dies, the remaining parameters of the experiment will be established.

The upper and lower punches were already available from former experiments. The important tip geometry of the punches have been designed according to the recommended guidelines given by the International Cold Forging Group [20]. The specific details of the punch tip design can be noted from the technical drawing shown in Figure 5.16. With

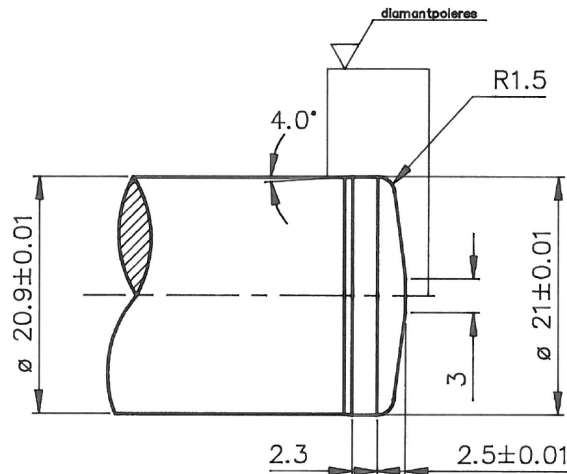


Figure 5.16: Drawing of the punch and ejector geometry in accordance with the general guidelines outlined by ICFG [20].

a punch diameter of 21mm and an inner diameter of 27mm the area reduction ratio is 60% as calculated by equation 5.4.

The work piece material is St C8C (also known as St Ma8) having a yield stress of about 520MPa. The material stress-strain curve, taken from literature, is shown in Appendix A.

With the chosen workpiece material and the reduction ratio of 60 % and a friction factor of $m=0,3$, the internal normal pressure is around 1200MPa according to simulations.

The billets to be formed were cut to an aspect ratio of 1:1 and phosphate surface coated and soap lubricated by an external partner.

The double cup pressing is done by a hydraulic press from the Swedish company Lagan Press. The Lagan Press is capable of punch forces up to 250 tons and is equipped with four cylinders (two at the top and two at the bottom). The four cylinder setup makes it possible to mount two punches (one at the top and one at the bottom) including ejectors.

A functional sectional drawing of the flexible tool and guiding system utilized in the pressing of the double cups are shown in Figure 5.17. The tool system was developed as a versatile and flexible system, incorporating short times for setting up in order to facilitate cold forging of smaller series of products [12]. The punch travel rate is about 10mm/sec and no force measurement instrumentation was available at the press.

A total number of 18 tests is conducted. For each die specimen a total of three tests pr. punch travel length is conducted. Each die is tested with a 40% and 60% punch travel

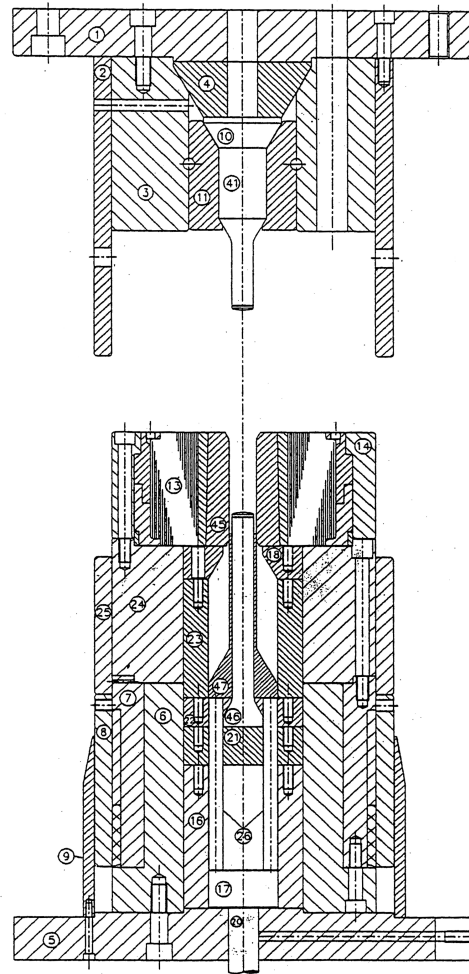


Figure 5.17: Tool system for double can extrusion [12]

length, giving rise to a total of 18 forging tests. The relation is specified in Table 5.2 below.

Die name	40 % punch travel	60 % punch travel
RAP 1 - blank	3	3
RAP 2 - functional	3	3
EDM - micro blast	3	3

Table 5.1: Indication of the number of DCE-test to be conducted.

Measurement of of Macro sized DCE-test specimens

To measure the cup height of the double cups a dial gauge from the company Sylac is used. The dial gauge is used due to the fact that it provides with an accuracy of $5 \mu\text{m}$ and is fairly easy to handle. The measurement setup is illustrated in Figure 5.18. To

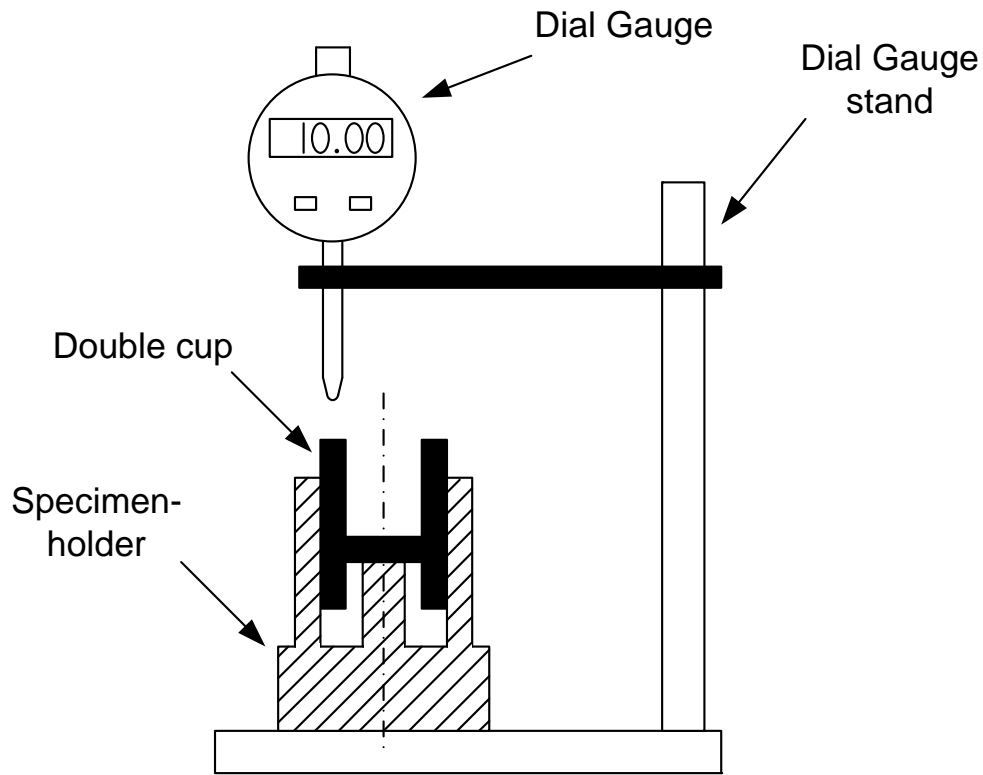


Figure 5.18: Sketch of the cup-height measurement setup

stabilize the cup during the measurements a specimen-holder is used. The bottom of the cup is balanced by the pin in the middle and the outer sides of the cup are supported by the internal sides of the cylinder (of the specimen-holder). In this way the outer sides of the cup is always kept perpendicular to the bottom plane of the specimen holder.

Since the result of the analysis is the quotient between the upper and the lower cup-height, the combined measurements uncertainty have to be evaluated including the influence of the relating function. The relating function is reproduced in Equation 5.7.

$$f = \frac{h_l}{h_u} \quad (5.7)$$

Now, the combined uncertainty of a general function relating several ingoing parameters and their respective uncertainties is given by Equation 5.8.

$$u_c^2(y) = \sum_{i=1}^N \left(\frac{\partial f}{\partial x_i} \right)^2 u^2(x_i) \quad (5.8)$$

Inserting and evaluating the partial derivatives, we arrive at:

$$u_c^2(y) = \left(\frac{1}{h_u}\right)^2 \cdot u_{h_l}^2 + \left(-\frac{h_l}{(h_u)^2}\right)^2 \cdot u_{h_u}^2 \quad (5.9)$$

However, when evaluating the complete influence of uncertainty contributions from temperature deviations, measurement procedure and equipment and relating function, the combined uncertainty is estimated to be below $\pm 10\mu\text{m}$. An uncertainty contribution of this magnitude is neglectable and will not be treated further in the analysis of the macro size specimens.

Results of the macro size DCE-test

The cup height measurement value of the conducted DCE-test are reproduced in Appendix H. The results of the double cup height ratio are plotted with the corresponding calibration curves in Figure 5.19. The calibration curves have been constructed from a range of FEM-simulations employing the constant friction model. Each subset of observations is indicated by averaging the cup height ratio of the three observations and the indicated confidence intervals are with a 95% convergence factor.

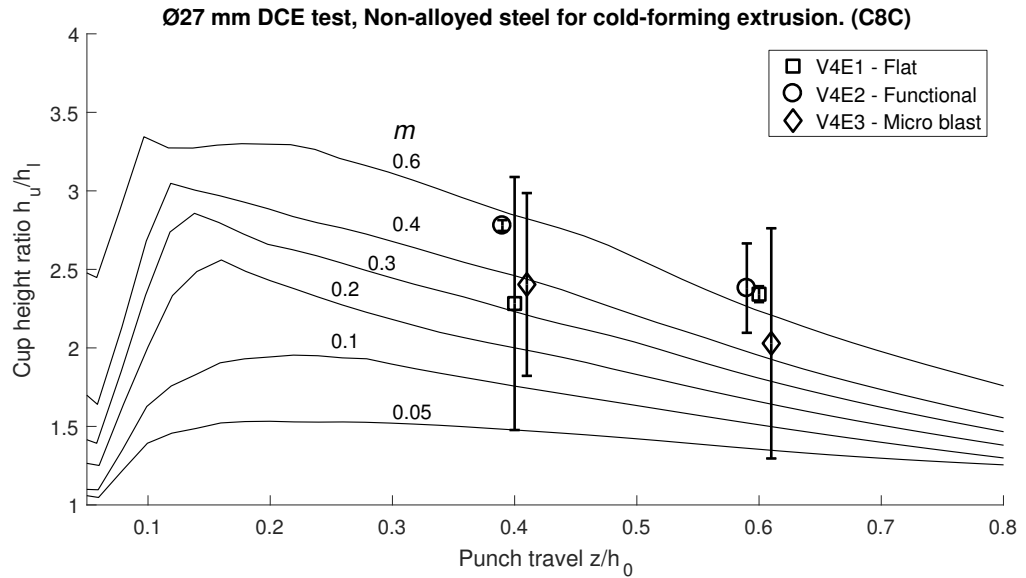


Figure 5.19: Results of the macro size double cup test. The indicated confidence interval is with 95 % coverage factor

It is clearly seen that the scatter of the measurement points is substantial. It is primarily due to a few outlier observations.

As a second result, a plot is made where the influence of the outlier observations is removed. This is done by allowing the manual removal of one observation out of three in each subset (die - punch travel). The resulting graph is shown in Figure 5.20. It can be noted that the cup height ratio results now meet in the diagram and that the confidence intervals have been narrowed down.

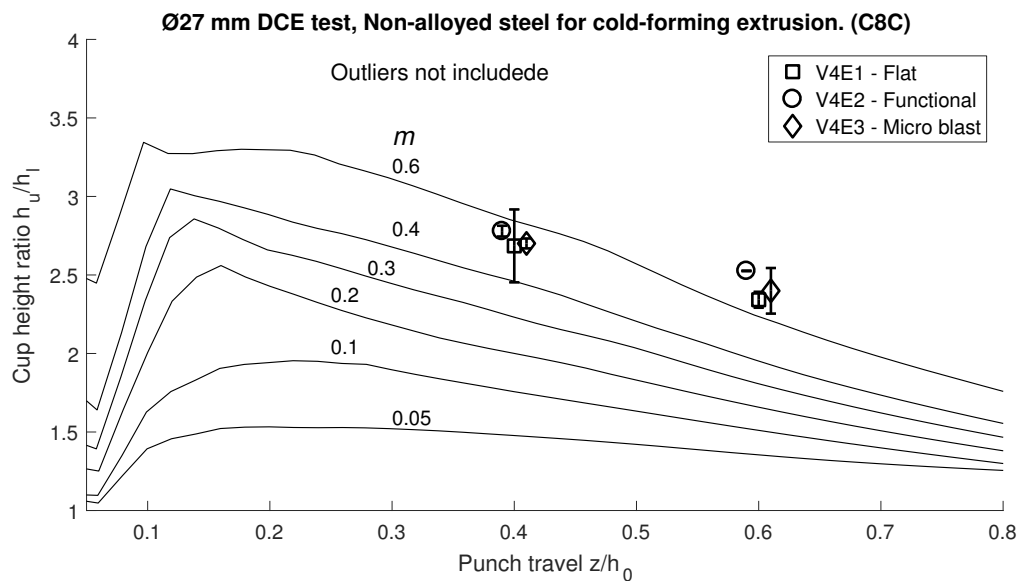


Figure 5.20: Results of the macro size double cup test, allowing the disregard of one outlier measurement pr. reduction height batch.

Conclusion

A number of double cup extrusion test have been conducted with the aim of quantifying the influence of surface topography of the die on friction during bulk metal forming. A container diameter of Ø27mm was used and the diameter of the two punches was 21 mm. This places the experiment in the so called macro length scale.

Two of the manufactured dies were polished using a novel semi-automatic polishing equipment developed by Strecon A/S. The third die was finished using the conventional wire-EDM process. The surfaces roughness parameters were determined, and plots of the 3D and 2D surface topography were shown.

The results of the experiment, meaning the ratio between the upper and lower cup height, show no distinct correlation with the surface characteristics of this test. Further, the measurement point which constitutes the average of three observations features large variation. The wide confidence intervals can primarily be attributed to isolated outlier observations.

In Figure 5.20 where outlier observations have been removed, the independence of the observations on the choice of die surface characteristics is manifested.

The reason for the independence of surface roughness friction shall be found in the lubrication regime. The phosphate coating and soap lubrication layer is simply thick enough to overrule the influence of the surface roughness asperities. The lubrication film is thicker than the surface roughness of the die and work piece billet, effectively placing the experiment in the *Hydrodynamic thick film* lubrication regime, rather than the *mixed-layer* regime, as outlined in section 5.1.

A friction factor in the areas 0,3–0,6 can be estimated from the calibration curves. This is a relatively high friction factor, that should give raise to some additional reflections. When comparing the DEC experiment to similar results obtained by other researchers, a friction factor m around 0,1 would be expected. The substantial difference in friction can be explained by the calibration curves used in this experiment not being correct. This is probably due to the work piece material stress-strain curves, taken from literature and used in the finite element simulation, not accurately representing the work piece material used in this experiment.

If a more viscous lubricant had been applied, placing the DCE-test in the *mixed* lubrication regime, it is likely that an influence of die surface topography would have been noticeable. However, a more viscous lubricant would also increase the risk of lubricant breakdown leading to galling and permanent scoring of the die surface.

A number of supplemental DCE-test in the micro scale have been conducted to investigate the influence of tool surface topography in the micro bulk forming process.

5.5 Micro size friction experiments

It is well established that the high friction encountered in micro forming is one of the key barriers prohibiting the evolution of this process into an industrial process. Recapitulating on the size effects in micro forming (section 3.3), the main contributors to the increased friction are the influence of the increased ratio of open- to closed lubricant pockets in combination with the in-scalability of the surface roughness [38, 64, 74].

These effects, leading to challenging tribological conditions in micro forming, have been reported to induce a range of complications in application of the micro forming process. The dominant increase in friction can lead to galling, excessive tool load, reverse forming and degradation the surface finish of the formed work piece.

The research work and experiments have been conducted at the Lehrstuhl für Fertigungstechnologie, Universität Erlangen-Nürnberg, Germany, deliberately using an equivalent of the experimental used by Tiesler in his micro DCE-test experiments [17]. This allows for subsequent comparison of results and reproducibility of the experimental results.

In the following a number of double cup extrusion tests (DEC-test) will be completed with the objective of researching friction dependence on die surface topology. The experiments can be seen as a continuation of the macro size experiment treated above. However, several important parameters have been altered, making a direct comparison non valid. The experiments are deliberately designed to have a high degree of similarity with earlier research, where the correlation between the size effect and frictional behavior were researched [17].

In order to ease the manufacturing of the tool elements, the ICFG guidelines for design of the punch form factor have been abandoned. Instead a simpler design incorporating a simple chamfer edge has been adopted. The simplified punch design is shown in Figure 5.21. It is noted that due to the chamfer on the punch tip, the punch travel must surpass the height of the chamfer before evaluation of the DCE-test becomes valid.

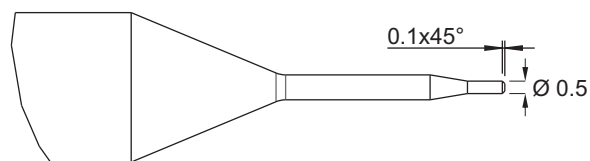


Figure 5.21: The punch geometry for the upper and lower punch.

A total number of six dies were manufactured. Three of these dies will feature a \varnothing 1mm hole while the remaining three will have a \varnothing 2 mm hole. The diameter of the punches will be \varnothing 0,5 mm and \varnothing 1 mm respectively, corresponding to an area reduction ratio of $r = 0.25$ during the formation of the cup. This areal reduction ratio is on the lower limit of recommendable areal reduction but will make the test more sensible to the influence of friction [68].

The α brass alloy CuZn15 was chosen a work piece material. Subsequently a number of upsetting tests were conducted to determinate parameters for the Ludwig-Hollomon type material model. The upsetting tests were conducted with a billet aspect ratio of 1:1 and using a Silicone based MoS₂ paste as lubricant. The results of the upsetting tests are visualized in the flow curves in Figure 5.22. An increased flow stress can be noted for

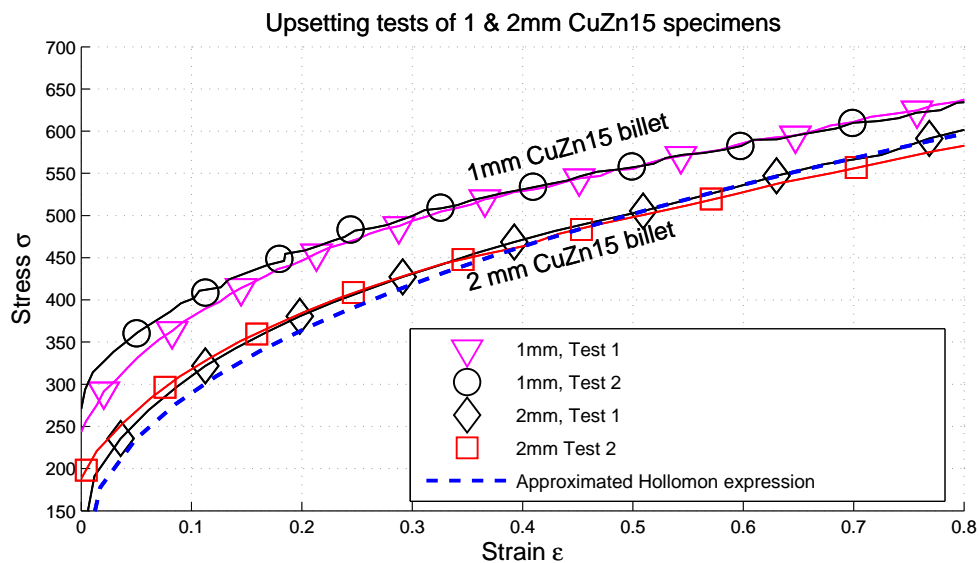


Figure 5.22: Results of the upsetting test of 1 and 2 mm CuZn15 α -copper alloy.

the 1mm specimens in comparison to the 2mm. This can be explained through through preexisting work-hardening of the materials, where the 1mm was further reduced in diameter. Ideally the work piece material should undergo annealing before undergoing deformation in the experiment. At the time of the experiment it was not possible to normalize the work piece material. However, according to several sources, an offset of the flow stress will only have minor influence of the material flow in the DCE-test, whereas the envelope of the curve (n-value) is strongly correlated with the material flow [67].

The acquired stress-strain curves are approximated a Ludwig-Hollomon expression as shown in Equation 5.10

$$\sigma = \sigma_0 + h\varepsilon^n \quad (5.10)$$

The values of the different parameters are as follows: $\sigma_0 = 77,56$ [MPa] ; $h = 571,7$ [MPa] and $n = 0,4294$ for the $\varnothing 2\text{mm}$ specimen. Corresponding values taken from the Ludwig-Hollomon expression are plotted in Figur 5.22.

Tool Design and Manufacturing

Preliminary numerical analysis of the die and punch stresses showed a maximum die stress of 1330 MPa. The results from the die stress analysis implied that cost-effective norm parts in HSS, according to DIN 1530 AH, could be used as a basis for the punches. The punch geometry was then manufactured using conventional grinding technique. The dies, having an outer diameter of $\varnothing 14\text{mm}$, were cut from a hardened punch needle of HSS material using wire-EDM. The internal geometry of the dies was manufactured using the wire-EDM process. This process, by virtues of its nature, generates a surface with a defined roughness and a high degree of randomness in the position of the individual asperities. By changing the process parameters, such as the number of passes and the shape of the electrical current pulses, different surfaces topographies can be created. One of the dies in each size-set was subsequently polished using a best effort approach.

An overview of the dies to be produced is provided in Table 5.2. The naming convention

Die name	Diameter [mm]	EDM-passes	Expected Ra [μm]
1-R	$\varnothing 1,0$	2	1,8
1-F	$\varnothing 1,0$	4	0,3
1-P	$\varnothing 1,0$	4+polishing	<0,3
2-R	$\varnothing 2,0$	2	1,8
2-F	$\varnothing 2,0$	4	0,3
2-P	$\varnothing 2,0$	4+polishing	<0,3

Table 5.2: Indication of the number of DCE-test to be conducted.

is a contraction of the die diameter and a suffix according to roughness, R for rough, F for fine and P for polished.

Roughness measurements

Due to the small internal diameter of the dies, it was not possible to measure the internal roughness parameters using a conventional stylus-type instrument. Instead, a number of replicas were made using a commercial silicone based replica compound with a resolution better than $0,1\mu\text{m}$. The replicated surfaces were then analyzed in a focus variation microscope where the roughness parameters were determined. Measurement lengths of $250\mu\text{m}$ were used for the roughness measurement and no cut-off filtering was applied to the roughness measurements. The acquired values for the achieved surface roughnesses of the dies are reproduced in Table 5.3.

Die name	Ra [μm]	Rz [μm]
1-R	1,947	11,75
1-F	0,227	0,965
1-P	0,150	1,084
2-R	1,581	7,456
2-F	0,227	1,139
2-P	0,08	0,579

Table 5.3: Achieved surface roughness parameters of the manufactured dies.

Minor deviations can be noted when comparing the expected Ra roughness values between the expected and achieved values. It should be noted that the application of the replica technique in conjunction with the non contact roughness measurement and the relative short roughness acquisition length, will increase the measurements uncertainty for the roughness parameters.

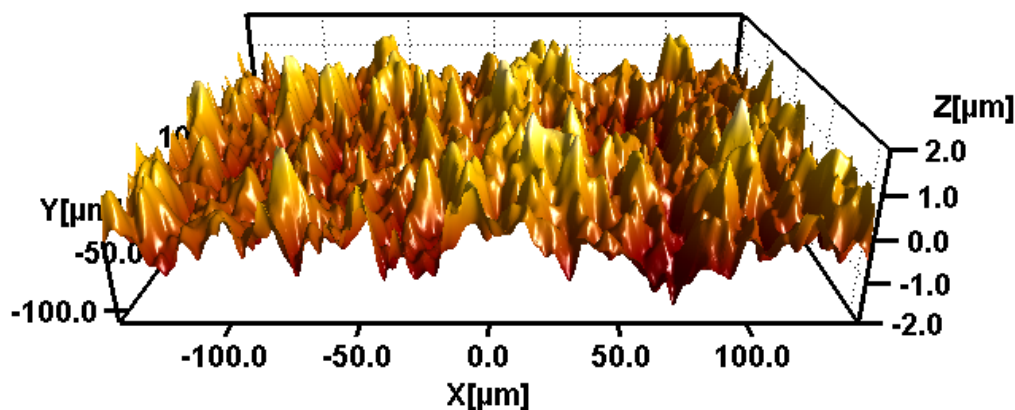


Figure 5.23: Example of surface topography after wire-EDM processing. This case is a surface scan of the 2-F die replica.

Lubrication and Tool Framework

Kubitrac 4096-1, a commercial tube drawing lubricant was applied to the billet before forming. The lubricant was applied using a hollow glass pipette and the billet was subsequently lightly wiped with a paper towel.

The punches and the die were mounted in a standard die-set and placed in a universal testing machine. The punch load was sampled during the forming operation and the result is plotted in Figure 5.24. The deviation between the course of the measured and predicted load curves can most likely be attributed to unintended additional elasticity of the tool die set and the press frame, that are omitted in the simulation. The predicted curve was simulated with a friction factor of $m = 0,3$ and with the stress-strain Ludwig-Hollomon expression derived during the preceding upsetting test.

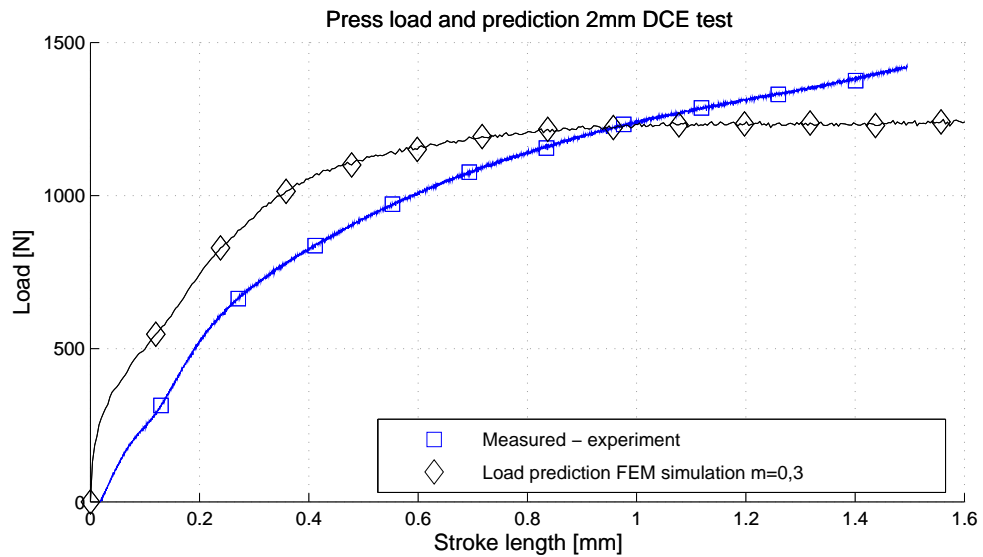


Figure 5.24: Comparison of predicted and measured punch load during double cup forming.

Finally, the individual work pieces were measured using an Alicona focus variation microscope. With the resulting 3D topography model at hand, the cup height could be extracted using a general purpose measurements data visualization software package.

The die set used in the experiments is shown Figure 5.25. The die set is relatively large compared to the specimen size, causing alignment of the individual tool elements to be challenging. The upper part of the die set, holding the upper punch, is in floating configuration and can be displaced by turning of adjustment screws in the top fixture. This allows for position adjustment of the punch position relatively to the center of the die set, something that is needed in order to get a well-formed backwards cub extrusion with the hole correctly centered. Due to the high dimensional size difference between the die set and the forming die, it is expected that the elastic deflections of the die set will be of dominant influence, as already noted above.

Results on Micro DCE-tests

For each die, a total number of 3 tests were performed, with punch travels of 40% ,60% and 80% respectively. Each test was repeated 3 times, giving raise to a total of 9 tests to be performed pr. die. Due to an unexpected large elasticity in the test-setup the measurements were shifted towards a lower actual punch stroke. This meant that the 40% punch stroke experiments were shifted to an actual punch stroke ratio of 10-20%. As this regime of the DCE-test is unreliable, the 40% experiments had to be discarded. The results of the 1 mm DCE-tests are plotted in Figur 5.26 in conjunction with a number of constant friction lines originating from the numerical simulations.

The results are rather comparable for the case of the fine and the polished dies. It is not possible to establish a distinct friction factor in this case, but the friction factor ranges

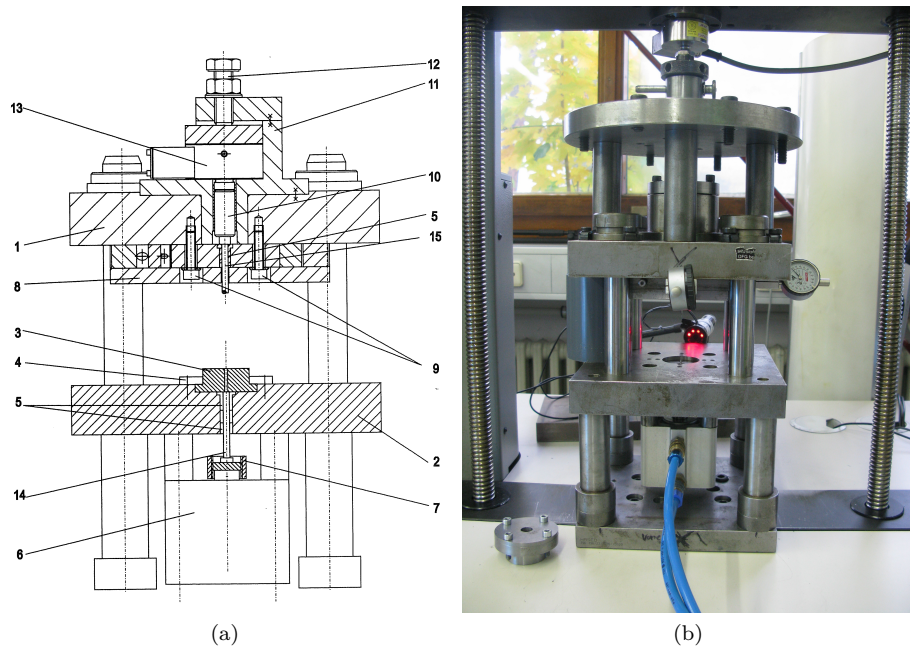


Figure 5.25: Sectional sketch of the die set utilized for the micro DCE-test (a) and a photograph of the tool system mounted on the general purpose testing machine (b).

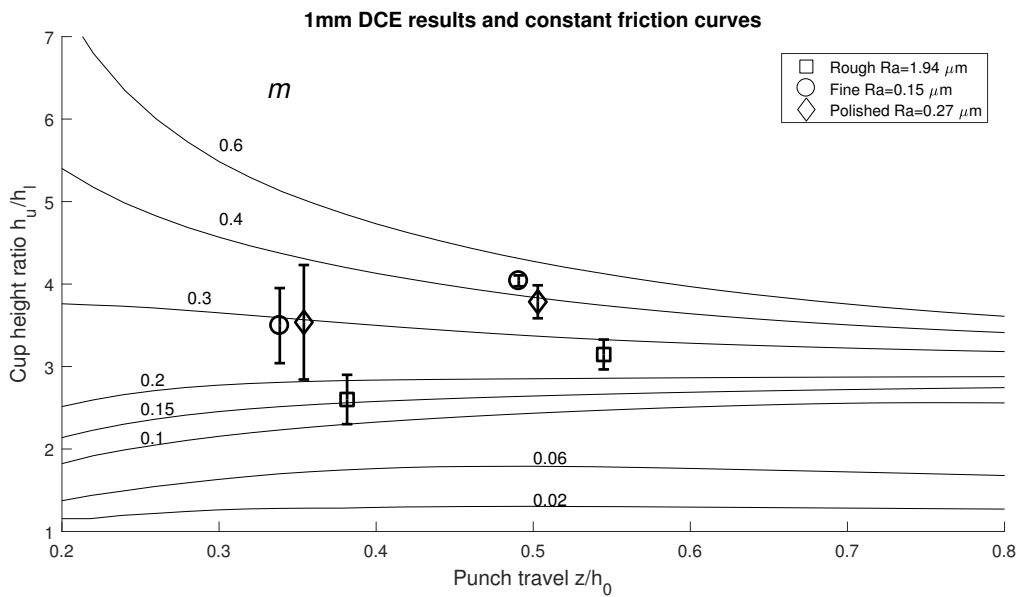


Figure 5.26: Results of the 1 mm DCE test plotted on top of the reference values from the numerical simulation.

between 0,3-0,4. For the case of the die with the highest roughness, a low frictional behavior is exhibited. The results for the 2 mm experiments are shown in Figure 5.27. In this case the rough die exhibits a friction factor of 0,4. For the case of the die with

the fine surface, the estimated friction factor is ranging between 0,08 and 0,2, depending on the reduction ratio. Finally the polished die exhibits a larger variability than the other experiments in the series. However, the results are comparable to the results for the die with fine surface finish. As a secondary parameter of the experiment, the

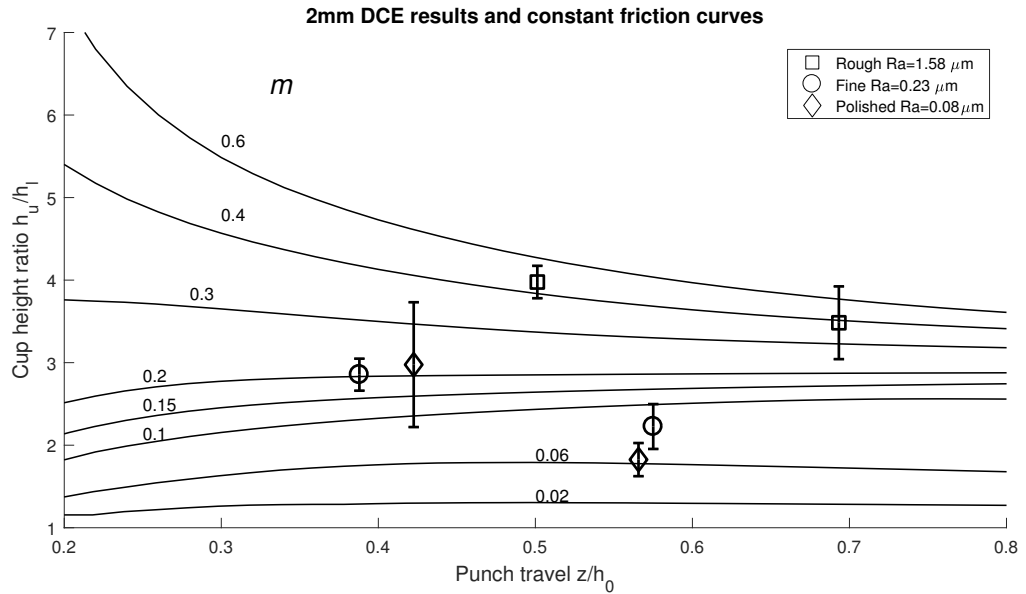


Figure 5.27: 2mm results from the DCE-test. Confidence intervals are 95% coverage.

press load for each experiment setup is plotted in Figure 5.28 and 5.29. The plots are showing the acquired load values for a representative sample, and not the average of the three repetitions of the experiment, but the trend was seen for all repetitions of the measurements.

The punch load measurements show a trend towards a 10-20% higher punch load for the polished dies with low surface roughness. This trend is seen across the 1 and 2 mm tests.

Conclusion on Micro DCE-tests

A number of micro DCE-test has been completed. The results generally show a high friction factor when compared with similar experiments made in the past [17]. An explanation for this behavior might be found in differences in the surface roughness on the work piece specimens in combination with the application of a different lubricant. However, it is more likely that the increased friction can be attributed to the amount of clearance between the die land and the work piece billet. Small play will translate to a thinner lubrication film, giving rise to higher friction - and vice versa. Also the grain size of the material and the amount of preexisting work hardening of the work piece material are deemed to have an influence.

For the 2 mm case, a proportional dependance between the measured die surface roughness values and the measured friction is noted. This is in accordance with established theory, where a higher surface roughness will lead to a higher real contact area α_{RC} , again leading to higher friction. The estimated friction factor from comparison with numerical

simulation is high when compared to earlier results [17], even for the polished die. This can possibly be attributed to a combination of a small clearance between workpiece and die, giving rise to a thin lubrication film and higher normal pressures in the die.

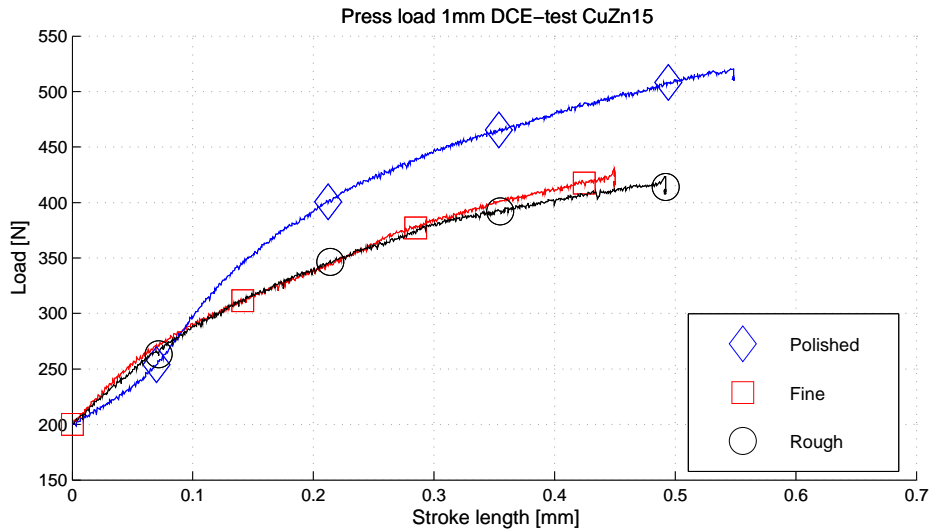


Figure 5.28: Punch load during micro DCE-test for 1mm specimens. Plot of three representative single samples.

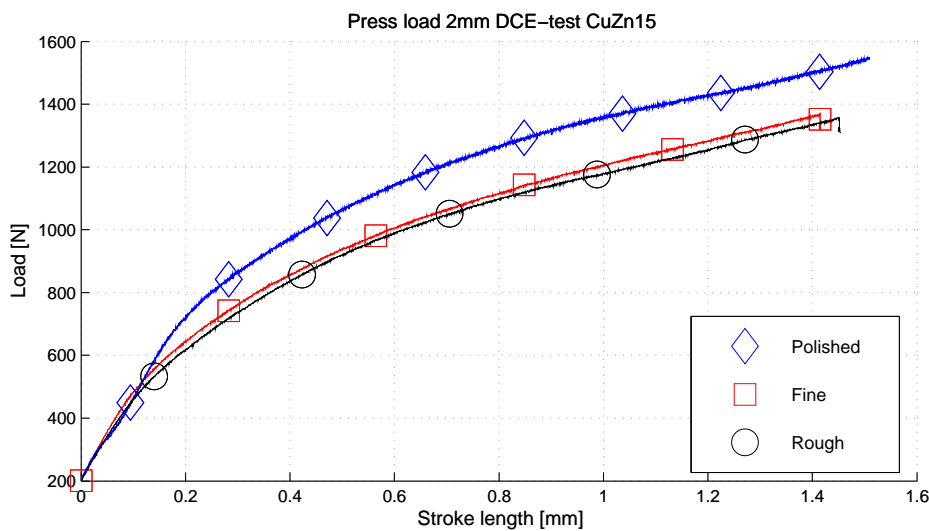


Figure 5.29: Punch load for 2mm DCE-test. Plot of three representative single samples

For the 2 mm specimens a similar cup height ratio is noted for the fine sparked and the polished dies, having a measured surface roughness value of $R_a = 0,23 \mu\text{m}$ and $0,08 \mu\text{m}$ respectively. Whereas the rough die, with a $R_a = 1,58$, exhibits a distinctly higher cup

ratio. This could imply a change of specific friction mechanics regime at a roughness values between $Ra = 0,23 - 1,58 \mu m$.

Moving to the experiments with $\varnothing 1mm$ tests, the relation between roughness and cup height is upturned. Again, the die with fine and polished surfaces, and comparable surface roughness parameters, show similar cup height ratio. The die with a rough surface finish demonstrates low cup height ratio and thus low friction. This behavior cannot be readily explained. A similar observation has been made during extrusion experiments with specimens of the same diameter and work piece material [17]. For convenience, the reference have been reproduced in Appendix E. Further, observations have indicated that the real contact area α_{RC} might depend on the viscosity of the lubricant in the case of surface characteristics with high surface roughness [64]. This might lead to low friction in the case of closed die forming with medium surface roughness and high lubricant viscosity. However, this statement has to be researched further.

Looking across the 1 and 2 mm tests, the expected trend of higher friction and smaller size is clearly seen. Where an approximate friction factor of $m = 0,2$ can be identified for the polished die in the 2 mm case, the corresponding value at 1 mm specimens is $m = 0,3$. This tendency is not seen for the tool with a rough surface finish.

When comparing the micro DCE-test against the Macro equivalent, an influence of the surface roughness characteristics can now clearly be noted. The reason for this should most likely be sought in the down-scaling of the experiment in combination with the radical change of lubrication base. The mineral oil based lubricant utilized in the micro DCE-test can be modeled as a Newtonian fluid, whereas the phosphate coated and soap lubrication more is to be regarded as a solid lubricant.

In the following, further investigations are undertaken to verify this frictional behavior found in this experiment using a newly developed linear-translocation micro friction testing apparatus.

5.6 Micro tribology tester friction experiments

As addition to the frictional results achieved in the two DCE-test above, some extra friction test have been conducted using a newly developed translocation friction testing apparatus. The Micro Tribology Tester (MTT) was developed in order to ease the study for tribological conditions in cold forging at micro scale. Further information on the design and working principle of the micro tribology tester, together with a range of preliminary results, can be found in literature [21, 75].

Working principle of the Micro tribology tester

The test principle is easy to comprehend and can be classified as a simulative test following the definition outlined in Section 5.3. The functional principle of the translocation friction tests is sketched in Figure 5.30.

The test principle is also known from the well known strip-test, where two plate tools are pressed against an intermediate strip, taking the role as workpiece material. The strip is then drawn or translocated, allowing friction force and surface of the strip to be studied.

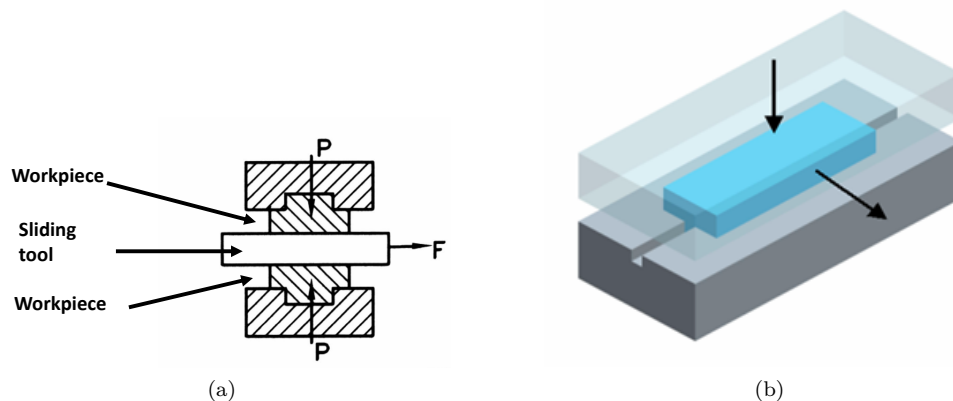


Figure 5.30: Sectional sketch of the working principle of the Micro Tribology Tester Figure (a). Figure (b) show the one-sided 3D model of the test, where the workpiece is marked blue and the tool is semi-transparent.

Following the principle, the MTT works by upsetting to identical cylindrical workpiece specimens against an exchangeable tool insert. By altering the lengths of the work piece billets and the clamping of the tester, strains between 0 and 1 can be reached.

The design parameters of the Micro Tribology Tester is reproduced below:

- Work piece dimension: \varnothing 0.3mm - 3mm
- Materials ranging from Al 99.5% (softest) to Steel C8C (Ma8) (hardest)
- Compression load: $5\text{N} \leq P \leq 10000\text{N}$
- Friction load: 0.4N - 2400N
- Separate load cells for vertical and horizontal forces
- Measurement accuracy: $\pm 1\%$
- Pull speed 1mm/s - 100mm/s

An exchangeable load cell provides measurement of the upsetting force, whereas the friction load is measured by a custom build force transducer based on strain gauge technology. The force for upsetting and drawing of the tool is delivered by two high precision actuators. The actuators are based on an a fusion of a rotational servo drive and an encoder with a high precisions ball screw featuring a prestressed nut. A third actuator is included to allow centering of the tool upon application of the drawing force. The control system and design of the MTT is shown in Figure 5.31. The equipment is composed by three linear actuators which are according to the following sequence:

- The up-setting motion is executed.

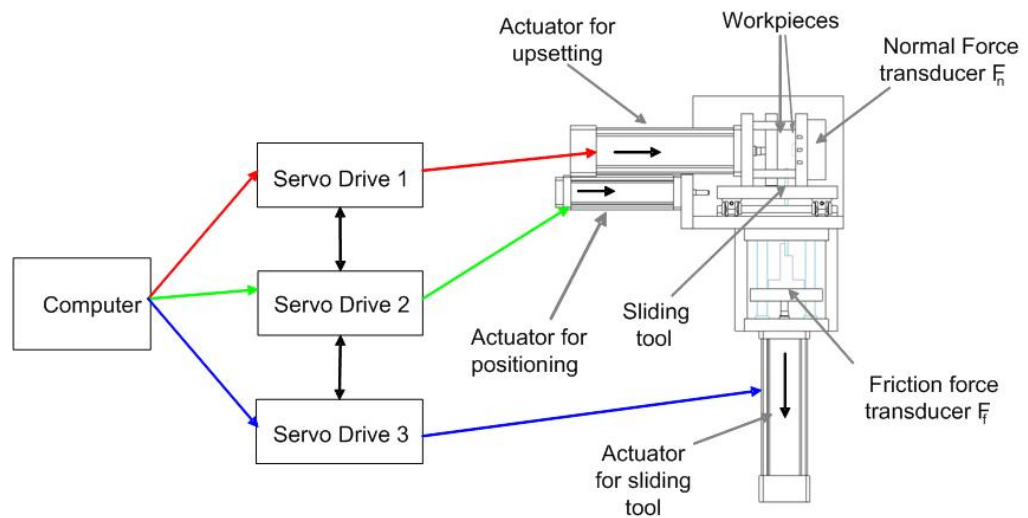


Figure 5.31: Outline of the mechanical design and control system for Micro Tribology Tester.

- The tool is centered, ensuring alignment between tool and center axis of the translocation motion.
- The vertical sliding of the drawing tool is executed.

The tool frame of the testing machine consists of standard four columned ball-cage die sets, ensuring good alignment and low friction contributions from the tool frame itself. A photograph of the central elements are shown in Figure 5.32. In the Figure, the center image (a) is taken from the internal cavity of the friction tester. Following the figure, the workpiece holders and the fixture holding the tool can be identified. To the left (b) an image of the oblong tool insert is shown. By preparing various tool inserts with different surface characteristics, the tribological conditions can be changed. Towards the top (c) examples on the work piece inserts are shown. To the left a virgin specimen is shown and to the right is an example of the workpiece after upsetting the MTT. Finally, to the right (d), the tool holder and friction force measurement transducer. This custom made transducer is based on a conventional full-bridge strain gauge patches.

Tool manufacturing and test setup

In order to replicate the tribological conditions of the Micro DCE-test as close as possible, the tool inserts for the MTT was manufactured using the same tooling chain. That is; a number of tool inserts were machined, hardened and finally calibrated using a wire-EDM machine. The tool inserts are manufactured in Vanadis 6 material, a high-alloyed chrome molybdenum vanadium powder metallurgy tool steel.

A total of four tool inserts were produced. Two of the tool inserts were later hand-polished to achieve a lower surface roughness. Using the R_a surface roughness as the primary indicator, the roughness values intended were: $R_a = 0,01; 0,1; 0,35$ and $1,8 \mu\text{m}$. The measured roughness values of the four dies are reproduced in Table

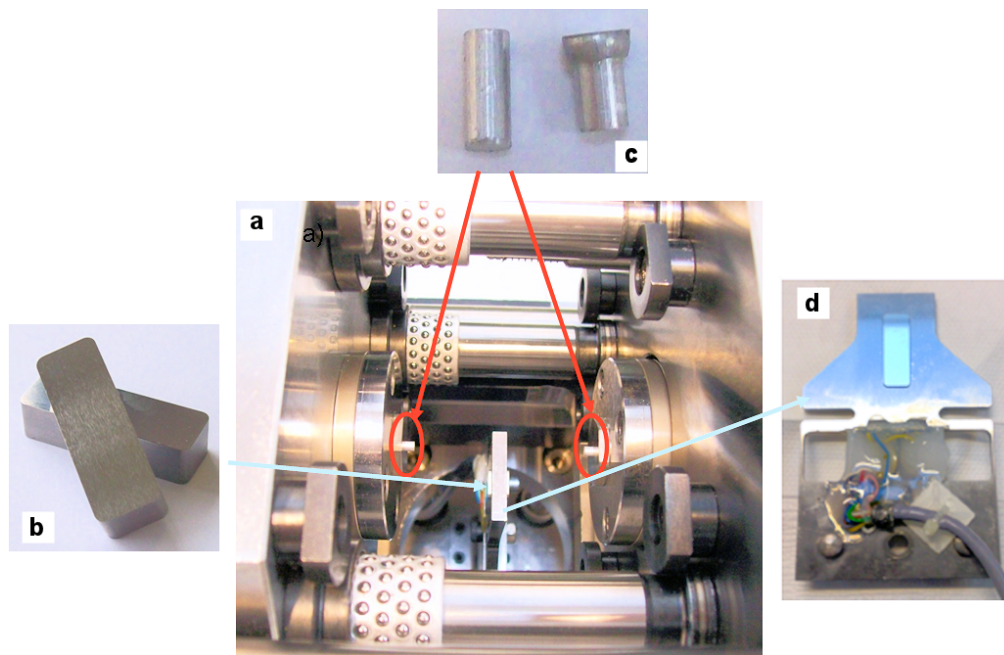


Figure 5.32: a) Close view of the testing equipment; b) Center tools made of high performance cold work steel Vanadis 6; c) Cylindrical test workpiece before and after the test; d) Friction force transducer [21].

5.4 below. The roughness values were obtained using a conventional contact stylus roughness measurement device. Evaluation lengths are chosen to comply with ISO 4788 standard [76].

Intended	Measured			
Ra [μm]	Ra [μm]	CI(95%)	Rz [μm]	CI(95%)
0,01	0,02	0,002	0,142	0,017
0,1	0,067	0,018	0,358	0,074
0,35	0,325	0,02	2,313	0,296
1,8	1,571	0,212	8,916	1,074

Table 5.4: Surface roughness parameters of the manufactured tool inserts for the MTT. Measured values are based on five repeated roughness measurements. The values marked CI(95%) are confidence intervals with 95% coverage for the five measurements, corresponding to the double standard deviation.

Figure 5.33 is a photograph of the tool inserts. The difference in tool roughness is readily visible for the tools with roughness values $Ra = 0,35$ and $1,8 \mu\text{m}$. These dies were finished using the wire-EDM process. Tools with surface roughness values $Ra = 0,01$ and $0,1 \mu\text{m}$ were polished to a high glossy state. Like in the case of the micro DCE-test, the α -brass alloy CuZn15 was used as work pieces material. The coiled work piece material with diameters $\varnothing 1 \text{ mm}$ and $\varnothing 2 \text{ mm}$ were cut using the wire-EDM process, achieving a

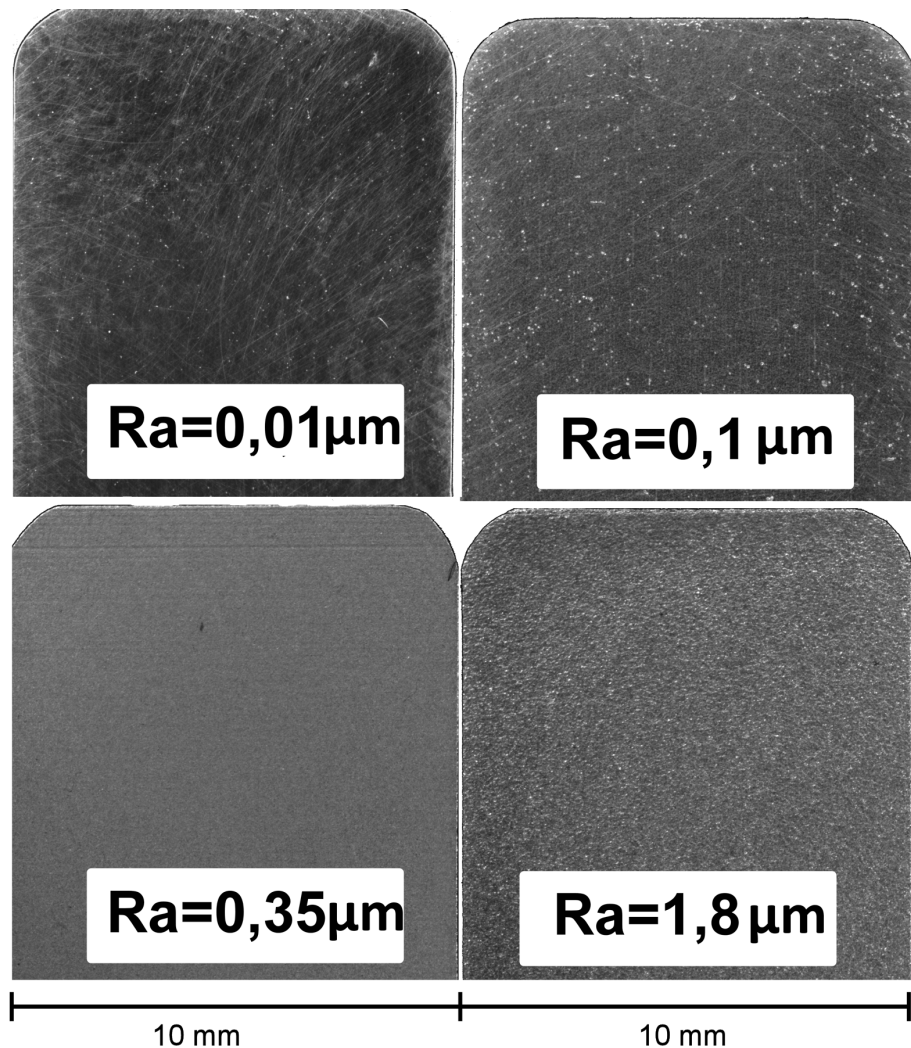


Figure 5.33: Microscope images of the tool inserts for the MTT apparatus. High roughness values show a diffuse scattering while the low roughness values exhibit specular reflection of the microscope light.

surface roughness value $Ra=0,7 \mu\text{m}$ on the end billet facets.

For lubrication, the Kubitrac 4096-1 oil, designed for tube drawing of copper is used. Almost no additives are present in this type of lubricant selected to be used in the tests to avoid possible boundary lubrication. The lubrication oil was applied in a thin layer to both the tool and the work piece specimens using a pipette.

Results from the Micro Tribology Tester

Apart from the parameters relating to the physical properties of the experiment, a number of parameters governing the dynamics of the experiment have to be established. These are the up-setting speed, governing the strain state during the initial upsetting of

the work piece specimens; the sliding speed, being the speed with which the translocation movement is executed and finally the sliding distance being the total length of the translocation movement. The parameters during the investigation are: up-setting speed = 1,2 mm/s, sliding speed 5 mm/s work piece material and height reduction of 40 % . These parameters have been chosen on the basis of the parameters from previous test made on the MTT equipment. The sliding distances were chosen to be 2,5 mm and 1,4 mm respectively for the billets with a starting diameter size of $\varnothing 2$ mm and $\varnothing 1$ mm. The two different lengths have been chosen a bit longer than the nominal diameter of the workpieces to ensure that static coefficient of friction have been overcome and the kinetic friction domain was entered. Each combination of specimen diameter and tool insert was repeated three times, meaning that a total of 24 tests must be conducted. Micrographs of the tool surfaces following the friction testing are shown in Figure 5.34.

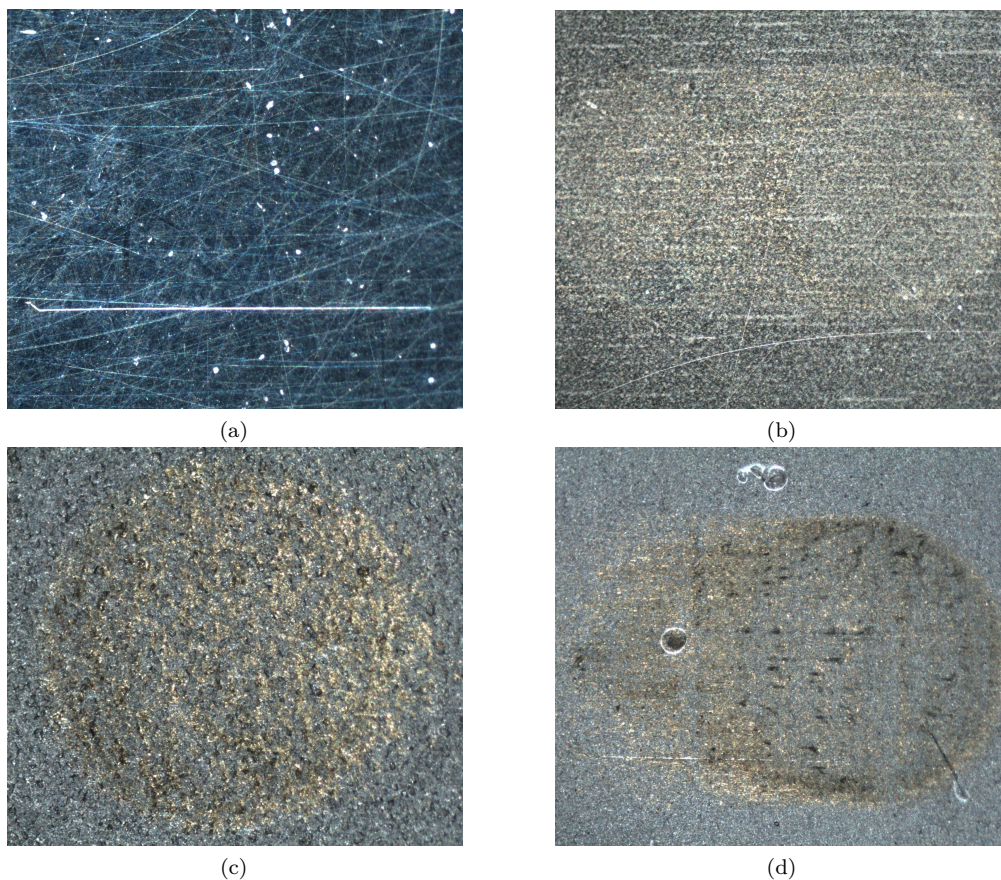


Figure 5.34: Micrographs of the tool surfaces after forming. (a) is the tool with surface finish $R_a=0,01 \mu\text{m}$; (b) is $R_a=0,1 \mu\text{m}$; (c) is $R_a=0,35 \mu\text{m}$ and (d) is $R_a=1,8 \mu\text{m}$. Remaining of the workpiece material is clearly visible for all roughness values except for the finest value.

Galling or pick-up of the work piece material is clearly visible in all cases, excluding the tool with the finest surface finish. Galling, also known as seizing, cold welding or pick up, is an unwanted effect in forming. It is however hard to avoid altogether, especially in case of a soft workpiece material with insufficient lubrication.

To observe the properties of the galling, the normal force, being normal to the friction shear force, can be observed. The micro tribology tester does not readjust the upsetting force during the translocation movement, meaning that the galling or grinding behavior will lead to a reduction of the normal force. The workpiece material has been upset against the work piece material, meaning that the work piece material has been able to flow into the surface asperities of the tool through displacement of the lubricant. Figure 5.35 illustrates a plot of the normal-, friction force and the friction quotient for the $Ra=0,01 \mu\text{m}$ and $\varnothing 2 \text{ mm}$ specimen. The same plot for the rough $Ra=1,8 \mu\text{m}$ tool is shown in Figure 5.36. It is evident that while the normal force remains constant

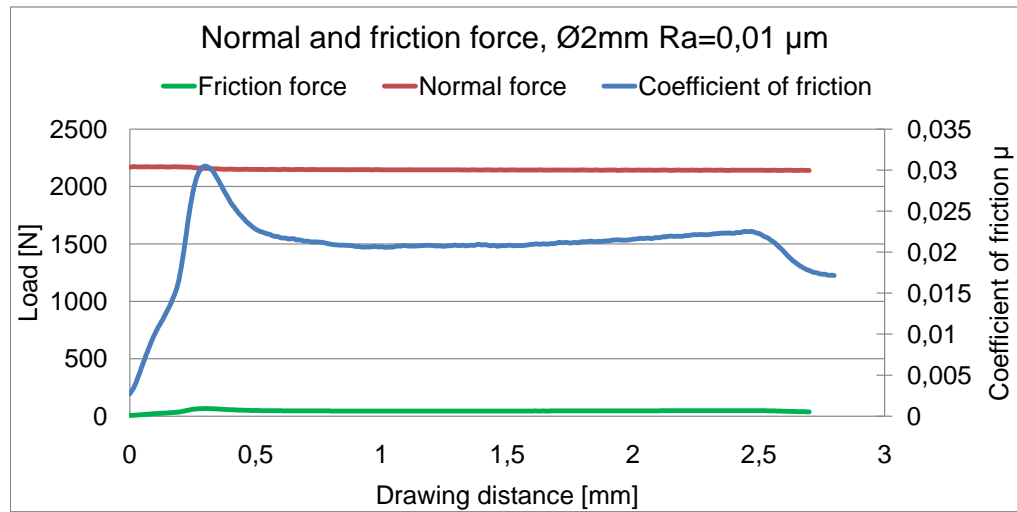


Figure 5.35: Plot of friction- and normal force measurements for a tool featuring a fine surface finish, $Ra=0,01 \mu\text{m}$.

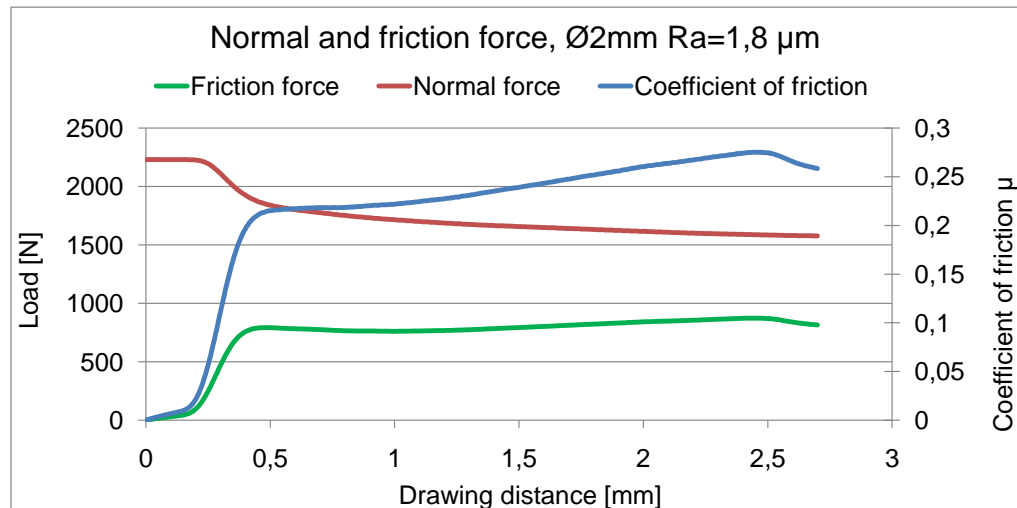


Figure 5.36: Plot of friction- and normal force measurements for a tool featuring a rough surface finish, $Ra=1,8 \mu\text{m}$.

for the smooth tool, an exponential decay behavior is seen for the experiment with the rough tool surface. As these two examples represent the upper and lower bound of the roughness values, it is expected that for intermediate roughness values will cover the transitional phase from low friction to shearing of the material becomes dominant.

Plotting that determined friction coefficient, as the quotient between the normal and the friction shear force, we arrive at the plots depicted in Figure 5.37 and 5.38 for the $\varnothing 1$ and $\varnothing 2$ mm specimens respectively. Each line represents a point to point average over three repetitions of the experiment. The error bars indicate the confidence interval with 95% coverage factor. Starting from the most rough tool and $\varnothing 1$ mm specimens, indicated in

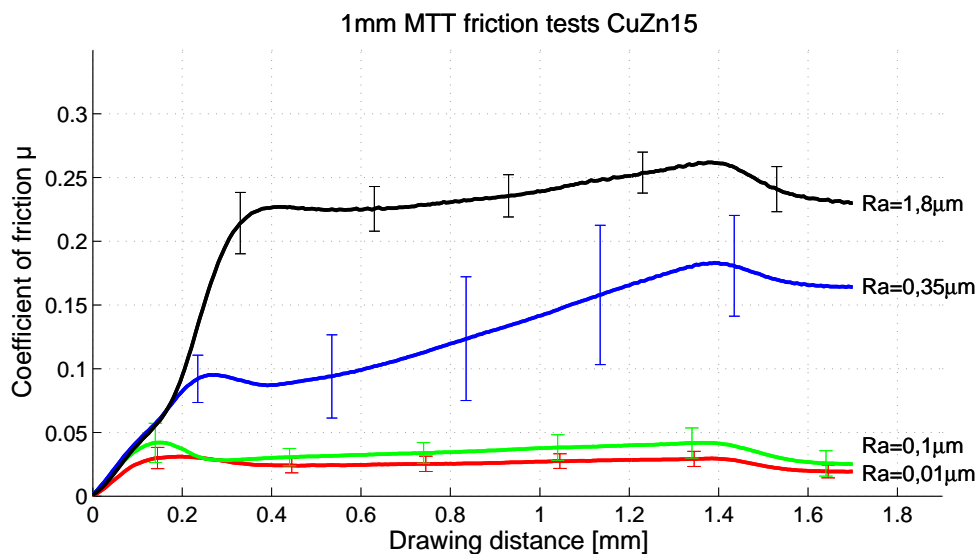


Figure 5.37: Plot of friction measurements for the $\varnothing 1$ mm specimens.

black color in Figure 5.37, the friction exhibits a threshold like behavior. The friction force ramps up and continues to stay at a high level. The expected transition from static to dynamic friction domain is not identifiable. For the tool having a surface roughness value of $Ra = 0,35 \mu\text{m}$ the situation differs. In this case the shift from static to the dynamic friction domain can be readily identified. The measured friction constant μ is initially around $\mu=0,1$, but is nearly doubles over the sliding length. Observing the scatter of the measurements, the curve for the $Ra=0,35 \mu\text{m}$ tool shown substantially more scatter. Finally the two cases with low tool surface roughness both shown low friction and only increase slightly over the course of the drawing length.

Moving on to the friction results for the 2 mm specimens, the trends from the $\varnothing 1$ mm specimens is repeated, with a few important deviations. With the exception of the highest surface roughness, an overall lower friction factor is seen for the $\varnothing 2$ mm experiments. Further, the increase of friction coefficient over the drawing length is lower for the 2mm case when compared against the 1mm ditto. Finally, a lower overall scatter of the measurement values is seen. The lower scatter is especially pronounced at low drawing lengths.

Finally, a comparison between the friction coefficient μ is undertaken between the $\varnothing 1$

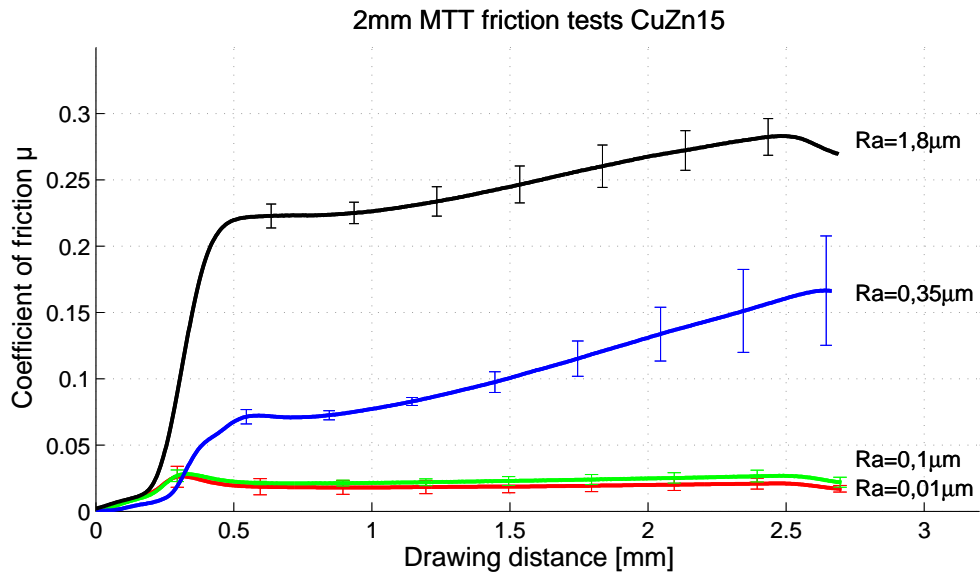


Figure 5.38: Plot of friction measurements for the \varnothing 2mm specimens.

mm case and the \varnothing 2 mm case. Figure 5.39 depicts a comparison between the friction coefficient measured at the end of the drawing operation. As expected, a smaller diameter

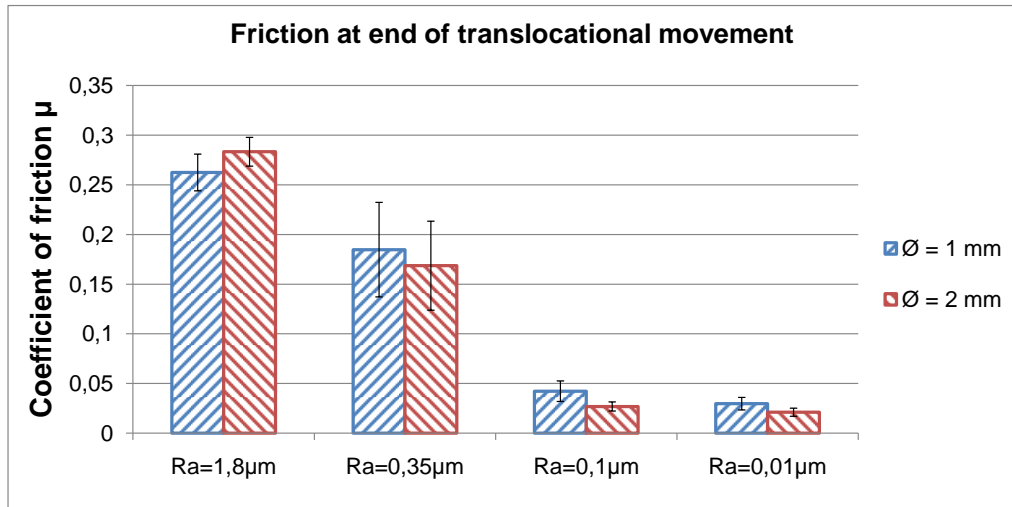


Figure 5.39: Bar plot of the ultimate friction coefficient, measured at the end of the translational movement.

gives rise to increase friction, with the exception of the very rough tool surface. It can also be noted that while the tools with roughness values of $Ra=0,01$ and $Ra=0,1$ show comparable friction results, the dies with higher roughness values exhibit substantially increased friction and higher values of scatter. In order to further establish the effect of increased friction a lower diameter workpiece, a repetition of the test could be carried out with a 0.5 mm work piece.

Conclusion in Micro Tribology Tests

For each tool roughness and diameter combination, a total of 3 tests have been performed. Using the same lubricant in the tool/work piece interface and the same surface roughness of the specimens, the histograms in Figure 5.37 and 5.38 show an increase in friction with increasing tool roughness. A slight friction increase from the bigger 2 mm specimen to the smaller 1 mm specimen is noted. This behavior is likely to be attributable to the known size effects in tribology. Further, the noted scatter effect for the smaller 1 mm specimen also complies with established theory, dictating that the ratio between open and close lubricant pockets increase with down-scaling of the specimen size. The growing scatter of the measurements for the tool with $R_a=0,35\mu\text{m}$, is likely to be attributed to physical variance in lubricant entrapment along the path of translocation as the lubricant is more likely to escape.

The high values of μ , acquired during the test via the roughest tool, are comparable to values obtainable in testing under dry conditions.

Visual investigation of the tool after test showed pick up of work pieces material on the tool in every case. However, there seems to be a correlation between the tool roughness and the severity of the galling on the tool surface, where higher roughness leads to more galling. For the tools having the highest roughness, the course of the friction curve is more to be regarded as a shear friction measurement than a friction measurement. A thesis could be: at higher roughness values the lubricant is able to escape, thereby increasing the area of real contact. This leads to grinding of the work piece material against the hardened tool. This observation is supported by the progress of the friction curve for the tool having a roughness of $R_a=0,35\mu\text{m}$. At this roughness, the tool start out as well lubricated. However, as the sliding length increase, allowing the lubricant to escape, the friction coefficient increases rapidly.

As a final remark it should be noted that the simulative MTT should be regarded as an open die forging scenario, whereas the DCE-test is to be regarded as a more close die operation. This makes direct comparison difficult. However, some comments to the observed interdependent of tool surface roughness values and measured friction coefficient for the three test will be given in the following section.

Conclusion on Macro- and Micro tribology experiments

In the above three different tribological tests have been undertaken, two double cup extrusion process tests and a novel translational direct testing method for testing of scale effects in metal forming friction. All of the tests have been conducted with the aim of researching the dependence of friction in metal forming processes on the tool surface roughness characteristics.

In the first DCE-test, conducted at macro scale utilizing a $\varnothing 27$ cylindrical billet in C8C material, three forming dies featuring different surface finishing were tested. Two of the dies had been polished using the prototype Strecon RAP machine, whereas the third die surface had been finished using a wire-EDM machine. The billets were lubricated with a conventional phosphate coated and soap lubrication approach. The experiment showed no dominant correlation between die surface finish and the measured cup height ratio of the formed specimens. It was concluded that the reason for the lacking interdependence

between surface roughness and friction could be attributed to the thickness of the lubrication film exceeding the height of the surface asperities.

The second DCE-test, performed at micro scale utilizing billets with diameters 1 and 2 mm, confirmed findings of an earlier experiment. That is, an increase in friction when the scale of the experiment is reduced. Further, it was generally found that a finer surface finish lead to a decreased friction factor. An exception from this behavior was seen for the very rough surface finish in the \varnothing 2mm case. The values of the estimated friction factor were generally high.

The friction measurements acquired using the micro tribology tester provided elaborate information of the tribological effects. Allowing the friction factor to be acquired over the drawing length of the tool, an increase of the friction factor over the drawing length of the tools could be noted. This effect was attributed to the escape of the lubricant, leading to non-pressurized lubricant pockets. Low coefficients of friction were measured in both the \varnothing 1mm and \varnothing 2 mm case for the tools with surface roughnesses $R_a=0,1 \mu\text{m}$ and $R_a=0,01 \mu\text{m}$. For the \varnothing 1 mm case lubricant escape could be noticed for the $R_a=0,1 \mu\text{m}$ tool, an effect not noticeable for the \varnothing 2 mm specimens. This observation manifest the established scaling effects and open-closed lubricant pocket theory. Finally, the 'reverse' frictional effect, also noted in the micro DCE-test, was noted. For the tool having a high roughness of $R_a=1,8 \mu\text{m}$, the friction measured for the \varnothing 1 mm specimens was lower than the for the \varnothing 2 mm ditto.

Summarizing across the three tribology experiments, a number of conclusions can be given. Even though different lubricants and work piece materials were used, some general comments between the macro and micro sized DCE-test can be made. Strong size effects were seen between the macro and micro sized DCE-test, placing the macro sized experiments in the full-film lubrication regime whereas the micro scale DCE-test must be considered as a mixed regime lubrication condition scenario. This shift towards more challenging lubrication conditions when downsized is a clear characteristic of the bulk forming process.

Comparing the micro DCE-test and the micro translocation friction test, with the fundamental difference of the tests in mind, some common ground can be established. Both experiments show decreasing friction for decreasing surface roughnesses. The direct dependence between tool surface roughness is clearer in the case of the micro translocation test, primarily due to the ability to study the friction as a function of drawing length. The DCE-test showed comparable scatter of the measurements across the \varnothing 1 mm and \varnothing 2 mm specimens, while the translocation test show a clear increase in the scatter when downscaled. This could imply better sensitivity of the translocation test. The odd observation, that for high tool surface roughness and \varnothing 1 mm specimens low friction is seen, is noticeable across both tests. This is only minor in the case of the case of the translocation test however.

The analysis could give a number of recommendations on suitable surface roughness for micro forming tools. From the friction measurements plotted in Figure 5.37, it can be concluded that surface roughness in the range of $R_a=0,1 \mu\text{m}$ and below is recommended for micro bulk forming. From the DCE-tests one could be led to believe that a high surface roughness is optimal. However, later inspections of the specimens from the \varnothing 1 mm DCE-tests have shown heavy plowing and surface degradation of the specimen

formed in the dies with high roughness. This is not desirable for most micro forming scenarios.

State of the art die sinking EDM machines are capable of delivering tools with surface finish down to $Ra \simeq 0,15 \mu\text{m}$. This is on the limit of what is tolerable for micro forming purposes, raising the need for methods of improving the surface quality. Manual polishing is precluded in most cases, due to the often strict tolerating, fine internal geometries and the unavoidable distortion of the die geometry. This is a suggestion for future work in this area.

Chapter 6

Tooling for the micro bulk forming process

Since the year 1455 when *Johannes Gensfleisch zur Laden zum Gutenberg* invented the printing process, replication techniques have been used extensively in mass production of almost every type of product. Application of replication processes are cost effective ways of mass producing components in several materials. When the replication process has been realized, almost infinite production volumes can be reached by a simple parallelization of the process.

Casting of steel, injection moulding of polymer and cold bulk forming of metals are all examples of replication processes used in the manufacturing industry. A common characteristic of family replication techniques is the need for a mould or die having the inverse shape of the desired component geometry. As part of the basic geometrical requirements, a number of practical and functional aspects influences the design of the tooling system. Within polymer injection molding, especially the material flow and the temperature cycling of the moulding cavity are important governing properties of the performance. Within metal forming process this is even more pronounced owed to the complex influence of strain hardening properties of the work piece material, springback effects, friction, tribological wear effects. Further, a typical bulk forming tool is often operated with narrow tolerance requirements and as close to the physical attainable internal pressure as possible, making the typical design marginal in more than one respect.

6.1 Introduction to tool design

Generally spoken, forging is an experience-oriented technology. Throughout the years, a great deal of knowledge and experience have been accumulated about forming technology, largely through trial-and-error methods. However, the forming industry has come a long way and has been able to supply industry with huge tonnages of high quality components, made of alloys with limited formability, while ensuring conformity to strict tolerances.

The physical effects involved in forming are hard to express explicitly through exact mathematical models. The correlation between microstructure and properties of materials, material flow, friction are tool/work piece interfaces, heat generation during the plastic

flow of material and the process conditions are all quantities which are hard to predict and analyze a-priori. Often a single forged component will go through several forming steps (preforms), where the level of geometrical complexity increase throughout the successive forming chain. Often the specimens have to go through tempering or annealing process between forming operations. Thus, the typical forming process is actually a collection of individual operations cascaded into a process chain. The most important methods of analysis are the once that assist the designer in analyzing the chain of forging operations, making it possible to arrive at a suitable tool design.

Tool analysis, design and manufacture for metal forming process have been studied extensively through decades and more than 50.000 scientific articles have been published on the subject. With tool design and performance being the dominant cost bearing element of the bulk forming process in combination with the substantial tool manufacturing costs, the search for performance optimization and shortening of the development time is understandable. From the design phase of a component to when the first successful component leaves the press, years can pass and the cost of design can be excessive. State of the art within bulk metal forming is still advancing as new tooling technologies become available [77,78] Especially net-shaping, where the specimen is forged as close as possible to the desired shape, has been researched [79,80,81,82]. But also the topics of tool wear, fatigue life and friction is studied actively [83,84,85,86]

The influencing variables of tool design include [18]:

- Design and geometry
- Surface finish, lubrication
- Stiffness of die, tool and press
- Mechanical and thermal effects under use

When considering tooling for micro bulk forming, the knowledge legacy of the macro scale cannot simply be applied. In the micro scale, the already marginal processing window of the metal bulk forming, is restricted further. Size effects change the physical rules of the process and the process window changes with it. This impacts tool analysis, design and manufacturing. Little research have been done in this area.

The following section will treat the subject of micro tooling for the bulk forming process. A number of tools are manufactured and the performance is evaluated through prototype trial runs.

6.2 Micro tooling characteristic and challenges

Apart from the parameters influencing tool design at macro scale, micro tooling incorporates further properties to be considered. Owed to the small size of the die system, tool alignment issues and the choice of tool manufacturing process impacts the performance of the tool system. Also, metrological assessment of the tool system during manufacture is challenging at micro scale.

The visualization in Figure 6.1 depicts the major influencing parameters in micro tool design.

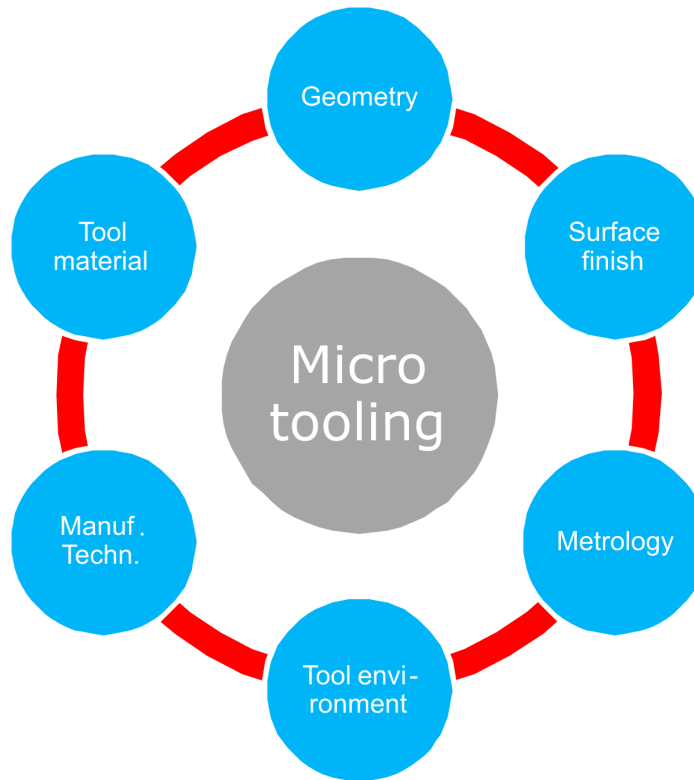


Figure 6.1: Parameters influencing the design of tools for micro bulk forming.

Starting from the top, geometrical aspects naturally play a role in the tool design process. The choice of tool structure and tooling technology is mainly dictated by the geometry in question. For example, a through circular hole in a hardened circular die for a backward cup extrusion would be made using the wire EDM process. However, a punch geometry would most likely be shaped using round grinding. Further, the geometrical scale of the workpiece, and with it the tool system, most often entail an implicit scaling of the tolerance bands of the tool geometry.

Surface finish is one of the strongest influencing parameters of micro forming, and thus important for the manufacturing of the tool system. The surface structure of the active tool elements will impact friction and lubrication conditions during forming. Often the tribological conditions is the single only parameters setting the forming limits for the bulk forming process. This effect is even more pronounced at micro scale forming, due to confined scalability of surface roughness characteristics.

Micro metrology is a variant of general metrology, dealing with metrological constructs and assessment at micro scale. Most of the techniques and machines utilized in conventional macro scale metrology is not practically scalable in size. Further, only few

mechanical measurement instruments can honor the precision required at micro scale.

Tool environment is meant as a common term for the framework and physical conditions surrounding the central die-set. Apart from bare environmental parameters, such as temperature and requirements of cleanness; the tool frame and the precision with which the adjoining press system is controlled, will influence the design of the tooling system. The importance of the parameters of tool environment is often erroneously disregarded.

The tool manufacturing techniques are an essential parameter in micro tool design. The choice of tool manufacturing process will impact the quality of the tool as well as many of the other variables of the forming process, such as surface finish, achievable geometry and the choice of tooling material.

Finally, the choice of tooling material is to be considered. Depending on load, surface requirement and manufacturing technology, the choice of material can be made. But the selection of tooling material is not only a dependent variable, since the resulting wear and lifetime of the tool system is closely bound to the choice of tool material. Further, a typical tool system for bulk forming almost always utilizes a combination of different tooling materials for different functional requirements in the system.

6.3 Geometrical limitations and tolerancing

Naturally, the design of a tool system takes offset in the intended geometry. As mentioned, the scale of the component in question and its features determine the condition for manufacture and operation of the tool. However, when the scale of the specimen is reduced, a domino effect is seen, requiring the process, tooling system and tool manufacturing process also to scale. In order to arrive at the final component, a tool with the right shape and quality is needed. This requires the availability of a manufacturing technology capable of producing the tool geometry in question - and with the right precision. Tool manufacturing technologies capable of producing dies for a micro bulk forming process will be treated later.

A secondary and intangible size effect is the desire to tighten the tolerance band as the overall envelope size of the produced part decrease. Even though tolerance setting in the ISO GPS system is defined as a separate entity, in reality it is often bound as a percentage of scale of the dimension to which it is attached. This means that the conformance interval, defined as the gap between the lower- and the upper tolerance for a geometrical entity, will be tighter in the micro scale. Or said in another way: small parts usually needs to be more precisely manufacture than bigger parts. The tight tolerance setting on small parts often leads to difficulties during quality and conformance assurance and special arrangements must be made to guarantee dimensional accuracy [14].

Restricting the view to a single micro forming step and considering the process level contributors to tolerancing, it is possible to define a general tolerance chain for the process. Figure 6.2 illustrates the main contributors to the variability of the forged specimen from a process standpoint. The press frame stiffness and distortion will impact the forging quality. Generally a rigid press frame is preferred because this will reduce the influence of the deflection of the frame. A technique exists for characterize the press frame deflections in a matrix formulation. From the 6-element formulation, the

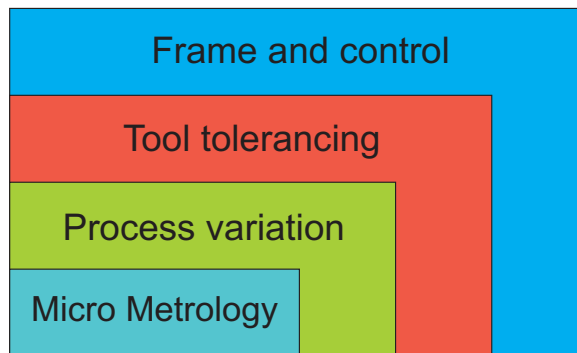


Figure 6.2: Contributors to deviation for nominal geometrical dimensions in micro bulk forming

deflections of the press frame can be predicted and counteracted [87].

The motion control system of the press and the accuracy with which the stroke length can be controlled is also important. In an open die reduction forming process, an inaccuracy of ten microns in the stroke length can mean inaccuracies in the forged component of several hundreds of microns. Further, an imprecise punch stroke can destroy the tool set or lead to underfilling of the die cavity.

Tool tolerancing is inevitably the most fundamental factor in the shape of the forged component. Any inaccuracy in the tooling system will directly be passed onto the forged component. Further, the influence of these effects is often substantial in comparison to other effects. Tolerance deviations in the tooling system can be further classified into direct and indirect effects. Direct tolerance effects are those that characterize inaccuracy in the central tooling elements, such as punches and dies. Indirect effects are the secondary effects attributable to misalignment, backlash and elasticity of the tool die set and other supporting elements of the central tool. Some of the forging inaccuracy originating from indirect tooling inaccuracies can be quantified and counteracted. By repeated measurement of the tool in between the various machining processes, the indirect deviations can be detected and counteracted. Active in-process measurement and correction is possible in some cases. An example is the placement of a length transducer close to the central tooling elements, allowing for in process verification and counteraction of the stroke length and tool elasticity changes.

The third contributor to geometrical deviations during the forming process is variations within the process itself. In a well designed forming process, only small process deviations are to be expected. However, changes in temperature, workpiece material, tribological and wear properties of the tool system can lead to changes in the forged geometry. For this reason it is common to see quality assurance specifications in the forging industry with a batchwise random sampling approach. When a forging process is scaled to the micro domain, increased process variations can be expected due to the increased 'inhomogeneity' of the work piece material [17]. This effect is strongly dependent on the grain size of the work piece material and can be neglected in the case of amorphous materials. Analytical analysis of the material flow in micro metal forming, incorporating

the stochastic nature of the grain size influenced material flow, has been developed [88].

Finally the metrological instruments and procedures will influence the process tolerance chain. It is debatable whether metrology is an integrated part of the process chain in micro bulk forming or an associated process. However, the finite measurement accuracy of the utilized instruments and procedures will have an impact on the geometries and tolerance bands that can be set and verified. A common understanding is that the uncertainty of the method of measurement should be about a tenfold better than the uncertainty or accuracy of the specimen in question. This requirement can be difficult to satisfy for micro bulk forming. Thus, the influence of metrology cannot be neglected during design, manufacturing and inspection of components with geometrical aspects in the micro scale.

6.4 Micro bulk forming analysis

The first step in a tool design process is an analysis of the forming procedure. Here the creativity, knowledge and experience of the designer are combined with computer aided design tools to evaluate the performance of the suggested design.

Once the concept for a forming procedure is established, a preliminary tool design is modeled in the CAD system. From hereon the CAD solid model can be imported into a simulation tool, where the elastic and plastic deformation of the material in question can be simulated. A number of commercial metal forming simulation tools are available both as 2D and 3D packages. Essentially all types of simulation tools work in the same manner, utilizing the finite element method for solving the problem at hand in a number of parts. There are, however, differences in the type of material libraries and friction model that are implemented in each package.

Once the simulation of the forming operation is concluded, the designer can evaluate the material flow, strain within each point of the part, damage, surface expansion, press load and more. With these data the designer can go back to the geometry of the tools and optimize the design and rerun the simulation with a new geometry. In this way costly tool manufacturing for each trial run can be avoided. Simulation tools for metal forming have a track record of more than a decade and the similarity between forged part and the simulated results are often within less than 1% error. However, in order to arrive at a good simulation result, the conditions for the simulation have to be set up correctly. First of all, a good material model is essential. But also the number of simulation steps, friction conditions and boundary conditions have to be chosen with care.

In conventional metal forming simulation algorithms, the work piece material is modeled as a homogeneous continuum. This is only valid in the case where the majority of the material grain structure is confined inside the volume of the material. In the micro scale, where a sizable part of the grains are bordering on the surface of the billet, the presumption of a homogeneous work piece material breaks down. In this case a surface model can be adopted, where grains contained inside the volume of the workpiece and grains located close to the surface are modeled differently [89]. This is dubbed a *surface layer model* and is regarded to have validity in open die forging primarily.

The next incremental development in the quest for an accurate material model capable of

including the grain size induced effects, was the introduction of synthetic grain structures in the material model. By compilation of a synthetic grain model, which statistically comparable values to that of the work piece material, the effects of inhomogeneity of the material can be simulated. Through introduction of a matrix formulation of in the Hall-Petch equation, the equation governing the relationship between grain size and yield strength in the material (Equation 6.1), good simulated predictions were made for yield strength and scatter of a micro cylinder upsetting experiment [49,90].

$$\tau = \tau_0 + \frac{K}{\sqrt{d_G}} \quad (6.1)$$

, where τ is the shear stress, τ_0 the critical shear stress, K is the Hall-Petch constant and d_G is the mean grain size.

Introduction of the mesoscopic model allows for an approximate evaluation the influence of the scattering effects in the material flow, provided that an accurate material model is available. However, the model is limited to single phase materials, the influence of the grain orientation is not taken into account and the procedure for establishment of the material model is not standardized.

Finite element analysis is an indispensable tool in the design phase of new bulk forming procedures. Currently in micro bulk forming the material models of the macro size is applied, well aware of the inadequacy of the material model. With future research into more accurate material models and a standardized formulation of the material parameters being the input to these models, precise simulation of the micro forming process can be accomplished.

6.5 Tooling elements and properties

When the geometry and forming process steps have been established, the actual tool design phase can be initiated. In traditional size tool manufacturing the typical tool manufacturing process chain is as visualized in Figure 6.3. Upon selection of the tool material, a bulk piece of material can be selected and cut. Depending on the geometry of the die or punch tool element, the bulk steel can either be already hardened or in the soft state.

The bulk piece is then machined, typically by milling or turning or grinding. Electrical discharge machining is also applied, especially for medium to complex internal geometries with high aspect ratio.

Often tools then undergo a number of heat treatment processes. The purpose of these is either to tailor the tooling material characteristics to the usage scenario or to relieve the tool of internal stresses originating from the cutting processes.

After heat treatment the tool is sent for polishing and coating. Polishing of the bulk forming tools is essential for the tool function and lifetime. If polishing is omitted the required tribological conditions of the bulk forming process cannot be met, primarily due to high friction and wear. Further, an unpolished tool will be more vulnerable to crack initiation, thereby increasing the risk of tool fracture. At times the active tool

Tool manufacturing for bulk forming

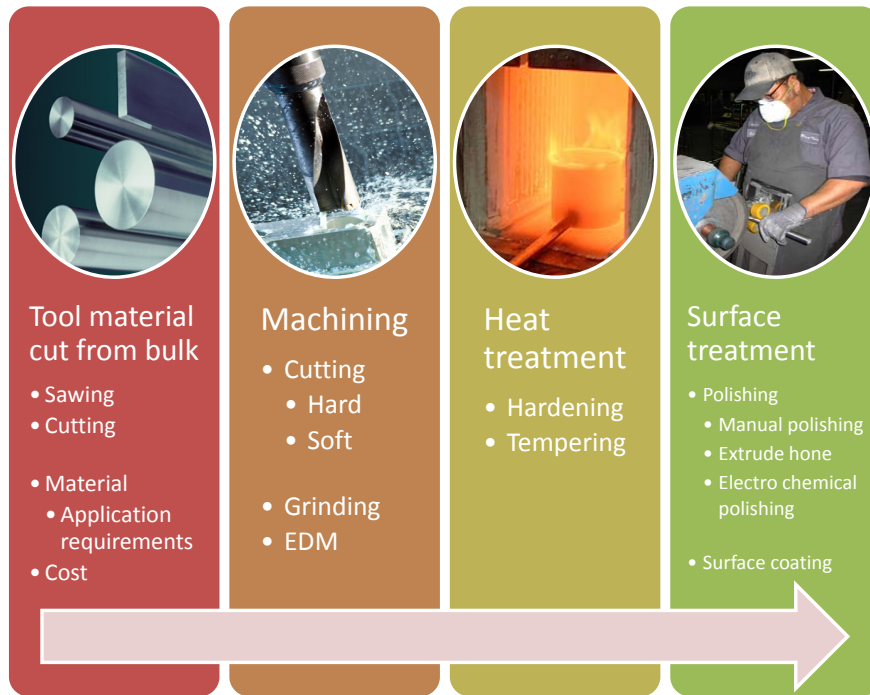


Figure 6.3: Typical processing sequence for a macro scale bulk forming tool

surface is coated with thin layers of coating. Depending on the nature of the forming operation and the materials used in the process, tool coating can help to increase cycle times, minimize friction, galling and can increase tool life. Coating is most often applied through physical vapor deposition process and requires the tool surface to be primed before the coating can be applied.

Examples of variants of the outlined processing chain for tool manufacturing can be encountered, but the outlined sequence is followed in most cases. In large bulk forming plants, tool manufacturing is systematized to high degree, often with the use of advanced logistics planning software. This is done in order to avoid bottlenecks in the production chain, increase flexibility and save cost by not having idle time on the tooling processes.

Altering our view to the production chain for a typical micro bulk forming tool, the tool process chain changes considerably. Due the tight tolerances for the geometry of the central forming tools, cut of tool material in the soft state is no longer possible. The reason for this is that a subsequent hardening process would cause intolerable geometrical distortion. The tool manufacturing process chain, as it typically looks for a micro tooling system, is shown in Figure 6.4. Starting from the beginning of the micro tool processing chain: Owing to the typical size of the tools, it is advantageous to take offset in the large family of standardized tooling elements, as specified in various ISO and DIN standards, available through a range of vendors. These norm elements form a cost effective basis for

Micro tool manufacturing



Figure 6.4: Typical processing sequence for a macro scale bulk forming tool

production of micro tooling elements directly in hardened material. Further, the norm tooling elements are available in bulk and is usually manufactured with good precision tooling machinery. The precision norm parts further form a good basis for reference system alignment during tooling processing and in the bulk forming machine.

Due to the hardness of the tool material and the size of the geometry to be fabricated, the number of milling, drilling and turning operations that can be applied is very limited. Cutting process can be achieved in hardened tool steel for geometries with limited width/depth aspect ratio by application of limited feed rates. Further, for micro mill tools the axial depth of cut is often measured in microns and the shaft length is often around 5 millimeters. This imposes a natural limitation of achievable forming tool geometry [36]. For external geometries, such as punch or ejector, grinding is the preferred method of machining. Grinding is applied extensively for standardized hardened tooling parts such as ejector pins, punch needles and bars for bearings. For internal geometries, electro discharge machining is applied as the variants μ wire-EDM, μ drilling-EDM, die sinking EDM and μ EDM-milling. These processes will be treated later in this chapter.

Surface roughness is a key parameters in any bulk forming process. Owed to the scaling of the bulk forming process, a low tool surface roughness is crucial at micro scale. However, the tool roughness cannot be chose arbitrarily and will often be a resulting

parameter of the chosen tool manufacturing process and process parameter settings. Surfaces roughnesses down to $Ra = 0.12\mu m$ can be achieved directly in electro discharge machining. However, this value should ideally be reduced to $Ra < 0.04\mu m$ in order to lower friction during the forming process to a tolerable level. Few processes exist to lower the surface roughness of micro tools. Manual polishing requires a customized shaped polishing body and polishing medium with fine grained abrasive particles. Electro chemical polishing can also be applied with a custom made electrode and careful selection of the process parameters. However, the area of surface creation and characterization for micro tooling is a complex matter and continues to be an area of research [36].

The condensed structure of the typical micro tooling process has the effect that the typical production time of a micro tool can be reduced. During some of the experiments done in this work, the complete tool manufacturing lead time was less than 24 hours, allowing for fast design iterations and trial runs to be made. Further, by utilization of a single processing step for machining of the central geometry, the inter-process alignment errors are avoided.

6.6 Tooling materials for micro bulk forming tools

Typical tooling requirements for micro bulk forming tools can be summarized as in the following:

- Temperature range typically from $20^{\circ}C$ to $200^{\circ}C$. For advanced forming operations, such as the forming of Titanium or bulk metallic glasses temperatures up to $500^{\circ}C$ are required.
- Pressures on the tool facets in the range of 2000 MPa requires hardened tool materials.
- Required precision of central tooling elements approximately $1-5\mu m$.
- The application of lubricant is advantageous in many cases, but lubricant entrapment should be avoided.
- Surface roughnesses should be below $0,1\mu m$, preferably in the range $0,01 - 0,05\mu m$ in order to keep friction low.

Material families suitable for honoring these requirements would be conventional tool steels, cemented carbides and advanced ceramics.

Tool steel refers to a number of different carbon and alloy steels that are well-suited to be made into machine tools. Tool steel can be processed using a range of processes and the hardness and metallographic grain structure can be tailored to the individual application. Tool steels are inexpensive and can be sourced easily. Steel is the most commonly used material for die and mould making and a lot of knowledge and experience regarding the use of this material has been accumulated. Soft and medium hard tool steel alloys are used for frame and supporting tool elements, whereas tool parts with high requirements for wear and load often are hardened.

Ceramic materials can be defined as any inorganic crystalline oxide material. Ceramic materials are generally brittle materials with high hardness, high strength in compression, weak in shearing and tension. Owing to the trend towards more net shape parts in bulk forming processes, cemented tungsten carbide, also called hard metal or tungsten-carbide cobalt, have found their way as interesting materials for die and punch tooling elements. The primary reason for this is the high compressive hardness of about 90 HRA, yield strength between 3000 and 4000 MPa and good wear resistance. As in the case of other polycrystalline materials, is the performance characteristics of advanced ceramic materials influenced by the material grain size. Small grain size equals high hardness but low fracture toughness. Cemented tungsten carbide has good tolerance towards compressive stresses but exhibits relatively low fracture toughness. When used in metal forming, a cemented tungsten carbide die needs to be prestressed in order to keep tensile stresses within an acceptable level and avoid tool fracture. Cemented Tungsten carbide can be applied in forming procedures up to about 400°C where oxidation of the material will begin. The material hardness is reduced by about 75% at 400°C. For hot to warm forging, other sorts of ceramic materials can be used. Ceramic materials are already known as mould material in sand casting and as main component of thermal insulation material. Especially nitride and silicon ceramics exhibit properties that make them suitable for application as high temperature tool materials. Ceramic materials can be applied at temperatures up to 1000°C and beyond without significant loss of mechanical strength, with the important exception of the none oxide types. The mechanical properties of modern ceramic materials are comparable to those of cemented tungsten carbide, with high hardness and little tolerance toward fracture and tensile stresses. Due to the widespread application of silicon in the electronics and MEMS industry, silicon and nitride ceramics have become interesting as micro tooling materials. Further, the availability of mature processing processes for these materials, mainly based on combination of a number of lithography and etching operations, make advanced ceramic materials interesting from both a research and application perspectives.

	tools steel	advanced ceramics
μ -machining	✓	NA
diamond cutting	(✓) non ferrous	
μ -EDM & μ -ECM	✓	(✓) electrically conductive
Chemical etching	slow	some
Laser ablation	slow	structuring

Table 6.1: Typical processability of metals and advanced ceramic material for micro tooling.

6.7 Micro tooling manufacturing processes

Once the choice of tooling material has been made, the tool manufacturing process chain have to be established. A number of tooling processes exists. These can be categorized as additive or subtractive processes, depending on their nature of operation. Further, the characteristics of each process makes it more or less attractive for a given application scenario. Key parameters in this sense are: accuracy, compatible materials, minimum corner radii, speed of operations and more.

Tool manufacturing holds an element of the classic chicken or the egg causality dilemma. In order to realize a manufacturing process, the need for a tool is evident. But in order to realize a tool; a tool manufacturing process is needed. The same relation can be applied to manufacturing precision. In this case the precision of manufacturing process equipment should exceed the required precision of the specimen be a factor of 5-10. But how is this high precision tool manufacturing process equipment realized?

In the following we will assess some of the most common processes that might be suitable for micro tool manufacturing. A list of commonly encountered additive processes are listed below:

- electroforming [7]
- laser sintering (SLS)
- physical and chemical vapour deposition [91]
- printing [92,93]

The group of additive processes generally function by surrounding the specimen with a chemical solution that is able to deposit on a base structure surface. In some cases the deposition can then be controlled through selectively altering of the localized physical environment at the spot where adhesion is desirable. These selective mechanisms are often controlled thermally, through lithography processes or by pre-structuring of the specimens surface. Finally, additive processes can be achieved by printing technology or sintering of material on top of a base. The latter type of processes is the core technology of the emerging rapid prototyping technologies.

Apart from electroforming, none of the additive processes are considered to have sufficient precision to be utilized for micro tool production. Physical vapour deposition is used to coat micro tools after main geometrical processing, but is generally not well suited for creation of tool structures with high aspect ratio.

Subtractive processes are processes that work by removal of the bulk material. Apart from classical cutting processes, a range of chemical, electro-chemical or thermal processes exist. Popular subtractive processes used for in micro fabrication include:

- milling, turning or other machining processes [35,36]
- electro discharge machining (EDM) [94,95]

- chemical etching processes [95,96]
- electrochemical machining (ECM) [95,97,98]
- laser machining/ablation [95,99]

Micro -milling, -turning and -drilling are scaled versions of the well know processes where a part of the workpiece material is removed by means of a cutting tool. However, due to burr surface generation, tool deflection and scaling effects, cutting processes experience a reduction of the processing windows at micro scale [36].

Electrode discharge machining is available in a number of variants. Wire- and die sinking EDM are the most commonly applied processes, but also μ EDM milling is frequently applied. The EDM processes are capable of working equally well in hard or soft materials, it only requires a certain level of conductivity of the workpiece material [94,95].

Chemical etching is applied frequently in the MEMS world, where typical $2\frac{1}{2}$ D geometries are made by alternating processes of deposition and etching of materials. Within micro tooling chemical etching rarely used for other purposes than surface structuring or as parts of chemical polishing processes [95,96].

Electrochemical machining is sometimes referred to as 'reverse' electroplating and is a niche technique. It can be used for machining of complicated parts and for de-burring of surfaces. Like in the case of die sinking by EDM, the ECM method often requires an electrode having the inverse shape of the finished workpiece geometry [95,97,98].

Laser machining and ablation is frequently used for engraving, cutting and welding purposes. The primary usage of laser technology in micro tooling is for cutting of thin plates and for surface structuring [95,99].

In the following the electroforming and μ EDM processes will be treated in more detail. Examples of application for micro tooling will be demonstrated and the process characteristics outlined.

As example of a micro forming die geometry, the die geometry shown in Figure 6.5 will be used. This die geometry is utilized for the first of a two step forming process of an aluminium potentiometer axle. The high aspect ratio and the small alignment feature in the conical part of the die are the most challenging elements of the manufacturing process of this internal geometry.

Electroforming of die insert

With the goal of evaluating if electroforming can be applied as method of tool manufacture, a tool manufacturing experiment will be conducted. First the basic principle of electroforming is outlined. Electroforming is used in an indirect tooling approach where an mandrel with the inverse shape is first manufactured. Typically the mandrel is machined using cutting or EDM processes. The mandrel is then submerged into a conductive electrolytic solution and is then connected as the cathode in a voltaic cell. The anode is typically a nickel based material, but can also be copper or any other metallic material to be transferred to the mandrel. The voltaic cell is then connected

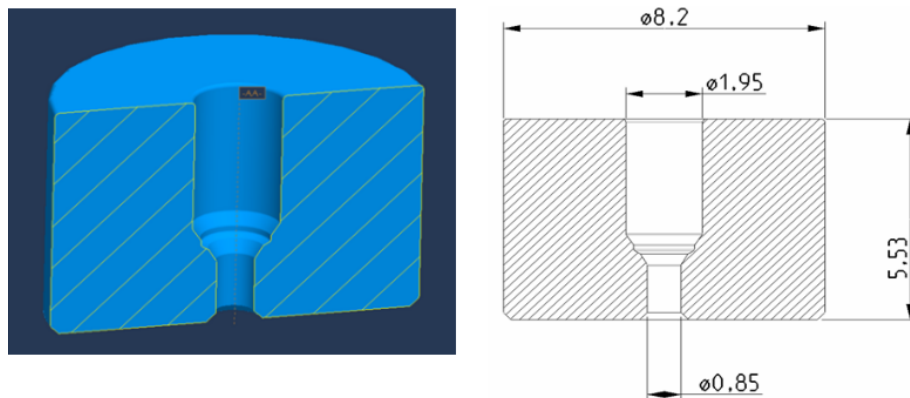


Figure 6.5: Die geometry to be manufactured. The die is a pre-forming die for a two step forming process for manufacturing of a micro axle for a potentiometer.

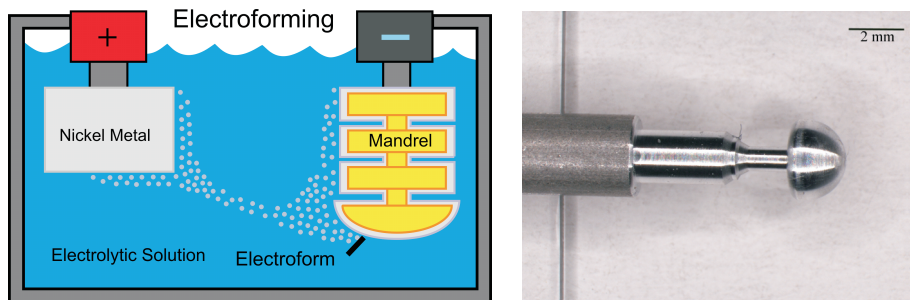


Figure 6.6: Principle of electroforming (left) and a turned geometry in aluminium to be used as stencil for electroforming.

to a direct current power supply and the electroplating process is started. The process often applied in a popular variant where a silicon base, often a silicon wafer, is machined and subsequently plated electroplated. It has been demonstrated that this method can be utilized for realization of precision tools for polymer injection moulding tools [33].

The plating rate is depending on the electrical current going into the two electrodes. Local plating rates are dependent on the current density or flux at every point at the mandrel. Thus, to assure a uniform plating rate, agitation and rotation of the mandrel is often needed. Basically any metal can be used for the electroplating process, also alloyed materials. However, for thick layers local stresses and voids tend to build up in the electroplated material. This effect can to some degree be reduced or controlled with chemical additives.

In order to electroform the die geometry show in Figure 6.5, a mandrel with the inverse shape has to be machined. Since the mandrel will be machined, electroplated and then removed, it is advisable to choose a mandrel material that is simple to machine and can be easily chemically dissolved. In this case an aluminium alloy EN AW-6060 is chosen. The finished mandrel is shown in the photograph right in Figure 6.6. In order to ease referencing after electroplating, a reference feature was machined onto the rod of

the mandrel.

The mandrel was then electroplated with pure nickel for 48 hours, leaving a layer of about 3 mm nickel on the mandrel. In order to access the quality and accuracy of the electroplated specimen, the electroplated specimen was casted in epoxy and ground. The aluminium mandrel was etched away using a NaOH solution. The result of the plating operation can be seen in Figure 6.7. In the closeup on the right hand side, the detailed quality of the electroforming operation can be evaluated.

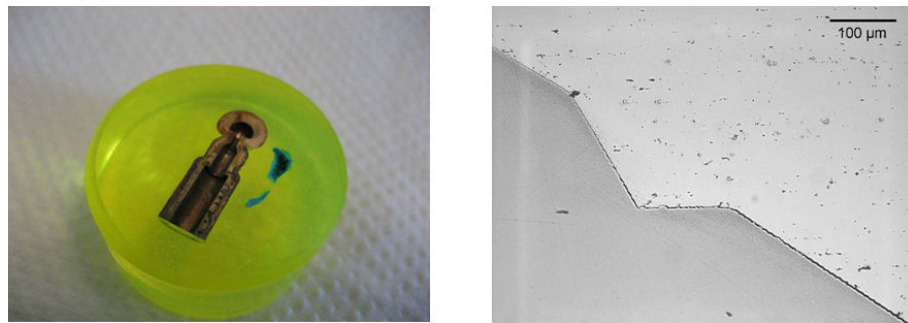


Figure 6.7: Micro bulk forming die to be manufactured using electroplating.

It is clearly seen that accurate replication is achieved. The sharp edge on the alignment feature of the die geometry is replicated onto the electroformed component with high precision. Indeed replication accuracies in the micrometer range have been reported for the electroforming procedure [33].

Due to the difference in yield strength of the mandrel material and the nickel layer and the following risk of bending of the aluminum mandrel, the wavy surface of the electroplated nickel could not be machined using a cutting operation. The mandrel was cut using wire-EDM and then press fitted into a stress ring made of Impax tool steel. The resulting tool insert can be seen later in this chapter in Figure 6.9.

Micro-EDM

In this section the forming die for a micro axle is manufactured using a Sarix Micro Electrical Discharge Machining (μ -EDM). The computer controlled machine is capable of wire eroding hard metal with high precision. The machine features a CAM extension, which makes it possible to reproduce complex geometries from a CAD-model. The machine works much like a traditional milling machine but uses a solid carbide electrode down to 60 μm in diameter as the active eroding electrode. The small size scale of μ -EDM process allows point-flooding with dielectric fluid of the sparking area, avoiding complete submersion of the workpiece and electrode. The central elements of the μ EDM process is depicted in Figure 6.8b.

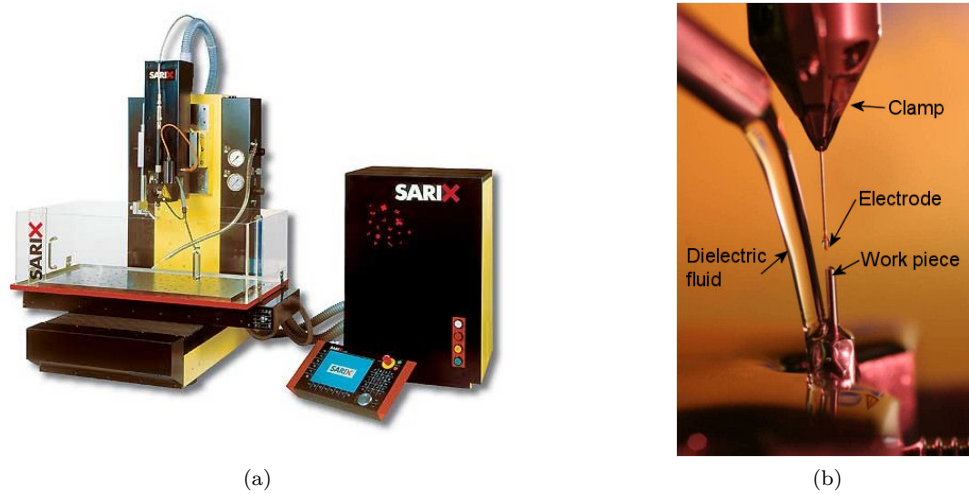


Figure 6.8: Photograph of the Sarix SX-200-HPM 3D Micro EDM machine (a) and a closeup image of the active components involved in the central spark erosion process line (b)

The μ -EDM process is divided into three operations. First a drilling operation is executed using a hollow $300\mu\text{m}$ brass electrode. The purpose of this operation is to ensure proper flushing of debris through the hole during subsequently machining of the internal geometry of the die. The processing time of the drilling operation is 20 minutes. Secondly, a rough sparking operation is performed. This operation removes the bulk of the material inside the die using a $300\mu\text{m}$ solid carbide electrode. The roughing operation leaves only a $50\mu\text{m}$ layer of stock material along the wall-sides of the die and has a processing time of about eight hours. Finally, a the fine sparking operation is executed with at running time of about eight hours. The purpose of the operation is to ensure good precision of the final geometry and to reduce surface roughness. The final surface roughness after the fine-sparking operation has a value of $R_a \cong 0,14\mu\text{m}$ and the precision is within $\pm 3\mu\text{m}$. Ultimately, the surface roughness should have a R_a value which is about ten times lower (about 0.01), but this is not realizable using the μ -EDM process. Due to nature of the electrical discharge technology it is not possible to achieve corner radii of less than $60\mu\text{m}$, but generally this figure scales with the diameter of the electrode. The reason for this is bound in the fact that a spark-channel is more likely to open at the point of a discontinuity [100].

Comparison between electroforming and Micro-EDM

The yield strength of the electro formed die was tested to be about 400 MPa. This is not sufficient for cold forming purposes as even with soft materials the die stresses will exceed 600 MPa . Recent studies have show that electro forming with a Nickel-Cobalt alloy is feasible. The first test-items showed problems with cracks and uneven plating of the substrate, but these problems were solved by using special additive in the plating-bath. Nickel- Cobalt has a yield strength of about 800 MPa, thus being better suited as die material [101].

As an additional case study a die was manufactured by the μ -EDM process and send for

coating with diamond-like carbon coating (DLC). The DLC coating is mainly applied to increase wear resistance of the coated surface. Special care should be taken when coating ferrous alloys with the DLC coating as this might lead to carburizing at higher temperatures, an effect that can lead to degraded hardness of the coating or substrate material.

A photograph of the manufactured die geometries can be seen in Figure 6.9. It should be noted that the electroformed die insert has been press fitted into a supporting holder. In order to access the results of the manufacturing processes and the coating experiment,

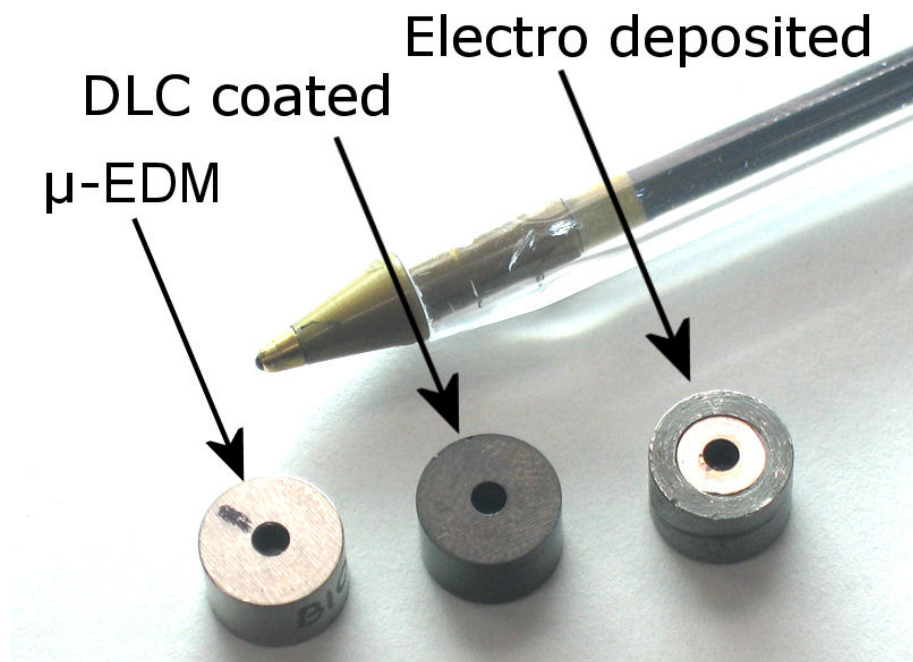


Figure 6.9: Photograph of micro forming dies manufactured using electroplating and EDM processes. The black colored die in the center has been coated with DLC coating.

silicone replicas were made of the respective dies. The resulting replica items have been photographed under microscope and are shown in Figure 6.10.

First considering the replica of the DLC coated die in Figure 6.10b, it is clear that the internal surface finish of the die have been deteriorated by the coating process. The tilting of the lower cylindrical part with the smaller diameter cannot be attributed to the coating process and is an artefact of the replication process. However, the coating inclusions in the replica compound is a indicator of poor adhesion inside the die. It is noted that the poor adhesion increase around the middle of the die and is only minimal close to the in- and outlets of the die. In conclusion is can be noted, that the utilized coating technology is not capable of successfully coating internal die geometries with high aspect ratios. The selected die geometry is representative of a whole class of micro forming dies, thus the findings is regarded as being a general observation for die geometries with these features.

Concluding on the comparison between the electroformed die and the spark eroded die geometry, the difference is evident. When looking at the figures 6.10a and 6.10c the overall geometry appear identical. However, when considering the achieved corner radii (marked with arrows) at the first reduction die land and around the neck of the alignment feature, a clear difference is seen. Where the electroforming procedure have achieved low corner radii, a clear rounding of the features are for the die manufactured with μ -EDM. This rounding is due to an unavoidable rounding of the micro electrode edge during erosion. The external corner radii are replicated as internal corner radii during machining, setting an lower bound limit on the achievable corner radii. The effect can be minimized by adding a finishing pass in the EDM process with a small diameter electrode.

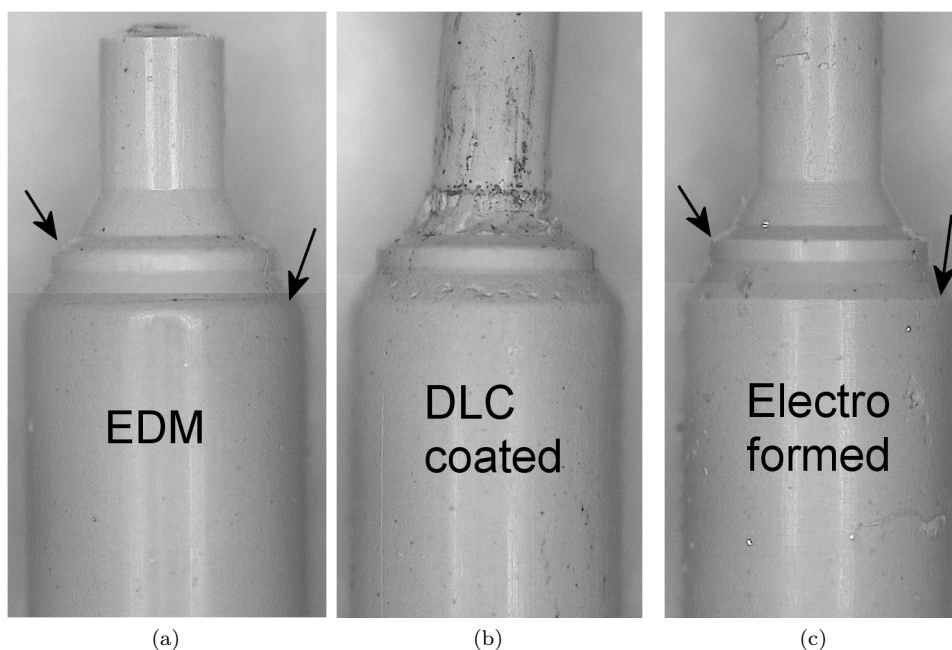


Figure 6.10: Silicone replica of forming dies manufactured by electroforming and by EDM.

Even though the increase in the internal corner radii of the die is unintentional, it is recommendable in metal forming to ensure rounding of internal edges. Sharp edges might induce shearing of the work piece material and thus lead to excessive damage or fracture during forming.

Conclusion of electroforming and Micro-EDM die manufacturing experiment

Concluding on the experimental results on the die manufacturing, some general observations have been made. With a machined mandrel and the electroforming procedure, a high quality die insert was manufacture. The electroforming method is capable of accurately replicating the geometry of the mandrel, including sharp corners and fine features. The electroforming process chain is longer and requires the pre-fabrication of a

mandrel as well as subsequent etching, machining and fitting of the formed geometry in a holder. The available materials for electroforming of forming dies are limited to nickel base alloys, thereby restricting the achievable hardness of the formed material. The tool roughness of the electroformed die will be comparable to that of the mandrel.

The micro EDM process is a direct process, where the intended geometry can be manufactured directly in virtually any alloy able to conduct electric charge. The material removal rate is low, when compared to cutting and the design and layout of tool path and process parameters requires an experienced operator. Further, the process is not capable of machining internal corners geometries with small corner radii and the minimal surface roughness is about $Ra=0.12\mu m$. The results have been published at the Esaform conference proceeding [102].

6.8 Micro forming tool for micro axle application

In the following we look at the possibility of forging of a micro cardan axle component using the micro forming process. The axle component is used in an application where a rotational movement must be translated laterally. The work piece material was specified to either stainless steel, Sterling silver or an aluminum alloy. The choice of work piece material suggests only limited requirements for the overall strength of the component. The technical specifications for the cardan-shaft are reproduced in Figure 6.11. Given the

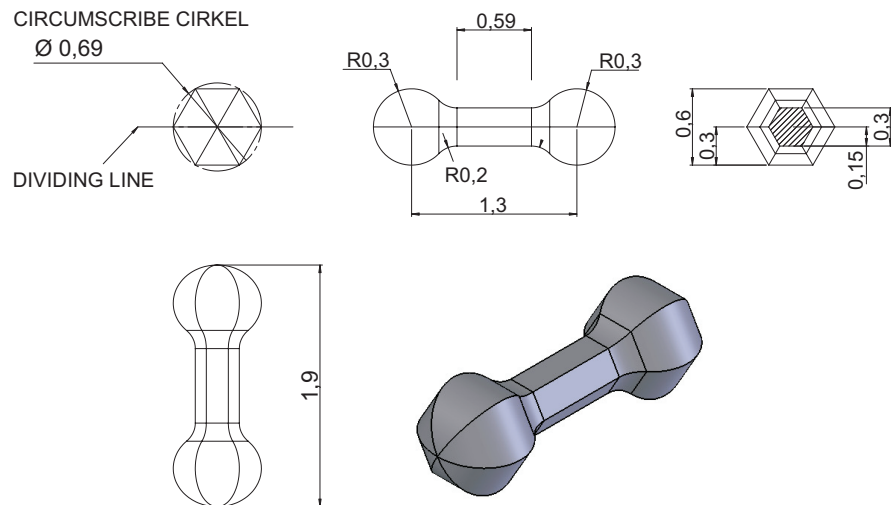


Figure 6.11: Technical drawing of the axle component. The general tolerances are $\pm 20\mu m$ on most geometrical elements

geometry of the axle component, a closed die forging approach is chosen. Two identical dies are pressed together around a small billet and the component is forged in a one step process. The material of the axle is unevenly distributed, with a cross sectional area of 0.31 mm^2 in the middle of the orb and 0.078 mm^2 in the middle of the cardan shaft, a cross sectional area difference of about four times. In such case it would normally be useful to design a forging process involving a number of pre-forming operations, where the work piece material can be positioned before the final forging procedure is executed.

However, this approach have been abandoned in this case to avoid alignment and transfer problems. The design of the die system was made to allow for flash to be generated during forming. This flash should subsequently be cut using a cropping or blanking procedure in a separate tool. The suggested forming procedure was simulated using the Deform 3D simulations software with 10.000 nodal elements and the simulation was run as rigid-plastic deformation. The resulting flow of the material can be seen in Figure 6.12 where (a) illustrates the initial position before the forming operation and (b) is the situation once the axle have been formed. It is clear from the simulation and

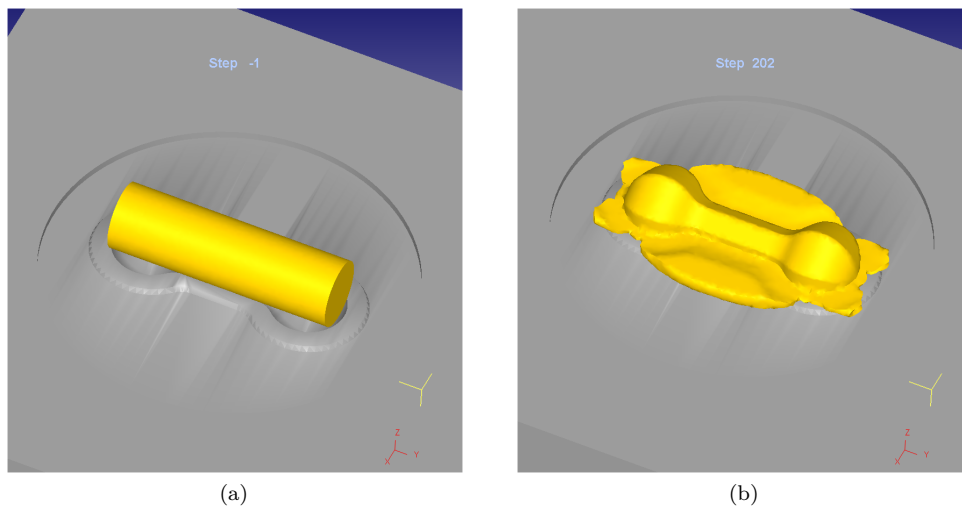


Figure 6.12: Simulation of suggested forming procedure of axle component.

visualization of forming process that some of the material is wasted as flash around the middle waist section of the component. The volume of the billet is 120% of the volume of the cardan-shaft, leading to 20% material waste.

The limited size of the component envelopes and the strict tolerance specifications imposes high requirements on the die geometry. A set of dies was manufactured using the Sarix SX-200 μ -EDM machine, utilizing the option of using dressed electrodes. Two electrode diameters were used, one electrode with a diameter of $150\mu\text{m}$ for roughening of the die and a $50\mu\text{m}$ for subsequent fine sparking of the die geometry. A total of three sparking operations were defined. First a rouging operation is executed where the bulk of the material is removed using a $150\mu\text{m}$ diameter electrode. During the roughing operation the voltage and current setting of the micro-EDM machine is set high in order to achieve a higher material removal rate. The operations was set to leave $100\mu\text{m}$ of stock material between the roughened machining and the final geometry; in order to leave material for a subsequent fine sparking operations. The second sparking operation is executed with lower voltage and current setting, thus realizing a fine surfacer finish. The fine sparking operations tracks the contour of the axle die, thereby lowering the surface roughness along the surface of the forming die. The second operation also uses a $150\mu\text{m}$ tungsten carbide electrode dressed on the wire dressing unit on the machine. The third and final machining pass uses a $50\mu\text{m}$ dressed electrode. This small diameter is required to reach as far as possible into the corner of the die bottom - especially at the orb bottom. The tool trajectory of the third and final pass is illustrated in Figure

6.13b.

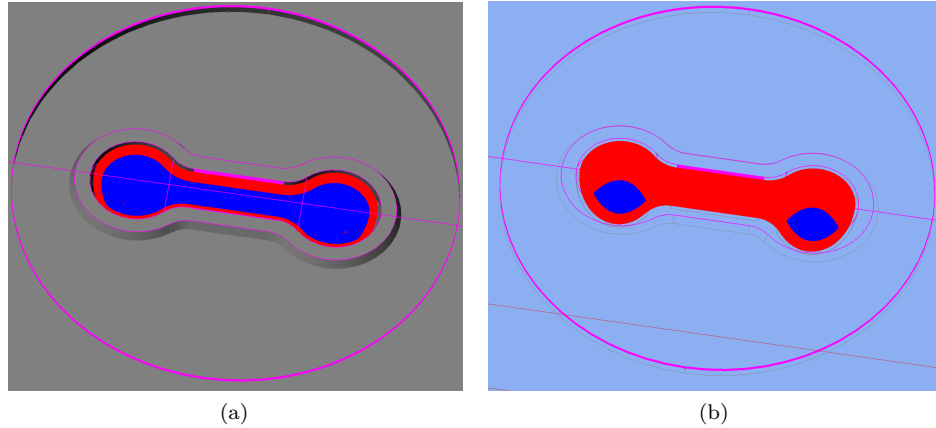


Figure 6.13: Micro-EDM tool path for machining of die for cardan-shaft.

The multistage machining operations was chosen in order to optimize machining time. With the chosen approach, the total machining time of the three operations was about 24 hours. If the complete geometry had been spark eroded using a $50\ \mu\text{m}$ dressed electrode, the complete machining time would exceed 100 hours due to lowered removal rate and time for dressing of electrodes. The die geometry was machined onto the end surface of a ground norm punch needle of HSS material and a brass bushing was machined to ensure alignment. Simulation of the forming procedure exhibited internal pressures around 800MPa, thus no yielding of the tool elements are expected as these are hardened to 62 HRC. A photograph of the tooling elements is reproduced in Figure 6.14.



Figure 6.14: Photograph of the manufactured forging dies for micro bulk forming of the cardan axle component. The brass bushing in the background is used for alignment of the two dies during forming.

Once the two dies have been machined they were characterized in the Alicona focus

variation microscope. In order to access the quality of the manufactured die, two profiles were extracted along the length of the die. The first profile, crossing one of the orb ends of the die is shown in Figure 6.15a, together with the 2D profile extracted along the marked line. Using the minimum square method, the length and the angles between the

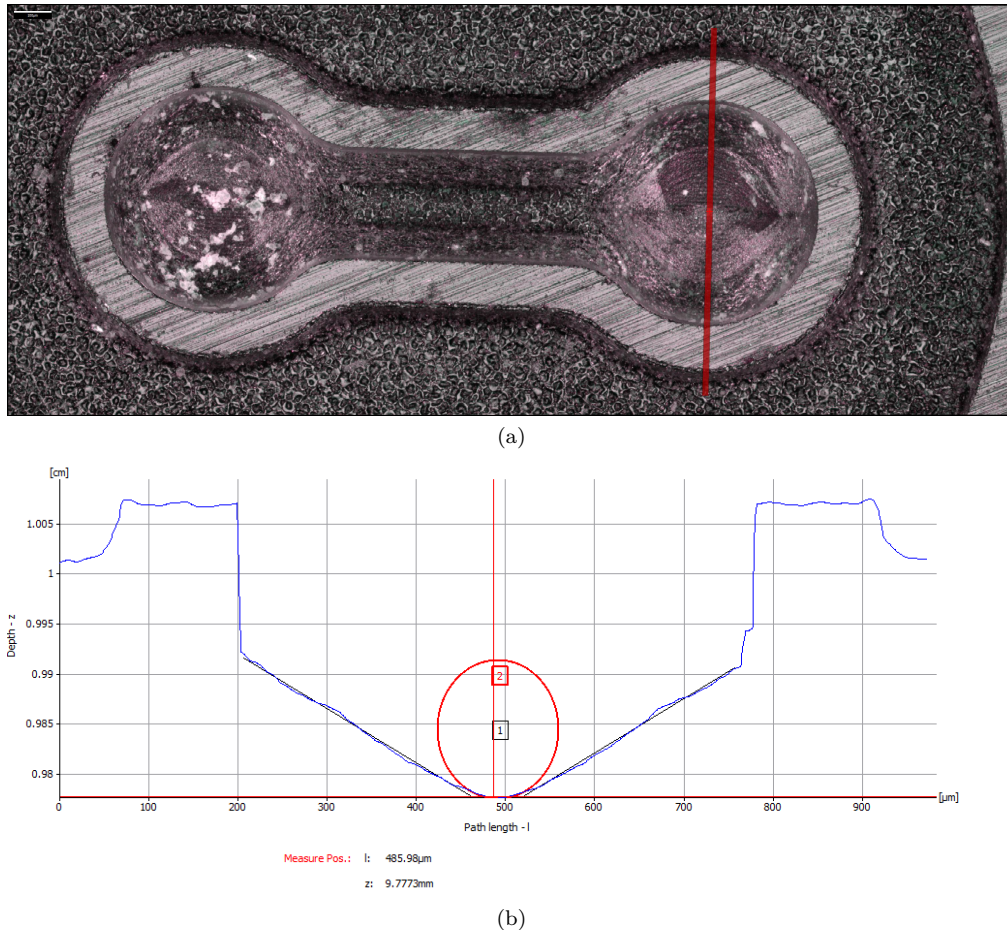
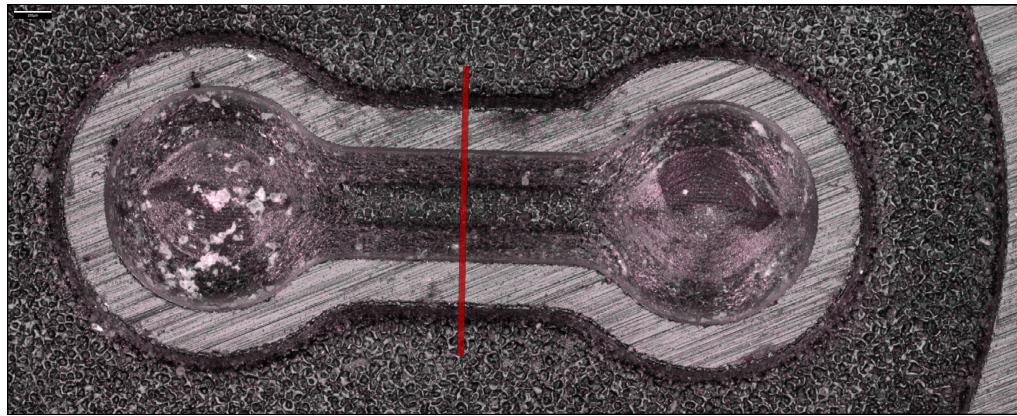


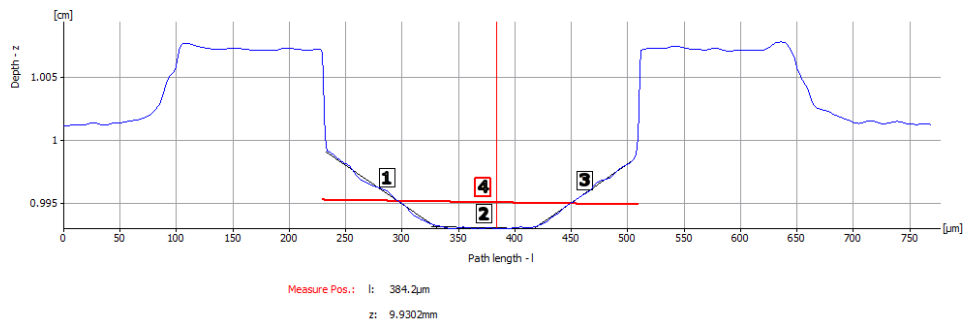
Figure 6.15: A photograph of the manufactured die geometry and profile line (a) and the extracted profile along the line (b)

two sides along the base of the die was measured. The values are as follows: $323\mu\text{m}$ and $303\mu\text{m}$ with an angle difference of 123° , with the nominal values citing $345\mu\text{m}$ and 120° respectively. Considering the estimated combined measurements uncertainty of $\pm 30\mu\text{m}$, these are acceptable values. With the same approach, the radii of the bottom corner can be estimated. The radius of the fitted circle is states to be $62\mu\text{m}$, a values comparable to the minimum achievable corner radii mentioned earlier in this section.

The other profile is taken at the waist of the cardan-shape, thereby representing the smallest feature and dimension of the cardan shaft. The line along which the profile have been extracted and the cross sectional profile have been reproduced in Figures 6.16a and 6.16b respectively. The line pieces 1,2 and 3, measures $120\mu\text{m}$, $88\mu\text{m}$ and $103\mu\text{m}$ respectively. These three section line should, according to the technical drawing,



(a)



(b)

Figure 6.16: Micro-EDM tool path for machining of die for cardan-shaft.

only consist of a V-shaped two section line piece. Each line pieces should have a line length with a nominal length specified as $0,15 / \cos 30 = 173 \mu m$. The occurrence of this geometrical artefact is due to the finite width of the erosion electrode, where the electrode dimension of $50 \mu m$ and the spark gap distance is estimated to about $80 \mu m$. This is an example of a case where the finite width of the electrode is limiting the smallest achievable size of an internal geometrical feature. The micro EDM machine holds a feature for producing tapered and non-circular electrodes, but this capability has not been explored further in this work. The distance between the two opposing vertical facets are measured to $279 \mu m$, with a nominal specification of $300 \mu m$.

The tool surface roughness characteristics were measured using a conventional stylus type roughness profilometer, the Form Talysurf FTS 50 from Tylor Hobson. The roughness data was not de-convoluted to account for the stylus tip influence or cutoff filtered, but rather the mean value of a third degree polynomial approximation was subtracted to minimize the influence of waviness. The evaluation length of the three profiles was $620 \mu m$, thereby only satisfying the required evaluation length roughness values up to $Ra=0,02$ and $Rz=0,1$ according the the ISO 4788 standard [76]. However, since the

roughness values are applied as an indicative measure of roughness in this experiment, the evaluation length requirement can be relaxed. Figure 6.17 illustrates the positions

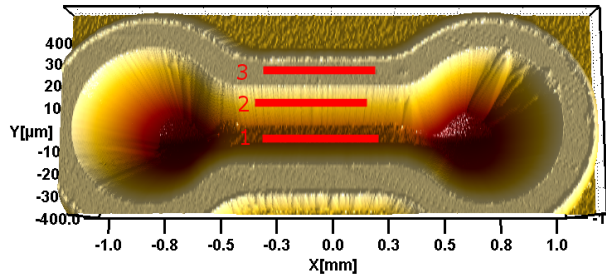


Figure 6.17: 3D representation of the surface roughness measurements. The three numbered lines indicate the position extracted roughness profiles.

at which the roughness profiles was extracted. The first profile is placed in the bottom of the unintended plateau of the cardan-shaft waist. The second profile is taken along one of the sides of the forming die. Owed to the 120° inclination of this surface special care should be excited when interpreting the measured roughness values for this profile. The third and final profile is placed on the rim plateau for thinning of the flash. The measured roughness values are reproduced in Table 6.2. Concluding on the measured

Profile number	Ra [μm]	Rz [μm]
1	0,63	5,76
2	0,31	3,22
3	0,16	1,00

Table 6.2: Measured surface roughness values of the cardan-shaft forming die. Profiles acquired as marked in Figure 6.17.

roughness values; an ideal roughness values for this kind of forming operation would lie in the range $Ra=0,01-0,1\mu\text{m}$. It is customary to encounter surface roughness values of $Ra=0,2\mu\text{m}$ in tool parts used in conventional cold forging. However, due the down scaling of the forging process in this experiment, it is expected that a lower roughness values is required.

For the roughness value of $Ra=0,63\mu\text{m}$ measured along profile no. 1, this high roughness is only expected to have a minor impact on the friction during forming. This is due to the fact that material is pressed perpendicularly into the surface, realizing little material shearing across the surface. The roughness values for the profiles 2 and 3 may be regarded as high for this micro forming operation. In theory, the Sarix SX-200 Micro-EDM machine should be able to achieve surface roughnesses down to $Ra=0,12\mu\text{m}$ with a substantial increase in machining time. Owed to the size and required precision of the process, the option of manually polishing the die surface is not considered viable.

Forging of cardan-shaft

A number of components was forged using the manufactured dies. A commercial lubricant, Molycote DX paste, was used for lubrication. The sterling silver work piece material

was drawn to a diameter of 0,65 mm, normalized and cut to the right length. A number of trials were conducted and the component was found to be fully forged with a press load of 900N. The photo shown in Figure 6.18a was acquired using a focus variation microscope and the profile along the red lines was extracted and plotted in Figure 6.18b

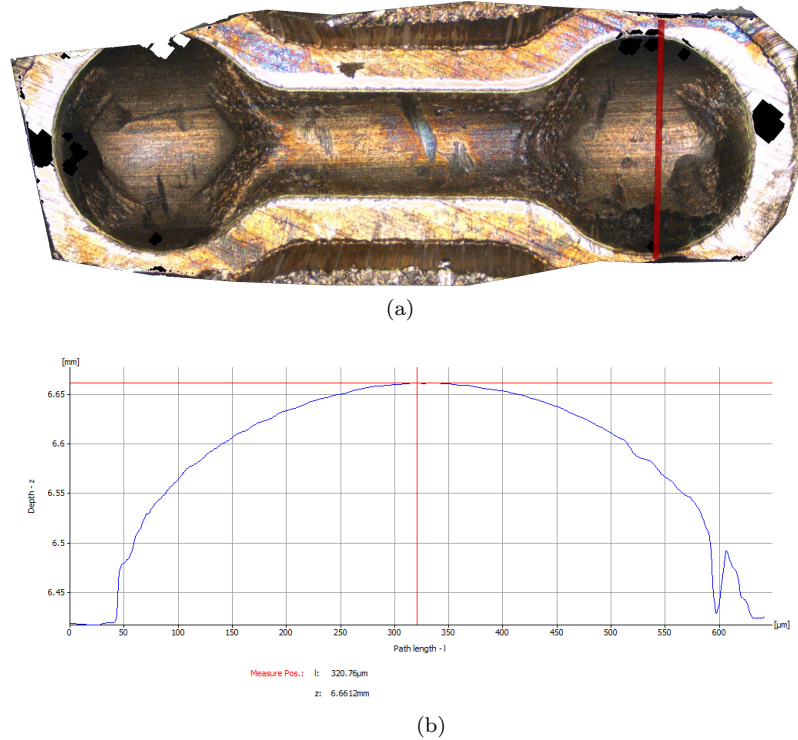


Figure 6.18: Forged cardan-shaft specimen. The shape of the forged readily recognizable. A profiled cross section can be seen in the plot (b).

When considering the cross sectional profile in Figure 6.18b, it is evident that full form filling has not been achieved. The round envelope of the orb end is the formed replica of the die geometry seen in Figure 6.15a. Looking at the forming filling around the middle waist of the component, shown in Figure 6.19, the situation is much the same.

The incomplete filling of the die and the inadequate replication of the die geometry is considered to be due to the combination of friction and flow characteristics of the work piece material. The relatively high roughness of the forming tool surface in combination with the limited size of the forged specimen has been shown to bring increased frictional influence [17]. Further, the classical polycrystalline structure of the silver material will impact the material flow during forging - typically leading to rounding of sharp geometrical features.

The experiment was concluded with a suggestion for a future development of a second generation forging system for this component. It is suggested that friction should be lowered through a decrease of the tool surface roughness. The better surface finish could be achieved through optimization of machine parameters and/or manual or chemical

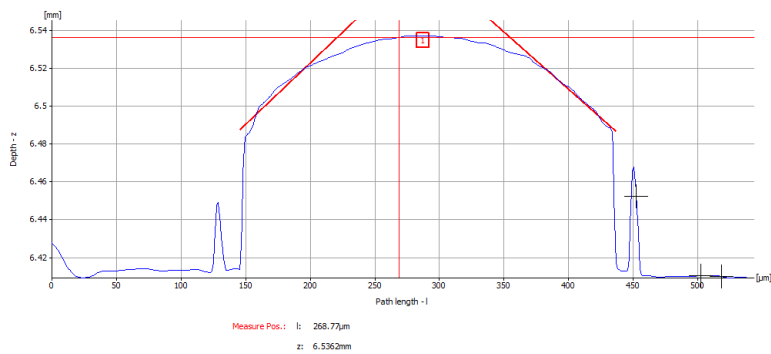
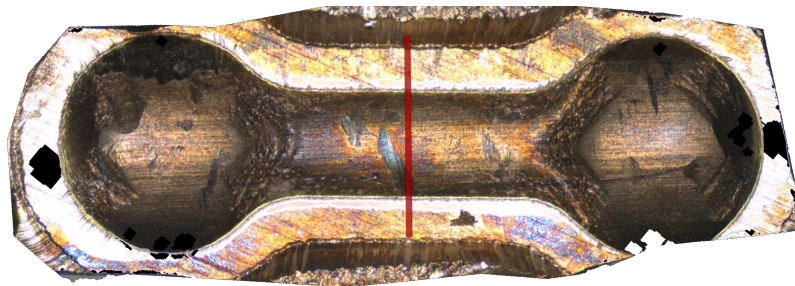


Figure 6.19: Micro-EDM tool path for machining of die for cardan-shaft.

polishing of the die surface. Further, it is suggested that a three step forging process is applied. The cylindrical bulk material would first be pre-formed into a string of pearls, whereby the work piece material would be repositioned into a more optimal position prior to the fine forging operation. After the final forging procedure, where extra material would be extruded axially along the shaft of the component, the individual cardan-shafts could be cropped from the chain.

The suggested die design for the central forming operation is shown in Figure 6.20.

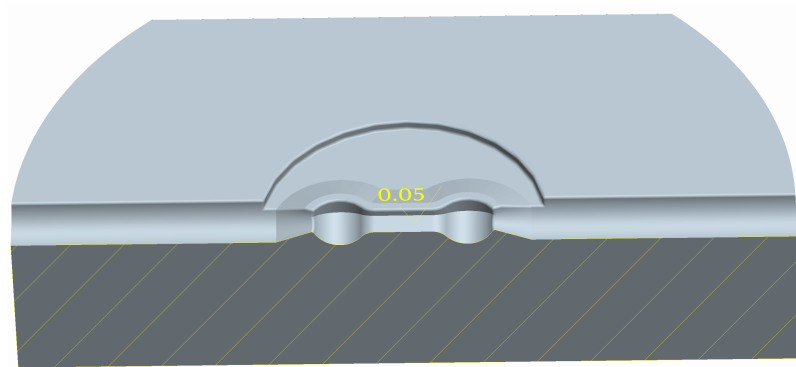


Figure 6.20: Suggested die geometry for the final forging step of the new three step forging procedure.

6.9 Alignment tolerances within micro bulk forming

Considering the tolerance chain of a typical tooling system, the tolerance requirements for the forming punch, the die or ejector elements are only one constituent of a compounded tolerance chain. Further, as practical tolerance deviations is summed up over inter-aligning tool elements involved in the bulk forming process, the total precision of the process is specified for the chain. To arrive at the tolerance requirement of an element in the tool chain, the tolerance chain must be broken into parts. A model for the typical tolerance chain encountered in micro bulk forming is shown in Figure 6.21. When

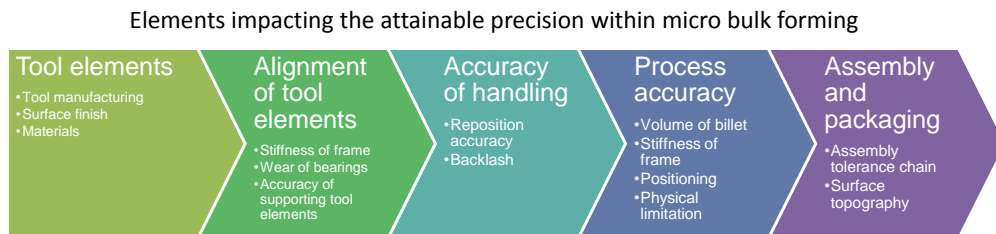


Figure 6.21: Typical tolerance chain for the micro bulk forming process.

considering the illustrated tolerance chain, it seen that an inaccuracy on a forming die will impact the tolerance conformance zone directly. Thus, realizing high accuracy for the central forming elements must have high priority. However, once a number of high permission tool elements have been realized, the question of how these discrete tool elements are aligned relative to each other arises. The question of ensuring proper alignment is often equally critical as the realization of the actual tooling elements. Further contributions to the tolerance chain includes the accuracy of handling and positioning of the work piece material in the tool system, process accuracy and the influences that can be attributed to packaging and assembly of the produced component.

Introducing the notion of primary and secondary effects in precision of a micro tooling system, the primary precision is the achieved accuracy of the individual discrete tool elements, whereas the secondary precision effects are the achieved dimensional precision

between the features residing on two different tool elements. Then, the secondary alignment effects of micro tooling elements are often challenging because the required precision of the primary forming tools also must be required for the secondary tool elements responsible for support and alignment. Or said in another way: a precise punch and die is only as precise at the relative alignment between the two.

Some of the common approaches to the alignment are listed below.

- Rigid fixture - rigid tolerance chain
- Floating dynamic fixture
- Adjustable floating fixture

The straightforward way of ensuring alignment of tooling elements is by a high precision framework supporting the tooling elements. This could be through utilization of a standard die set where ball-cage bearings ensure alignment of the upper and lower part of the die set. The use of a reference plane as depicted in Figure 6.22, such as a ground back plate, is another way of ensuring good alignment. By placing the high accuracy reference element in the middle of the tolerance chain, it is possible to reference all other tooling elements to this element. This approach requires strict control of the tool tolerance chain to ensure that alignment errors are within an acceptable level. It is often challenging to realize the macro size framework tooling elements, such as stand and base-plate, with the precision required for the alignment of the microsize forming tools. One way of ensuring good alignment of the upper and lower tool elements is by

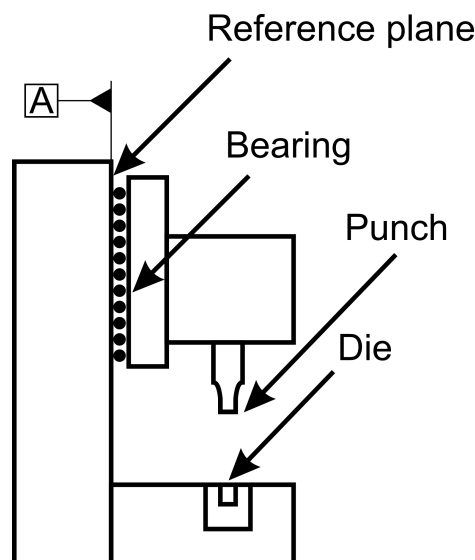


Figure 6.22: Rigid fixation of tool elements through high precision support elements.

machining the parts in one run. Consider the die holder shown in Figure 6.23. In this case the die is the floating element and the ejector is the rigid element whereupon the die is aligned. The top of the die holder is aligning the punch through a tight fit. Good

alignment is ensured by precise alignment of the upper and lower tool holder and through machining of the upper and lower alignment facets in the same run. The through hole was drilled first and subsequently widened using a wire EDM machine. This approach ensured alignment within a few microns of the facets guiding the ejector (and die) and the punch. The guiding facets have been highlighted in red color in Figure 6.23.

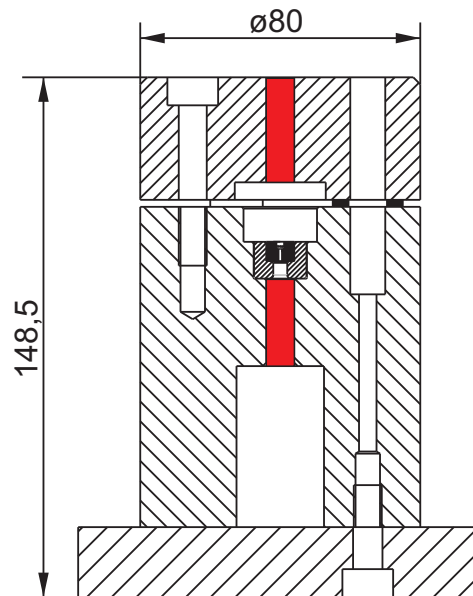


Figure 6.23: Suggested die geometry for the final forging step of the new three step forging procedure.

An other approach is the one of Figure 6.24, where the punch is loosely fitted in a slot of the moving fixture; thereby allowing the punch to center on the die during closure. It is important that the alignment happens before any load is applied to the punch, meaning that self-alignment should be included into the design of the primary forming tools. This approach for alignment is simple and self-contained, but is generally only suitable for simple forming operations of rotational-symmetric components. The floating fixture approach can also be applied as a hybrid solution where two high precision fixtures with embedded forming tool inserts are placed on a floating bed. The alignment is then ensured through the relative alignment between the two fixtures. The fixtures then passes the precise relative alignment onto the forming tool inserts. An example of a tool employing the hybrid alignment approach is depicted in Figure 6.25.

An popular third option for alignment is the inclusion of an adjustable floating stage. This spring loaded stage makes it possible to adjust the position of either punch or die relative to the mating part. This makes the running-in and commence of the tool system more complicated, because the alignment stage must be carefully tuned. However, the presence of the adjustment stage relaxes the strict tolerance demands for the tool frame elements and thereby the manufacturing costs of these parts. It is however important, that the tool is able to reproduce the position motion accurately and that no backlash exists. An illustration of an adjustable floating stage tool system is show in Figure 6.26.

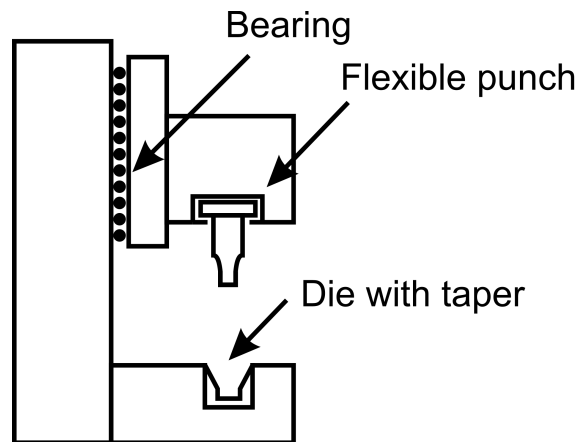


Figure 6.24: Illustration of self-alignment between tool elements through floating tool elements.

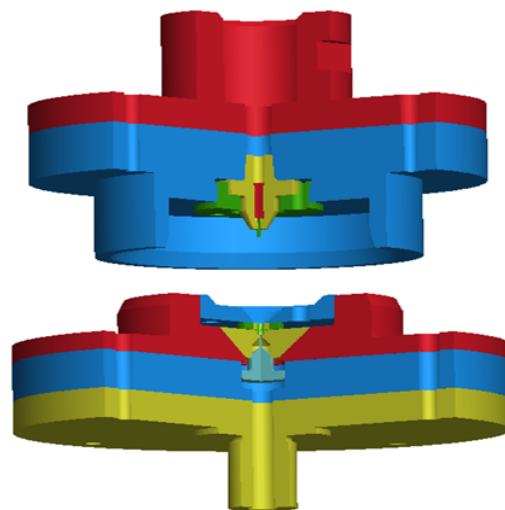


Figure 6.25: Illustration hybrid alignment approach. Alignment of the upper and lower die is ensured through relative alignment of the two tool holders. The holders are self-guiding through the conical surfaces [22].

6.10 Conclusion

A suggested procedure for micro bulk forming tool design has been presented, touching on the challenges and possibilities for good design practice. The most influencing requirements for tooling for the micro bulk forming process were identified, including suitable manufacturing processes. Suggestion for a process chain for micro tool design were given and the basis for the process were elaborated. Suitable tool materials have been presented and the properties in relation to micro tool design were outlined.

A comparative study of three different forming die examples were developed. One die

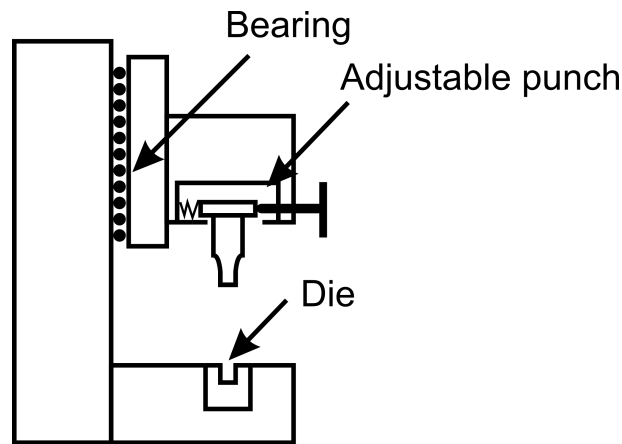


Figure 6.26: An adjustable punch fixture allows for alignment of punch and die through an adjustment screw

was manufactured using an alternative tool design method. This method utilize the electroforming process were described and an experimental qualification was conducted. The two other dies were manufactured by state of the art μ -EDM technology. One dies prepared by μ -EDM were send for coating. The quality of the three dies were compared using silicone replica technique. It was found that the die manufacture by electroforming had too low yield strength for application in bulk forming but had good replication accuracy. The coated die had an unsatisfactory surface quality, confirming that the PVD coating process can not be applied for coating of high aspect ratio micro forming dies. The un-coated μ -EDM die was found to be satisfactory for application if forming. However, the surface roughness and minimum achievable corner radii of the μ -EDM could pose problems.

A micro forming experiment of an axle component was conducted. The tool were manufactured using μ -EDM directly in hardened tool steel. The achieved tool system was analyzed, confirming the constraint of the μ -EDM process. The resulting formed specimen showed signs on material flow and grain size influence.

Finally, strategies for tool alignment and ways of achieving these were given. The notion of primary and secondary effects of a micro tooling system was in introduced and elaborated. The chapter was concluded with examples of rigid, floating and adjustable alignment strategies.

Chapter 7

Micro bulk forming framework

The vision of table-top manufacturing facilities for production of micro components have already been discussed. The following chapter will outline some of the aspects and analysis relating to realizing a facility for mass production of formed micro components. According to literature, the integration and analysis across the process-chain is of great importance [34, 103]. Current research activities in micro manufacturing is mainly focused on the realization and optimization of the individual micro manufacturing process, disregarding the increased influence system and process-chain aspects at micro size [42].

In the current chapter aspects such as billet preparation, press frame and system design will be discussed. A prototype design for a second generation dedicated micro press station design is presented and the design decisions outlined. Further, an example of an inline transfer and ejection system is presented. Finally, a piezoelectricity driven device for stress relief during ejection of a forged micro component is explained. The chapter is concluded with a short discussion on the possibilities for subsequent processing of forged components, including machining and surface treatment.

7.1 Billet preparation

Prior to any forging operation, a billet or slug piece of material must be obtained. Normally, the bulk material for the forming process gets delivered from mill in the shape of long bars or wound on a coil. This bulk material must be split into billets of the right volume and dimension prior to the forging process.

The separation of billets from the bulk material can be done using abrasive processes, such as sawing or cutting on a lathe. These processes usually produce billets with low volume variance and does not alter the grain structure around the shear zone of the billet. Cutting using ablation based cutting processes, such as flamecutting or laser cutting generally produce a cutting edge comparable to that of the sawing or cutting processes. However the ablation processes leave a heat-affected zone around the cutting edge, leading to thermal hardening on some steel types, thus making subsequent forging difficult.

Separation of the billet by cropping is a process without material loss. In this process

the billet material is sheared between a stationary and moving cutting blades. The working principle of the cropping process illustrated in Figure 7.1. Due to the simplicity of the cropping process, the production yield is much higher when compared to abrasive and ablation based processes. Normally the shear blade cavity encloses the billet with

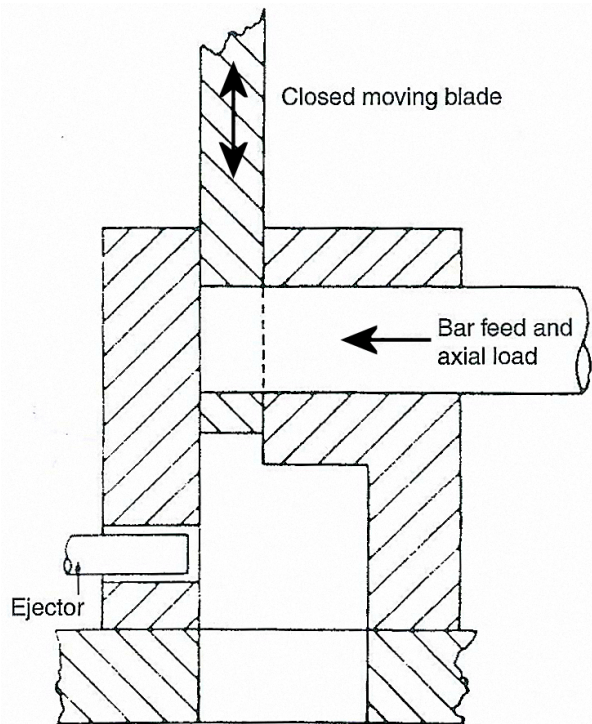


Figure 7.1: Schematic of a shear with axial load to improve shear quality [18].

a narrow tolerance, thereby limiting the geometrical distortion in the shear zone. It is possible to use a shear blade with a flat edge, with a considerable amount of distortion of the billet cross section. The process works by plastically deforming the billet material until the point where the deformation limit in the shearing zone has been reached. If the shearing continues, the material will crack or fracture, leaving a less perfect crescent shaped fracture area. Depending on the material and the tolerance requirements for the subsequent forming operation, the cracking behavior is tolerable or not.

Some classes of materials cannot be cut by cropping with sufficient accuracy with respect to the length and volume of the billet. High strength steels with a yield strength exceeding 400 MPa are generally heated prior to cropping. Aluminium, magnesium and copper alloys require sawing or cutting with a friction saw blade. Superalloys and Titanium is normally cut using sawing or abrasive disk processes [18,104].

In order to investigate options for production of billets for micro forming, a test device for cropping has been constructed. The idea is to investigate the possibilities of cropping micro billets for later use in the micro bulk forming process. The constructed device is shown in Figure 7.2. The device was constructed to allow for flexible investigation of different cropping scenarios, including the following:

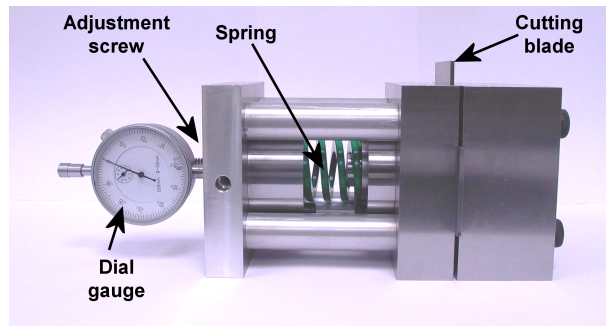


Figure 7.2: Test equipment for cropping of micro billets [23].

1. Cropping with flat shear blade
2. Cropping with enclosing shear blade
3. High speed cropping
4. Cropping with enclosing shear blade - billet under hydrostatic pressure.

Aluminium EN6061 and α -copper alloys were used as work piece materials for the cropping process.

Early investigations showed that cropping with a flat shear blade yielded billets of unsatisfactory quality. The flat shear blade would distort the cylindrical work piece material to such a high degree, that it would not align in the bulk forming die subsequently.

For the enclosing shear scenario, a hole was machine in the hardened cutting blade using a Micro-EDM machine. The cutting blade is then positioned so that the billet rod material aligns in the blade hole and pushes again a hard stop. The cropping is initiated by applying force on the shear blade.

High speed cropping is identical to the case of cropping with enclosing blade, with an increased velocity of the shear movement. Theoretically, at very high shear speeds the deformation of the billet material becomes adiabatic, as the induced heat in the billet material have little time to escape.

In the final case, where the billet is cropped under hydrostatic pressure, an axial load is applied to the billet before shearing. By applying an axial pressure exceeding or close to the yield strength of the billet material, crack zones and other defects can be avoided altogether. Equation 7.1 can be used to calculate the required shear stress necessary to initiate shearing of the billet. The formula is based on the Von Mises yield criterion. The equation applies for stresses less or equal to the flow stress of the material.

$$\sigma_T = \sqrt{\sigma_N^2 + 3\tau^2} \Leftrightarrow \tau = \frac{1}{\sqrt{3}} \sqrt{\sigma_T^2 - \sigma_N^2} \quad (7.1)$$

, where σ_T is the normal yield stress of the material, σ_N is the axial stress the normal direction and τ is the shear stress.

Similar analysis can be applied to show that for normal stresses σ_N above the flow stress of the work piece material, the theoretical required shear stress is zero. Figure 7.3 plots

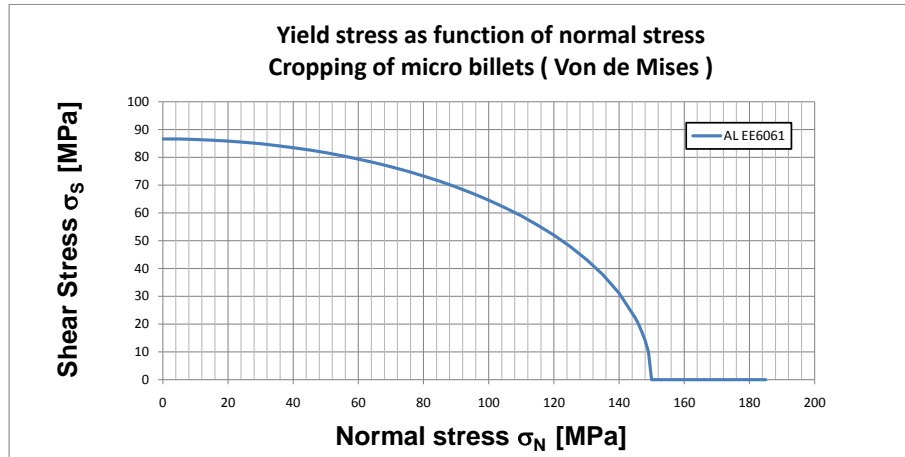


Figure 7.3: Required shear stress (τ) as a function of axial stress (σ_N).

the required shear stress of an aluminium EE6061 alloys, having a flow stress of 150 MPa, as a function of the axial stress applied. This theoretical curve traces one quadrant of the Von Mises yield ellipses. It should be noted that this theoretical curve does not include the influence of strain hardening of the material, friction and reduction of the billet cross section during cropping.

Figure 7.4 depicts a simulation of the high speed cropping process with a shearing speed of 10 m/s. The high velocity of the cutting blade was achieved using a spring-suspended

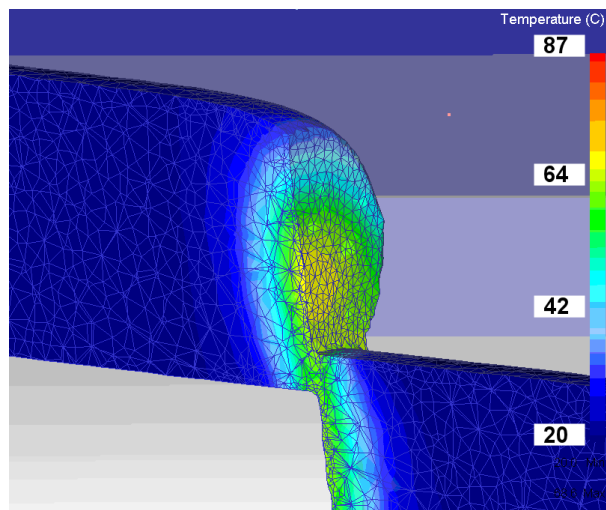


Figure 7.4: FE-simulation of high speed cropping process. Temperatures up to 87 °C can be noted.

drop hammer setup. A length transducer was mounted on the hammer to monitor the

velocity at impact with the cutting blade.

The results of the three cropping experiments can be seen in Figure 7.5. For the picture a) a clear two facet end surface is noted. A smooth part with clear tracks showing the shear direction and a second part where the material have suffered brittle fracture.

For the case where hydrostatic pressure have been applied, depicted in b), the billet is sheared over the complete surface. Further, a low distortion of the billet envelope is noted.

In the case of high speed cropping, Figure 7.5 c), no fracture zone can be noted. However, the cropped specimen suffers distortion of the circular perimeter. Looking closer at the sheared surface, an uneven surface finish can be noted. The reason for the medium quality of the high speed cutting experiment should most probably be found in the high heat conductivity of the aluminium alloy prohibiting the adiabatic conditions in the shear plane of the material. This is confirmed by the FE-simulations of the high speed cutting process in Figure 7.4. Further, the low yield strength of the material makes it prone to distortion of the high impact rate of the shear blade. Following the

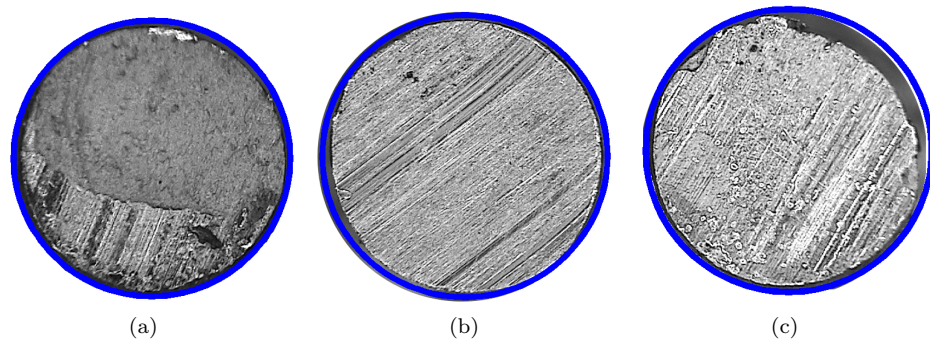


Figure 7.5: Results of the three different cropping experiments. (a) is the end surface achieved when cutting with an enclosing blade. (b) is cropped with the addition of hydrostatic pressure and (c) is cropped under high speed with the blade speed exceeding 10 m/s.

successful results of the micro billet cropping device, a device for volume cropping under hydrostatic pressure has been constructed. A photograph of the prototype cropping machine is shown in Figure 7.6. Driven by a manual handle, two eccentric camshafts translate the rotational movement into two transversal ones - a movement for the feeding of the bulk material and a second for the actuation of the cropping blade. The cropping of the billets happens between two hardened dies and a set of conical shaped grippers ensure feeding and pressurizing of the work piece material during cropping. A trial run of the cropping machine was conducted, using α -brass as work piece material. A total number of 50 representative specimens were cropped and subsequently weight off on a high precision scale. Through the density and weight, the length was calculated and plotted in the histogram seen in Figure 7.5. The intended length was set to 1,55 mm on the cropping machine. The histogram in Figure 7.7 show a high number of the cropped specimens that have lengths close to the intended nominal length and a number of outlier specimens that are shorter. No specimens featuring a length significantly longer than

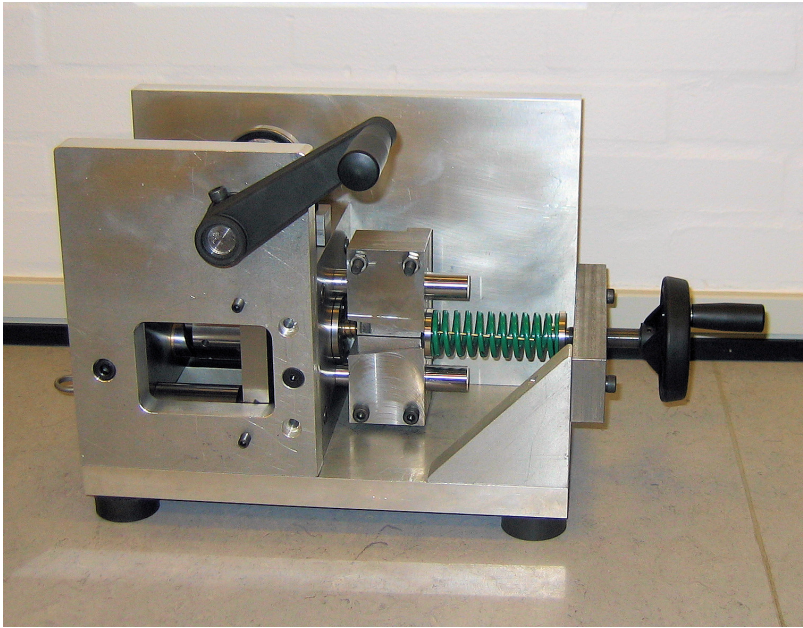


Figure 7.6: Prototype cropping machine for cropping of micro billet under hydrostatic pressure.

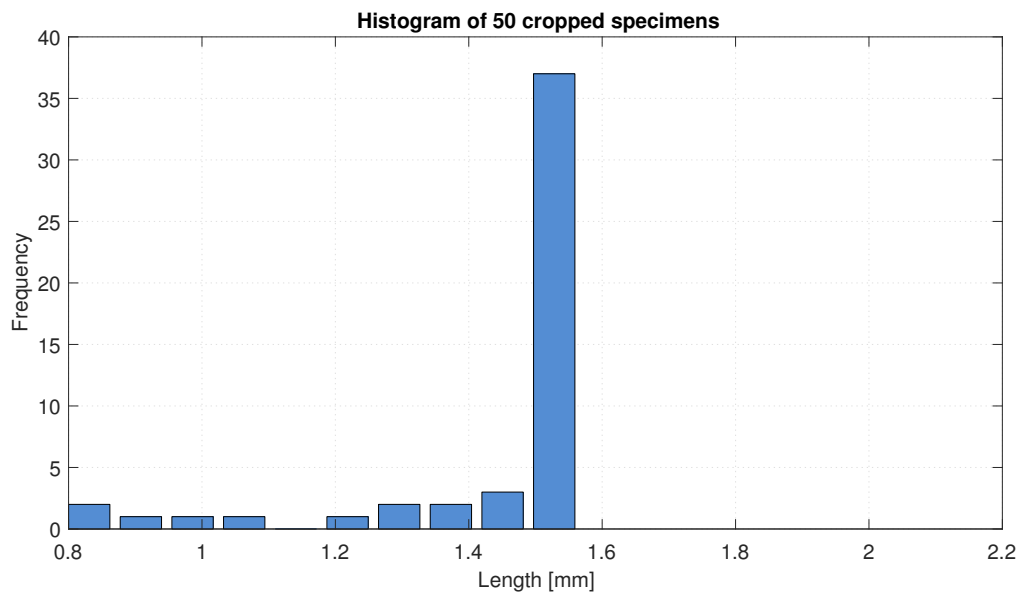


Figure 7.7: Results of the a trial run of the cropping machine with brass material. A total of 50 specimens were produced and weight on a high precision scale. The cropped length could then calculated.

the intended can be noted. This is due to the hard end-stop at the end of the cropping cavity prohibiting any overshooting of the billet length.

It is clear that the achieved length, and thereby also volume, scatter of the cropping process is not satisfactory for fabrication of billets for the micro bulk forming process. The shorter billets will mean faulty components in the forming process and can lead to complications during ejection and handling operations.

Inspired by industrial common practice, where the cropped billets go through a weight based sorting device, an outlier subset of the billets have been discarded. This correspond to 26 % of the observation population or a total of 13 specimens.

A histogram of the sorted subset of the observations is shown in Figure 7.8. Apart from the fitted normal distribution function and the matching standard deviation values, two blue colored punctuated lines indicate the billet lengths corresponding 1% volume deviation from nominal. A total of two observations lie outside the 2% volume span,

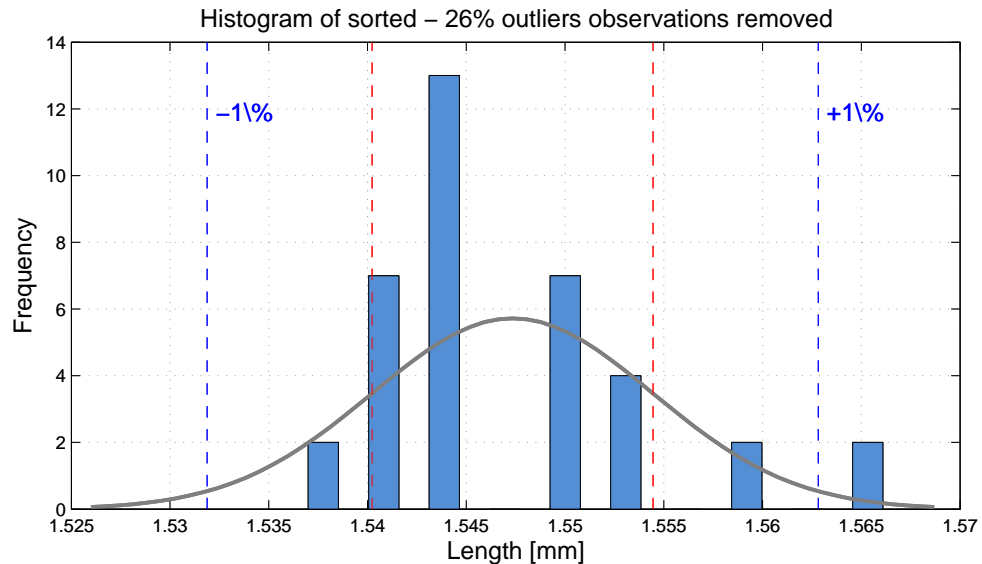


Figure 7.8: Histogram of the cropped billet lengths after disregarding a 26 % subset of outlier observations. Punctuated blue lines indicate the upper and lower bound of a 2 % volume conformance zone.

but on the higher side of the minimum required billet volume. For the sorted data set the resemblance between the fitted normal distribution curve and raw data is relatively good for the small sample size. This indicates that the sorted data subset is a better representation of the achievable accuracy of the cropping process itself, rather than being a result of a number of data outliers due to a faulty feeding mechanism.

Conclusion of billet preparation experiments

In order to realize the micro bulk forming process as an industrial production process, the need for a high yield billet or slug production method is evident. The cropping process fulfills most of the requirements but has not been evaluated at micro level. A number of different cutting strategies have been studied, including cutting utilizing a

flat cropping blade, cropping with a enclosing blade, high speed cropping and shearing under hydrostatic pressure.

The latter approach showed promising results and was advanced into a prototype for a production type cropping machine. Apart from a relatively high level of specimens that deviates substantially from normal length, the machine was able to produce billets with volume accuracy and low geometrical distortion.

Acknowledgements

The work in the section above is a part of a B.Sc. thesis by Jakob Duus Dolriis and Jakob V. Holstein [23].

7.2 Press and system design for micro forming

The different types of press technologies utilized in metal forming can be divided into displacement-related, force-related or work-related presses, depending on the controllable parameter of the press technology. Hammer forging and screw presses are quantifiable as work-related press technologies, whereas mechanical and hydraulic presses can be run as displacement or force-related press systems.

For the established forming processes, such as blanking, deep drawing and cold forging, the choice of press and handling systems is often given a priori. For blanking, stamping and bending of smaller sheet metal parts, conventional open-front eccentric driven mechanical presses are dominant. In combination with low-cost pneumatic feeders, high production volumes can be reached at low cost.

For more advanced forming operations or higher stroke rates, the linkage drive press offers several benefits. A more constant stroke velocity and a more controlled buildup of the forming force makes the kinematic characteristics of the linkage press ideal for deep drawing processes. Further, the magnitude of the dynamic forces are lower, yielding a longer lifetime of the press components such as clutch, brake and transmission.

The choice of press technology is mostly application driven but may also be primed by legacy or 'cultural' influences. However, a good tool process design involves the right choice of press technology. The main process parameters driving the choice of press system is outlined below:

- the pressing - this determines the required size and rigidity of the frame and actuation
- the dimension of the tool system - determines the size of the tool area
- work area accessibility - determines the shape of the press frame
- required precision of guidance - influences the shape and stiffness of the frame.

The complex dynamic interaction between tool, work piece, press force actuator and press frame stiffness in a typical metal forming operation makes it difficult to analyze the

exact behavior of the complete metal forming system. No explicit method for qualifying a given press for a given forming operation is existing, but general guidelines are given in literature [104]. Besides the load capacity and physical design, the stiffness of the press system is a vital parameter in selection of a suitable press system.

Stiffness of frame and guiding system

The use of prestressed press frames has become standard in press systems with capacity exceeding 4000kN. The prestressing reduces the elastic deflections of the press frame during the forging operation. As the the actual stroke length of the tool is calculated as the stroke length of the press actuator minus the elastic deflection of the press and tool system, the prestressed frame makes the control of the stroke length less dependent of the load of the system. Further, the prestressing of the frame will make the press more tolerant towards off-center loading, allowing a number of tools for a sequence forging operation to be mounted in the same press frame. Off-center loading of the *press crown*, the vertical moving base plate driving the tool, also puts requirements on the guiding system. Depending on the configuration of press frame, force transmitting elements and guiding system a maximum allowable turning moment of the individual press is obtained. This parameter is usually cited in data sheet of the press system as a single maximum value. It has been shown that the stiffness behavior of the press will influence the achieved product quality. Further a method for obtaining and formulating the stiffness behavior of an individual press system has been developed [105]. Some hydraulic presses are equipped with an active adjustment system for parallel control of the press slide.

Considering a press system for a micro bulk forming operation the scale difference between the press system and the component to be forged is often increased. Thus, the design and strength of the press frame is less critical as the press frame dimensions will tend to be oversized by default. On the other hand, the influence of elasticity and backlash will be increased and can exceed the actual desirable stroke length. For forming operations that depend on accurate stroke length control, such as backward can extrusion, this poses a challenge. Through trial and error methods it is possible to estimate the total amount of backlash and add this length to the desired stroke length of the forming operation. However, often the elasticity and backlash will change over time or when the tool is replace after a service, requiring the stroke length adjustment to be repeated. A displacement transducer build into the core tool system can be connected to the press control system, allowing the stroke length to be controlled according to the inserted transducer. This effectively eliminates the influence of elasticity of the press frame and backlash between the tool and the press.

Actuation of presses

In conventional forging, the press systems are generally divided into mechanical and hydraulically driven presses. Mechanical presses include excentric, knuckle-joint and screw systems where a rotary angular momentum from an electric motor is converted into a high force linear motion. A mechanical press system often features a pneumatically driven clutch and a flywheel for storage of the rotational energy. Mechanical presses are less flexible in application as the available stroke- and ejector lengths are closely coupled with the mechanical design of the press transmission system. However, high stroke rates can be reached which is why mechanical press systems are generally recommended for

high production volumes. A mechanical press is often paired with an automatic transfer system for the work piece handling and are recommended for production batches of 10.000 parts and yearly production rates exceeding 1.5 million.

Hydraulically driven forging presses offers flexibility and extended stroke lengths over the family of mechanical presses. Hydraulic presses are versatile and can be used both in single and multiple step forging. They are frequently used for pressing of long shafts and for large parts with weights up to 15 kg. Press forces of several thousand metric ton can be reached and numerical control systems allow flexible configuration and control. As hydraulic presses have the ability to reverse at any point of the forging process, the press operation can be controlled either as a force-, work- or stroke controlled forging process. Further, the flexible control of the hydraulic press piston allows the forging operation to be discontinued in case a malfunction is detected. This could be in the form of a broken punch, a sudden increase in friction or a misplaced workpiece specimen. Thus, the flexible control possibilities of the hydraulic press can help to avoid tool fracture, saving cost and downtime. The drawback of using hydraulics are the unavoidable oil leaks, the need for external cooling, low productions speed and an a low overall efficiency of the system. Also, a hydraulic system is often noisy due to cavitation in the pump station. New developments in hydraulic press systems go towards higher pumping pressures around 300 bars, leading to a reduction of required oil flow and the reduction of cylinder diameters.

Servo driven presses have recently become technically feasible and cost effective enough to be used in metal forming processes. The main driver for this development is the availability of high quality spindles with low leads. Further, servo drives, planetary gears and controls systems have dropped in prices, making the cost of a servo driven press system comparable to that of the mechanical and hydraulic systems. The main reason for switching to a servo driven press system is flexibility. A servomotor gives a press slide motion flexibility and accuracy in terms of speed, motion, and position control. This flexibility means that an infinite number of slide motion variations can be realized. The increased flexibility can help to increase tool lifespan, precision of the forged parts and can allow for forming and assembly operations to be integrated in one stroke. Present commercial servo presses are available from 35 metric tons to 1.000 tons. On average a servo press system consumes 1-5% of the energy it would take to drive a similar hydraulic based press system.

Heating and cooling of tool and workpiece

Forming at elevated temperatures is often required for advanced geometries or when the work piece material is deformed excessively. The primary reason for forming at elevated temperatures is to lower the flow stress of the work piece material thereby lowering the stress and chance of fracture of the forming tools. Further, at elevated temperatures the ductility of most materials increase and the strain hardening coefficient n is reduced. Thus warm forging offers the potential of forging more complex parts at lower loads and with greater toughness of the finalized part.

Typical temperature ranges for warm forging of steel is between 600-900 °C with the exception of austenitic stainless steels, which are usually forged between 200 and 300 °C.

Drawbacks of utilizing warm forging is mainly related to an increased complexity of the

tool design and challenges in qualification of a good lubricant and surface finish. In conventional warm forging the tool system is heated by insertion of resistance heater cartridges. Typical steady state temperatures of the forging tool range between 300-800 °C, depending on the die material and configuration of the forging process. The work piece billet is then typically heated in an external furnace, normally through the application of induction heating. The forming temperature of the work piece will typically exceed the temperature of the forming tool by 200-600 °C. The temperature difference between the tool and work piece material temperature gives rise to thermal equalization effect during the forming process, effects known from the moulding of thermoplastics. It is important to consider these dynamic thermal conditions, both from the point of the forming of the work piece material as well as the tool, in order to achieve good precision of the forging operation.

The installation of a temperature controlled tool system in a forging press frame at ambient temperature, inevitably introduces a temperature gradient across the tool system. This can lead to thermal deflection of the tool frame, causing misalignment of tool elements and stiction and locking of the tool guiding system. Application of thermal insulating filler material, heat shields and passive cooling elements can help to reduce the influence of thermal deflections effects. However, for precision warm forging active cooling, using temperature controlled water circulation, of the tool frame might be unavoidable.

For micro manufacturing processes involving heating and cooling elements, these effects are even more pronounced. The decrease in tool material volume can give rise to thermal steady state thermal gradients in the forming die itself, leading to internal stresses. Also, the tighter tolerances met in micro manufacturing requires careful design of the dynamic and static temperature behavior of the forming process.

Finally, the large relative decrease of the work piece volume in a micro forming process means that any temperature difference between forming tool and the billet will equalize within seconds. The thermal capacity of the forming tool is normally substantial when compared to that of the work piece billet. For this reason, the work piece material in a micro bulk forming is not preheated upon insertion into the heated tool, but inherits the temperature of the forming tool.

A recurring complication of warm and hot forging is the challenging tribological conditions. Oil based lubricants vaporizes above the flash point temperature and few good replacements exists. Graphite powder in a volatile solution can be applied as well as solid molybdenum disulfide. By selection of the right lubricant and by application of different metallic or ceramic based coatings on the tool and work piece elements, tolerable tribological conditions can be achieved in most cases. However, no universal applicable lubricant exists for warm forging scenarios.

Inline monitoring

Intelligent process supervision is an area of increasing interest within manufacturing technology. Through inline monitoring of different process parameters and real-time comparison with a priori values or values acquired through earlier processing, a number of common process errors can be caught and the forming process can be halted. The micro bulk forming tool shown in Figure 7.9 has been equipped with two piezo-type force

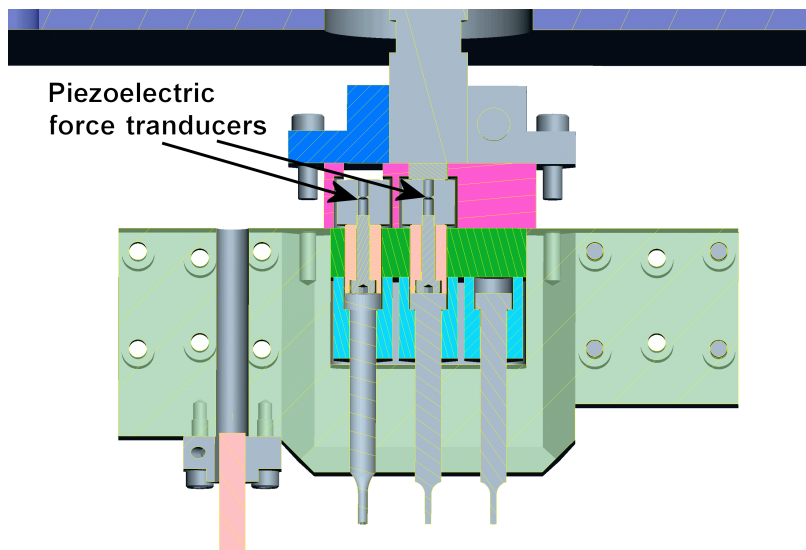


Figure 7.9: CAD model of a dedicated tabletop two step micro forming press with two integrated piezoelectric force transducers for process control.

transducers which measures the forming- and ejection forces on each of the two forming cells. By correlating the forming force with the stroke length, given by the actuator position encoder, the load-stroke curve can be determined. The acquired load-stroke is then compared in real-time with some pre-established curve envelope, only allowing deviations within a certain threshold. If the threshold is momentarily exceeded, the press is stopped. With this type of setup it is possible to detect machine errors such tool breakdown, stuck workpieces and misplaced workpieces due to transfer errors. Also secondary fault causes such as inconsistency in workpiece material, lubricant breakdown and tool wear can be monitored. Data logging of the monitored values can serve as quality assurance parameter of the manufactured components. As it is not uncommon to encounter inspection requirement rates of 100 % within micro manufacturing, the addition of traceability and inline quality inspection provides adding tangible value to the manufactured items. Furthermore, the ability to stop the bulk forming machine in case of misalignment of workpiece or general tool malfunction can avoid machine breakdown, save tooling costs and help to minimize production downtime.

The simple force-stroke curve detection can be supplemented with temperature measurements in the tool, vibration measurements of the press frame and sensor verification of the lubrication system.

Flexibility and set-up

Even though the bulk forming process primarily is regarded economical attractive for medium to large size production volumes, the flexibility of production system and fast change-over times has high priority in the industry. As the *just in time*-principle has been adopted in most production facilities and the stock of finished products is small, flexibility of production equipment is of key importance. A typical bulk forming plant produces a range of different components and can keep a portfolio of thousands different

bulk forming tools. This implies that the logistics and flexibility of the bulk forming equipment is a priority. Since a typical tool system will weigh more than one metric ton, the press system must facilitate access for tool lifting and handling equipment.

For micro bulk forming the tool system is small and light. The complete die-set can normally be moved by hand and the hard metal die inserts can reside inside a matchbox. The press framework must support easy changeover of tool systems, but the light weight tools make handling easier.

Considering the vision of realizing future dynamic micro production chains, each functional element in the production chain must be as versatile as possible. Thus, the production station should be easy to rearrange and store up, meaning that the weight and number of interfaces should be limited. Further, the preferred production chain elements themselves should be capable of performing a range of operations.

The C5K press for micro forming

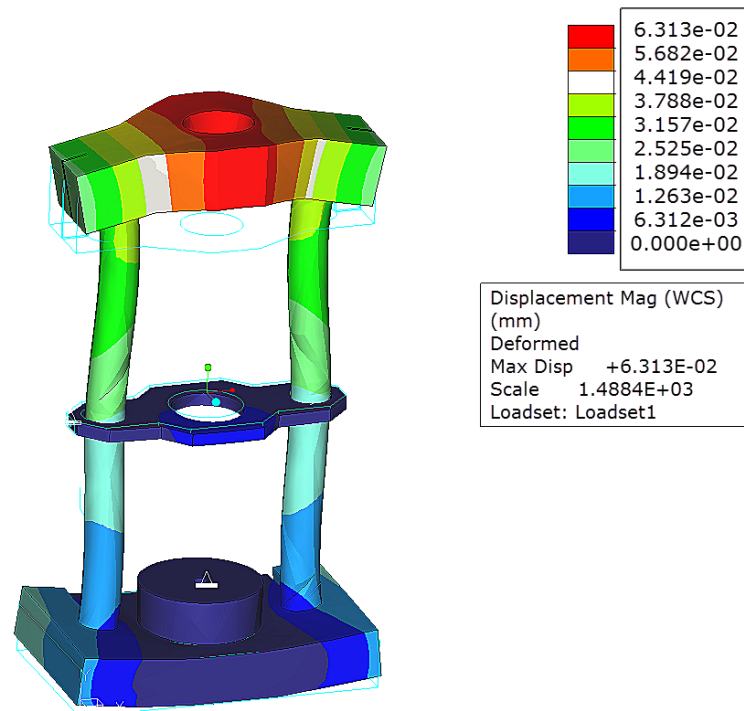


Figure 7.10: FEM-simulation of the frame stiffness under full 50 kN load. Maximum deflection of the frame is around 60 μm total.

The C5K press was designed with the vision of a dynamic micro production line in mind. The goal was to create a cost effective prototype press system intended for a range micro bulk forming processes. The load capability of the press was specified to 50 kN to allow for forming of small macro size components and allow for assembly of die and

7. MICRO BULK FORMING FRAMEWORK

pre-stressing rings directly in the press. Further, it was a requirements that the press was able to position accurately and was able to operate both force- and stroke length drive forming processes. The main design driving criteria are listed below:

- High stiffness of frame
- Capable of delivering a load of 50 kN
- Punch speed up to 1 cm pr. second
- Up to 10 strokes pr. minute
- Cost effective
- High precision control of stroke length, 1-2 μm
- Flexible tool insert
- Inline force measurement
- Mobile, can be moved with a small lifting truck
- Applicable for research and prototype production purposes
- Compliant with European safety machine directive ISO-13849-1

To allow for tool inserts of different height, the two side-stanchions are exchangeable. This allows for refitting of different stanchion sets, thereby making the height of the press frame adaptable.

The slide is guided by a column guiding system featuring a teflon bearing cylinder insert. The slide guiding system based on teflon bushings makes the bearing system intolerable towards radial loads. This limits the amount of off-center load that can be tolerated by the press frame. This is a deliberate design choice due to the fact that the press system is intended for research and prototype use, meaning that only one stage tools will be used. Further, the press is well oversized for micro forming purposes, allowing the operation of multistage micro bulk forming tools with moderate off-center loads.

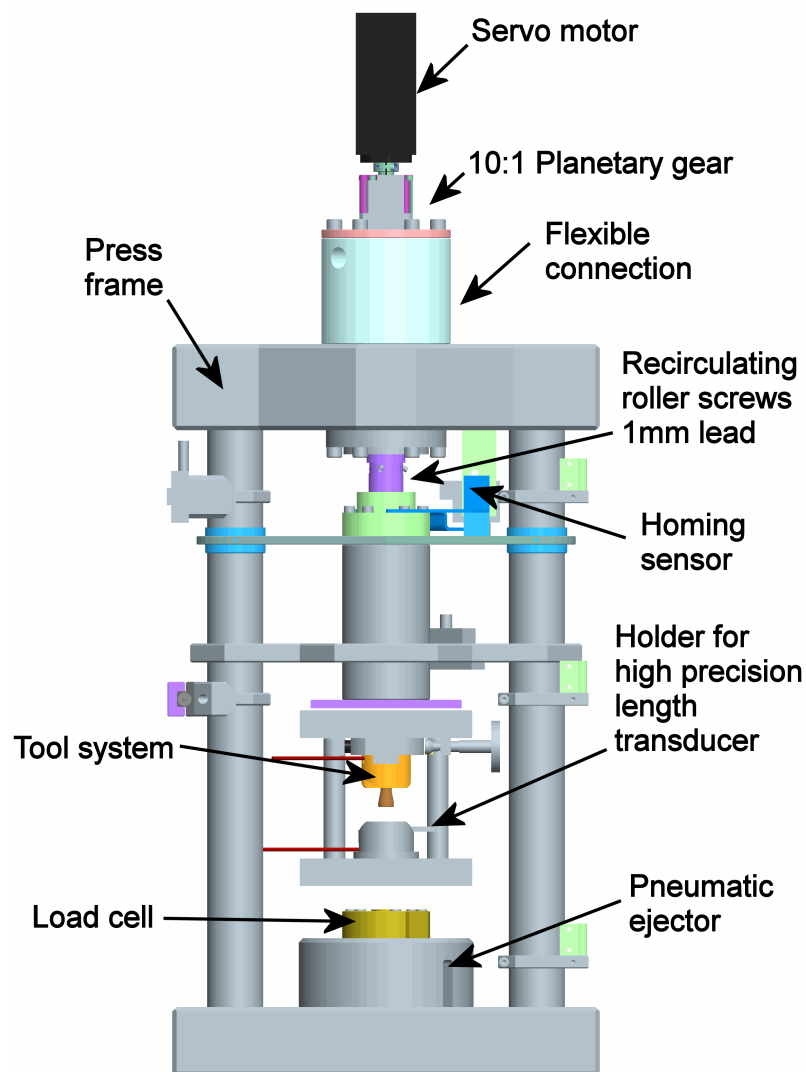


Figure 7.11: Illustration from the C5K press CAD model with indications of vital elements and components.

The elastic deflection behavior of the press tool frame was analyzed using the finite element method. The basis for the simulation was to estimate the amount of elastic deflection of the press frame under full and centered 50 kN load. The result of the elasticity analysis is depicted in Figure 7.10. The total deflection between to base and top is around $60 \mu\text{m}$.

The main elements of the C5K press are shown in the CAD model shown in Figure 7.11. Starting from the top, a 650 W servo motor is mounted on a 10:1 planetary gearbox. This output of the gear-box is connected to the main roller screw through a flexible rotation coupler, allowing slight misalignment between the motor and gear-box and the main screw spindle. The planetary gear is included in order to shift the working domain,

being the combination of rotational speed and torque, into the desirable domain of the press system.

The central part of the press is the \varnothing 40 mm recirculating roller screw with a lead of 1 mm. The screw can sustain a dynamic load of 79 kN and a static load exceeding 200 kN. This type of roller screw is particularly suitable for a high precision press application as it offers fine resolution, minimum drive torque and heavy load carrying capacity. The roller screw can be supplied with different nut configurations, including pre-tensioned version with no axial play. In this application a flank version was chosen without backlash compensation, as the press operation only requires high precision position accuracy in one direction. The total stroke length of the C5K press is 300 mm, exceeding the typical demand of most small and micro bulk forming processes.

The screw nut is mounted on a cylinder kept in place by a transversal alignment piece. The alignment piece is guided by a couple of teflon bushings, marked in light blue on the CAD model.

The bottom of the press is fitted with a dome part containing a pneumatic cylinder for component ejection. The 50 kN load cell includes a bore for the ejector pin to come through, allowing measurement of both forming and ejection force.

The C5K press is equipped with a number of limit-switches, prohibiting overrun of the roller screw. Further, a high precision inductive homing sensor is included. Finally a high precision displacement transducer, based on the linear variable differential transformers principle, can be attached to the tool.

The model depicted in Figure 7.11 is fitted with a general purpose tool system capable of executing a range of bulk forming processes at ambient as well as elevated temperature.

A photograph of the C5K press is reproduce in Figure 7.12. The yellow safety switches and the transparent safety enclosure can be noted.



Figure 7.12: Photograph of the functional C5K press with tool system.

C5K press control system

The control system of the C5K press has been designed to be small and movable. The control system only requires a normal 230 volt 10 A plug hook-up and is controlled with a standard IBM compatible PC through a RS-232 serial connection. The software interface features a number of control options as well as data acquisition options, allowing realtime plotting of motor current, load, motor position and position sensor state. The data can be saved in text format, allowing subsequent data processing. The C5K press has been fitted with a required security system according to the newly published ISO 13849-1 standard. The security system is made up of a mechanical enclosure of transparent

7. MICRO BULK FORMING FRAMEWORK

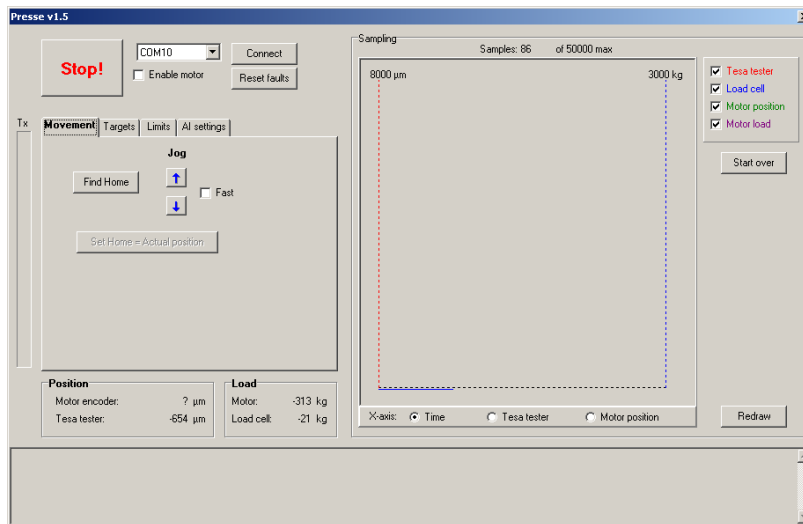


Figure 7.13: Control screen of the C5K press system software. The interface features a number of control options and realtime plotting of process values.

polycarbonate. The enclosure is supervised by a number of safety switches, only allowing the press to operate when the enclosures are closed.

A three-position safety handle is supplied for commencing and set-up purposes, allowing the press to be operated with an open enclosure. The operating option is only allowed during supervision of a second person. The complete control system and three-position safety handle is shown in Figure 7.14

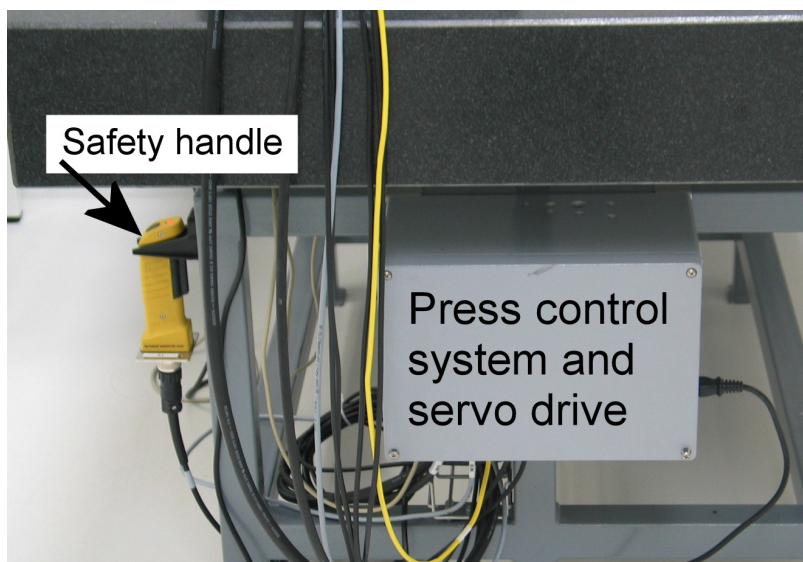


Figure 7.14: Control system for the C5K press. The the left the three position safety handle can be noted.

7.3 Handling, ejection and transfer of components

A key challenge within micro manufacturing is the physical handling of the billets, pre-formed specimens and finished components [34, 53, 106]. In conventional manufacturing the finished components are often piled in boxes when they leave a production line. Upon any subsequent processing, the pieces are then placed into a circular vibration feeder, aligning the specimens onto a linear feeding rail. From here the specimens can easily be fed into an automatic screw machine or grabbed by a pick and place robotic system.

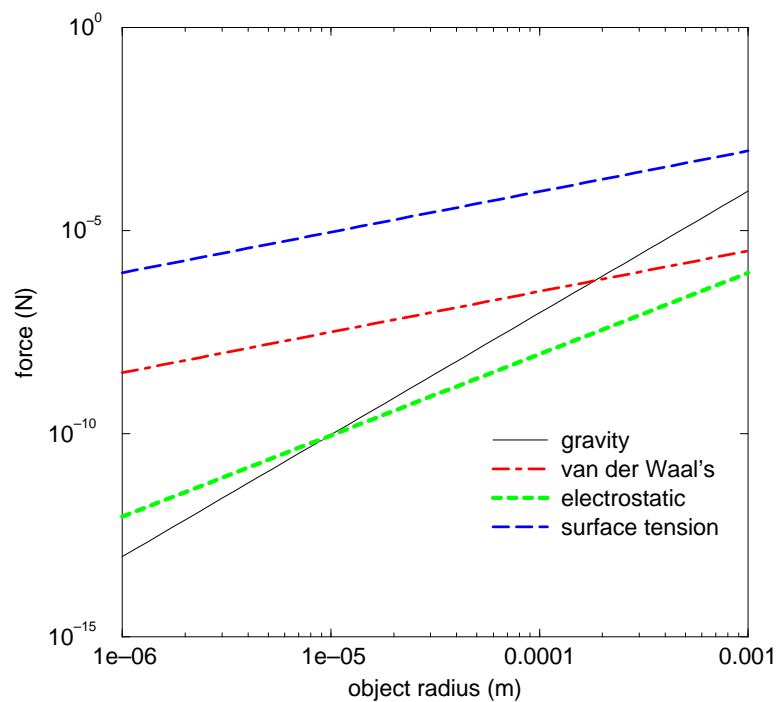


Figure 7.15: Gravitation, electrostatic, van der Waals and surface tension forces. Attraction between a sphere and a plane [24].

In a multistage micro bulk forming scenario, transfer and component handling is complicated by size limitations and stiction forces. Thus, a new approach for handling and transfer of the micro sized components is needed. In the following we will consider a component transfer system proposed for effective and simple handling of micro bulk formed components. A plot of some of the dominant forces acting on a micro component is reproduced in Figure 7.15. It can be noted that as the influence of gravitational pull is greatly reduced as the components size is reduced. This effects can be ascribed to the difference in scaling of volume and surface area.

Handling and transfer systems for the micro bulk forming process

The handling, manipulation and assembly of micro size parts is a key challenge to be overcome. Often when a novel micro manufacturing process is realized, the required physical manipulation of the bulk material and semi-manufacture elements turn out to be equally challenging to realize. This strict bound between micro manufacturing process and supporting micro handling and transfer system entails that a holistic design approach is applied. Thus, elements from the concatenated production chain have to be integrated into every process, thereby enforcing a top-down type design approach.

When considering the micro bulk forming process, the main challenges in handling and transfer of bulk, semi-manufacture and finished micro elements are listed below:

Flexibility A successful transfer and carrier system can easily be adapted to various component geometries.

Speed Naturally, the handling system must be able to follow up with the achievable process production rate.

Reliability Very few errors are tolerable as these will stop production, require human interaction and can cause tool damage.

Precision The specimen handling system must be able to precisely align with process tools and have a high degree of repeatability.

A number of these challenges are conflicting by nature, such as speed and precision, meaning that a tradeoff will have to be found.

When compared with other micro manufacturing process, the micro bulk forming process have some common characteristics that can be considered when designing a suitable transfer and handling system:

- High production rates.
- Medium to large series.
- Often rotational symmetric specimens.
- Metallic materials.
- Presence of lubricant can be expected.

Considering each individual characteristic, a well suited handling system can be designed. The high production rates translates into high speed. Thus, a general purpose micro robotic arm is not deemed a good choice of component manipulator, as it will introduce a production speed bottleneck. Instead a dedicated carrier system will have to be developed with only few degrees of freedom.

The typical production batch size makes it feasible to design manufacture and component dedicated holders for each forming operation. By fitting a number of specially adapted

component holder tools with a standardized outer envelope dimension, into a more general purpose transfer carrier, a certain flexibility can be retained. Owing to the frequent rotational symmetric geometry of bulk formed specimens, a helpful carrier system would be designed for this scenario. Further, a number of free shape geometry bulk formed components would be possible to take advantage of a carrier system designed for cylindrical specimens, as long as the height to width ratio is comparable. The fact that the carrier and handling system will be working with metallic elements sets demands for clearances and wear resistance of the specimen holder system. Finally, the carrier system will have to be able to operate successfully in combination with the process lubricant and other impurities.

With the above observations at hand, a prototype system has been designed for testing purposes [25]. The mockup type test transfer rig was constructed to validate the basic concept of the proposed transfer mechanism. A cross-sectional view of the test-transfer mechanism can be seen in Figure 7.16. The \varnothing 1.89 mm billet is located in the stationary

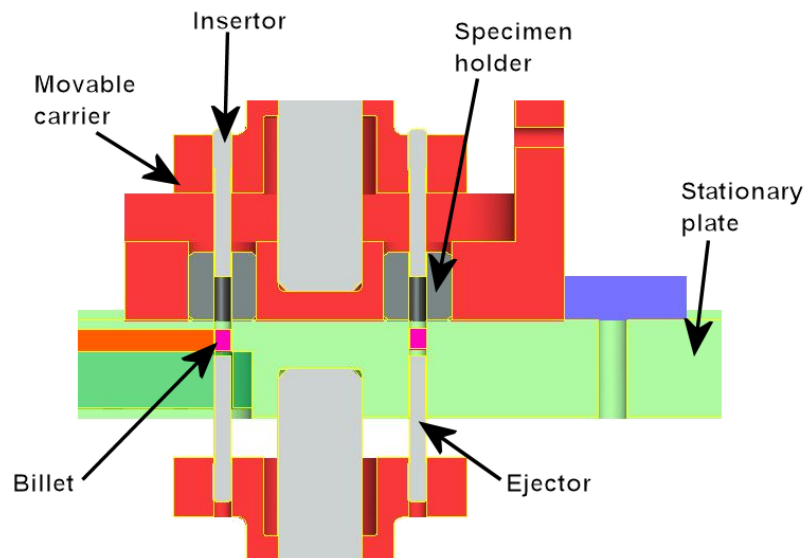


Figure 7.16: Mock-up type test transfer rig [25].

plate of the tool and is transferred to the first specimen holder insert of the carrier wagon by means of the ejector pins. The billet is held in place in the carrier by dry stiction forces or capillary forces arising from the surface tension of the lubricant. The carrier is then moved and the billet can be re-inserted into the stationary plate, which has the role of mimicking a micro forming cell.

It was found that a maximum center-to-center misalignment of $15\ \mu\text{m}$ between the bore of the stationary plate and the specimen holder in the carrier was tolerable [25]. If the two holes are offset by more than $15\ \mu\text{m}$, the transfer can not be achieved successfully. It can be noted that the alignment tolerance includes tolerance contributions from the carrier linear bearing backlash, re-positioning accuracy of the carrier actuator and a number of mechanical tolerances. The strict tolerance requirements of the transfer system causes it to be classifiable as a micro precision mechanical system. However,

as outlined in Section 6.9, a flexible adjustment option can be included to relax the tolerance requirements.

Further, the accuracy of chosen SMAC LAL 35/025/51 moving-coil actuator systems was quantified. The actuator was found to have a linear deviation of $+36 \mu\text{m}$ over the full stroke length of 20 mm. However, the repositioning accuracy was found to be within $\pm 1 \mu\text{m}$.

Following the qualification trials of the handling and transfer system, a functioning prototype system was build and integrated with a micro bulk forming process. The precondition for the handling system is that billets are feeded into the system on a rail and are removed using a vacuum suction apparatus, conditions that are commonly found in industrial metal forming processes.

The four-step handling and transfer sequence is outlined in Figure 7.17. In the initial step the unformed billet is moved from the feeding rail into the first slot of the transfer unit. Simultaneously, any formed specimens from the two cold forming cells are inserted into the two other slots of the transfer unit. The three micro sized parts are held in place by stiction forces.

The transfer unit is then moved horizontally to the second position, effectively moving the billet to the position of the first forming tool, the formed specimen from cell one to cell two and the finished specimen to the ejection position. The forming punches are then lowered, touching the spring loaded insertion mechanism in the transfer unit. The three components are then transferred back to the forming cells and the finished component is ejected.

Upon insertion, the carrier is repositioned to allow the forming punches to reach the forming cells. The finger-shaped geometry of the transfer unit allows the forming punches to lower vertically in between them.

In the final step the forming punches are lowered, completing the forming operation in the two cells. The third punch runs idle. When the forming operation has completed, the punches are returned to their starting point and the sequence is repeated.

Owed to the high constraint of the specimens during transfer and tight mechanical tolerances, the system is believed to be able to operate at high production rates. The micro bulk forming operation have been rated at a production volume of 300 strokes pr. minute and the transfer system has been designed to sustain this high production rate.

The system was tested at low production rates with a few complications. The difficulties experienced during commencing of the transfer system generally related to mechanical adjustment and ensuring sufficient alignment between the transfer carrier and the forming cells. It is estiamted, that with a few adjustments, the system would function as intended.

Die pre-stressing experiment

The influence of friction in micro-forming and the consequential difficulties with ejection of the formed specimens have been confirmed in literature as well as in the experiments of the present work [4, 17]. Primarily due to the increased friction, the high surface

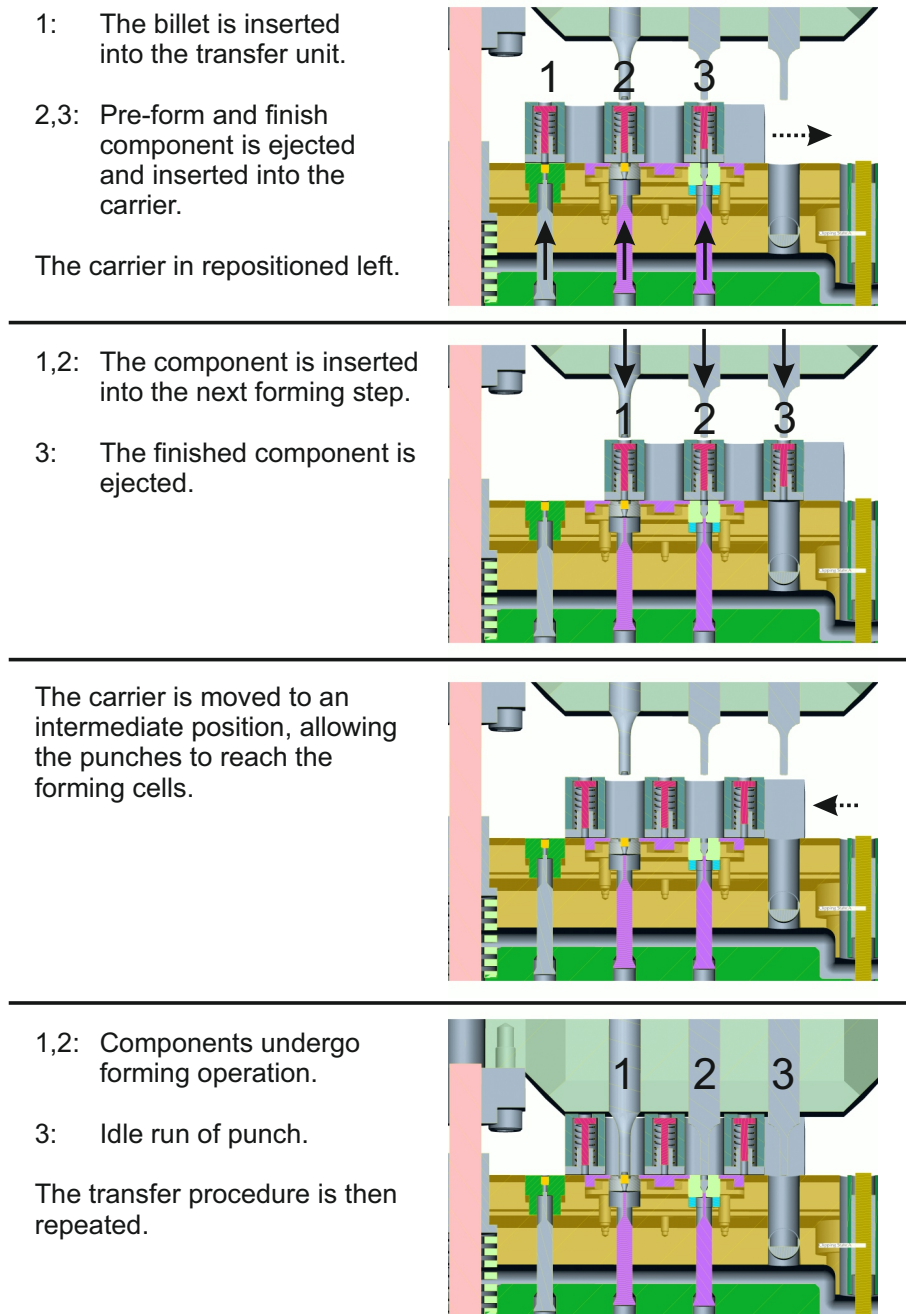


Figure 7.17: Example of transfer sequence of a two stage micro bulk forming process.

area and the often tapered geometry of the specimens to be formed, reverse-forming or collapse of the geometry during ejection is commonly observed. Further, the die of the micro forming cell will expand radially during the forming operation, due to presence of an internal pressure of typically 1000-2000 MPa. When the forming operation is

concluded and the internal pressure is relieved, the die will contract elastically, giving rise to a static stress clutching the specimen to the die. The joint effects contributing to the sticking of the specimen in the forming die can complicate or even preclude the realization of the micro bulk forming process.

The addition of slip-angle to the tool surfaces are well known from thermoplastic moulding of polymer materials. The slip angle helps to relieve any remaining stresses during ejection and the technique is normally advisable for moulding of micro polymer components. The utilization of tools with slip angles on the vertical faces have been attempt for the micro bulk forming process. However, it showed minor effect on the ejection forces of the forged micro specimen. The reason for this shall be sought in the higher internal pressures of the bulk forming process and the higher mechanical stiffness of tool system in metal forming. The combination of high internal pressures and high stiffness of the tool, will lead to high remaining 'clamping' stresses working on the specimen. This causes the main reverse-forming damage to happen at the initial state of the ejection process, whereas employment of a slip angle will help relieve stresses later in the ejection process.

As a possible solution to the challenges related to ejection of a bulk formed micro component, a piezoelectricity actuated pre-stressing tool system have been constructed.

The idea of elastically deforming the die in bulk metal forming is not novel. Radial and axial prestressing systems designed for cold forging dies are commercially available. These pre-stressing systems have helped to increase the dimensional quality of the forged components as well as tool life [78]. Adjustable die pre-stressing systems are also available. These systems feature variable pre-stressing capability, allowing fine adjustment of the overall die geometry through small elastic deflections. Using these tool systems a precision extrusion of macro steel gear wheels with a maximum solid tolerance deviation of $\pm 30 \mu\text{m}$ has been realized. It should be noted that the variable pre-stress tool systems normally require the tool to be removed from the press and undergo light disassembly.

Lately, inline dynamic pre-stressing systems have been researched. With the use of conical inserts, much like the system known from a chuck of a drilling machine, the amount of pre-stress on the die can be adjusted. Now, if the pre-stressing system is controlled using a separate actuator, the die system can be dynamically pre-stressed and relieved. This can help to ease ejection of the finished part and improve the tribological conditions of the forming operation.

Details of piezo driven prestressing system

The tool system is designed for rod extrusion of a AA6062 from $\text{Ø } 0,5 \text{ mm}$ down to $\text{Ø } 0,3 \text{ mm}$. The strength of the extruded part is so low, that conventional ejection systems will cause problems as described in the introduction of this chapter. The process is simulated by the commercial FE code Deform 2D and consists of 3 objects. The die is simulated as elastic and the billet as elasto-plastic. The prestress pressure is applied as a pressure boundary condition on the outer surface of the die. The die is simulated as axis-symmetric in the 2D simulation, but the elastic deformation of the die has been verified by 3D simulations of a square die. Snapshots of the simulated pre-stress sequence is shown in Figure 7.19.

Initially the billet is inserted and the tool is ready for the forming operation, Figure 7.18a. In Figure 7.18b the piezo actuator system is energized, giving rise to an effective stress of about 500 MPa. The forming operation is then executed, leaving a static elastic stress acting on the forged components. The stress distribution can be noted from Figure 7.18b and is ranging between 1000 - 1500 MPa. In the final step of the sequence the applied pre-stressing is eased, allowing the die to expand elastically. This relieves the internal stress clamping the forged components by 500 - 1000 MPa, as can be noted from Figure 7.18d.

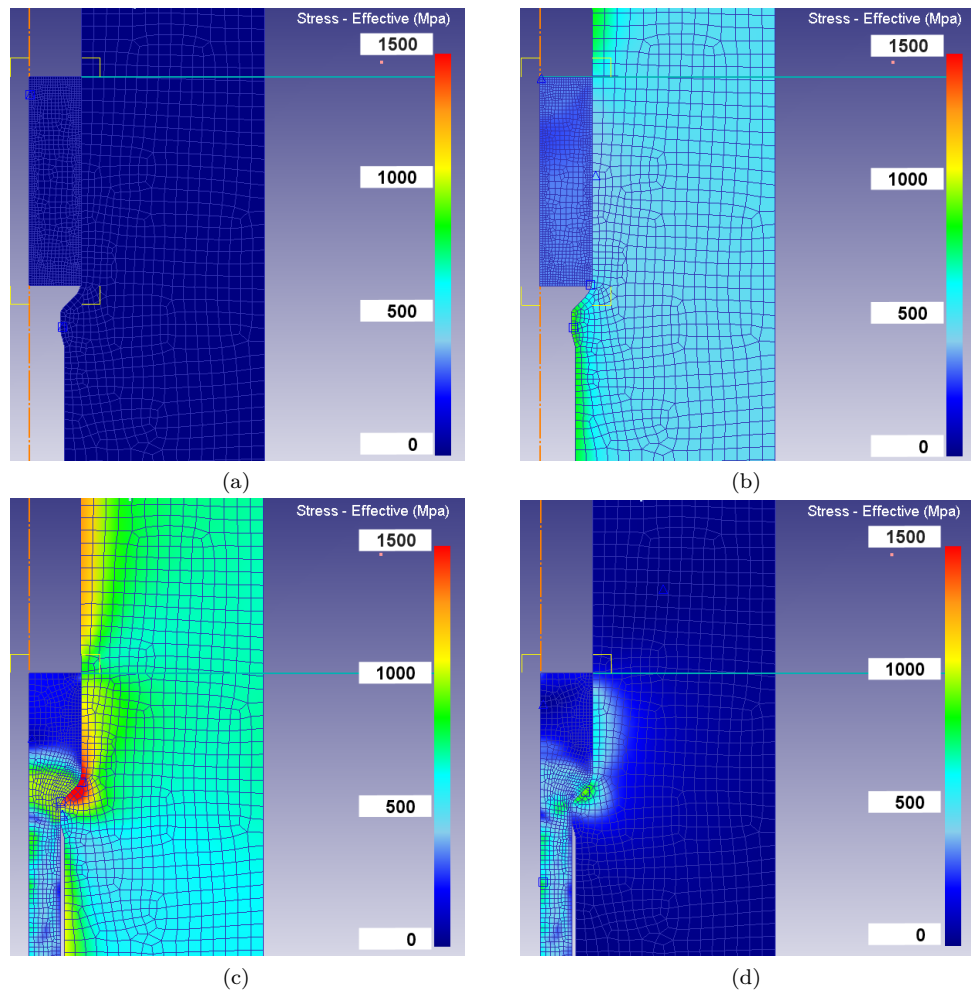


Figure 7.18: FE-simulations of dynamic piezo driven pre-stressing sequence. The system is intended for micro bulk forming.

Figure 7.19a shows the extrusion process, with a red mark at the point of the contact analysis on the inside die surface. In Figure 7.19b, the blue curve shows the normal pressure, which during the process reaches approximately 310 MPa. The red curve represents the inside diameter of the die insert, where the expansion of the die insert during the forming process, can be identified as a small positive stepwise increase of the

curve. The third phase is where the process benefits from the controlled pre-stressing device. The punch is withdrawn and the piezo actuators are de-activated. Hereby the die insert expands to the initial diameter, as shown in Figure 7.19b. The interesting part is the internal pressure in the reference point, which during the un-loading phase becomes zero. This indicates that there will be a gap between the formed component and the container after un-loading. Hereby a significant reduction in the ejection force can be anticipated.

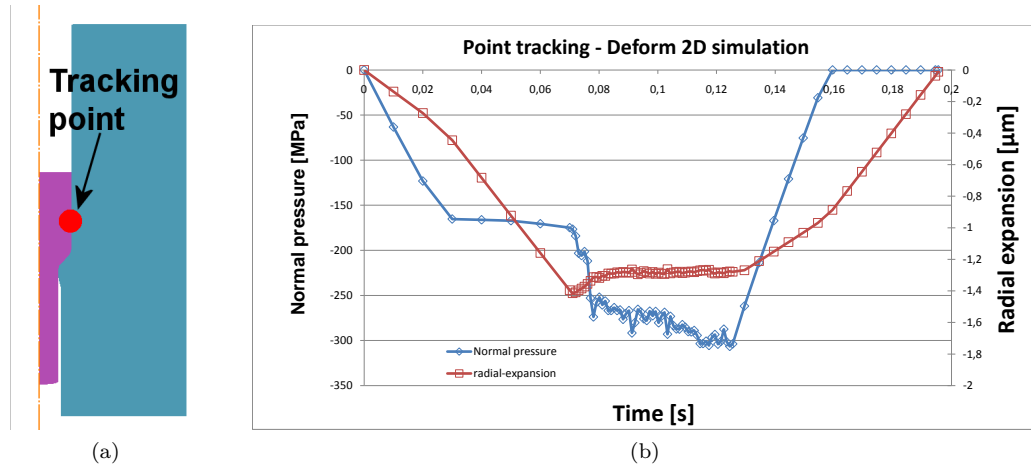


Figure 7.19: Simulation of the force interaction of the piezo driven pre-stress system. Data is acquired at the point indicated (left).

Tooling elements

The actuator elements of the tool system are depicted in Figure 7.21 (left). The actuator consists of a block of multilayered piezo elements in the middle, a stress amplifier towards the front and two opposing wedges at back for adjustment purposes. The dimension of the piezo ceramic actuator stack is 10 X 15 X 10 mm. The stress amplifier elements and the adjustment wedges have been included to account for the available working curve of piezoelectric actuators, showing an inverse linear connection between available load and stroke length. Thus the maximum stress is available at zero stroke whereas the fully extended piezo ceramic actuator will exert zero force. A typical force - stroke characteristic for a ceramic piezo actuator is shown in Figure 7.20. The theoretical block force of the piezo stack is 4000 N and the maximum stroke length is 149 μm. However, the elasticity of the system will quickly exceed the maximum stroke length, prohibiting the piezo actuator to perform correctly. Thus, application of the right amount of pre-stressing force onto piezo actuators is critical. This is done by adjusting the wedges. Strain gauge elements have been mounted on each piezo stack to allow for monitoring the stress during pre-adjustment and operation of the stack.

The assembled configuration of the dynamic pre-stressing system is shown in Figure 7.21b. The four actuator elements are placed in a cross configuration around the die. The stress amplifier pyramid, having a cross sectional area ratio between the front and back faces in contact of 35, will shift the low stress of the actuator into the higher stress needed to elastically deflect the die. The stress amplifiers pyramids have been made

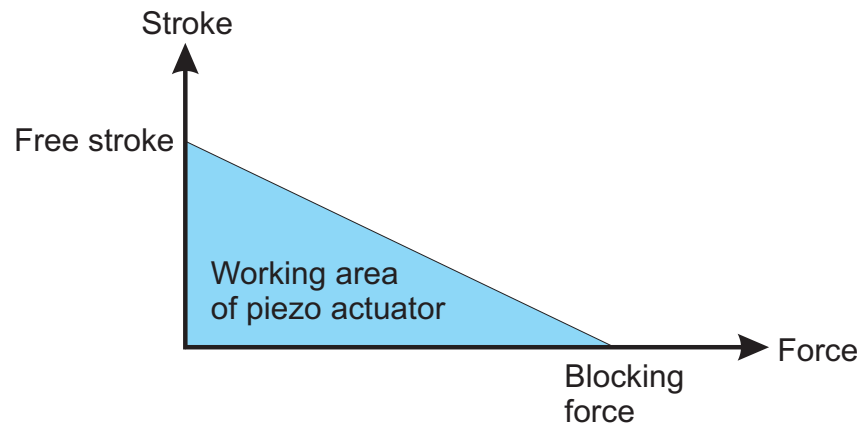


Figure 7.20: Working curve of a ceramic piezo actuator. The product of the exerted force and the stroke length is constant.

in tungsten carbide material to reduce the elastic loss at the point of contact between the amplifier and the die. The die is made of hardened high alloy powder tool steel and

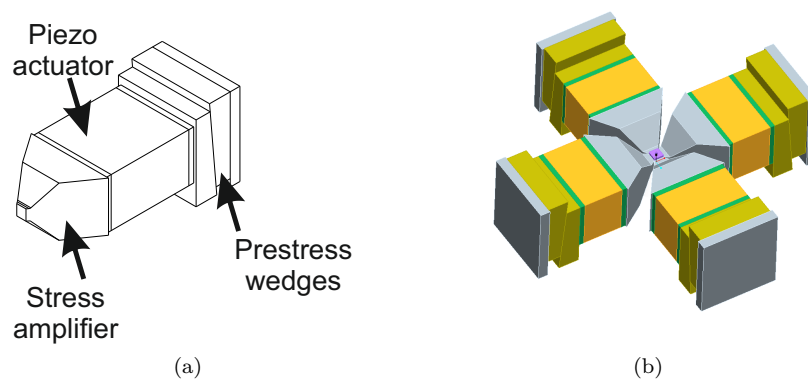


Figure 7.21: Illustration of the pre-stressed piezo stack with stress amplifier element (a). Figure (b) depicts the placement of four piezo stack elements around the centermost square tool die element.

was delivered as a dice with a side length of 2 mm. The center hole was machined as a through hole using the Sarix micro-EDM machine using a dressed electrode option. The diameter of the center hole was specified to $\text{Ø } 0.5$ mm. The diameter was subsequently measured using the optical Demeet 200 CMM giving a nominal diameter of $\text{Ø } 0,4928$ mm, corresponding to a deviation on the diameter of $-7,2 \mu\text{m}$. The uncertainty associated with the diameters measurement is estimated to $\pm 2 \mu\text{m}$. A photograph of the centremost tool die is shown in Figure 7.22b. A human hair has been included in the photo to give the reader an impression of the scale of the tool element. The photograph in Figure 7.22a show the assembled pre-stress system prior to testing. The brown-colored strain gauge pads can be noted on top of each piezo actuator as well as the stress amplifier



Figure 7.22: Photograph of the dynamic piezo pre-stressing system (a) and a closeup of the small forming die with a overlaid human hair (b)

pyramids and the center die.

The movement of the actuators is controlled in pairs, i. e. the two x-actuators and the two y-actuators each share a voltage supply. This allows for a simple electronic setup, where two analogue outputs ranging from 0-10 volts from a computer running Labview, are amplified by a fixed amplification constant. The design voltage is 200V direct current, but the amplifier allows twice as much if testing at extreme conditions are needed.

Results from test of piezo driven prestressing system

From the FE-simulations shown in Figure 7.19b it is known that elastic deflections in the order of 1 μm can be expected. Such small deflections are difficult to measure using normal metrological equipments. The situation is further complicated by the fact that the die center bore will tend to shift position during pre-stressing and relieve cycles, as a result of an unavoidable unbalance between the forces exerted by each opposing actuator pair.

Due to the dimensional size of the expected deflections and the following complications with accurately quantifying the geometrical distortion of the die, a conventional strict metrological analysis was abandoned. Instead an indicative approach was adopted, based on a number of consecutive diameter measurements of the central forming die. The diameter measurements were acquired using a ZEISS UPMC 850 CARAT CMM mounted with stylus ball-probe with a diameter of \varnothing 0,3 mm. By using the CMM machine as comparator, relying on the precision or repeatability of the machine measurements, rather than relying on the absolute traceable accuracy, the combined measurement uncertainty is reduced as seen in Chapter 4.

The diameter measurement values acquired for the three successive measurement rounds are shown in Table 7.1. Here the first collumn show the diameter initially measured. The second collumn is the a measurement of the internal die diameter during excitation of the piezo system with a voltage of 200V. In the third collumn the voltage is reduced to zero and the diameter is once again measured. In the final collumn series the piezo

actuators are operated at a increased voltage of 250V.

The row marked *Average* in Table 7.1 donate the geometrical average of the three above measurements, whereas the Δ *initial* row is quoting the numerical difference between the average value of the first column - to each following collum. The last row is solely included in order to assist the reader in comparing the dynamic performance between the four states of the tool pre-stressing system.

	Initial	$V_p = 200V$	after 200V	$V_p = 250V$	after 250V
Measurement 1	0,4873	0,4870	0,4874	0,4867	0,4873
Measurement 2	0,4875	0,4869	0,4875	0,4868	0,4874
Measurement 3	0,4876	0,4867	0,4874	0,4867	0,4875
Average	0,4875	0,4869	0,4874	0,4867	0,4874
Δ initial		$-6,00E-04$	$-3,33E-05$	$-7,33E-04$	$-6,67E-05$

Table 7.1: Diameter measurement values take with a ZEISS UPMC 850 CARAT CMM at DTU-MEK having a resolution of $0,1\mu m$. Measurements are not corrected. *Average* values are the average of the three preceding measurements and Δ *initial* is the difference between the initial averaged diameter and the averaged diameter values measured following the excitation of the piezo actuators.

7.4 Conclusion

The chapter above described framework considerations in relation to the bulk forming process. Research on ways of preparing billets for the forming operation was presented. A prototype apparatus for investigation cropping of micro billets was constructed. It was found that micro cropping under hydrostatic pressure could achieved high quality billets with volume deviations within $\pm 1\%$.

The influence of press frame stiffness in relation to the micro bulk forming process was described. A design for a new prototype micro press system was presented. The press was designed specifically with the special needs of the micro forming process in mind. Further, considerations for tool design a elevated temperatures was presented. Also, suggestion for a system for in-line process control was given and the properties described.

Further, a handling an transfer system for micro components was presented. Measurements on the acquired accuracy of the transfer system was presented together with characterization of the actuating servo system. Finally, the concept for application of the transfer system in a real life two step micro forming machine was presented.

The chapter was concluded with an experiment involving the utilization of piezo ceramic actuators for dynamic pre-stressing of a micro forming die. The design and machine elements of the prestressing system was described together with control strategies. Simulations of the pre-stressing system showed promising results. Finally a number of measurements on the realized pre-stressing was conducted. The measurements showed an influence of the pre-stressing. However, the elasticity of the system was grater than expected, making the stress output of piezo actuators smaller than expected.

Chapter 8

Results of advanced micro forming experiments

The following chapter will outline some of the micro forming experiments undertaken throughout this work. The experiments have been conducted with the aim of researching the feasibility of utilizing the micro bulk forming method for production of a range of advanced components with industrial relevance.

The text will be initialized with a concise passage dealing with micro forming of an axle component in Aluminium for a potentiometer application. This work was carried out under the course of the European Commission research framework 6 project, *MasMicro* at the author's institute.

The chapter will be continued with results from forming experiments of a small gear wheel intended for a drug delivery system. The component was manufactured through conventional extrusion of aluminium in cold condition. Further, the gear wheel was manufactured in a range of amorphous metals using closed die forging. The amorphous BMG metals are formed at temperatures between 150 °C and 450 °C.

In the final section of the present chapter, the results from a two-step forging operation of a small dental implant in medical grade Titanium will be described. In order to lower the yield strength of the hard Titanium material, the forging operation is carried out in warm condition with temperatures around 400 °C. The two cascaded forging operations may be characterized as an extrusion and a heading process respectively.

8.1 Micro forming of axle for a potentiometer application

In the following section the results of a micro cold forging development are treated. The results are the outcome of a three year research project *MasMicro*. The main activities in this research project have been undertaken by Mogens Arentoft and Nikolas Paldan from IPU, but the author have assisted with practical and theoretical aspects of tool design and manufacturing.

The demonstrator component chosen for this project is a militarized axle for a potentiometer application. The axle is currently being manufactured using conventional

cutting processes and the material of choice is a low cost brass alloy. The envelope dimensions of the axle is \varnothing 3mm and a length of 2,95 mm. The component is symmetric around the rotational axis as shown in Figure 8.1. In terms of forging the axle component

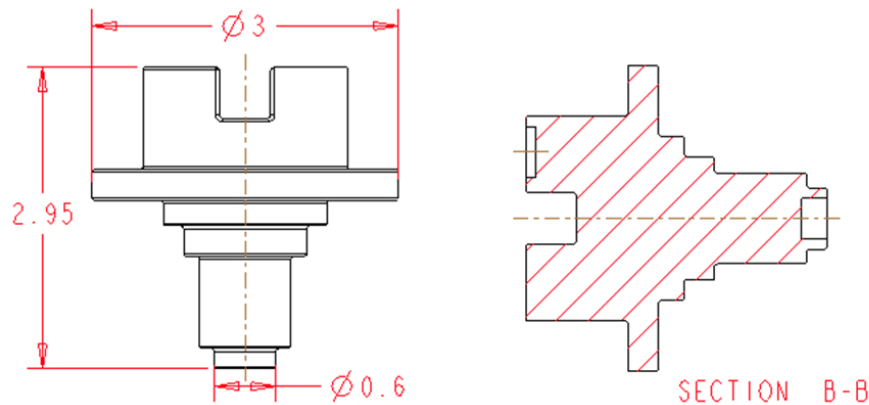


Figure 8.1: Technical drawing of the potentiometer axle component.

geometry and material choice has several implications. The overall geometry is generally well suited for forging, due to the conical progression of the component envelope and the absence of under-cuts. Further, brass and copper alloys are well suited for cold forging at macro scale. However, micro forming of conventional copper alloys, with grain sizes in the range 50 -70 μm , are known to be prone to grain size influences at micro scale leading to anisotropy in the material behavior at micro level [107]. Due to preliminary complications of the grain size influence, the work piece material was changed to a soft aluminum alloy EN AA6061. A few other complications can be mentioned when seeking to replace the cutting based manufacturing method of the axle component with forging operations. One of these difficulties are related to realization of internal and external corners with small rounding radiuses, often requiring excessive internal pressure in the forging die. This leads to high load requirements of the press system, high tool wear and can lead to problems during ejection due to elastic clamping of the component. The same can be said about the small indentation at the very end of the axle component, where presumably the material will have difficulties flowing into the small sharp groove of the die. An other abutting difficulty is realizing the forging system; complete with tools, transfer and ejection system and press system. Owing to the small size of the component, no pre-fabricated production equipments exists at present and a custom system will have to be developed.

The forging process was split into a two-step operation. This was done in order to reposition the component material before the final forging step is executed. As known from conventional forging, this helps in achieving the intended component geometry while lowering the stresses on the tool system. A technical drawing and photo of the formed component is reproduced in Figure 8.2. The axle preform geometry has been designed to be self-aligning in the subsequent forging cell by virtue of its conical side-facets. The self-aligning property of the second forming operation eases the tolerance requirements of the handling system.

The preform forming operation is a classical extrusion process with a 'shoulder' for

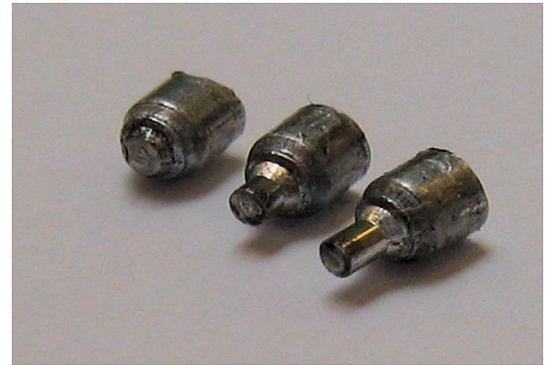
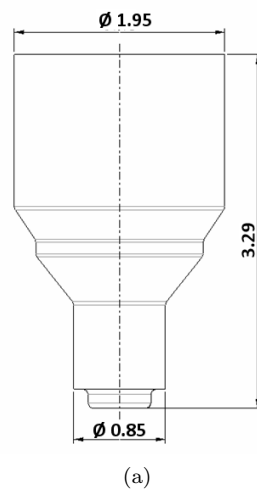


Figure 8.2: Technical drawing of the pre-form component (a) and a photograph of the micro formed specimen, in a soft aluminium alloy, at different extrusion lengths (b).

subsequent forming of the mid-section of the axle. The punch for the extrusion process was a flat-faced norm punch needle of hardened high alloy powder tool steel. The same material was used for the die which was machined using a micro EDM process and the die was subsequently polished with diamond paste to lower the surface roughness. The commercial mineral oil based paste containing white solid lubricant Molycote DX paste was used as a lubricant.

Following the design, optimization and execution of the pre-form forging operation, the second forming step was designed. The second forming operation will realize the final component geometry and was designed to mimic the shape of the axle as close as possible. The forming operation was executed as a closed die cold forging operation and could be classified as a heading operation. The geometry of the component 'mid-waist' and up was machined into the forming punch. The remaining lower geometry is to be formed by the die. Figure 8.3 show results of the gradual change of the preform into the finished geometry during forming. An undesirable material flow characteristic was discovered during the final forging step, requiring increased press load to successfully form the second step. In order lower the press load and tool stresses, a second generation of the tool design for both forging operations had to be made.

The required press load of the first forging operation was about 3 kN while the second forming step required 5.5 kN, exhausting the full capability of the utilized linear actuator. The actual measured press load values were about 20 % higher when compared to values obtained from FE-simulations, a behavior that most probably is attributable to increased friction.

Figure 8.4 shows a side by side comparison between the original axle component, realized through cutting of brass material, and the formed aluminium ditto realized through the two step micro bulk forming process. Comparing the two photographs in Figure 8.4a and 8.4b some noticeable differences are apparent. Starting from the top of the axle, the screwdriver slot is less defined for the forged axle. Especially around the lower internal

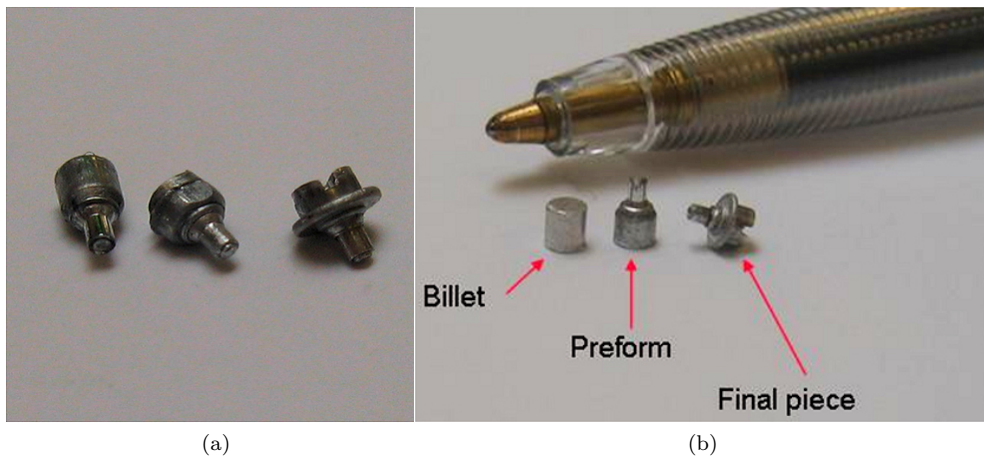


Figure 8.3: Photographed aluminum axle component - from preform to final component. Photographed aluminum axle component (a). The photo show gradual forming from the shape of the preform to the final component geometry. The image (b) illustrates the scale and gradual change from billet to preform to final geometry of the micro axle.

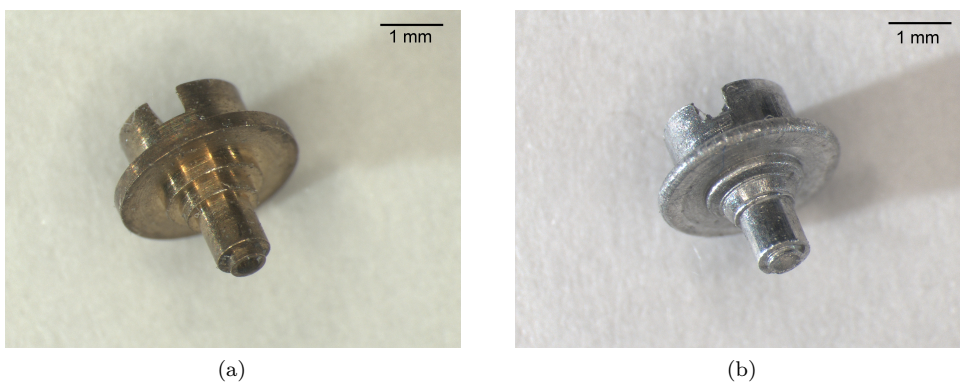


Figure 8.4: Machine brass axle component (a) and the micro bulk formed aluminium axle realized in this work (b).

corner of the slot, some unintended rounding appear. Continuing to the 'waist' of the axle, a clear rounding of the outer edge is noticeable. Further, the surface finish of this side-facet is not very good for the formed axle. As this facet is a functional surface, ensuring proper guidance of the axle in the polymer potentiometer casing, the surface finish is critical.

Following the axle further down a few other differences can be noticed around the staircase-midsection of the axle. As before, a rounding tendency is noticed and the smaller staircase ring is not well defined on the formed specimen.

Despite the imperfection of the micro bulk formed axle component, there is generally good agreement between the cut and formed specimen.

Conclusion on axle forming experiment.

When comparing the general envelope of the two specimens in Figure 8.4, good agreement was found. The experiment has proven that it is possible to manufacture small components with good accuracy using bulk forming technology. The physical properties of the bulk forming process have shown to introduce unintended rounding of edges intended to be sharp. Further, the surface finish of the formed axle was rough when compared against the specimen manufactured by cutting.

By taking into account the physical constraints of the bulk forming method during the design phase of the micro metallic component, its neighboring mechanical elements and the requirements of the ingoing application, it should be possible to incorporate these constraints. This could mean that some corners or functional surfaces should be given higher priority in the design of the forming operation, thus realizing a better finish, while other non critical geometries could tolerate the rounding and possible under-filling effects that might occur during a bulk forming operation.

Finally it is debatable if subsequent machining, as known from conventional bulk forming industry, will ever be attractive at micro level. Just the costs associated with handling and logistics alone will likely make it more attractive to machine the micro component from bulk, avoiding forming process altogether.

The axle component has later been successfully formed in an amorphous bulk metallic glass alloy [26].

This successive bulk forming of the axle component has set the foundation for work of this thesis.

8.2 Comparative micro forming operation of Gear-wheel component.

In the following section the results from a number of forming experiments of a small gear wheel will be given. The gear wheel component is a critical element of a portable drug delivery system and is currently mass produced using powder metallurgy technology. The current material is stainless steel AISI 316.

The general dimensions of the gear wheel can be noted from the specifications in Figure 8.5. The tolerance requirements ranges between $\pm 20\text{-}50\ \mu\text{m}$ and are mutual dependent through the option to inherit unused tolerance deviation between several entities. The net volume of the gear wheel component, excluding the center hole, is $27,8\ \text{mm}^3$.

The gear wheel has been selected as object of study as it represents a small metallic component, dimensionally close to the micro range, with medium complex geometry. Further, the tolerance settings bound to the gear wheel geometry are comparable challenging in terms of production quality. Finally, a forming process have the potential to lower the production cost substantially when compared to the powder pressing method currently applied.

The following experimental analysis will be split two ways. In the first part of the section the gear wheel will be produced using cold extrusion of aluminium alloy. Extrusion of

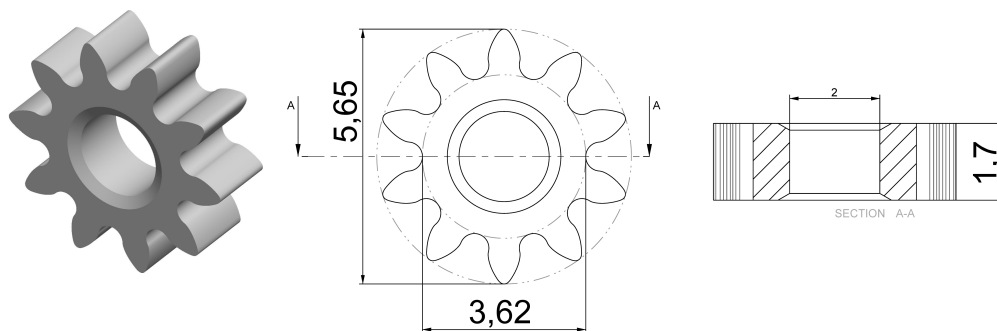


Figure 8.5: Technical drawing of the gear wheel component. Tolerances are ranging between $\pm 20\text{-}50\ \mu\text{m}$.

aluminum is well known for which reason the analysis will take the role of a reference process rather than a novel addition to known technology. In the second part of the section, a number of special metallic glass alloys will be formed using closed die forging at elevated temperatures.

As a whole the gear forming experiment seeks to demonstrate two viable alternative routes of achieving the gear wheel - one using conventional methods and one using a new choice of material and process combination.

Gear wheel cold extrusion in Aluminium

Extrusion is probably the most frequently applied forming method within processing of aluminium. The process can be applied in a wide range of scales, ranging from extrusion of the hollow profiles making up the carriages of trains down to the cores of an electrical conductor. The process is well described and imposes few complications.

In the current work the extrusion process will be examined as potential production method for production of the gear wheel geometry. In order to simplify the tool design the internal center hole has been filled in.

Naturally, the extrusion process will not realize discrete gear wheels but rather a lengthy rack. The rack will subsequently have to undergo cropping or sawing in order to arrive at the gear wheel geometry. If production volumes are sufficient, the extrusion and cropping methods could offer a substantial cost reduction over powder pressing processes.

A number of numerical simulations were undertaken in order to identify good process conditions. Properties such as area reduction ratio and die angle were varied in the simulations to arrive at a suitable extrusion die design. An example of a simulation of the extrusion process can be seen in Figure 8.6 where high strains around 4 can be noted. Concluding on the simulations a suitable area reduction ratio of 65% was chosen and a die angle of 45° .

The extrusion die was prepared in high alloy powder tool steel in the annealed state. The die was then hardened and the toothed rim then cut with a wire-EDM machine utilizing a machine with parameters set for low surface roughness. Finally, the tool system was

8.2. Comparative micro forming operation of Gear-wheel component.

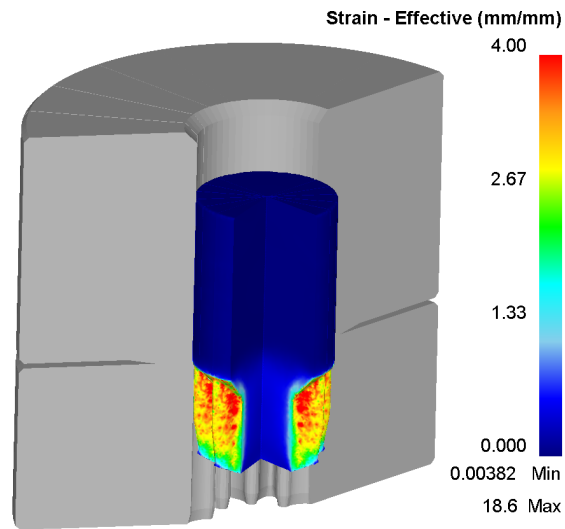


Figure 8.6: Simulation of the gear wheel extrusion process.

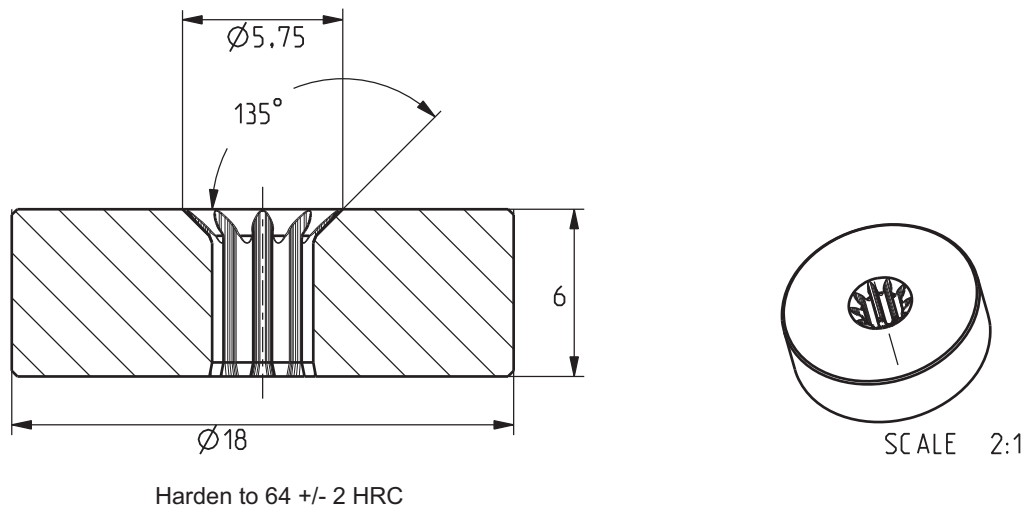


Figure 8.7: Technical drawing of gear wheel extrusion die.

completed with die container, punch and tool holder. The tool elements were fitted into a preexisting fixture, ensuring good alignment between the punch and die geometry. The alignment fixture is allowing a maximum die height of 18 mm, determining the maximum allowable height of the tool insert for this experiment. The complete extrude tool system, excluding the alignment fixture, is visualized in Figure 8.8.

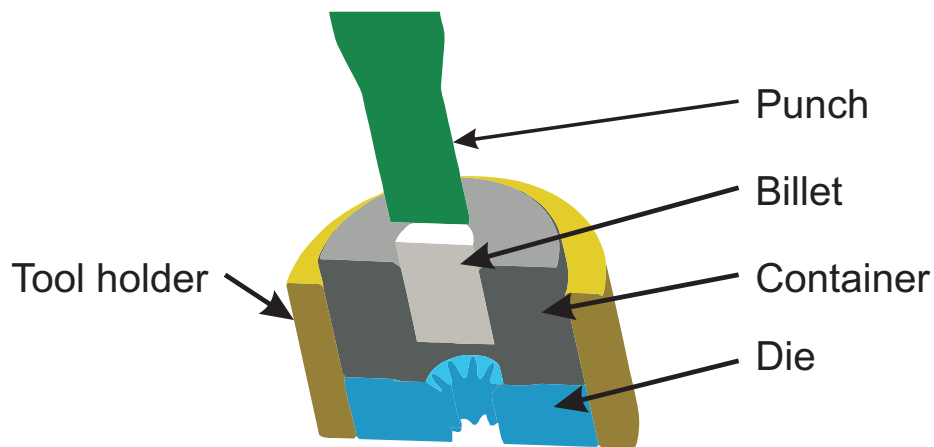


Figure 8.8: CAD model of the extrusion tool elements. General tolerances are $\pm 50 \mu\text{m}$.

The tooling elements were manufactured, assembled and a number of extrusion tests were carried out. The photos in Figure 8.9 show the extrusion tool elements mounted in the alignment fixture (a) and an example of a billet halfway through the extrusion die (b). As can be noted from the photo in Figure 8.9a, a chamfer have been machined on the die container in order reduce the area of contact between die and container, allowing higher contact pressures to be reached. Upon assembly of the extrusion tool, a number of

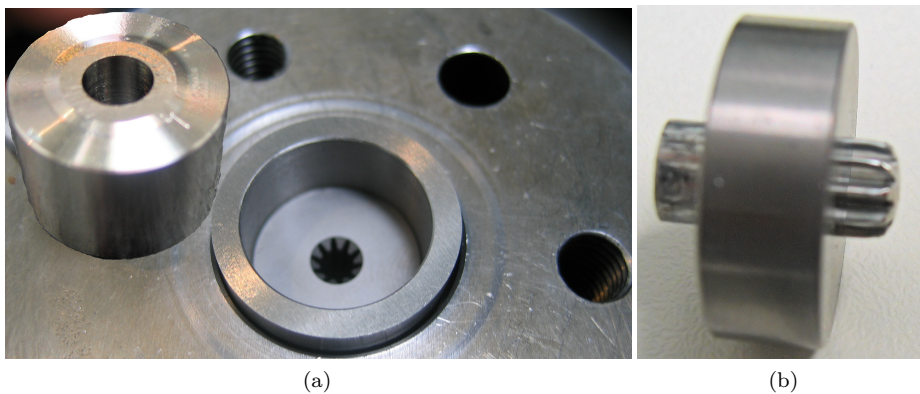


Figure 8.9: Photograph the extrusion tool parts (a). In this image the die and the tool holder ring is mounted in the aligning fixture. The container die can be noted on the side. The photo to the right (b) shows a billet pressed half-way through the extrusion die.

extrusion experiments were conducted. Figure 8.10 depict plots of the press load and a

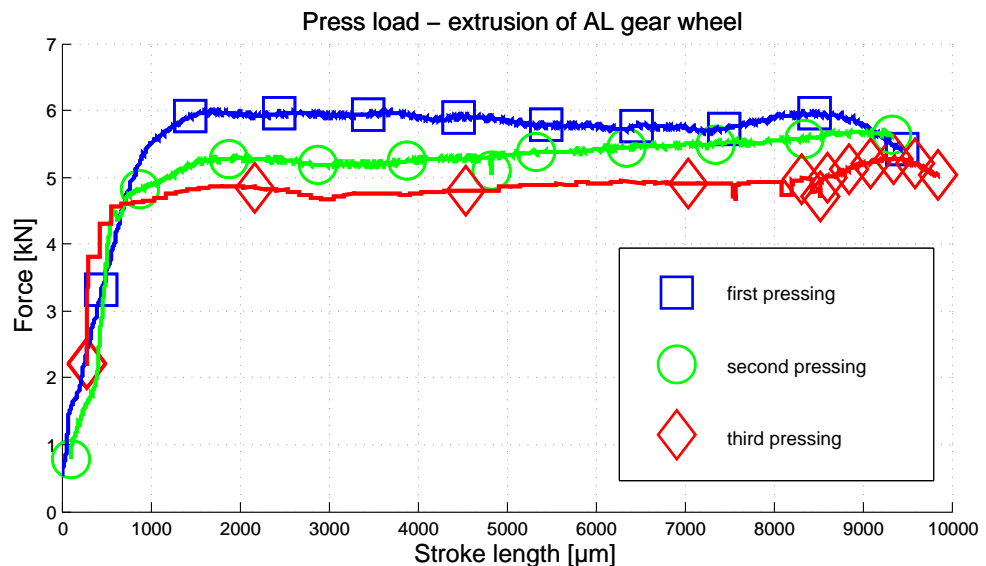
8.2. Comparative micro forming operation of Gear-wheel component.

photograph of the extruded specimens. A commercial mineral oil based paste containing white solid lubricants was applied as lubricant.

As can be noted from the plots in 8.10a, a slight increase in the process load can be noted towards the end on the extrusion process. This signals the end of the current billet and the process should be stopped. Further, a decrease in the process load can be noted over the successive experiment. This is normal behavior and can be explained by the flattening of die surface asperities and the slow filling of the successive ingress lubricant into the die surface 'valleys'.

With a total billet length of 10 mm and a area reduction of 65%, the extruded billet length is about 15 mm long.

Upon forming, the billets were cut and the center hole was drilled on a conventional lathe. The results are described in the end of this section together with the results of the forming experiments of the bulk metallic glass alloys.



(a)



(b)

Figure 8.10: Plots of the press load over three successive extrusion experiments (a). (b) is a photo showing the result of a number of successive extrusions.

Closed die forming of gear wheel in BMG materials

In this section we look at the closed forming of the gear wheel geometry. In a conventional closed die forming scenario, involving crystalline material, the typical forming operations are sub-divided into a number of forging steps. The successive forming operations gradually shift the material volume to the right position. The final forging step then is then responsible for a final calibration of the component envelope dimension. An attempt to form a near-net shaped component using a single closed die forging approach, will most likely lead to excessive tool stress and fracture of die or punch elements.

Bulk metallic glasses, described earlier in Chapter 3, are a family of materials that under special conditions behave like a supercooled newtonian viscous fluid. The supercooled phase can be sustained for a limited time when the material is tempered between the glass transition temperature, noted T_g , and the onset crystallization temperature T_x . The viscous behavior of these amorphous materials allow closed die forming in one operation with little tool stress - much like thermoplastic moulding of polymer materials. Further, the amorphous structure of the BMG material allow replication of features with dimensions in the sub micrometer range. Figure 8.11 plots the flow stress of a Magnesium based bulk metallic glass alloy as a function of temperature. A rapid drop in the flow stress at the onset temperature of 153 °C is noticeable for the amorphous alloy, whereas a normal crystalline Magnesium alloy material exhibits a linear decrease in flow stress.

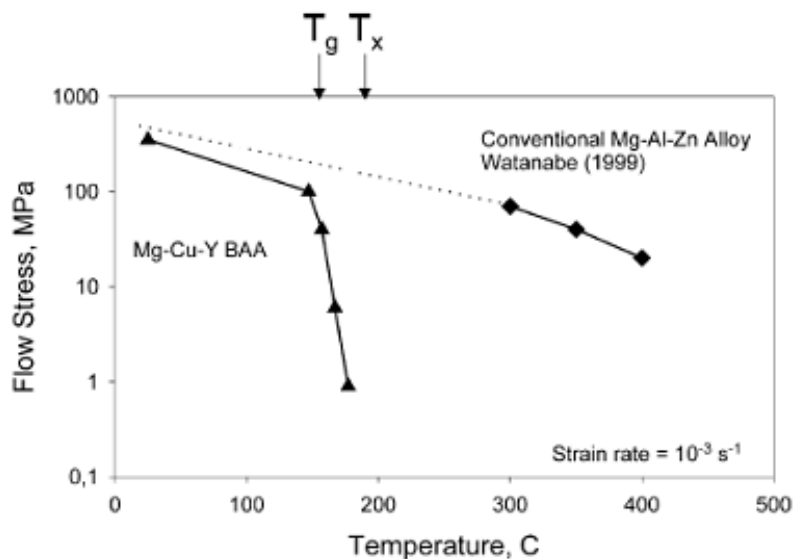


Figure 8.11: Example of transfer sequence of a two stage micro bulk forming process [26].

Recalling that in the super cooled viscous state, bulk metallic glasses are strongly strain rate dependent, care must be exercised to keep the punch travel speeds to a low limit. The viscosity of a matter and the measured force during forming can generally be related through the basic formula in 8.1. However, this relation only holds for steady state flow, low speed movement of newtonian matters and under some strict bounds on the physical dimensional relations. For this reason, further comparison between the

theoretical viscosity of the metallic glasses and the measured forming load have been omitted here.

$$\sigma(t) = 3\eta\dot{\epsilon} \quad (8.1)$$

, where σ is stress, η is newtonian shear viscosity and $\dot{\epsilon}$ represents the strain rate. The equation is not valid for the beginning of the experiment ($\dot{\epsilon} \neq 0$). More elaborate exposition on the relation between viscosity and forming force for bulk metallic glasses can be found in literature [108].

Tool system

Owed to the limited tool stresses involved in forming bulk metallic glasses, the range of suitable tool material is broad. The low tool strength requirements in BMG forming allow for soft or brittle materials such as copper, stainless steel or advanced ceramics to be utilized as tool material. But also conventional warm forging tool steels, such as ORVAR can be utilized. The elevated temperature brings a number of challenges relating to oxidization of tool surfaces and the general complications of tool temperature and tolerance control involved in warm forging.

Especially for closed die forming with small tolerance and narrow clearances, uneven thermal deflections and surface oxidation effects can complicate the tool design. Additionally, a thermal cycling procedure, required for some BMG forming operations, elastic clamping can occur as a result of differences in thermal expansion coefficients between the bulk and tool material. An elaborate investigation can be found in a co-authored article dealing with the required ejection force of a bulk metallic glasses component as function of surface finish and tool materials [2].

For the gear wheel case, a simple closed die tool system has been constructed. As can be noted from the CAD-model drawing in Figure 8.12a, the system is made up of two identical punch and ejector elements. The die, featuring the gear star geometry in the center hole, is made as a through container die with vertical internal facets. The tool material is classified as a high speed steel and all machining is done using the wire-EDM process technology.¹

To simplify the tool manufacture and the experiments, the center hole of the gear component has been omitted in the tool design. The chosen tool design contains a number of interesting potentials for evaluating ejection force, ejection approaches and flow of the material in the punch-die clearance.

The wire-edm tool process offers an easy and cost effective method of realizing a narrow fit between tooling elements required when forming amorphous metals. Figure 8.12b shows the finished tool parts. These parts are fitted in a die-set with electrical resistance heaters and a matching temperature control system. The die-set is then placed in the C5K micro process, delivering the required forming force for the operation.

¹It has been commented by the PhD thesis examiner that a dedicated warm working tool steel would have favorable properties in comparison to high speed steel. It was proposed to utilize a AISI Type H13 Hot Work Tool Steel, such as Orvar supreme from Uddeholm.

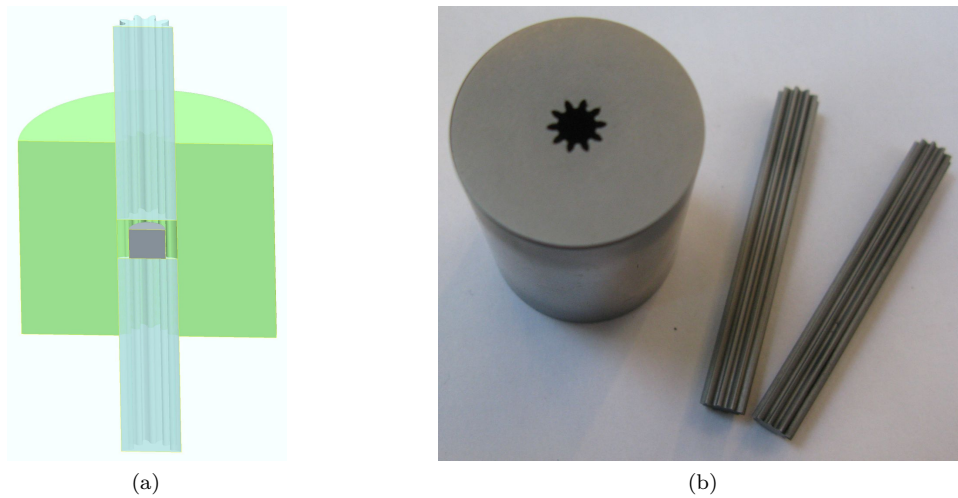


Figure 8.12: CAD model of the closed die forging tool system (a) and a photograph of the constructed tool system (b). The bulk metallic glass billet, colored gray, can be noticed inside the die in figure (a).

Gear wheel forming with $\text{Mg}_{60}\text{Cu}_{30}\text{Y}_{10}$ BMG material.

The forming experiment was initialized with forming of the $\text{Mg}_{60}\text{Cu}_{30}\text{Y}_{10}$ alloys. The bulk metallic glass was manufactured at the Risø-DTU National Laboratory using special arc-melting and quenching techniques. The sample was then exposed to x-ray diffraction (XRD) analysis to confirm amorphicity of the material.

The $\text{Mg}_{60}\text{Cu}_{30}\text{Y}_{10}$ bulk metallic glass has a glass transition temperature, T_g of 153°C and a crystallization temperature, T_x , of 192°C and processing should take place in this range between these two temperatures. Within the range, higher temperatures lead to lower viscosities. Refer to Figure 8.11 for details.

The tool temperature was set to 170°C and the temperature was verified with a calibrated thermocouple probe instrument. Billets with an internal diameter of 3,435 mm and a height of 3 mm, were cut using wire-EDM tooling machine. A birds-eye picture of the billet can be seen in Figure 8.13a. The diameter of the billet was chosen in such way that the volume of the billet would match the volume of the gear wheel being $27,8\text{mm}^3$. The forming operation will be carried out without application of lubricant. Earlier experiments have shown a degradation of the component surface quality due to an undesirable integration of the lubricant and the bulk material during forming [26].

A number of preliminary experiments had to be conducted to establish the required dwell time before forming. A sufficiently long dwell time is necessary to allow the heat from the tempered tool die to propagate onto the cold billet upon insertion. Evidently the required dwell time depend strongly on the temperature of the forging process, the die geometry and the billet volume. For the 170°C $\text{Mg}_{60}\text{Cu}_{30}\text{Y}_{10}$ forming process a dwell time of 8 minutes was found to be sufficient, when the BMG billet was pre-stressed between the ejector and punch after insertion. Figure 8.13b show a side-view photo of a specimen formed with a dwell time of only 4 minutes. It is clearly seen that the material

8.2. Comparative micro forming operation of Gear-wheel component.

in thermal contact with the ejector and punch have experiences viscous flow, while the center material has been tempered below the glass transition temperature, T_g .

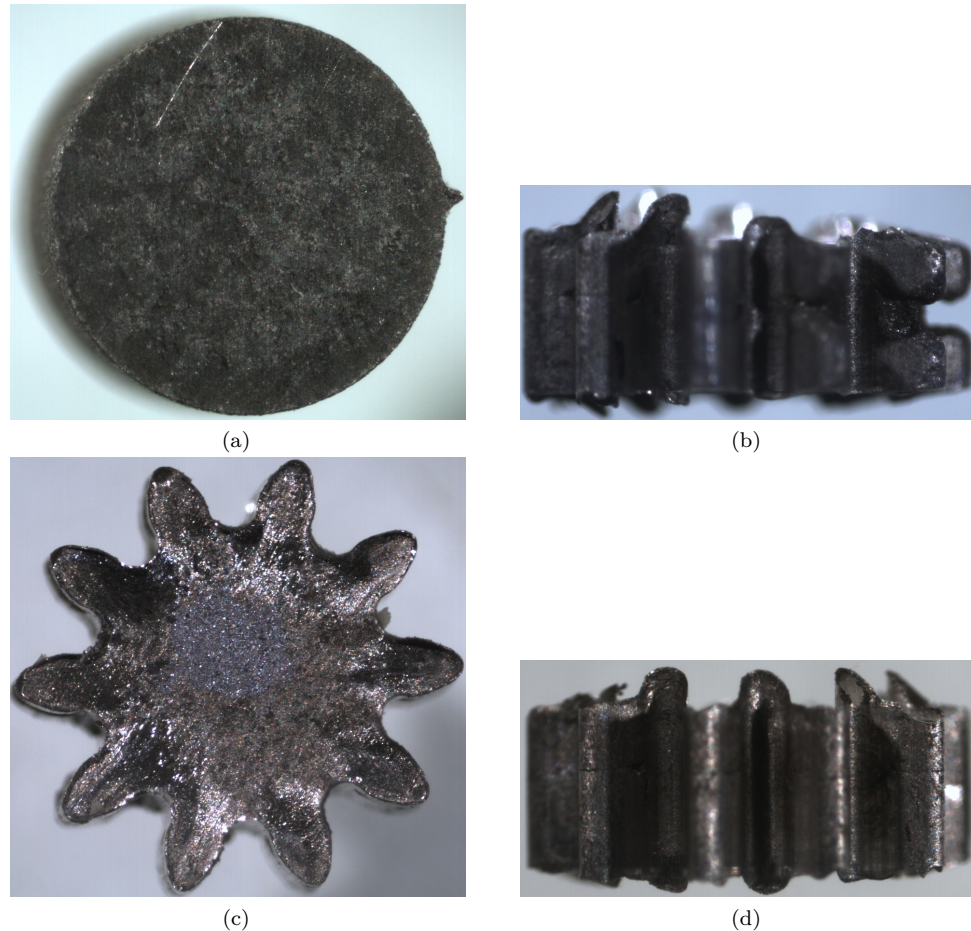


Figure 8.13: Micrographs of the $Mg_{60}Cu_{30}Y_{10}$ specimens. The cut billet is shown in (a), where the chip originating from the wire-EDM cutting is visible to the right. Figure (b) is an imperfect forming experiment due to under-heating. (c) and (d) show a good example of a the formed gear wheel geometry.

The photo in Figure 8.13c shows a top view of a successfully formed gear wheel. A thin rim along the contour of the wheel is noticeable. This rim is a result of the flow of the amorphous bulk material into the narrow clearance between the punch and the die. The backward extrusion through the die-punch clearance is clearly noticeable on the image in Figure 8.13d. The length of the thin backward-rim can be limited through optimization of the cutoff-load and the forming temperature. This is shown later in the chapter. Also, the burr rim is easily removed through utilization of a tumbler or alike.

The load stroke curve in Figure 8.14 shows low scatter between the three successive forming experiment. Full die filling is achieved at a stroke length of about $1000 \mu\text{m}$ and only 800 N load at a low punch stroke rate of only $10 \mu\text{m pr. second}$. A characteristic

bend can be noticed on the stroke-load graph above a stroke length 1000 μm . This can be ascribed to the backward extrusion in the punch-die clearance.

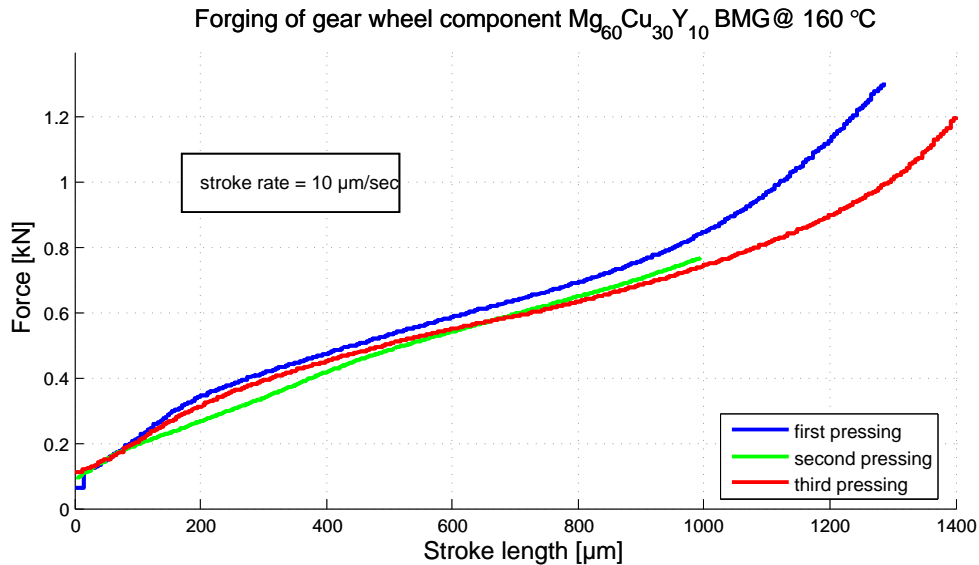


Figure 8.14: Load stroke curve of three successive forming of the gear wheel component in the $\text{Mg}_{60}\text{Cu}_{30}\text{Y}_{10}$ metallic glass.

At higher stroke rates the load of the forming operation increase exponentially. The strong strain rate dependance is exploited during ejection of the component. Instead of having to cool the tool system or wait for the metallic glass to turn crystallin, ejection is done at a high strain rate. At high strain rates, the component will be hard and collapse during ejection can be avoided.

Forming in $\text{Mg}_{61}\text{Cu}_{28}\text{Gd}_{11}$ BMG material

The $\text{Mg}_{61}\text{Cu}_{28}\text{Gd}_{11}$ bulk metallic glass is a Mg-based BMG with comparable properties to that of the earlier section. The glass transition temperature for the $\text{Mg}_{61}\text{Cu}_{28}\text{Gd}_{11}$ alloy is 149°C and the crystallization temperature is 210°C . As for other low temperature Mg-based BMG alloys the $\text{Mg}_{61}\text{Cu}_{28}\text{Gd}_{11}$ is very brittle when cooled having a fracture strength in the range 461-732 MPa.

The forming window and the crystallization time of the $\text{Mg}_{61}\text{Cu}_{28}\text{Gd}_{11}$ can be noted from the plots in Figure 8.15. The acquired load stroke curves of the forming experiments is plotted in Figure 8.16. Forming at increased strain rates yield higher loads. Increasing the temperature decreases the viscosity of the material, thus lowering the load, but shortens the crystallization time.

The course of the load stroke characteristics in Figure 8.16 is comparable to that of the $\text{Mg}_{60}\text{Cu}_{30}\text{Y}_{10}$ in Figure 8.14. However a higher punch stroke rate can be applied in the case of $\text{Mg}_{61}\text{Cu}_{28}\text{Gd}_{11}$ before the load of 800 N is reached.

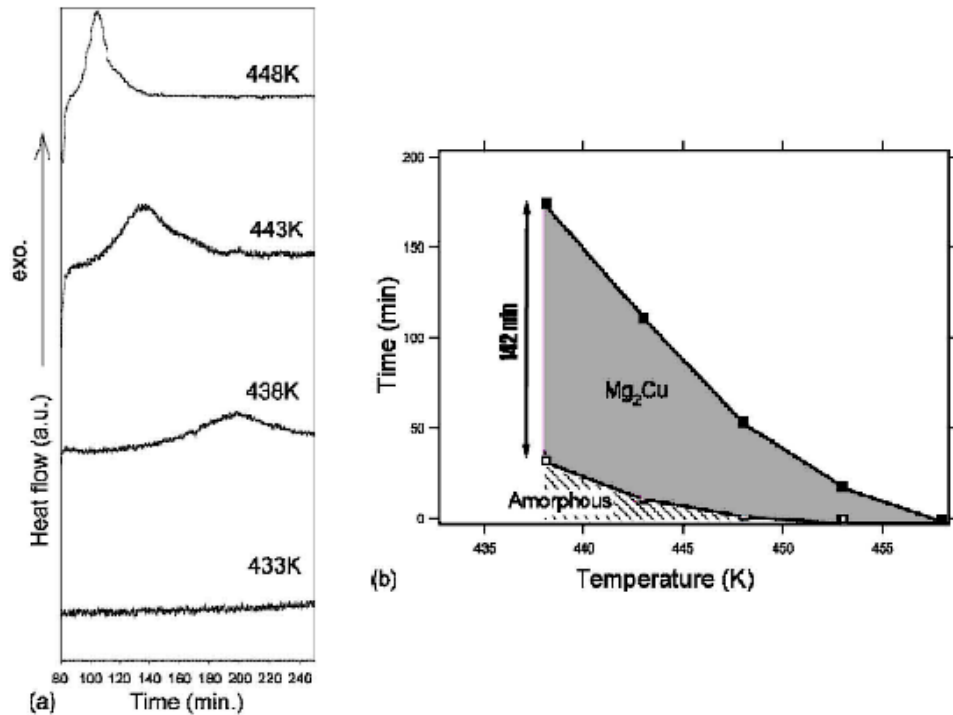


Figure 8.15: Thermal behaviour of Mg₆₁Cu₂₈Gd₁₁ BMG material. (a) plots experimental values for crystallization of the material. As the crystalline material is at a lower energy state, the exothermal response of the crystallization is a sign of when crystallization happens. Figure (b) show that super cooled forming window and the time to crystallization [26].

A number of the forming experiments failed due to high loads and brittle fracture of the billet material. This is likely due to the material being crystalline upon delivery due to challenges in the production process. The need for rapid cooling of the BMG material are known to lead to part-crystallinity in case high cooling rates cannot be sustained.

Forming in Zr₄₄Ti₁₁Cu₁₀Ni₁₀Be₂₅ BMG material

The Zr₄₄Ti₁₁Cu₁₀Ni₁₀Be₂₅, subsequently referred to as Vitreloy 1B, is a second generation development of the first commercial BMG; Vitreloy 1. Both metals have been developed by Liquid Metals Inc. The bulk material is delivered in the form of rods with a diameter of Ø25 mm, making one of the thickest amorphous alloys yet to be realized. The Vitreloy 1B has a glass transition temperature, T_g of 350°C and an onset crystallization temperature of 470°C. Figure 8.18 shown experimental values of viscosity and crystallization time. It should be noted that the crystallization time depends inversely on the heating rate, meaning that rapid heating will shorten the crystallization time substantially. Further, technical data of the Vitreloy 1B and other BMG materials can be found in Appendix F. From the temperature-viscosity curve a suitable forming temperature of 450°C was chosen.

At this temperature the punch, ejector and die material will suffer oxidization. The

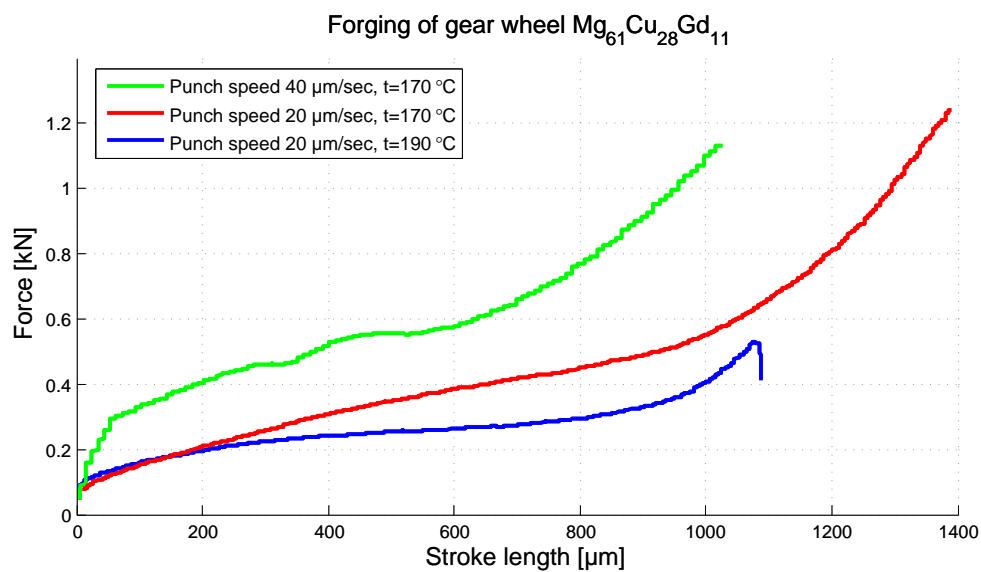


Figure 8.16: Load stroke curve of forming with different process parameters.

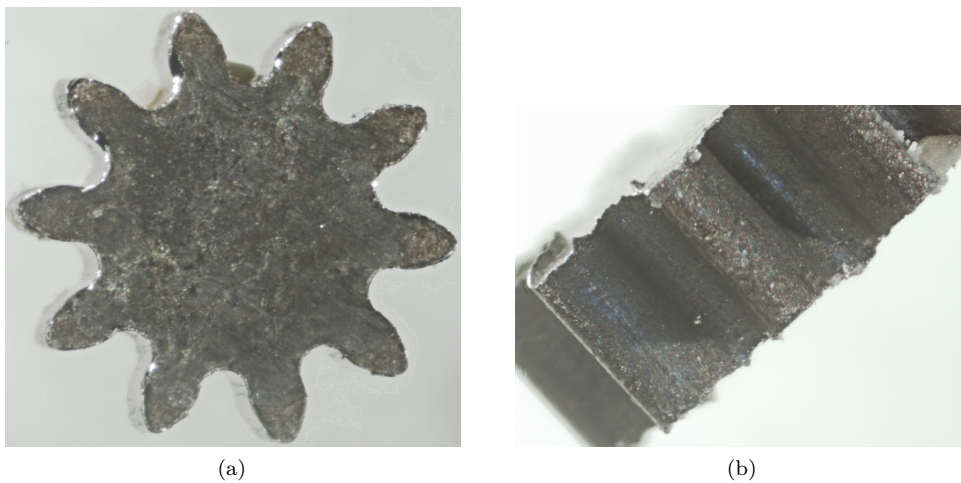


Figure 8.17: Microscope images of the formed gear wheel specimens, $Mg_{61}Cu_{28}Gd_{11}$. (a) is a top-down image while (b) is acquired from the side.

surface oxidation layer will generally worsen the tribological conditions for the forming process and between the tool parts. Especially the narrow clearance between punch and die is prone to clearance reduction and increase of friction. A common method of limiting tool oxidation is through different ceramic surface coatings. However, the small diameter and the high aspect ratio between height at diameter makes it impossible to coat the inside of gear wheel die using conventional vapor deposition methods. However, the punch and ejector tools was coated with a titanium nitride coating the avoid thermal oxidation of these tool parts.

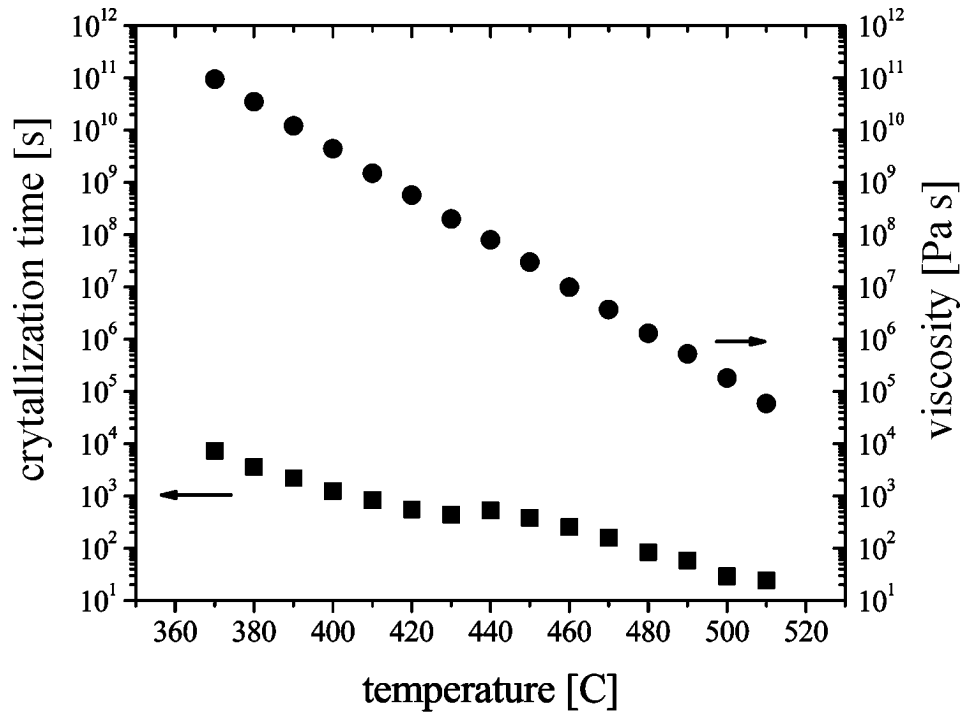


Figure 8.18: Plot showing the expected crystallization time and viscosity of the Vitreloy 1B BMG as a function of temperature [27].

A MoS₂ based graphite compound was used as a lubricant in the forming experiments. The lubricant will lower friction, also between the die and punches, but will lead to degradation of the surface finish of the formed specimen.

A number of forming experiments were carried out. Initially the forming temperature was too high owing to thermal radiation losses across the die. When a thermal probe, mounted on the external surface of the tool, was measuring 450°C, the internal temperature would be about 30° higher. Thus the BMG material would crystallize before any forming had happened. The temperature was then lowered so that the internal temperature would measure close to 450°C.

Upon insertion of the Vitreloy 1B BMG billet and immediate fitting of the punch with a pair of pliers, the gear wheel component was formed under the low pressure exerted with the manual pair of pliers. It is estimated that during the manual down-pressing of the punch a maximum force of 10 N was exerted. The forming time is estimated to be about one second. The scanning electron microscope images in Figure 8.19 show a formed gear wheel with very little rim backward extrusion.

The need for a dwell time between insertion of the billet and execution of the forming operation, had to be reduced to a couple of seconds. The thermal equalization between billet and tool temperature will happen fast due to the contribution of heat radiation.

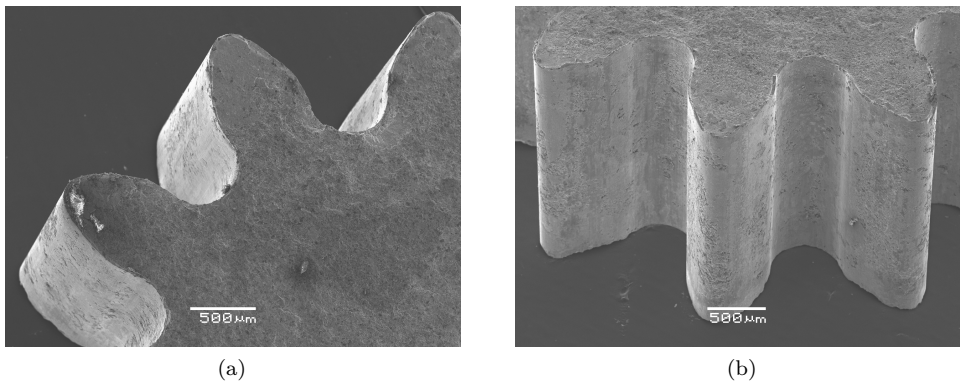


Figure 8.19: SEM images of the gear wheel formed at 450°C with only manual down-pressing of the punch.

In order to investigate the influence of temperature on the process load, the internal die temperature was lowered to 430°C. Now the C5K press micro press was used to form the specimen. The load-stroke curve of the experiment is reproduced in Figure 8.20. The

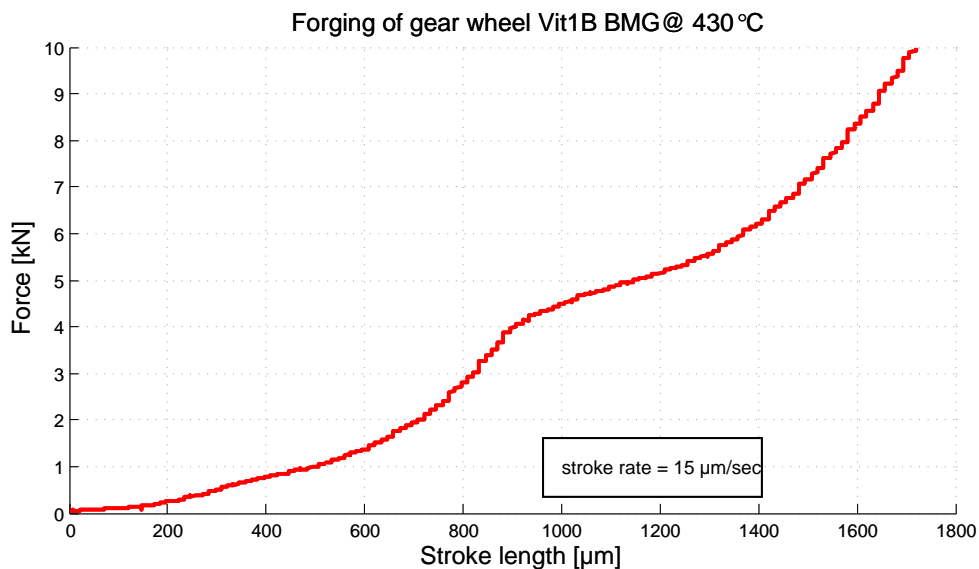


Figure 8.20: Load-stroke curve of gear wheel forming experiment of the Vitreloy 1B alloy tempered at 430°C.

press load at full form filling is about 6kN at a punch stroke rate of 15 $\mu\text{m}/\text{sec}$. The envelope of the stroke-load curve is comparable to that of the earlier experiments with low temperature BMGs. The SEM images of the resulting specimen is shown in Figure 8.21.

The SEM images show a layer of lubricant graphite remaining on the formed gear wheel specimen surface. The lubricant entrapment is especially pronounced on the top and bottom surfaces of the formed gear wheel. Additionally, the lower temperature and the

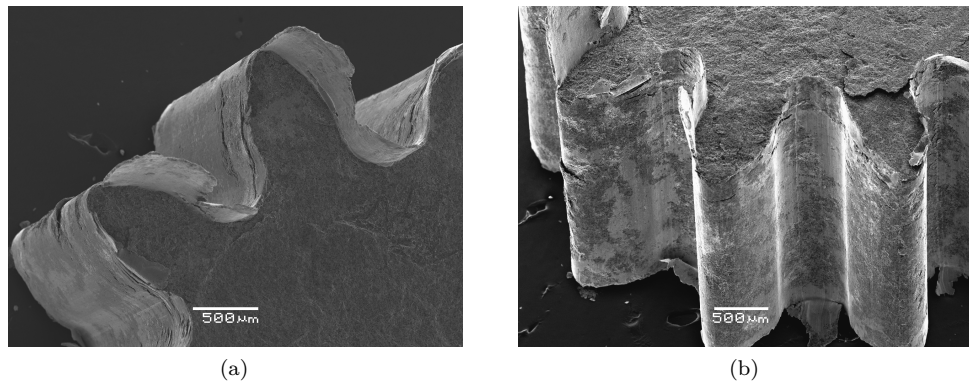


Figure 8.21: SEM micrographs of the gear wheel specimen formed at 430 °C. SEM micrographs of the gear wheel specimen formed at 430 °C. Figure (a) show the thin rim formed in the clearance between the punch and the die. Figure (b) depicts the gear wheel specimen from a different angle, where the remains of the MoS₂ lubricant is clearly visible as a flaky layer on the top of the specimen.

higher press force has led to the formation of a back-ward flowing rim. The width of these rims will be evaluated in the SEM images in the following section. Finally the vertical surfaces on the gear wheel show no traces of shear marks or other surface defects. Only the thin sheets of MoS₂ lubricant remains.

Conclusion of gear wheel forming results

A total number of four forming experiments have been conducted in order to evaluate alternative manufacturing methods for a miniaturized gear wheel component. The first experiment was a forward extrusion of a soft aluminium alloy through an extrusion die. Extrusion of Aluminium is well known, why the experiment is regarded as a reference process.

The following experiments have been dealing with closed die forming of various bulk metallic glasses in their amorphous state. Elevated temperatures between 170 °C, 180 °C and 450°C have been applied forming the BMG alloys Mg₆₀Cu₃₀Y₁₀, Mg₆₁Cu₂₈Gd₁₁ and Zr₄₄Ti₁₁Cu₁₀Ni₁₀Be₂₅ (Vitrelloy 1B) respectively. The stroke-load curves for the experiments have been recorded for comparison.

SEM micrographs of the forming experiment of the Vitrelloy 1B alloy are shown in Figure 8.22. The width of the unintended back-ward rim formed in the clearance between the punch and the die can be estimated to a geometrical width of about 15 μm to 20 μm through the images in Figure 8.22a and 8.22b. The results show a good replication of the die geometry. The Vitrelloy 1B alloy is easy to work with and can be moulded with low load if properly tempered. Through careful control of the stroke length and the temperature of the die, it is possible to form this alloys using a single step closed die forging process. The ability to regulate the viscosity and crystallization time of the material, through control of the tool temperature, can allow for advanced forming operations to be realized. Further, the degree to which the material replicates clearances and surface asperities can be control through adjustment of the viscosity through the forming temperature. Finally, the strain rate dependence can be used limit defects and

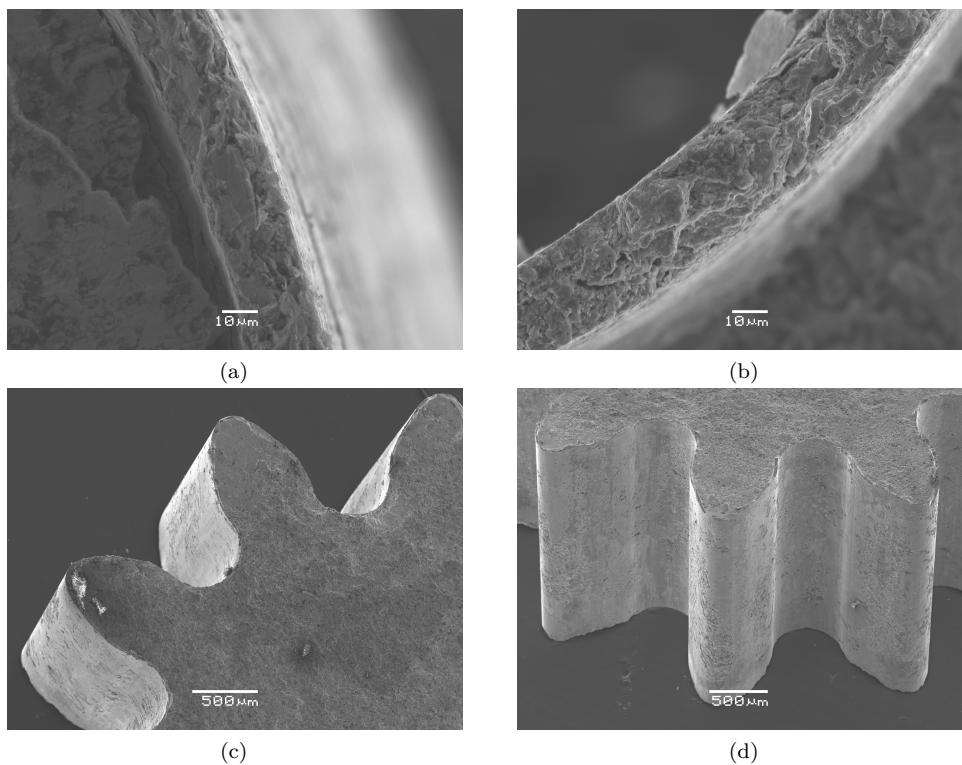


Figure 8.22: SEM images of the unintended back-ward rim formed on the Vitreloy 1B specimen moulded at 430°C is shown in ?? and ?. The images (c) and (d) show the results of the manual pressing of the Vitreloy 1B alloys at 450°C.

reverse forming during ejection.

Figure 8.23 is a SEM micrograph of the extruded gear wheel profile that has been machined to the nominal dimensions. Clear turning-marks from the machining can be noted from the surface in 8.23a. The small marks at the gear tooth tip is due to indention from the turning lathe gripper, rather than being an artefact of the extrusion process. The extruded and machined gear wheel has been submitted for mechanical performance testing at the industrial partner. Figures 8.23c and 8.23d shown the results of the low temperature forming of the magnesium based $Mg_{60}Cu_{30}Y_{10}$ BMG alloy. This alloy is well described and easy to form owed to the low temperature. However, the alloy must be formed employing very low strain rates and the resulting specimen is very brittle. For these reasons this alloys is practically only interesting for research purposes and will have little industrial relevance.

In summary it has been proven that the gear wheel demonstrator can be manufactured through extrusion and closed die forming of the advanced bulk metallic glasses. The extrusion process is a simple and stable process but subsequent machining is required to arrive at the intended component geometry. Forming of vitreous alloys in a single step closed forming operation have been demonstrated. With a more advanced tool setup it is considered feasible, on the back of the present results, that the complete gear wheel

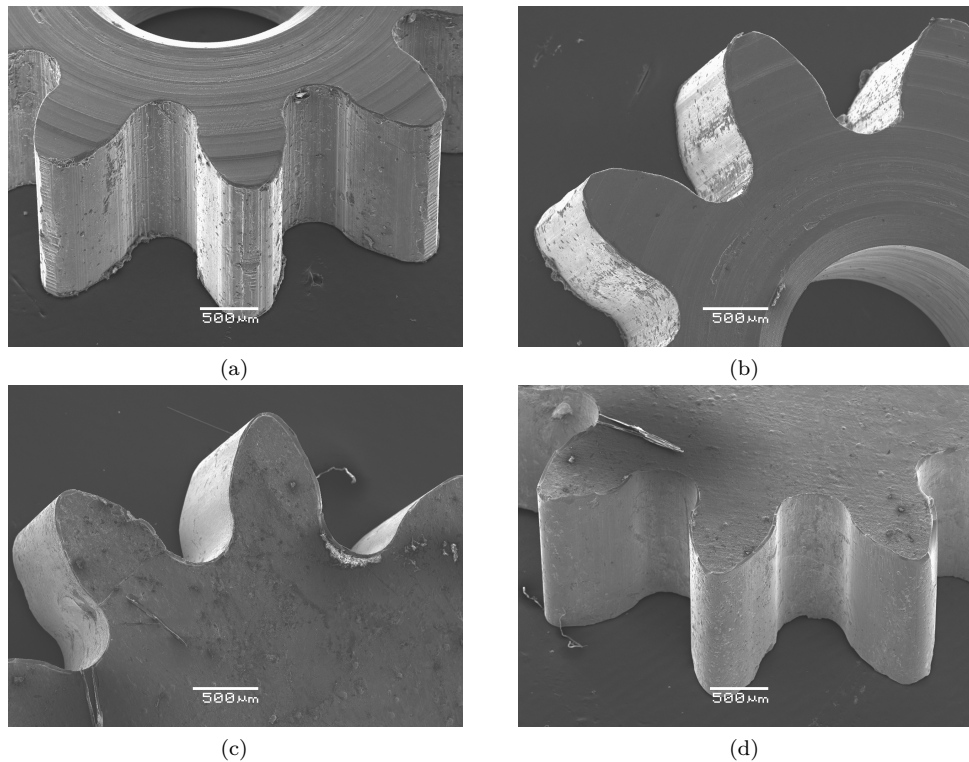


Figure 8.23: Figure (a) and (b) is a machined gear wheel from the extruded aluminium profile. Figures (c) and (d) show the gear wheel obtained through forming of the $Mg_{60}Cu_{30}Y_{10}$ low temperature BMG.

could be formed in a single operation. This would include the center hole and guiding surfaces.

Further research efforts have to go into effective ways of preparing the vitreous alloy billets required for forming. Also the correlation between forming method and surface topology to the fracture strength and stability of the formed specimen must be established. For the higher temperature vitreous alloys, such as the Vitreloy 1B employed in this work, process times around 1 second is feasible, thereby being relevant for industrial production rates.

8.3 Micro forming of dental implant in medical grade pure titanium

Titanium is a popular material for medico components, primarily due to its excellent properties as regards strength, resistance to corrosion and biocompatibility. The disadvantages are mainly the low formability at room temperature and the material cost. As an alternative to conventional machining, the component can be plastically formed by a range of warm established forming operations.

In this experiment a number of upsetting test of pure titanium, grade 1, 2 and 4 is tested

to investigate the effect temperature on the yield strength of the material. From these tests, a heat treatment procedure is derived and reliable data for a numerical model is acquired. Following the material characterization and modeling, a tool system for warm forging of a dental implant is developed. The tool system is analyzed using the acquired material data and a suitable forming strategy is found. A two-step process design with pre-stressed die inserts is realized; owed the high yield strength of the titanium material that causes internal pressures above 2500 MPa under forging. Finally the results of the forging trials are described. The section is concluded with outlook and suggestions for future work.

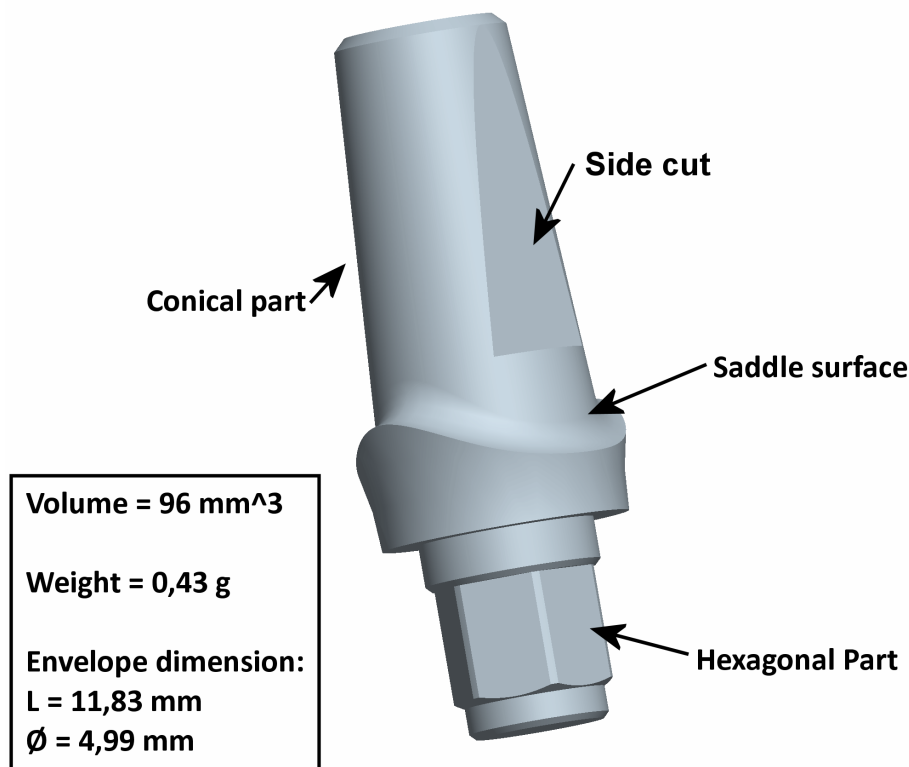


Figure 8.24: 3D drawing of the Saddle component with markers denoting the features of the component.

The component; the "Saddle", from an industrial research partner, is a semi axisymmetric component. The "Saddle" is intended for a dental implants application and is manufactured in Titanium, primarily due to its biocompatibility and ability of osseointegration with the human body. The main dimensions are seen in Figure 8.24. The largest diameter dimension is $\text{Ø}4.99$ mm and the length is 11,83 mm. Today, the component is primarily manufactured by turning, the HEX key and flank on the side and the holes through is done by milling and drilling respectively. All tolerances are within $\pm 10 \mu\text{m}$ and the corner radii must be kept below $50 \mu\text{m}$.

Owed to the regulatory and safety requirements associated with the application of this dental component, only commercial pure Titanium is allowed as workpiece material.

Pure Titanium is subdivided into the grades 1-4, depending on their tensile strengths, as in 170, 275, 380, 483 MPa UTS. Metallurgically speaking, the difference has to do with sub-percentage traces of oxygen and iron in the Titanium. The more of these impurities there is, the harder the metal becomes.

In order to evaluate the temperature effect on the material compressive yield stress, a diagram consisting of the three grades of Titanium, G1, G2 and G4 at 400 °C and 20 °C using Ø4 mm specimens, is generated.

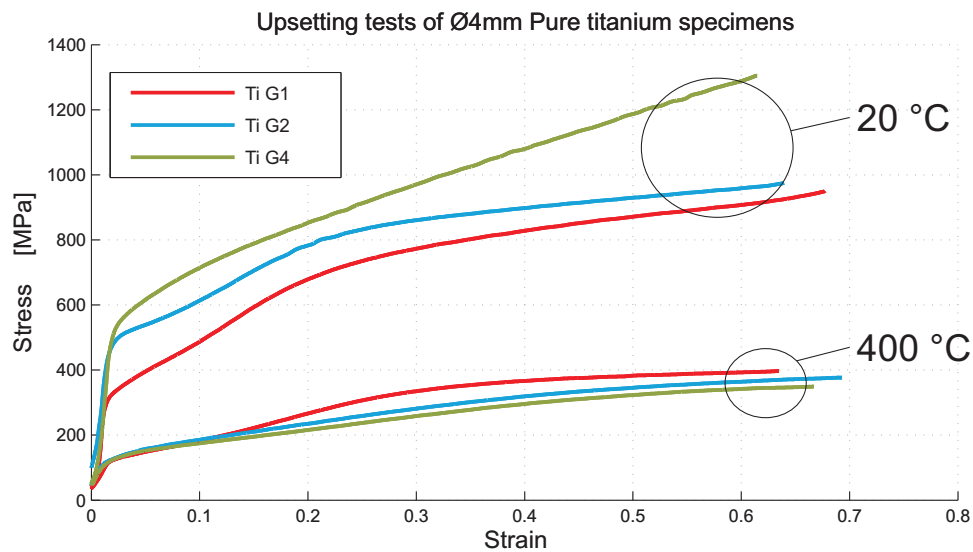


Figure 8.25: Stress-strain curve for Ø4 mm upsetting of Titanium alloy specimens G1,G2 and G4 at ambient- and elevated temperature.

Figure 8.25 depicts the stress-strain curves of the tested alloys at room- and elevated temperature. Concluding on data, the flow stress is lowered approximately 70% at high temperature with a minor dependence on the grade of alloy. Further, the effect of heating is significant, compared to the similar results for Magnesium [109]. The data depicted in Figure 8.25 indicates a reduction in flow stress gained by going from 20 °C to 400 °C, the effect is most predominant for the G2 and G4 alloys. The plot also shows a smaller dependence of forging temperature for the G1 alloy in comparison to the grades G2 and G4. With respect to this observation, it will be reasonable to use G4 in the following forming experiment, given that the cost of G4 is about half when compared to G1 and G2 alloys but the yield strengths are comparable at elevated temperature.

8.4 Tooling design

The tool design phase was initiated with a number of numerical simulations to establish forming strategies, load requirements and to optimize the tool stress load. The maximum load needed for the first forging step equals 15 kN, resulting in a maximum internal pressure of 2000 MPa to 2200 MPa. This means that core die material must be able to sustain a yield stress of about the same value. However, a dedicated tool stress

analysis to establish the actual die stress and thereby the requirements on material an pre-stressing system. The second forging step also requires a peak load of 15 kN, resulting in a maximal internal pressure of 2500 MPa. The accumulated pressure inside the die is determined to 1700 MPa with a safety margin of 200 MPa. The forces of the internal pressure distribution was interpolated onto the tooling dies, giving the tool stress distribution. In this way the effective tool stresses can be evaluated and the tool material and pre-stressing system can be established. Results of the die stress analysis is shown in Figure 8.26. Depending on the value of the friction factor and thereby the amount of peak load of the forming operation, normal tool stresses up to 2000 MPa can be noted.

The number of stress-rings, die-diameter and required hardness of die and stress-ring material is established using an analytical framework [110]. The high alloyed powder metallurgical high speed steel, Vanadis 60, was chosen as die material for both steps and also for the pre-stressing rings. Hardened Vanadis 60 does not soften considerably below 500 °C, which is compatible with working temperature of tool of up to 450 °C. Analysis of the prestressing systems show nearly identical results, justifying the decision to make prestressing system for both forging steps identical. The stress ring measures 24 mm in outer diameter and 10 mm in internal diameter, with conical angle of 1 degree. The dies of the tool system was hardened to 64 HRC while the stress rings where hardened to 54 HRC as taken from the calculations of the prestressing system.

The geometry of the die inserts where produced with die-sinking EDM while the ejector and punches where manufactured by grinding. The remaining tool elements have been produced using conventional machining.

In the first forming operation the hex-nose of the component is formed through extrusion. The component is then ejected and placed in the second forming operations. Here the diameter of the hex-geometry is calibrated, the conical head is formed on the billet and the skirt is flashed out. Illustrations of the procedure is shown in Figure 8.27.

Figure 8.28 show sectional drawings of both forming steps, including heaters, heat shield, thermal insulation, stress rings, dies and punch and ejectors. Upper an lower parts of the two forming operations are place in a die-set, ensuring alignment and handling of the tool. Sectional drawings of the complete tool system is printed in Appendix G.

As the amount of friction is the driving parameter for the process load and thus the amount of stresses acting on the tooling, a number of simulations with different friction factors are conducted. The purpose of the simulations is to check the process window in relation to the amount of stress the tool system can sustain. By comparing the hoop stress from the simulations with composite strength of the die and stress-ring combination, the maximum allowable friction factor can be found. Further, the analysis gives an idea of the weakest elements of the tool system. An overview of the values found during the tool analysis can be found in Figure 8.29. As seen from the data regarding the safety factor calculation for die of the first forming step, does the design become marginal at a friction factor $m=0,3$. However, the results of numerical simulations should be used as guidelines, since especially simulations of friction phenomenons have shown to be difficult. This is also noticeable from the simulated results of the load-stroke curves in Figure 8.29.

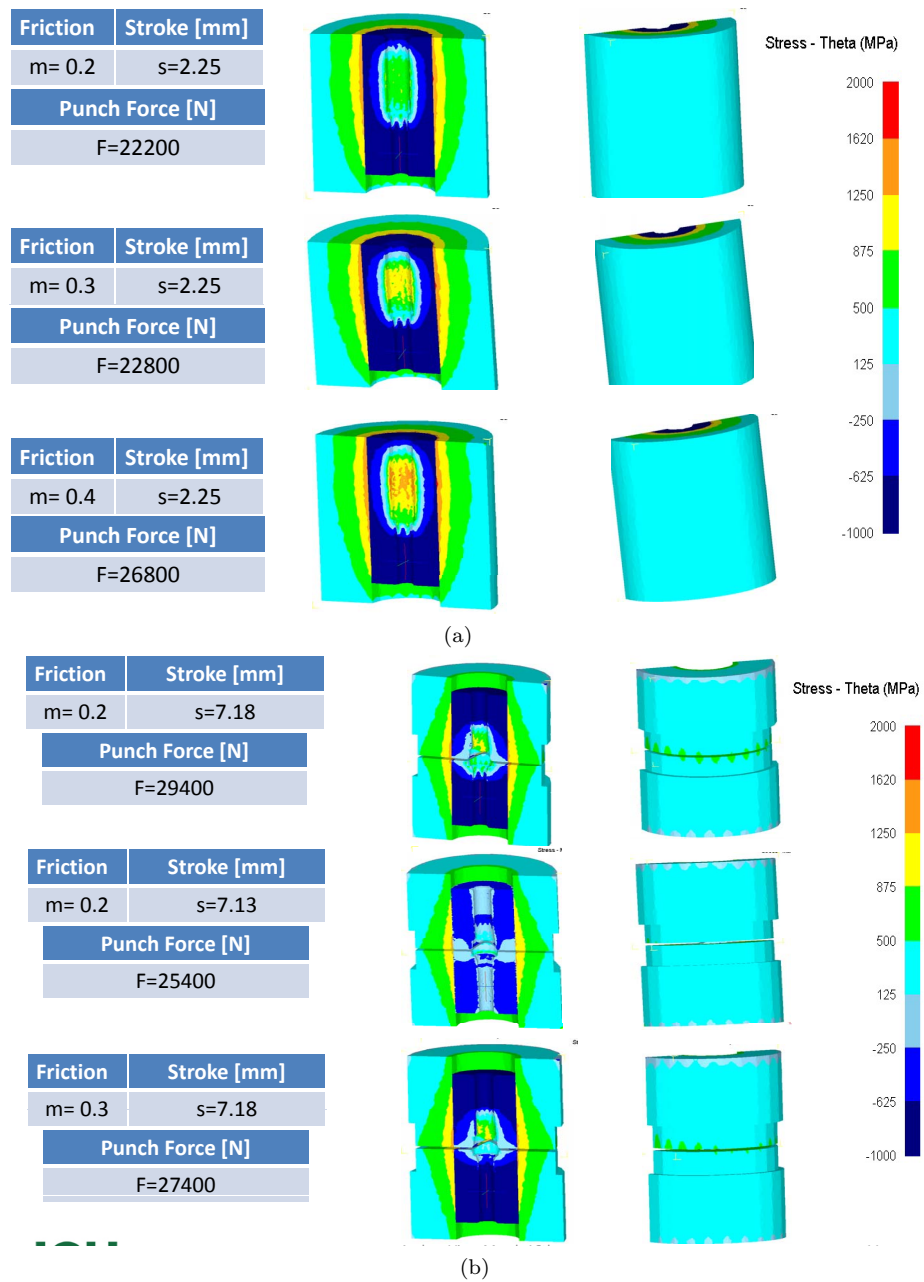


Figure 8.26: Tool stress analysis at different levels of friction and stroke length. (a) is the die geometry for the first forming step and (b) is the second forming step.

The simulations of the two forming operations further yield a number of load curves for different values of the friction factor m . The curves, plotted in Figure 8.30, can be used as calibration curves for estimation of the forming friction. For both cases a peak forming load of about 15 kN is expected. Finally the filling of the die is investigated through the simulations. Especially in the second forming step, involving forming of a

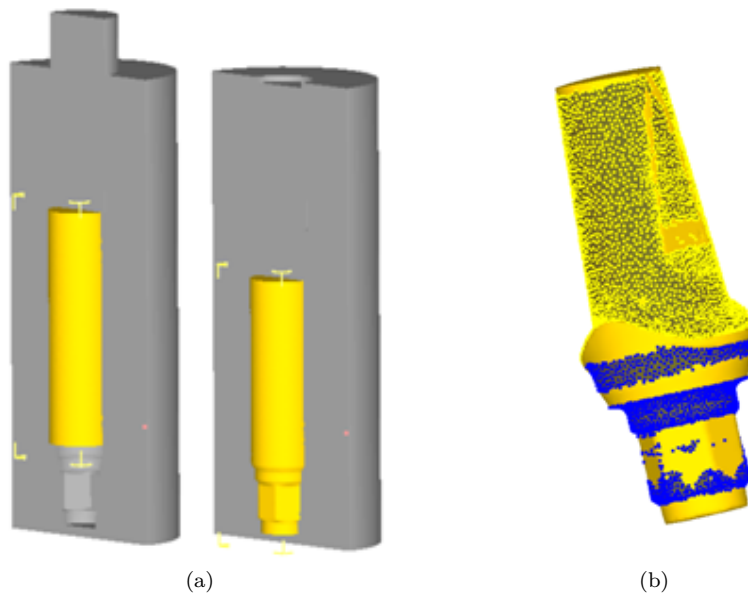


Figure 8.27: Illustration of the two-step forging process. In (a), showing the first step, the hex-geometry is extruded. In the second step, (b), the conical head is pressed onto the billet and the skirt is vertically extruded as flash.

large conical surface on the upper part of the component, the friction plays an important role on the final results. Figure 8.31 shows simulations of the form filling in the second forming operation with different friction factors. It is clearly noted that when a friction factor of $m=0,4$ is chosen, the length of the conical part upper part of the component is not fully formed and more material is flashed out at the skirt of the component.

Results of test forging of step one using aluminium alloy 6061

In order to verify the alignment of the tool elements and the basic concept of the constructed tool system, a number of commencing test forgings are carried out in a soft aluminium alloy. The forming tests of aluminium is carried out at ambient temperature and with a different material, but is otherwise comparable in any way. Figure 8.32 show the result of the forming of an aluminium billet in the first forming step. The color variation along the hex-shaped nose of the geometry reveal the presence of vertical surface roughness originating from the extrusion process. The commercial lubricant Molycote DX paste was used for the aluminium forming experiments.

Figure 8.33 show the load-stroke curve of the aluminium pressing. When noticing the acquired load-stroke curve, no major difference can be noted between two successive pressings. This indicates a stable forging process and stable tribological conditions. The peak load for the forming of aluminium is about 7 kN and the stroke length is close to 2700 μm . The stroke length is based on the rotation of the servo press motor and includes electricity and backlash of the press and tool system. The result of the forming process prove successful and the first forging operation is ready to be run with the titanium alloy specimen.

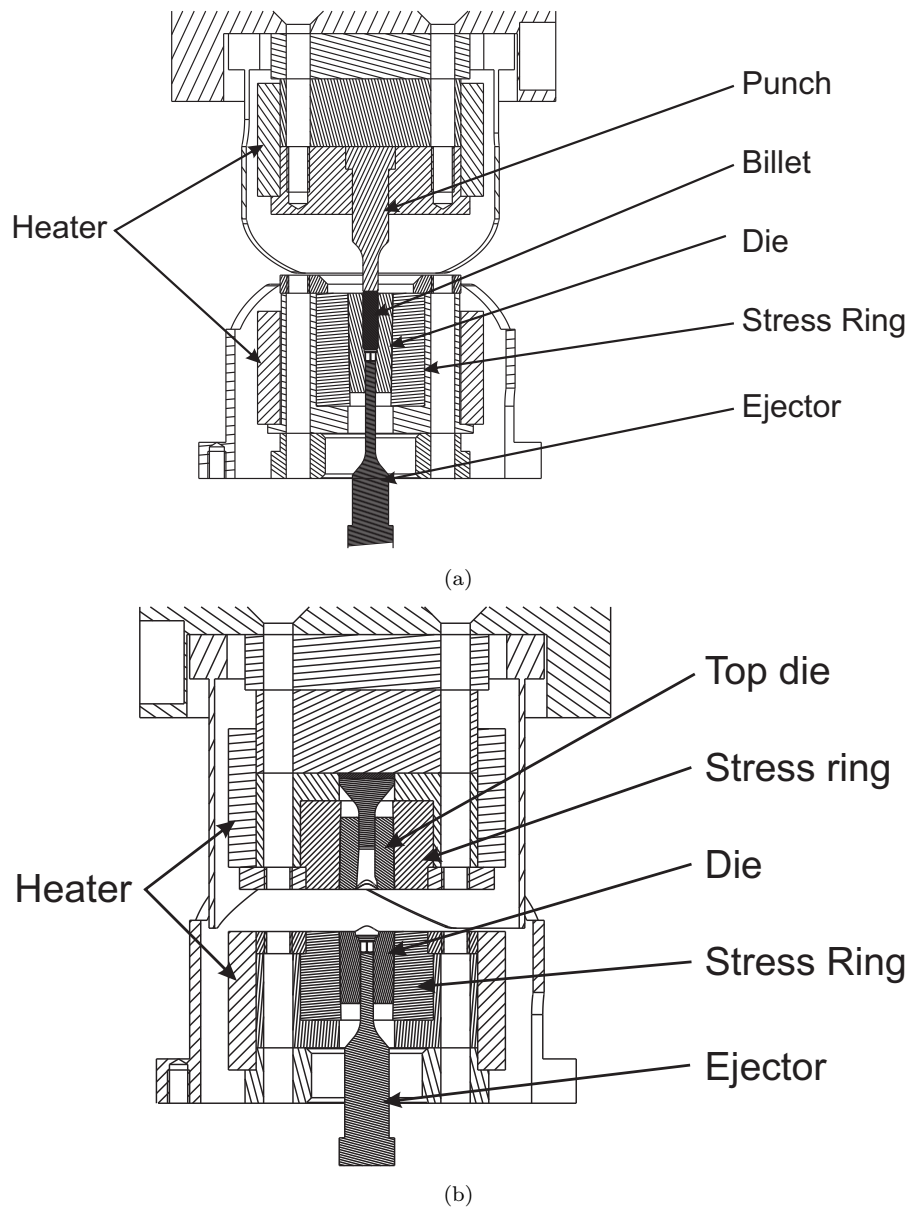


Figure 8.28: Sectional drawings of tool system for warm forging of titanium. (a) show the preform extrusion of the hex geometry and (b) depict the sectional drawing of the second forming step.

Forging of step1 in pure titanium grade 4

A number of titanium grade 4 billets were prepared using turning. The tool system was heated to 400 °C and allowed to thermally stabilize. A commercial lubricant, primary consisting of molybdenum disulfide particles suspended in a volatile carrier, was used as lubricant for the warm forging operation. The lubricant was applied to the billet and inside the forming die.

8. RESULTS OF ADVANCED MICRO FORMING EXPERIMENTS

St.	Friction "m"	Comp.	Stroke [mm]	Punch Force [N]	Mat.	HRC	Resistance [MPa]	Normal Pres. [MPa]	Hoop Stress [MPa]	"Safe Factor"
1	0.2	Punch	2.25	22200	Van 23	66 $m=2.5$		2800		
	0.3		2.25	22800				3100		
	0.4		2.25	26800				3700		
1	0.2	Ejector	2.25	22200	Van 23	66 $m=2.5$	3100→ 12920 N	2200		1.41
	0.3		2.25	22800				2400		1.29
	0.4		2.25	26800				2700		1.15
1	0.2	Die	2.25	22200	Van 23	66 $m=2.5$	$\sigma_c=-2460$ $\sigma_t=+1000$		700	1.43
	0.3		2.25	22800					1100	0.91
	0.4		2.25	26800					1400	0.72
1	0.2	Stress Ring	2.25	22200	Van 60	54 $m=1.3$	$\sigma_c=-1900$ $\sigma_t=+1460$		1400	1.04
	0.3		2.25	22800					1400	1.04
	0.4		2.25	26800					1400	1.04

(a)

St.	Friction "m"	Comp.	Stroke [mm]	Punch Force [N]	Mat.	HRC	Resistance [MPa]	Normal Pres. [MPa]	Hoop Stress [MPa]	"Safe Factor"
2	0.2	Top Ejector	7.18	29400	Van 23	66 $m=2.5$		2600		
	0.2		7.13	25400				2300		
	0.3		7.18	27400				2500		
2	0.2	Bottom Ejector	7.18	29400	Van 23	66 $m=2.5$	3650→ 15160 N	2300		1.6
	0.2		7.13	25400				1200		3
	0.3		7.18	27400				1000		3.65
2	0.2	Top Die	7.18	29400	Van 60	64 $m=2$	$\sigma_c=-2350$ $\sigma_t=+1150$		1000	1.15
	0.2		7.13	25400					380	3.02
	0.3		7.18	27400					900	1.3
2	0.2	Bottom Die	7.18	29400	Van 60	64 $m=2$	$\sigma_c=-2350$ $\sigma_t=+1150$		600	1.9
	0.2		7.13	25400					220	5.2
	0.3		7.18	27400					400	2.87
2	0.2	Top St. Ring	7.18	29400	Van 60	54 $m=1.3$	$\sigma_c=-1900$ $\sigma_t=+1460$		1300	1.12
	0.2		7.13	25400					1100	1.33
	0.3		7.18	27400					1400	1.04
2	0.2	Bottom St. Ring	7.18	29400	Van 60	54 $m=1.3$	$\sigma_c=-1900$ $\sigma_t=+1460$		1200	1.21
	0.2		7.13	25400					1200	1.21
	0.3		7.18	27400					1300	1.12

(b)

Figure 8.29: Results of forming process simulations and calculations of tool stress resistance for the first (a) and second (b) forming step.

Subsequently a total number of three forging experiments was conducted using the titanium grade 4 alloy. The results of the experiments can be seen in Figure 8.34.

The resulting titanium specimens show decreasing extrusion for the same amount of peak press load. The first specimen to be formed, shown in Figure 8.34a, is full formed and show little sign of galling. The length of extruded hex-shaped tip and base is a little longer than nominal, but this can be corrected through a readjustment of the position of the ejector.

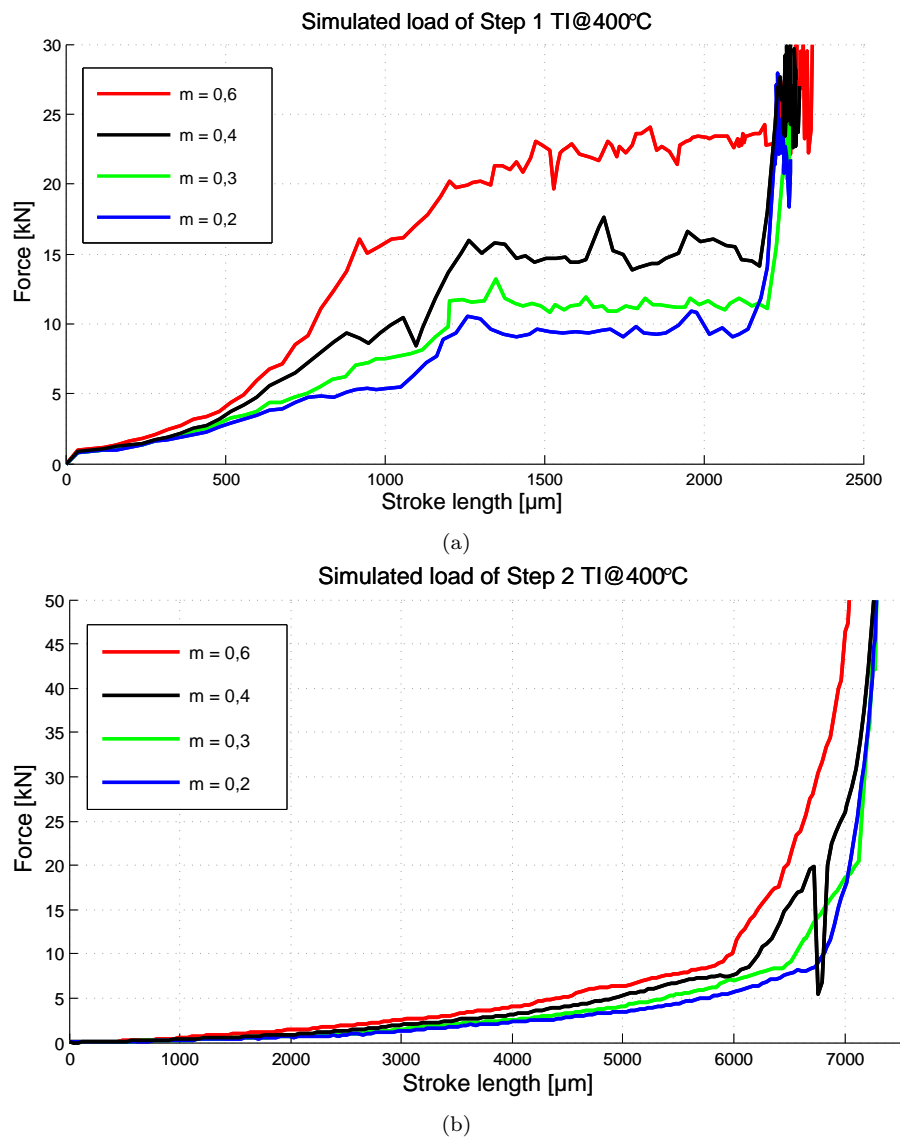


Figure 8.30: Simulated load of the two forming operations with different friction factors. The load curve shown in Figure (a) exhibit a staircase progression. For the second forming step, shown in figure (b), the load increases exponentially once the component is close to formed. The sharp dip in the load curve for friction factor $m = 0,4$ is attributable to numerical discontinuity during re-meshing.

In the second forming, shown in Figure 8.34b, the extruded part is shorted by approximately 200 μm and the front end of the extruded hex-geometry now show clear signs of galling or pickup. The galling, leading to severe increase of friction, have prohibited full forming of the component, leading the an unsatisfactory forming result.

The clear trend towards worsening of tribological conditions is continued in the third

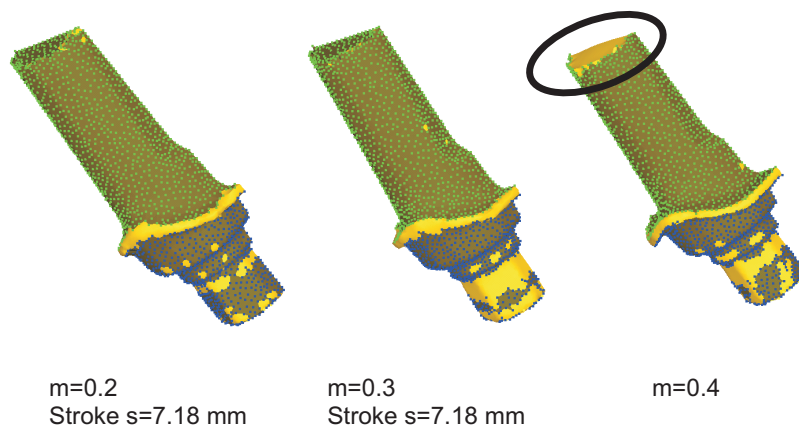


Figure 8.31: Simulation on the forming filling during heading of the abutment component. The green and blue dots donate areas of die contact.

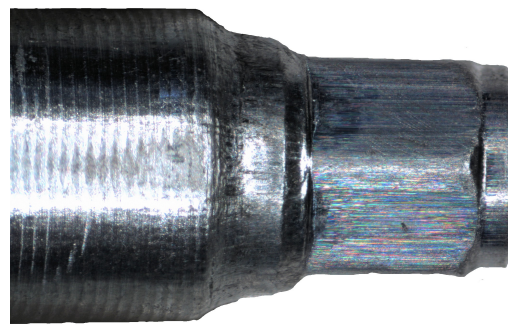


Figure 8.32: Micrograph image of the first forming.

example. As seen in Figure 8.34c the extruded pin is again reduced in length by approximately 200 μm . The surface quality of the extruded pin is further decreased with clear scoring marks in the lengthwise direction. In this final experiment audible noise was heard during forming, probably due to sticking and surface plowing in the die.

When consulting the acquired load-stroke curve in Figure 8.35, the hypothesis of galling and gradual degradation of the tribological conditions during the forming operations is confirmed. The load-stroke curve for the first pressing trace a profile that is overall comparable to the curve obtained through simulation or forming of the aluminium specimen. While for the second forming, the exponential surge, normally signaling the finalization of the forming operation, is noticed at a shorter stroke length. When comparing the curves of the first and second pressing, it is noticeable that the last vertical plateau on the curve, attributable to the extrusion of the hex-nose, has been shortened in the second pressing. This effect is further pronounced on the curve originating from the third forming experiment. The third curve also show increased scatter, originating from the jerky movement of the extrusion process.

The overall load requirement of this first forming process can be compared to the load

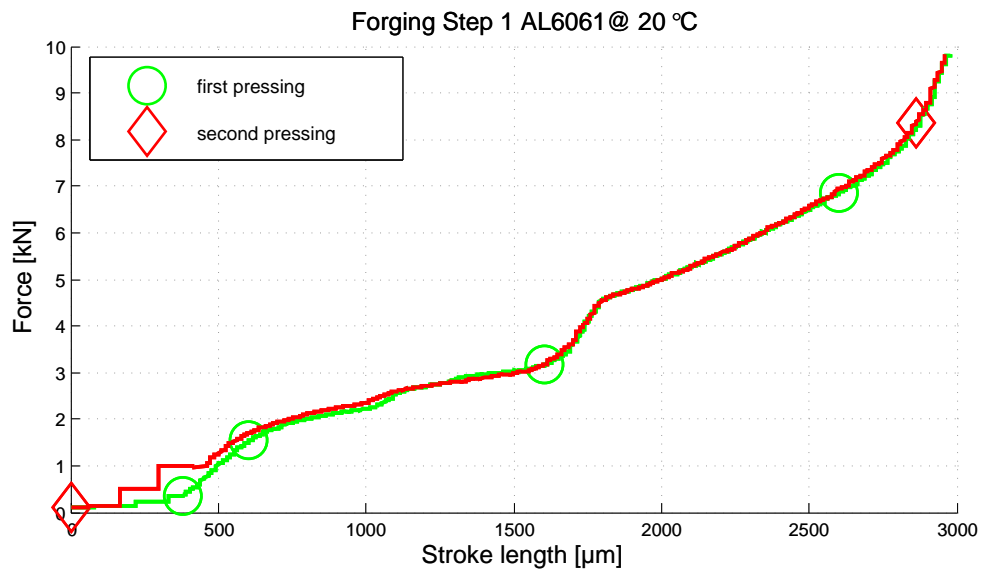


Figure 8.33: Load-stroke curve for commencing trial of first forging operation.

predictions of the simulations, shown in Figure 8.30a. Comparing the peak load of the first forming operation using the titanium alloy, having a value of about 7 kN, the friction factor is estimated to reside in the range between $m=0,2-0,3$. This is in good accordance with guidelines values cited from literature [18].

The experiment was stopped after the third forming due to the presence of increasing galling. The die was then demounted and polished to remove titanium than have been welded into the die surface.

When consulting literature on the tribological conditions of warm forging of titanium alloys, it repeatedly concluded that galling during forming is a key difficulty [18,111]. Graphite based lubricants are mentioned as a recommended together with boron nitride based lubricant types. For hot forging, in the temperature range 600 °C to 800 °C, a mixture of glass powder and conventional graphite based lubricants are recommended. However, there is no universal applicable lubrication strategy when it comes to plastic deformation of titanium at elevated temperature [111].

Forging copper coated titanium billets

Based on earlier experience of forming titanium at elevated temperatures and advise from industrial partners, a repetition of the failed forming operations was planned. The new experiment involved coating the billets with a thin copper coating by means of an electro plating process. The utilization of copper coatings to better tribological conditions are known from forming processes involving stainless steel.

The photo in Figure 8.36 shows the copper plated titanium billets prior to insertion in the forging process. The copper coated billets were again sprayed with a MoS_2 based lubricant and inserted into the heated die. The forming operation was then performed

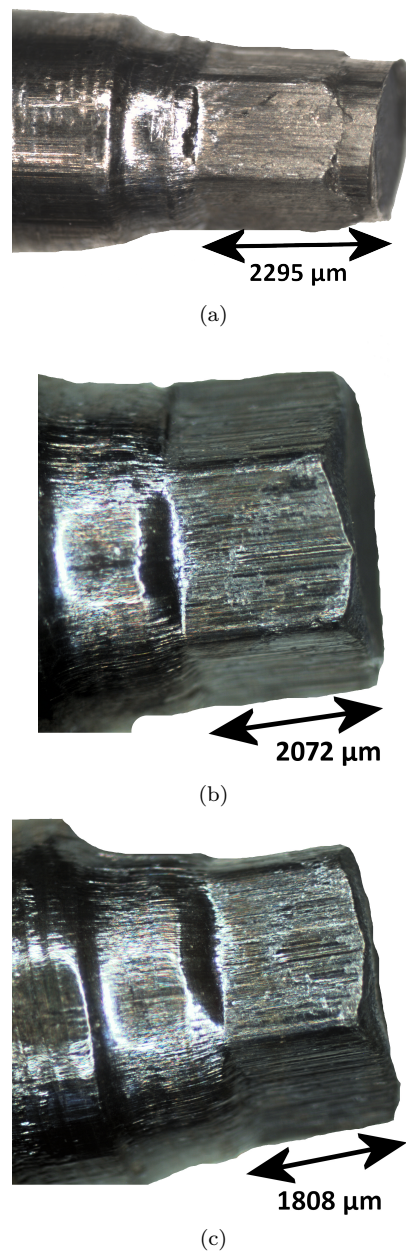


Figure 8.34: Micrographs of three successive forming experiment of the first forming operation. The specimen in (a) is the first specimen to be formed and the (c) is the last.

and the load curves were acquired. The load curves for two consecutive pressings of the copper coated titanium billets are shown on the plot in Figure 8.37. When compared again the earlier load measurements using non-coated specimens, the forming load have doubled. This could be due to remaining cold welded titanium still present in the die from earlier experiments. However, since the die had been re-polished, it is more likely to be attributable to the copper coating.

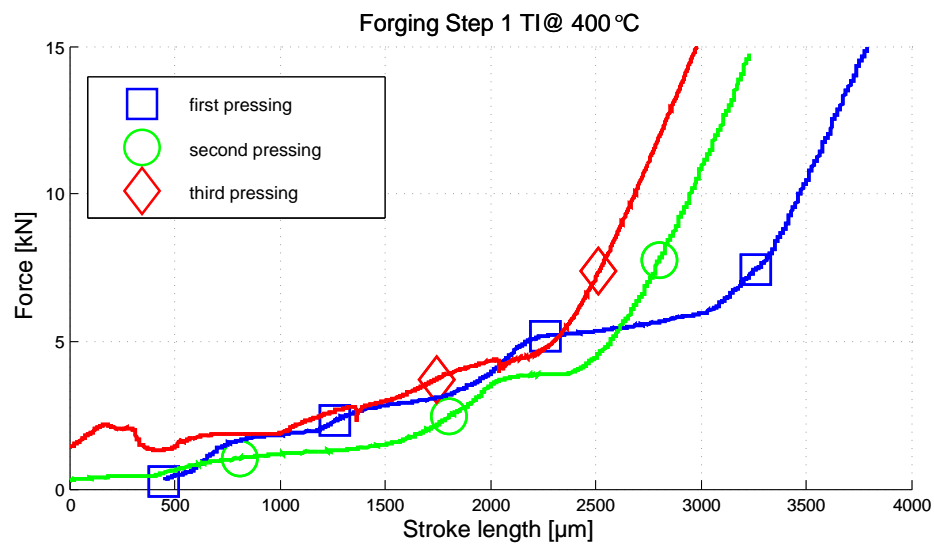


Figure 8.35: Load-stroke curves of the three consecutive warm forming experiment utilizing the pure G4 titanium alloy.



Figure 8.36: Copper coated titanium billets. The copper coating have been applied through electro plating as earlier described. The estimated layer thickness is around 10 μm.

When noticing the load plot in Figure 8.37, an increase in the required forming load is noted. This implies that the gradual worsening of the tribological conditions had not been resolved. Further, the copper coating has induced a substantial increase in friction, leading to increased tool stress. The increase in friction also impacted the ejection of the component, that had to be done manually by means of a hammer.

During the attempt to form a third copper coated specimen, the forming punch failed due to buckling. The measure load passed 25 kN and the punch deformed plastically.

Due to time constraints, no further attempts were made to improve the tribological behavior of the forming process. It is likely that the process could be optimized by selection of the right lubricant and surface coating in combination with a step-wise forming approach, where the specimen is formed in a number of steps with intermediate application of fresh lubricant.

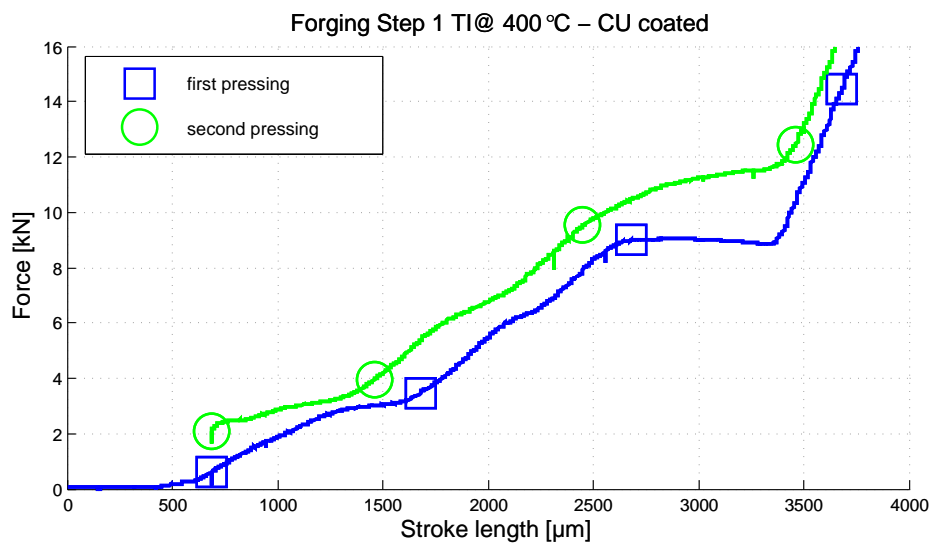


Figure 8.37: Measured forming load during the execution of the first step of the forming process with the copper coated specimens.

Forming utilizing the second forming step

In continuation of the forming trials conducted on the first forming step, a number of test were conducted on the second forming step. As in the prior step, the forming operations is firstly tested with a soft aluminium alloys to qualify the performance.

The aluminium piece, already preformed by the initial forming operation, was inserted into the second step forming tools. The tools were tempered at room temperature and the lubrication paste was applied. The first result of the second step forming operations can be seen in Figure 8.38. Clearly the upper and lower forming die is misaligned,



Figure 8.38: First specimen to leave the second forming step. A clear misalignment between the upper and lower forming die is noticeable.

leading to an off-center alignment between the upper and lower part of the component. Further the component unexpectedly stuck to the upper forming die during opening of the forming tools. This meant that the tool had to be disassembled to remove the formed component from the upper forming die.

The upper and lower forming die were aligned and a new forming operation was executed. The result, shown in Figure 8.39. The overall geometry of the formed component

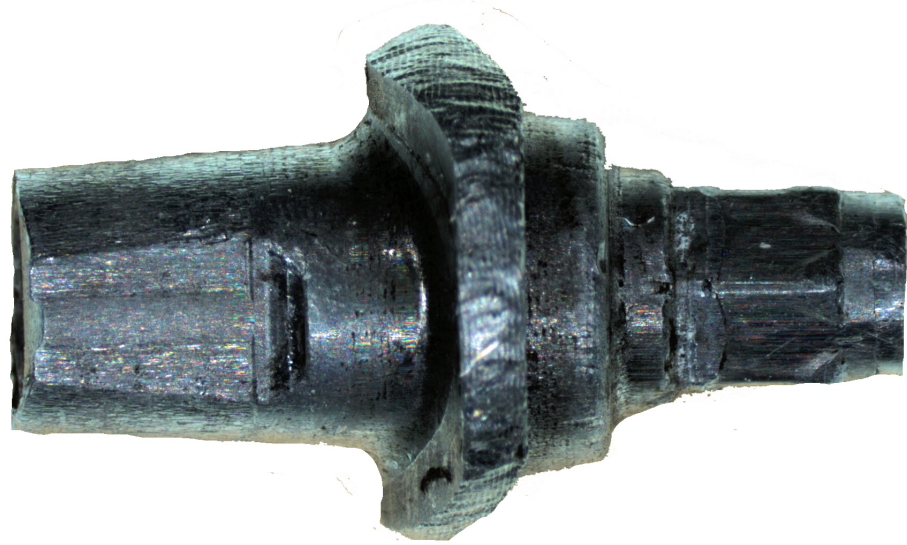


Figure 8.39: Component formed after alignment of the upper and lower forming die. The component length is short measured and the material is flashed out at the skirt prematurely.

resembles the original 'saddle' geometry to high degree. However the upper conical part of the formed specimen is too short. This might be due to the difference in material strain hardening behavior between the aluminium and titanium alloy. An alternative explanation might be that the friction in the upper conical forming die is unexpectedly high.

The upper forming die was used in its unpolished state with the surface finish left from spark erosion process. The internal free-form surface geometry makes the die hard to polish using conventional methods, usually involving a mandrel and some diamond paste. To investigate further on the method to lower the friction in the upper forming die, the die was polished using a wooden mandrel and some $6\ \mu\text{m}$ diamond paste. The polishing process lowered the surface roughness but also removed some of the die material around the side cut facet, making the upper die a cylindrical-conical die.

After the polishing operation had been completed, another aluminium specimen was formed. The resulting part is shown in the microscope image in Figure 8.40. The length of the third component is close to the nominal length. When looking close at the bottom part of the extruded hexagon, an unintended cam is noticed in the bottom corner.

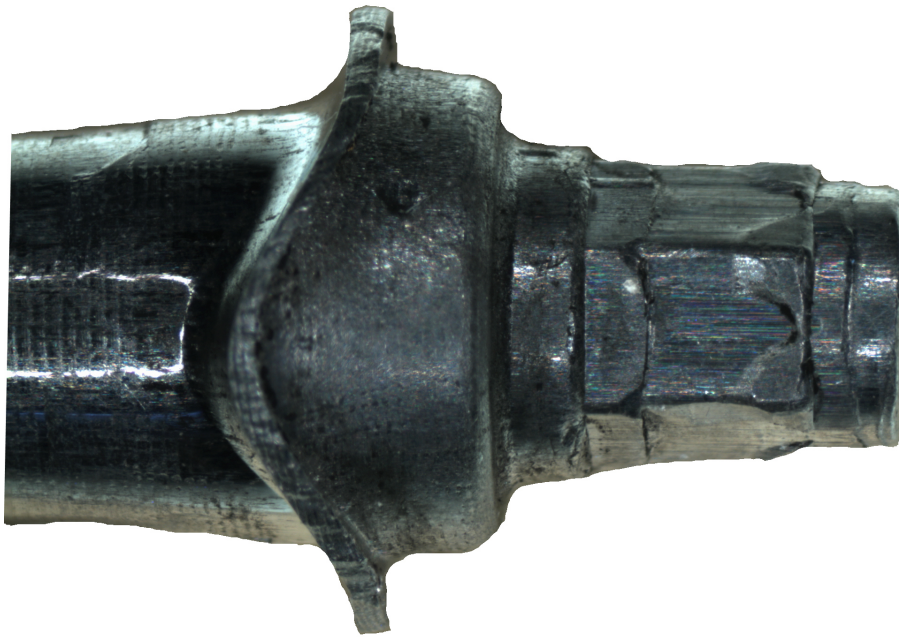


Figure 8.40: Aluminium component formed after polishing of the upper forming die. The polishing removed much of the side cut in the conical die.

To investigate whether the cam is due to damages of the die, a silicone replica is take of the die. The replica, shown in Figure 8.41, show no sign of defects, thus the cams seen on the hexagon edge must be attributable to dynamic die deflections or originate from the ejection process.

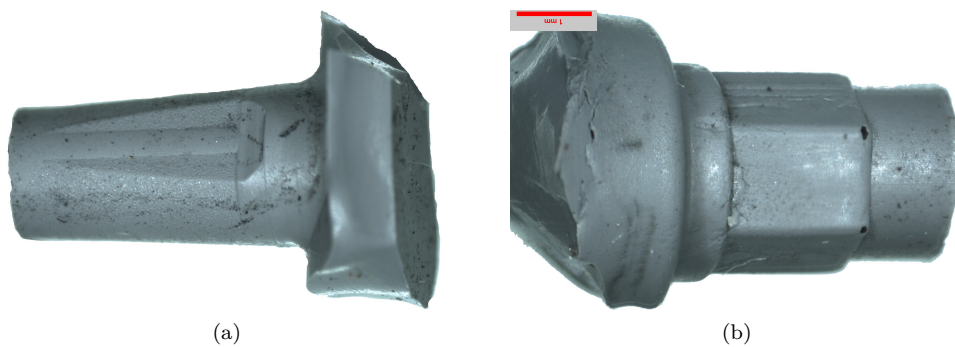


Figure 8.41: Silicone replica of the second forming step upper and lower forming die.

Finally the acquired press load during the forming operation is plotted. The diagram in Figure 8.42 show a peak press load off about 6 kN when the component is fully formed. Good reproducibility is noted between the two forming operations, implying that galling is not a problem.

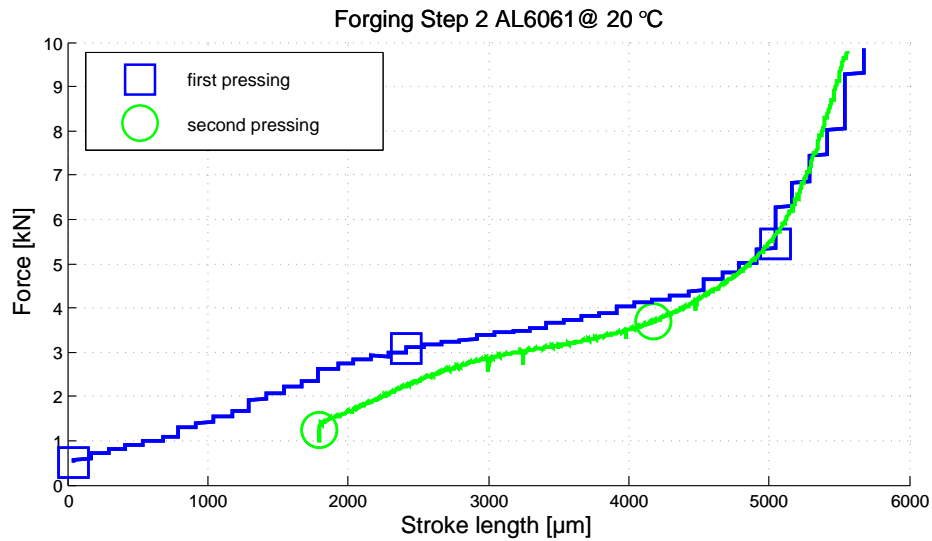


Figure 8.42: Plot of two successive forming operations.

Owed to the tribological issues encounter during the forming of the titanium in the preform operation and the unexpected sticking of the component to the upper forming die in the second step, no titanium specimens have been formed in the second step. The tool system must be changed, possibly the upper and lower die of the second forming step can be reversed. Also, the tribological challenges have to be overcome before further experiments can be conducted.

Conclusion on dental abutment forming

A forming process has been developed for forming of a dental implant geometry in pure titanium material at elevated temperatures. It has been shown that by elevating the forming temperature of pure titanium alloys to about 400 °C, the material yield stress is lowered by approximately 70 %.

A two step close die forming process design has been proposed. A number of numerical simulations were conducted on the tool system, showing satisfactory performance for friction factors not exceeding $m = 0,3$. The magnitude of the internal pressure during forming, required the application of a pre-stressed die in the tool design. Thermal design analysis has been conducted to investigate the steady-state thermal stability of the proposed tool design. It was proven possible to realize the two step forming process as two compact heated core tools, inserted into a standard die-set. The application of heat shields and ceramic insulation material eliminate the need for external cooling of the tool set.

Forming tests were carried out using the manufactured tool set. Preliminary forming experiment were conducted with a soft aluminium alloy billet to qualify the operational performance of the process and the tool system. The first forging step, characterizable as an advanced extrusion process, show promising results during the commissioning trials.

The subsequent forming using the grade 4 titanium alloy yielded satisfactory component geometry at an estimated friction factor of $m \cong 0,2$. However, severe galling was noted with a heavy impact on the following forming operations.

As an option for improving the tribological conditions, application of copper coating on the titanium billets was investigated. Testing of the coated specimens in the first forging step showed increased friction and only minor relieve of the titanium buildup in the die.

The second forming step was tested using aluminium alloy only. This is due to unexpected adhesion of the forged component in the upper forming die, causing ejection problems. Further, the tribological challenges appearing in the first forming step would also be present in the the second forming step.

Results from the second forming step with aluminium material showed good results. A few complications relating to achieving sufficiently low surface roughness was noted. Also the alignment of the upper and lower forming dies had to be dealt with. Finally, some unexpected cams appeared at the end of the component hexagon geometry. These could not be attributed to damages of the forming die and must therefore be due to dynamical phenomenons, such as die deflections or forming during ejection.

Summarizing on the achieved results, the overall process analysis, tool manufacture and experiments have proven successful. The tribological challenges are a main hurdle to be overcome. The results show that by applying the right lubrication strategy it should be possible to realize the dental abutment geometry using a micro bulk forming process.

Acknowledgements

The author wishes to acknowledge contributors to work involving warm forming of the titanium dental abutment. Jacob W. Holstein for a corporation and establishment of the groundwork through his thesis *Micro forging of titanium in warm conditions* [112]. Dr. Mogens Arentoft and M.Sc. Nikolas A. Paldan is acknowledge for numerous valuable discussions and input. Finally all contributors to the realization of the tool design is acknowledged, including the mechanical workshop at DTU-MEK and the company J.A. Tool design in Greve,DK.

8.5 Conclusion to advanced micro forming experiments

A number of forming experiments have been conducted with the objective of researching the practical aspects of utilizing the bulk forming processes for fabrication of small- and micro metallic components.

Three distinct component geometries have been produced utilizing bulk forming processes. The selected components have been chosen based on present industrial specimens, to ensure practical relevance of the experiments. The components have been formed in materials aluminium, titanium and bulk metallic glass, representing low cost, advanced high strength and amorphous materials respectively.

Valuable experience has been gained through each of the forming investigations. The novel empirical knowledge will form the basis for further investigation into the micro forming subject and serve as guidelines when a new micro forming processes are designed.

8.5. Conclusion to advanced micro forming experiments

The main findings from the series of experiments in relation to tool design are as follows:

- Tribological conditions, especially friction, play a major role in micro forming.
- Net- or near-net shaped components can be achieved through close integration of process design, tool design and tool manufacture procedures.
- The influence of the forging operation and tool design on the mechanical properties of the realized specimen needs to be better understood. This is especially important for the series of amorphous materials.

Based on the experimental results above among others, an industrial partner participating in the research consortium of this project has invested in a prototype micro bulk forming plant. The plant is based on the design of the C5K press and experimental learning obtained in the experiments above.

Chapter 9

Conclusion

9.1 Summary

Micro bulk forming has been identified as a suitable manufacturing process enabling mass production of micro metallic components.

The research undertaken during this Ph.D. project has been devoted to further development of the micro forming technology with respect to tool design and analysis.

Six main topics of study have been identified: tooling process chain and tool process characterization; Design of tool-, handling and press systems; Micro Metrology; Tribology and friction in micro forming; Manufacturing accuracy of tooling elements; Forming of advanced and amorphous materials. The most relevant results within each area is summarized below:

Tooling process chain and tool process characterization

A number of suggestions for viable process combinations for micro tool manufacturing have been proposed. A novel approach, using electroforming as tool manufacturing process for micro bulk forming has been demonstrated. A comparative study between the electroformed die and a die manufacture by means of μ -EDM were undertaken. The result showed best geometric accuracy of the electroformed die, but low yield strength of the nickel alloy. The family of EDM processes have been utilized extensively for micro tool manufacturing with good results. The difficulty in achieving low surface roughness, as required by the micro forming process, remains. Investigations on manual polishing have proven unsuccessful due to the unavoidable distortion of the die geometry.

Design of tool-, handling and press systems

A number of micro forming tools have been realized and the design philosophy behind these given. It was shown that a typical tool design at micro scale must consider the joint and complicated effects of process, tool, tool manufacture and end application requirements from the beginning. Methods for attaining high precision tool manufacturing results have been developed, including experimental examples of manufactured tools. Issues of tool alignment have been described. Different strategies for alignment of critical tool elements have been given, considering the needs of a typical bulk forming process. Finally, a micro handling system, satisfying

the special properties of the micro bulk forming process, have been constructed and characterized. The handling system proved successful but required high precision during manufacture and alignment. A maximum misalignment error between the forming die and transfer carriage of 15 μm was established. Finally a new micro forming press was designed and manufactured. The C5K press includes features making it suitable for utilization in a range of micro bulk forming process. Further, the machine has been designed with the vision of *micro factories* in mind, meaning that the press should be flexible, mobile and precise. Finally, the C5K process has been designed to comply with the strictest European norm requirements for machine safety.

Micro Metrology

Metrology has been identified as a key element in tool manufacturing for the micro bulk forming process. The micro scale assessment of manufactured tool elements and formed specimens has proven to be challenging due to the small size. A thorough analysis of available equipment for metrological assessment of sized elements has been undertaken. No universal 'whole-in-one' solution was found, but rather a range of different methods and techniques was identified. The silicon replica technique was characterized and showed good applicability for assessment of internal micro geometries. A round-robin style manufacturing and measurement experiment was conducted. The results of the experiment showed that dimensional accuracy within microns for simple tool geometries could be reached. However, dimensional differences between the manufactured specimens exceeding 10 μm were seen. The analysis further concluded that accurate micrometer scale dimensional assessment of tool elements requires dedicated measuring equipment. Finally, a comparative study of a range of measurements conducted on a 3D micro sized specimen was conducted. The analysis showed that small flat features could be characterized with high accuracy, while the overall dimension of the gear wheel component could be determined within $\pm 20 \mu\text{m}$ accuracy.

Tribology and friction in micro forming

The influence of high friction was noted throughout the experimental work of this thesis. The combination of high surface pressures, finite surface roughness of the tools and unfavorable lubrication conditions has led to complications. A number of macro- and micro sized friction investigations have been conducted, seeking to establish the relation between tool surface roughness and friction during forming. It was found that low tool surface roughness ($R_a < 0,05-0,1$) should be achieved. A novel transactional micro tribology test was applied for friction characterization. The results confirmed the noted size effects in friction. The results are further in accordance with the established theory of open- and closed lubricant pockets and escape of lubricants in open die forming.

Novel approaches in relation to micro forming tool design

A number of new ideas, additions and approaches for the bulk forming process have been presented. The Piezoelectric-driven pre-stressing system is an example of a novel addition. The tough tribological conditions and component ejection issues met in micro bulk forming can be eased with the application of a dynamic pre-stressing system. Further, the C5K micro press holds novel ideas for achievement of high accuracy, flexibility and mobility of a micro process chain element. Also the proposed transfer system for handling and transfer of micro bulk formed components is a new addition to state of the art. Finally, the core of the work, relating to

design and manufacturing strategies for micro forming tools and framework have demonstrated novel additions to the field.

Forming of advanced and amorphous materials

The forming experiments conducted in this work showed a dependence between tool design and quality of the forged element. The range of experiments have shown a wide selection of forming scenarios, including closed die forming, extrusion, warm forging and forming of advanced materials. The comparative closed die forming of different bulk metallic glasses is a new addition to state of the art. The warm forging of titanium shows interesting prospects for the future. Once the tribological challenges have been solved, micro forming of dental and medical titanium elements is a viable mass production method.

As such the project has made contributions to state of the art within micro forming technologies in several way. The design of the C5K press has been adopted and further developed by a Danish company seeking to explore the potential of the micro bulk forming technology. A minor part of this work has resulted in a patent application for a new lubricant carrier [5] for enhancement of tribological conditions in micro forming. Further, parts of the findings of this work have been selected for publication in a handbook of micro production technologies [1]. A number of supplementary publications have been planned based on the work of this thesis.

9.2 Suggestions for future work

A number of suggestions for future work have been identified through the course of this project.

Friction and tribology in micro forming of Titanium

The warm forming experiment conducted in this work showed severe galling problems. This led to cold welding of work piece material in the forming die and unsatisfactory specimen quality. A suitable combination of tool/billet coating in combination with a suitable lubricant should be found. Ideally the lubricant and coating should be easy removable after forming and should be able to operate at elevated temperatures around 400 °C.

Ways to produce smooth tool surfaces without degrading the dies

As encountered numerous times through this work, the current inability of manufacturing miniaturized tooling elements with sufficiently smooth surface finish is identified as real problem. Even the most advanced tooling methods are incapable of directly realizing sufficiently low surface finish for making the tools suitable for utilization in metal forming processes. The conventional route of lapping and polishing processes are ill-suited in the micro domain, since the geometric distortion of these processes are intolerable at small scale. In many ways, the surface finish challenge is a key barrier to be overcome before micro forming can be realized as an economically viable mass manufacturing technology.

The influence of forming method and tool characteristics on BMG fracture strength

The low fracture strength of bulk metallic glasses is a huge drawback of utilizing these materials. It is known that the forming strategy and tool surface roughness have substantial influence to fracture strength of the formed BMG component. The reason for this effect shall be sought in the presence of micro cracks in the surface of the formed specimen. The micro forming method and the tool surface roughness will be the main parameters influencing the formation of micro cracks. It is suggested that this relation is researched further.

Coating of micro forming tools

The area of coating is already actively researched for the case of conventional bulk forming. The size of typical micro forming tool makes it difficult to utilize conventional coating technology. The high aspect ratios of a micro forming die makes it virtually impossible to apply coatings to the active forming facets. This has already been demonstrated in chapter 3 of the present project. New methods of coating, possibly through the application of paste or an other carrier element and subsequent heat treatment, should be researched further.

Fine grain material for micro forming

The grain size influence in micro forming is one of the most dominant limiting factors. Methods for grain refinement already exist and the grain refined materials have shown enhanced mechanical properties, such as strength and anisotropy. However, the formability of fine grained materials have shown to be limited, with an increase risk of crack formation and other damage effects during forming. Realizing a fined grained material with excellent formability is important for any micro forming process. Thus it is suggested that continued research efforts are put into design and realization of special materials tailored for micro forming processes.

Author Publications

- [1] Mogens Arentoft, Rasmus Solmer Eriksen, and Hans Nørsgaard Hansen. *Micromanufacturing Engineering and Technology*, chapter 7. Elsevier Limited, 2010.
- [2] Cormac J. Byrne, Morten Eldrup, Masato Ohnuma, and Rasmus S. Eriksen. Free-standing bulk metallic glass microcomponents: Tooling considerations. *Journal of Materials Processing Technology*, In Press, Accepted Manuscript:–, 2010.
- [3] Rasmus Solmer Eriksen, Mogens Arentoft, Nikolas Aulin Paldan, and Jakob Viggo Holstein. Micro forming of titanium. *International Journal of Material Forming*, pages 601–604, 2009. Presented at: Esaform 2009 ; 12 : Twente, NL, 2009.
- [4] Nikolas Aulin Paldan, Mogens Arentoft, Rasmus Solmer Eriksen, and Charles Mangeot. Piezo driven prestressing of die-system for microforming of metal components. *International Journal of Material Forming*, 2008. Presented at: ESAFORM2008 : Conference on material forming ; 11 : Lyon, France, 2008.
- [5] Mogens Arentoft, Niels Bay, Peter Torben Tang, Jørgen Dai Jensen, Nikolas Aulin Paldan, Io Mizushima, and Rasmus Solmer Eriksen. Deposited micro porous layer as lubricant carrier in metal forming. In *Advanced Technology of Plasticity : Proceed. 9th International Conference on Technology of Plasticity*, pages 139–140, Korea, 2008. Korean Society for Technology of Plasticity. Presented at: 9th International Conference on Technology of Plasticity : Gyeongju, Korea, Sept., 2008.
- [6] Mogens Arentoft, Nikolas Aulin Paldan, Rasmus Solmer Eriksen, and Hans Nørsgaard Hansen. Innovationskonsortiet mikrometal - cold forging of industrial micro components. In *Metallurgi, Design og Innovation, Dansk Metallurgisk Selskab*, 2007. Vintermøde 2007, Middelfart, DK.
- [7] R. S. Eriksen, M. Arentoft, and N. A. Paldan. Tool design and manufacturing for bulk forming of micro components. *AIP Conference Proceedings*, 907(1):457–462, 2007. Presented at: ESAFORM2007 : Conference on material forming ; 10 : Zaragoza, Spain.
- [8] N. A. Paldan, M. Arentoft, and R. S. Eriksen. Production equipment and processes for bulk formed micro components. *AIP Conference Proceedings*, 907(1):463–468, 2007. Presented at: ESAFORM2007 : Conference on material forming ; 10 : Zaragoza, Spain.
- [9] M. Arentoft, N. A. Paldan, R. S. Eriksen, T. Gastaldi, J. A. Wert, and M. Eldrup. Bulk forming of industrial micro components in conventional metals and bulk metallic glasses. *AIP Conference Proceedings*, 907(1):665–670, 2007. Presented at: ESAFORM2007 : Conference on material forming ; 10 : Zaragoza, Spain.

AUTHOR PUBLICATIONS

- [10]Rasmus Solmer Eriksen. Lessons learned from entrepreneurial hot-spots and academic entrepreneurship in north america. Presented at: DREAM : Doctoral Retreat on Entrepreneurship As Making ; 1 : Sønderborg, 2008.
- [11]Mogens Arentoft, Nikolas Aulin Paldan, and Rasmus Solmer Eriksen. Cold forging of industrial micro components. In *39. Plenary Meeting of the International Cold Forging Group proceedings*, 2006. Presented at: Plenary Meeting of the International Cold Forging Group ; 39 : Changwon, Korea, 2006.

References

- [12] L. S. Nielsen, S. Lassen, C. B. Andersen, J. Grønbaek, and N. Bay. Development of a flexible tool system for small quantity production in cold forging. *Journal of Materials Processing Technology*, 71(1):36 – 42, 1997.
- [13] *ISO 5436-1:2000 Geometrical Product Specifications (GPS) – Surface texture: Profile method; Measurement standards – Part 1: Material measures.*
- [14] G. Tosello, H. N. Hansen, and S. Gasparin. Applications of dimensional micro metrology to the product and process quality control in manufacturing of precision polymer micro components. *CIRP Annals - Manufacturing Technology*, 58(1):467–472, 2009.
- [15] H. N. Hansen, K. Carneiro, H. Haitjema, and L. De Chiffre. Dimensional micro and nano metrology. *CIRP Annals - Manufacturing Technology*, 55(2):721–743, 2006.
- [16] Léonard de Vinci. Tribomètre de léonard de vinci. <http://en.wikipedia.org/wiki/Tribology>.
- [17] Nicolas Tiesler. *Grundlegende Untersuchungen zum Fließpressen metallischer Kleinstteile*. Meisenbach Verlag Bamberg, Erlangen-Eltersdorf, DE, 2001. Ph.D thesis.
- [18] Taylan Altan. *Cold And Hot Forging: Fundamentals And Applications*. ASM International, 2004.
- [19] P. Martins N. Bay, O. Wibom. Testing of friction and lubrication in bulk metal forming. Technical report. Keynote paper presented at Int. Mech. Engn. Conf. and Exhibition, IMECE98, Anaheim, Nov. 1998.
- [20] ICFG. Icfg - general recommendations for design, manufacture and operational aspects of cold extrusion tools for steel components, 1982. Doc. No. 6/82.
- [21] Matteo Calaon. Friction and lubrication in metal forming of micro components. Technical report, DTU, 2010. M. Sc. Thesis, Department of Mechanical Engineering.
- [22] C.P. Withen, J.R. Marstrand, M. Arentoft, and N.A. Paldan. Flexible tool system for cold forging of micro components. *First Int. Conf. on Multi-Material Micro Manufacture*, 2005. Forschungszentrum Karlsruhe, Germany.
- [23] J.V. Holstein and J. D. Dolriis. Automatisk cropping udstyr til fabrikation af mikro emner, 2006.

- [24] Ronald S. Fearing and Kg The. Survey of sticking effects for micro parts handling. In *International Conference on Intelligent Robots and Systems 95. 'Human Robot Interaction and Cooperative Robots', Proceedings. 1995 IEEE/RSJ*, pages 212–217, 1995.
- [25] Matteo Trevisan. Transfer system for mass-production of micro components. Technical report, DTU, 2006. M. Sc. Thesis, Department of Mechanical Engineering.
- [26] John A. Wert, Christian Thomsen, Rune Debel Jensen, and Mogens Arentoft. Forming of bulk metallic glass microcomponents. *Journal of Materials Processing Technology*, 209(3):1570 – 1579, 2009.
- [27] Jan Schroers, Tranquoc Nguyen, Sean O’Keeffe, and Amish Desai. Thermoplastic forming of bulk metallic glass—applications for mems and microstructure fabrication. *Materials Science and Engineering: A*, 449-451:898 – 902, 2007. Proceedings of the 12th International Conference on Rapidly Quenched & Metastable Materials.
- [28] Jens Grønbaek. Koldflydepresning: Procesteknisk begrænsning og muligheder for udvidelse af det hidtil kendte procesområde. Lic. forelæsning, DTH, 1982.
- [29] Peter Scheel Matthias Mullenborn, Jochen F. Kuhmann. Surface mountable transducer system, 05 2007. US patent no 7221767.
- [30] Ulf Engel and Emil Egerer. Basic research on cold and warm forging of microparts, 2002. TY: GEN.
- [31] Neil Krishnan, Jian Cao, and Kuniaki Dohda. Study of the size effects on friction conditions in microextrusion—part i: Microextrusion experiments and analysis. *Journal of Manufacturing Science and Engineering*, 129(4):669–676, August 2007 2007.
- [32] B. Eichenhüller, U. Engel, and S. Geißdörfer. Process parameter interaction in microforming, 2008. TY: GEN.
- [33] Guido Tosello. *Precision moulding of polymer micro components : Optimization, Simulation, Tooling, Quality Control and Multi-Material Application*. Technical University of Denmark, Department of Mechanical Engineering, Manufacturing Engineering, Lyngby, Denmark, 2008. Ph.D thesis.
- [34] L. Alting, F. Kimura, H.N. Hansen, and G. Bissacco. Micro engineering. *CIRP Annals - Manufacturing Technology*, 52(2):635 – 657, 2003.
- [35] H. Weule, V. Hüntrup, and H. Tritschler. Micro-cutting of steel to meet new requirements in miniaturization. *CIRP Annals - Manufacturing Technology*, 50(1):61 – 64, 2001.
- [36] Giuliano Bissacco. *Surface Generation and Optimization in Micromilling*. Technical University of Denmark, Department of Mechanical Engineering, Manufacturing Engineering, Lyngby, Denmark, 2004. Ph.D thesis.
- [37] T. Masuzawa. State of the art of micromachining. *CIRP Annals - Manufacturing Technology*, 49(2):473–488, 2000.
- [38] M. Geiger, M. Kleiner, R. Eckstein, N. Tiesler, and U. Engel. Microforming, 2001. TY: GEN.

-
- [39] U. Engel and R. Eckstein. Microforming-from basic research to its realization, 2002. TY: GEN.
- [40] R. Wechsum et al. Nexus market analysis for mems and microsystems iii, 2005-2009. *Wicht Technologie Consulting*, 2009.
- [41] N.A. Paldan M. Arentoft. Press design, transfer mechanism and tooling for micro forming. *9th ESAFORM conference*, pages 579–582, 2006.
- [42] Yi Qin. Micro-forming and miniature manufacturing systems – development needs and perspectives. *Journal of Materials Processing Technology*, 177(1-3):8 – 18, 2006. Proceedings of the 11th International Conference on Metal Forming 2006.
- [43] N. Kawahara, T. Suto, T. Hirano, Y. Ishikawa, T. Kitahara, N. Ooyama, and T. Ataka. Microfactories; new applications of micromachine technology to the manufacture of small products. *Microsystem Technologies*, 3(2):37–41, 02/25 1997. M3: 10.1007/s005420050052.
- [44] Yuichi Okazaki, Nozomu Mishima, and Kiwamu Ashida. Microfactory—concept, history, and developments. *Journal of Manufacturing Science and Engineering*, 126(4):837–844, November 2004 2004.
- [45] Rachel B. Cruise and Leroy Gardner. Strength enhancements induced during cold forming of stainless steel sections. *Journal of Constructional Steel Research*, 64(11):1310 – 1316, 2008. International Stainless Steel Experts Seminar.
- [46] Michael R. Notis. The history of the metallographic study of the japanese sword. *Materials Characterization*, 45(4-5):253 – 258, 2000.
- [47] Bradley Dodd. The making of old japanese swords. *Journal of Mechanical Working Technology*, 2(1):75 – 84, 1978.
- [48] F. Vollertsen, D. Biermann, H.N. Hansen, I.S. Jawahir, and K. Kuzman. Size effects in manufacturing of metallic components. *CIRP Annals - Manufacturing Technology*, 58(2):566 – 587, 2009.
- [49] Stefan Geissdorfer, Ulf Engel, Manfred Geiger, Elias Cueto, and Francisco Chinesta. Mesoscopic model - advanced simulation of microforming processes, 2007. TY: GEN.
- [50] M. Arentoft, S. Bruschi, A. Ghiotti, N.A. Paldan, and J.V. Holstein. Microforming of lightweight metals in warm conditions. *International Journal of Material Forming*, 1:435–438, 2008. Presented at the Esaform conference 2008, Lyon, France.
- [51] B. Eichenhüller and U. Engel. Microforming of titanium - forming behaviour at elevated temperature. *Proceedings of the Institution of Mechanical Engineers – Part B – Engineering Manufacture*, 222(1):77 – 82, 2008.
- [52] Francisco Chinesta and Elias Cueto. *Advances in Material Forming*. Springer, Heidelberg, esaform 10 years on edition, 2007.
- [53] T. Eriksson, H. Hansen, and A. Gegeckate. On the use of industrial robots in microfactories. *The International Journal of Advanced Manufacturing Technology*, 38(5):479–486, 08/01 2008. M3: 10.1007/s00170-007-1116-7.

- [54] F. Planitzer, T. Hatzenbichler, and B. Buchmayr. Microforming of lightweight metals in warm conditions. *FEM-Supported Development of a Radial Forging Process for Surface Densification of P/M Gears*, 2(0):93–96, 08/01 2009.
- [55] A. Weckenmann, T. Estler, G. Peggs, and D. McMurtry. Probing systems in dimensional metrology. *CIRP Annals - Manufacturing Technology*, 53(2):657 – 684, 2004.
- [56] *Guide to the expression of uncertainty in measurement, GUM 1995, with minor modifications*. Pavillon de Breteuil F-92312 Sèvres Cedex FRANCE, (e)1993 edition, 2008.
- [57] V. Fano, P. U. Gennari, and I. Ortalli. Dimensional stability of silicone-based impression materials. *Dental Materials*, 8(2):105–109, 3 1992.
- [58] Keith R. Marcroft, Raymond L. Tencate, and Eugene W. Skinner. The effects of heat, aging, and mold separation on the dimensional stability of silicone rubber. *The Journal of prosthetic dentistry*, 14(6):1091–1098, 12 1964.
- [59] *ISO/TS 15530-3:2004 Geometrical Product Specifications (GPS) - Coordinate Measuring Machines (CMM): Technique for Determining the Uncertainty of Measurement - Part 3: Use of Calibrated Workpieces or Standards, pp. i-v, 1-16*.
- [60] Jean-Yves Dantan, Alex Ballu, and Luc Mathieu. Geometrical product specifications – model for product life cycle. *Computer-Aided Design*, 40(4):493 – 501, 2008.
- [61] Kevin Swallow. 3-d microprobe metrology. Technical Report KCP-613-8519, Kansas City Plant (KCP), Kansas City, MO, 2008.
- [62] Z. X. Chao, S. L. Tan, and G. Xu. Evaluation on the probing error of a micro-coordinate measuring machine. In Chenggen Quan and Anand Asundi, editors, *International Symposium on Laser Metrology No9, Singapore ISBN 978-0-8194-7398-1 ; 0-8194-7398-*, volume 7155, page 71550K. SPIE, 2008.
- [63] Shiro Kobayashi, Taylan Altan, and Soo-Ik Oh. *Metal-Forming and the Finite-Element Method*. Oxford University Press, Oxford New York, 1989.
- [64] S. Weidel, U. Engel, M. Merklein, and M. Geiger. Basic investigations on boundary lubrication in metal forming processes by in situ observation of the real contact area. *Production Engineering*, 2009. Accepted for publication 17 November 2009.
- [65] N. Bay. The state of the art in cold forging lubrication. *Journal of Materials Processing Technology*, 46(1-2):19 – 40, 1994.
- [66] Yifei Mo, Kevin T. Turner, and Izabela Szlufarska. Friction laws at the nanoscale, 2009. TY: GEN.
- [67] M.I. Ghobrial, J.Y. Lee, T. Altan, N. Bay, and B.G. Hansen. Factors affecting the double cup extrusion test for evaluation of friction in cold and warm forging. *CIRP Annals - Manufacturing Technology*, 42(1):347 – 351, 1993.
- [68] Timothy Schrader, Manas Shirgaokar, and Taylan Altan. A critical evaluation of the double cup extrusion test for selection of cold forging lubricants. *Journal of Materials Processing Technology*, 189(1-3):36–44, 7/6 2007.

-
- [69] R. Komanduri, D.A. Lucca, and Y. Tani. Technological advances in fine abrasive processes. *CIRP Annals - Manufacturing Technology*, 46(2):545 – 596, 1997.
- [70] V.C. Venkatesh, I. Inasaki, H.K. Toenshof, T. Nakagawa, and I.D. Marinescu. Observations on polishing and ultraprecision machining of semiconductor substrate materials. *CIRP Annals - Manufacturing Technology*, 44(2):611 – 618, 1995.
- [71] Parshuram B. Zantye, Ashok Kumar, and A.K. Sikder. Chemical mechanical planarization for microelectronics applications. *Materials Science and Engineering: R: Reports*, 45(3-6):89 – 220, 2004.
- [72] R. Komanduri. On material removal mechanisms in finishing of advanced ceramics and glasses. *CIRP Annals - Manufacturing Technology*, 45(1):509 – 514, 1996.
- [73] C.J. Evans, E. Paul, D. Dornfeld, D.A. Lucca, G. Byrne, M. Tricard, F. Klocke, O. Dambon, and B.A. Mullany. Material removal mechanisms in lapping and polishing. *CIRP Annals - Manufacturing Technology*, 52(2):611 – 633, 2003.
- [74] Ulf Engel. Tribology in microforming, 2006. TY: GEN.
- [75] P.S. Nielsen, N.A. Paldan, M. Calalon, and N. Bay. Direct testing of scale effects in metal forming friction and lubrication. In *Int. Conf. on Tribology in Manufacturing Processes, ICTMP2010, Nice 13.-15. June*, 2010.
- [76] *Geometrical product specifications (GPS) - Surface texture: Profile method - Rules and procedures for the assessment of surface texture.*
- [77] Jens Groenbaek and Torben Birker. Innovations in cold forging die design. *Journal of Materials Processing Technology*, 98(2):155 – 161, 2000.
- [78] J. Grønbaek. Stripwound cold-forging tools – a technical and economical alternative. *Journal of Materials Processing Technology*, 35(3-4):483 – 493, 1992.
- [79] J. Cai, T. A. Dean, and Z. M. Hu. Alternative die designs in net-shape forging of gears. *Journal of Materials Processing Technology*, 150(1-2):48 – 55, 2004.
- [80] R. Cominotti and E. Gentili. Near net shape technology: An innovative opportunity for the automotive industry. *Robotics and Computer-Integrated Manufacturing*, 24(6):722 – 727, 2008. FAIM 2007, 17th International Conference on Flexible Automation and Intelligent Manufacturing.
- [81] Si-Young Sung and Young-Jig Kim. Economic net-shape forming of tial alloys for automotive parts. *Intermetallics*, 14(10-11):1163 – 1167, 2006. EUROMAT 2005 European Congress on Advanced Materials and Processes.
- [82] Eckart Doege and Jürgen Thalemann. Quality control of injection moulded micro mechanical parts. *4M/ICOMM 2009 - The Global Conference on Micro Manufacture*, pages 175–178, 2009.
- [83] T. Nellesmann, N. Bay, and T. Wanheim. Real area of contact and friction stress – the role of trapped lubricant. *Wear*, 43(1):45 – 53, 1977.
- [84] U. Popp and U. Engel. Microtexturing of cold-forging tools – influence on tool life. *Proceedings of the Institution of Mechanical Engineers – Part B – Engineering Manufacture*, 220(1):27 – 33, 2006.

- [85] S. Weidel and U. Engel. Surface characterisation in forming processes by functional 3d parameters, 2007. TY: GEN.
- [86] S. Weidel and U. Engel. Characterisation of the flattening behaviour of modelled asperities, 2009. TY: GEN.
- [87] M. Arentoft, M. Eriksen, and T. Wanheim. Determination of six stiffnesses for a press. *Journal of Materials Processing Technology*, 105(3):246 – 252, 2000.
- [88] S. Geißdörfer, U. Engel, and M. Geiger. Fe-simulation of microforming processes applying a mesoscopic model, 2006. TY: GEN.
- [89] M. Geiger U. Engel, A. MeXner. Advanced concept for the fe-simulation of metal forming processes for the production of microparts, 1996. Proceedings of the Fifth ICTP.
- [90] S. Geißdörfer, U. Engel, and M. Geiger. Fe-simulation of microforming processes applying a mesoscopic model, 2006. TY: GEN.
- [91] G.G. Fuentes, R. Rodriguez, J.C. Avelar-Batista, J. Housden, F. Montalá, L.J. Carreras, A.B. Cristóbal, J.J. Damborenea, and T.J. Tate. Recent advances in the chromium nitride pvd process for forming and machining surface protection. *Journal of Materials Processing Technology*, 167(2-3):415 – 421, 2005. 2005 International Forum on the Advances in Materials Processing Technology.
- [92] Frederik C. Krebs, Jan Alstrup, Holger Spanggaard, Kaj Larsen, and Esben Kold. Production of large-area polymer solar cells by industrial silk screen printing, lifetime considerations and lamination with polyethyleneterephthalate. *Solar Energy Materials and Solar Cells*, 83(2-3):293 – 300, 2004. The development of organic and polymer photovoltaics.
- [93] Frederik C. Krebs, Mikkel Jørgensen, Kion Norrman, Ole Hagemann, Jan Alstrup, Torben D. Nielsen, Jan Fyenbo, Kaj Larsen, and Jette Kristensen. A complete process for production of flexible large area polymer solar cells entirely using screen printing—first public demonstration. *Solar Energy Materials and Solar Cells*, 93(4):422 – 441, 2009. Processing and Preparation of Polymer and Organic Solar Cells.
- [94] Kun Liu, Bert Lauwers, and Dominiek Reynaerts. Process capabilities of micro-edm and its applications. *The International Journal of Advanced Manufacturing Technology*, 47(1):11 – 19, 2010.
- [95] K.P. Rajurkar, G. Levy, A. Malshe, M.M. Sundaram, J. McGeough, X. Hu, R. Resnick, and A. DeSilva. Micro and nano machining by electro-physical and chemical processes. *CIRP Annals - Manufacturing Technology*, 55(2):643 – 666, 2006.
- [96] Laxmikant V Saraf. Site-specific pt deposition and etching on electrically and thermally isolated sio 2 micro-disk surfaces. *Journal of Micromechanics and Microengineering*, 20(4):045031, 2010.
- [97] Shi Hyoung Ryu. Micro fabrication by electrochemical process in citric acid electrolyte. *Journal of Materials Processing Technology*, 209(6):2831 – 2837, 2009.

-
- [98] Zhi-Wen Fan, Lih-Wu Hourng, and Cheng-Yu Wang. Fabrication of tungsten microelectrodes using pulsed electrochemical machining. *Precision Engineering*, 34(3):489 – 496, 2010.
- [99] Peter Heyl, Thomas Olschewski, and Roelof W. Wijnaendts. Manufacturing of 3d structures for micro-tools using laser ablation. *Microelectronic Engineering*, 57-58:775 – 780, 2001.
- [100] Elman C. Jameson (Author). *Electrical Discharge Machining*. Society of Manufacturing Engineers, 2001.
- [101] P.T. Tang, M. Jaskula, M. Kubiczek, I. Mizushima, K. Pantleon, and M. Arentoft. Pulse reversal plating of nickelcobalt alloys. *Transactions of the Institute of Metal Finishing*, 87:72–77(6), March 2009.
- [102] R. S. Eriksen, M. Arentoft, and N. A. Paldan. Tool design and manufacturing for bulk forming of micro components. *AIP Conference Proceedings*, 907(1):457 – 462, 2007.
- [103] A. Islam, H. N. Hansen, P. T. Tang, and J. Sun. Process chains for the manufacturing of molded interconnect devices. *The International Journal of Advanced Manufacturing Technology*, 42(9):831 – 841, 2009.
- [104] Schuler GmbH. *Metal Forming Handbook*. Springer, Berlin Heidelberg, 1998.
- [105] M. Arentoft and T. Wanheim. A new approach to determine press stiffness. *CIRP Annals - Manufacturing Technology*, 54(1):265 – 268, 2005.
- [106] Yuichi Okazaki, Nozomu Mishima, and Kiwamu Ashida. Microfactory—concept, history, and developments. *Journal of Manufacturing Science and Engineering*, 126(4):837–844, 2004.
- [107] M. Arentoft, N. A. Paldan M., and R. S. Eriksen. Cold forging of industrial micro components. *Presented at: Plenary Meeting of the International Cold Forging Group. Changwon, Korea, 2006*, 2006. In: 39. Plenary Meeting of the International Cold Forging Group proceedings.
- [108] Frank Richter. *Upsetting and Viscoelasticity of Vitreous SiO₂: Experiments, Interpretation and Simulation*. TU Berlin, Berlin, DE, 2005. Ph.D thesis.
- [109] M. Arentoft, S. Bruschi, A. Ghiotti, and N.A. Paldanand J.V. Holstein. Microforming of lightweight metals in warm conditions. *International Journal of Material Forming*, 1(0):435–438, 04/01 2008.
- [110] N. Bay. Cold forging, 1993. MM.93.32 compendium, MEK-DTU, DK.
- [111] E. W. Collings and Gerhard Welsch. *Materials Properties Handbook: Titanium Alloys*. ASM International, 1995.
- [112] J.V. Holstein. Warm forging of titanium in warm condition, 2009. DTU-MEK.

Appendix A

Flow curves of popular cold forging materials

A. FLOW CURVES OF POPULAR COLD FORGING MATERIALS

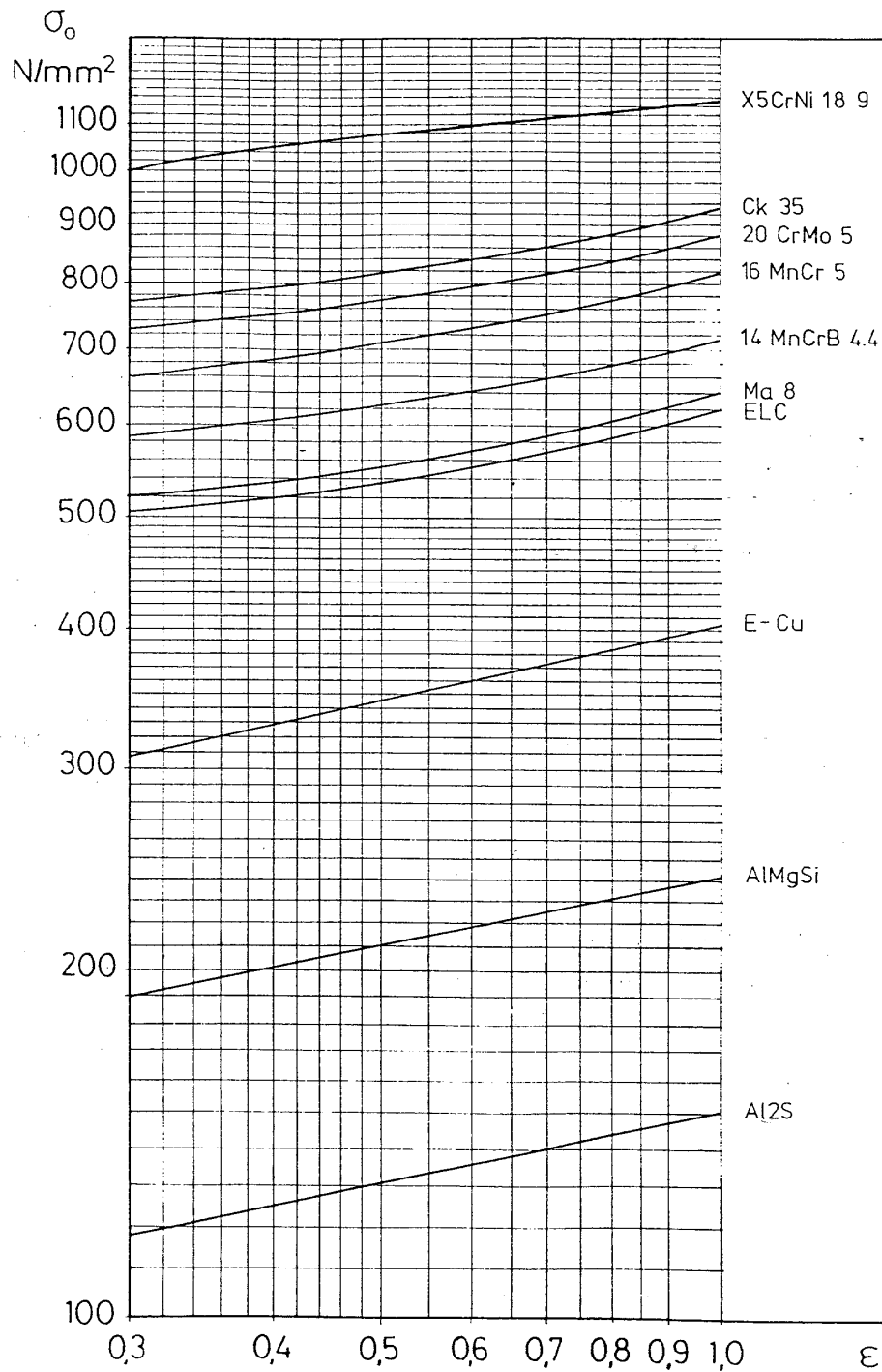
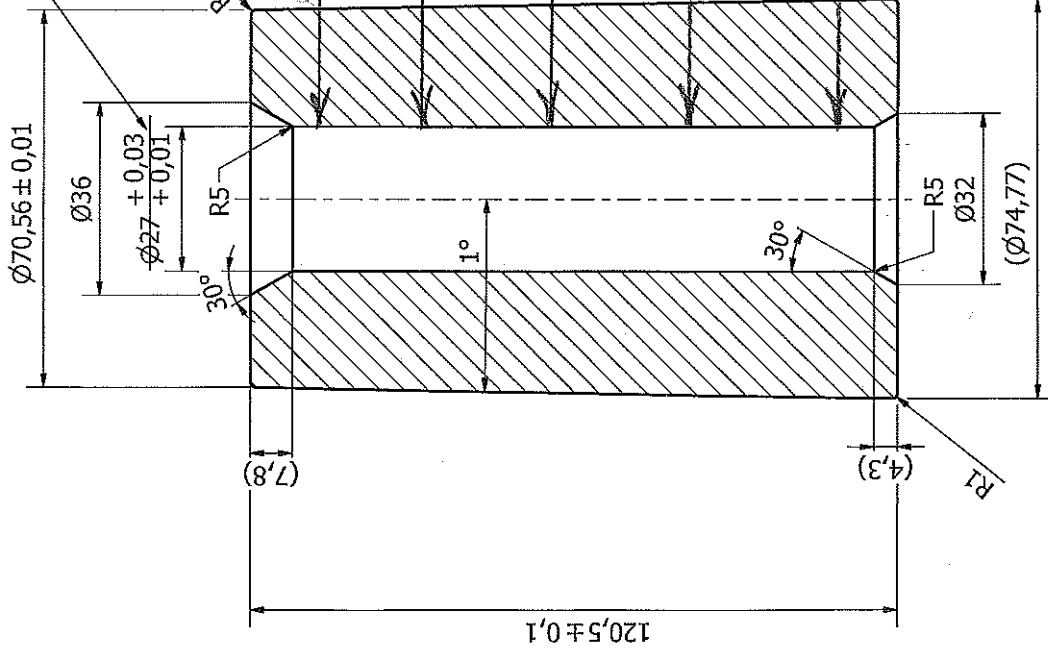


Figure A.1: Stress strain curves for various cold forging materials [28].

Appendix B

RAP EDM die deflection

ferdig mål efter ipresning i båndarmring
Arbejdsmaal = Ø26,8 (der er kompenseret med 0,2)

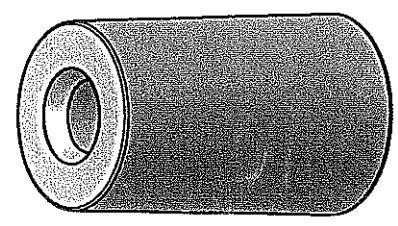


ipresset nr. 2

odpesset nr. 1

ipresset nr. 2

$\varnothing 27,015$	$\varnothing 27,230$	$\varnothing 27,230$	$\varnothing 27,230$
$\varnothing 27,015$	$\varnothing 27,210$	$\varnothing 27,210$	$\varnothing 27,210$
$\varnothing 27,012$	$\varnothing 27,205$	$\varnothing 27,205$	$\varnothing 27,206$
$\varnothing 27,010$	$\varnothing 27,196$	$\varnothing 27,196$	$\varnothing 27,202$
$\varnothing 27,010$	$\varnothing 27,172$	$\varnothing 27,172$	$\varnothing 27,175$



Projektion	Scala	Mat./Spec
		Vanadis 4 E HRC.61
Replace	Design	10-02-2009
	Karin Bak	
<small>Confidential. Property of Strecon A/S. Denmark. Not to be handed over to, copied or used by third party. Two- or three dimensional reproduction of contents to be authorized by Strecon A/S.</small>		
IPU-DTU Lyngby		No. D5701
Nano RAP		

Appendix C

RAP polishing procedure - mirror finish

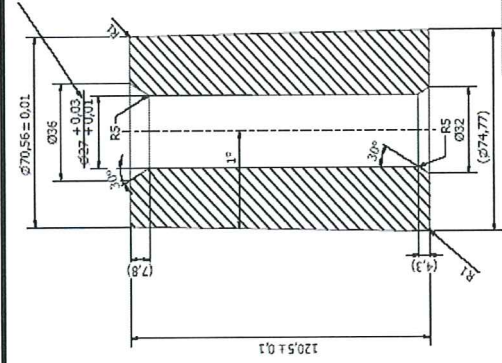
Emnetype	Matrice
Overfladetype	Slebet

Ra. før poléring	0.29
Ra. efter poléring	

Tegn.

Materiale	Vanadis 4E
HRC.	61

Flexstang nr.	02
Længde mm.	168



Medie:	MF600	DF900	15µm	3µm
Programkørsel:	Uden repetition	Uden repetition	Uden repetition	Uden repetition
Puls	2000	0	3000	0
Puls længde	1.5	0	1.5	0
Spindel	150	300	300	800
Tryk	1000	2000	2000	2000
Speed	3~5	5	3~5	6

Tid pr. overløb	00:00:59	00:00:44	00:00:59	00:00:46	Bemærkning
Overløb	10				Speed 3.
	10				Speed 5.
		20			Magic lab, speed 5.
			10		Spindel 150, tryk 1000, speed 3.
			10		Træ, puls 0, spindel 120, tryk 1000, speed 3.
			30		Filt.
				20	
				10	Puls 3000.
Overløb i alt	20	20	50	30	Samtlige overløb
Effektiv tid	00:19:40	00:14:40	00:49:10	00:23:00	Samlet effektiv tid
					120
					01:46:30



MarSurf XR 20
V1.40-3

STRECON A/S
Tool & Polish
RAP

Lars
P000_001.PCD

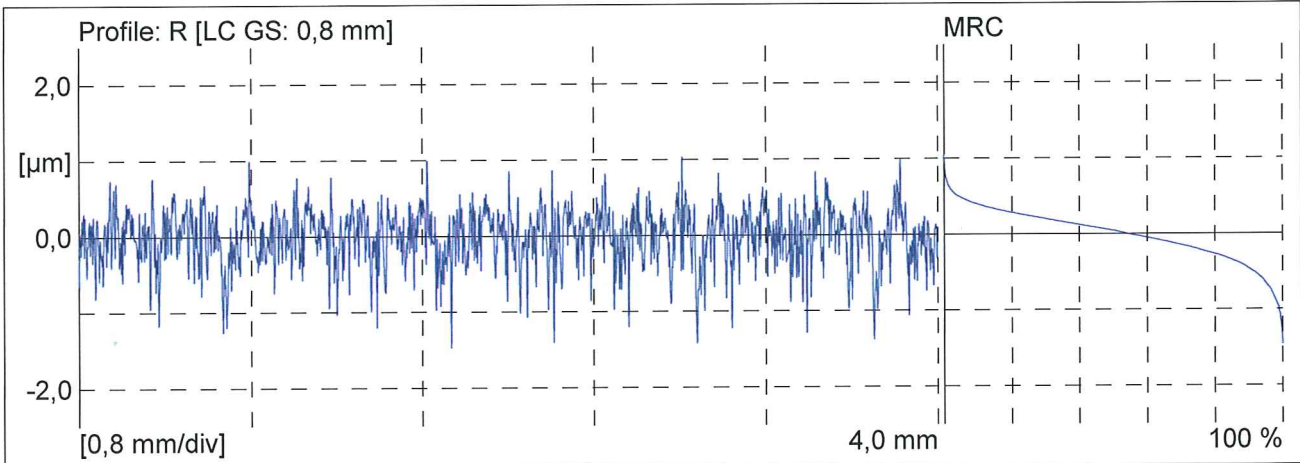


03/26/09

Object: D5701
Number: 01
Comment: Startoverflade. Slebet.

Meas. Instrum.: PS1
Drive Unit: PS1
Pick-up: PHT 350

Lt: 5,6 mm [N=5]
Ls: 2,5 μm
VB: $\pm 200,0 \mu\text{m}$
Vt: 0,50 mm/s
Points: 11200



Profile: R [LC GS: 0,8 mm]	
Ra	0,274 μm
Rq	0,350 μm
Rz	2,305 μm
Rt	2,51 μm
Profile: R [LC ISO 13565: 0,80 mm]	
Rk	0,82 μm
Rpk	0,24 μm
Rvk	0,52 μm



MarSurf XR 20
V1.40-3

STRECON A/S
Tool & Polish
RAP

Lars
P000_002.PCD

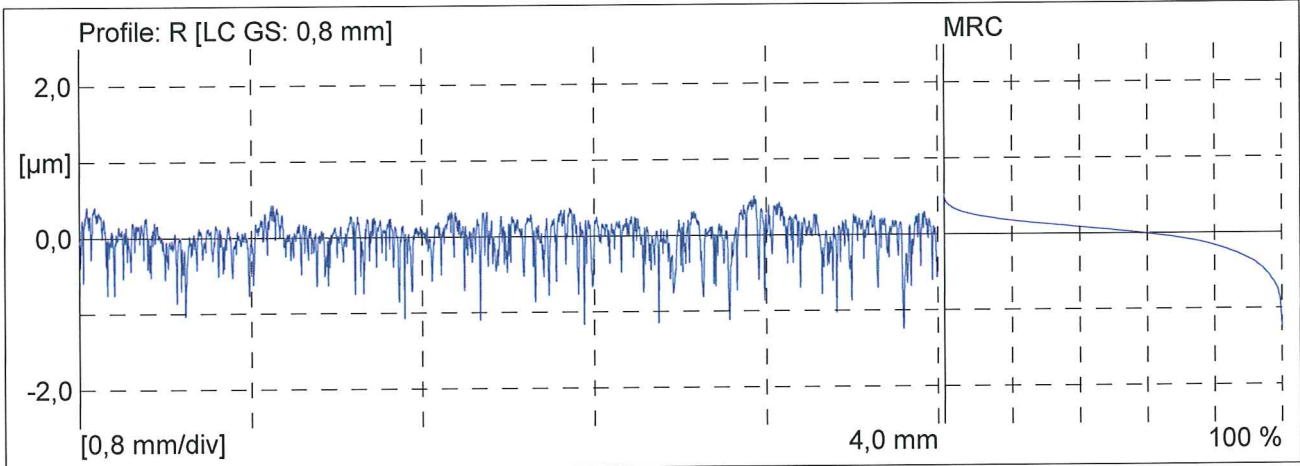


03/26/09

Object: D5701
Number: 01
Comment: MF600 10 overløb.
Puls 2000, spindel 150, tryk 1000, speed 3.

Meas. Instrum.: PS1
Drive Unit: PS1
Pick-up: PHT 350

Lt: 5,6 mm [N=5]
Ls: 2,5 µm
VB: ±200,0 µm
Vt: 0,50 mm/s
Points: 11200



Profile: R [LC GS: 0,8 mm]

Ra	0,180 µm
Rq	0,243 µm
Rz	1,566 µm
Rt	1,76 µm

Profile: R [LC ISO 13565: 0,80 mm]

Rk	0,45 µm
Rpk	0,15 µm
Rvk	0,46 µm



MarSurf XR 20
V1.40-3

STRECON A/S
Tool & Polish
RAP

Lars
P000_003.PCD

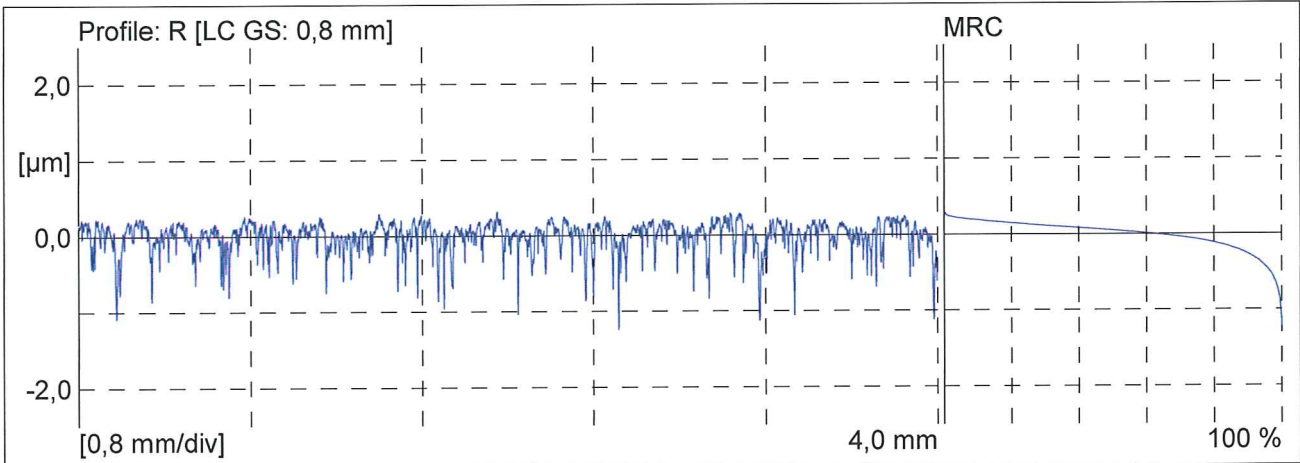


03/26/09

Object: D5701
Number: 01
Comment: MF600 30 overløb.
Puls 2000, spindel 150, tryk 1500, speed 5.

Meas. Instrum.: PS1
Drive Unit: PS1
Pick-up: PHT 350

Lt: 5,6 mm [N=5]
Ls: 2,5 µm
VB: ±200,0 µm
Vt: 0,50 mm/s
Points: 11200



Profile: R [LC GS: 0,8 mm]

Ra	0,147 µm
Rq	0,204 µm
Rz	1,343 µm
Rt	1,55 µm

Profile: R [LC ISO 13565: 0,80 mm]

Rk	0,33 µm
Rpk	0,04 µm
Rvk	0,43 µm



MarSurf XR 20
V1.40-3

STRECON A/S
Tool & Polish
RAP

Lars
P000_004.PCD

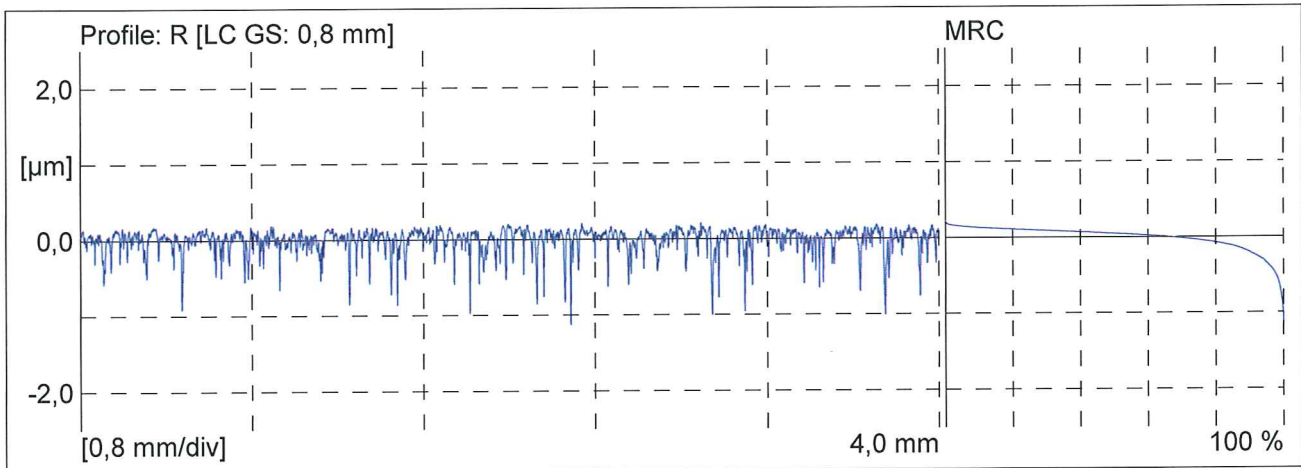


03/26/09

Object: D5701
Number: 01
Comment: MF600 50 overløb.
Puls 2000, spindel 150, tryk 1500, speed 5.

Meas. Instrum.: PS1
Drive Unit: PS1
Pick-up: PHT 350

Lt: 5,6 mm [N=5]
Ls: 2,5 μm
VB: $\pm 200,0 \mu\text{m}$
Vt: 0,50 mm/s
Points: 11200



Profile: R [LC GS: 0,8 mm]

Ra	0,113 μm
Rq	0,164 μm
Rz	1,176 μm
Rt	1,34 μm

Profile: R [LC ISO 13565: 0,80 mm]

Rk	0,20 μm
Rpk	0,03 μm
Rvk	0,37 μm



MarSurf XR 20
V1.40-3

STRECON A/S
Tool & Polish
RAP

Lars
P000_005.PCD

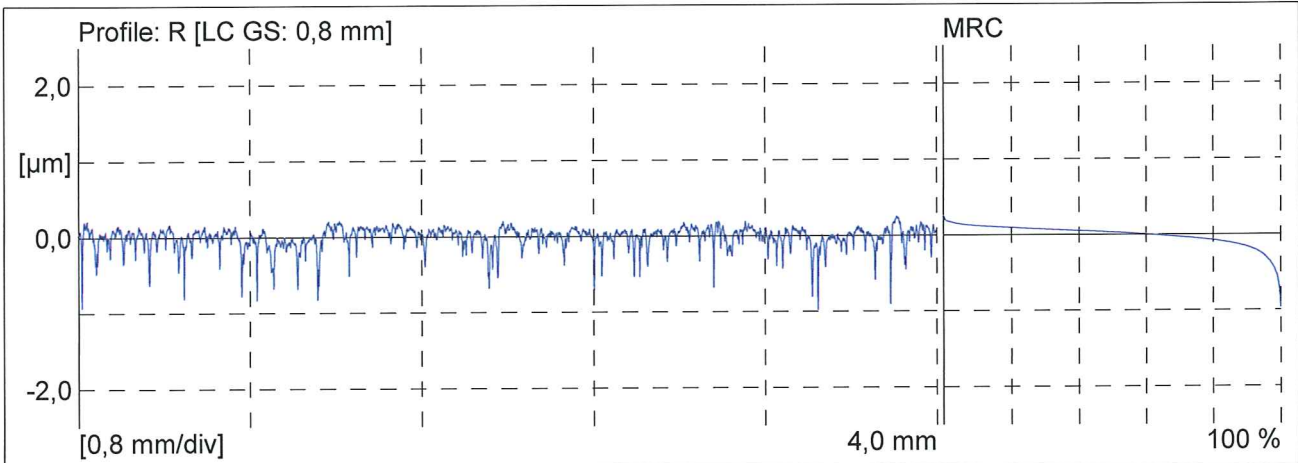


03/26/09

Object: D5701
Number: 01
Comment: 14µm 20 overløb.
Puls 1000, spindel 500, tryk 1500, speed 5.

Meas. Instrum.: PS1
Drive Unit: PS1
Pick-up: PHT 350

Lt: 5,6 mm [N=5]
Ls: 2,5 µm
VB: ±200,0 µm
Vt: 0,50 mm/s
Points: 11200



Profile: R [LC GS: 0,8 mm]

Ra	0,098 µm
Rq	0,139 µm
Rz	1,041 µm
Rt	1,23 µm

Profile: R [LC ISO 13565: 0,80 mm]

Rk	0,24 µm
Rpk	0,05 µm
Rvk	0,28 µm



MarSurf XR 20
V1.40-3

STRECON A/S
Tool & Polish
RAP

Lars
P000_006.PCD

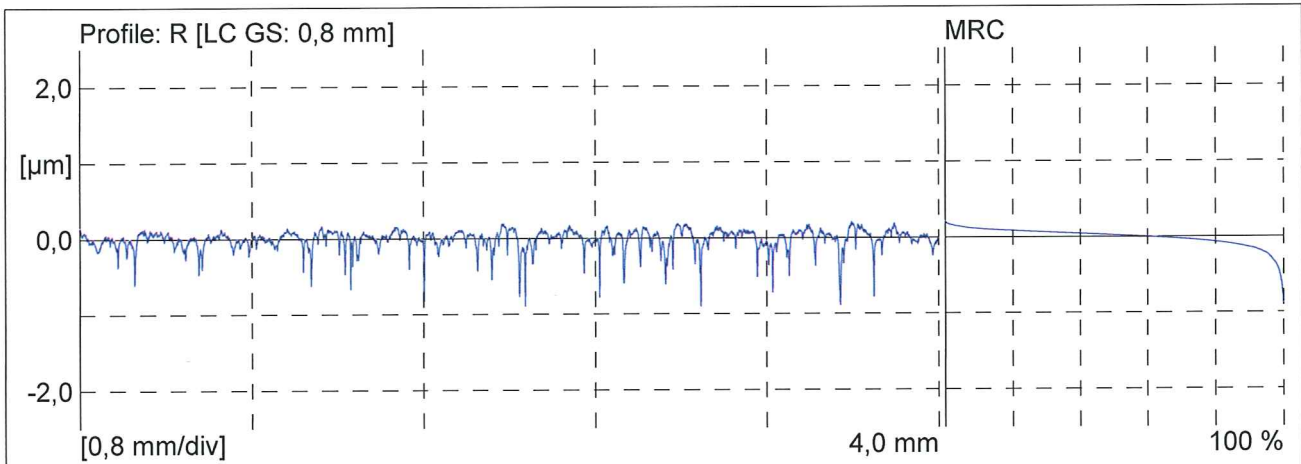


03/26/09

Object: D5701
Number: 01
Comment: 14µm 60 overløb.
Puls 1000, spindel 300, tryk 1500, speed 5.

Meas. Instrum.: PS1
Drive Unit: PS1
Pick-up: PHT 350

Lt: 5,6 mm [N=5]
Ls: 2,5 µm
VB: ±200,0 µm
Vt: 0,50 mm/s
Points: 11200



Profile: R [LC GS: 0,8 mm]

Ra	0,086 µm
Rq	0,125 µm
Rz	0,971 µm
Rt	1,11 µm

Profile: R [LC ISO 13565: 0,80 mm]

Rk	0,20 µm
Rpk	0,05 µm
Rvk	0,25 µm



MarSurf XR 20
V1.40-3

STRECON A/S
Tool & Polish
RAP

Lars
P000_007.PCD

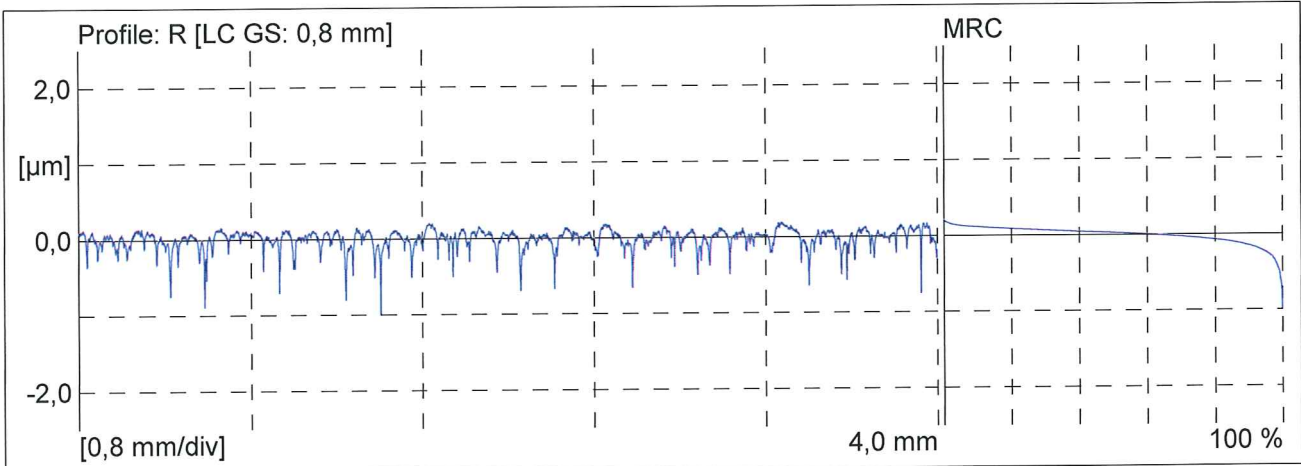


03/26/09

Object: D5701
Number: 01
Comment: 14µm 80 overløb.
Puls 3000, spindel 150, tryk 1000, speed 5.

Meas. Instrum.: PS1
Drive Unit: PS1
Pick-up: PHT 350

Lt: 5,6 mm [N=5]
Ls: 2,5 µm
VB: ±200,0 µm
Vt: 0,50 mm/s
Points: 11200



Profile: R [LC GS: 0,8 mm]

Ra	0,088 µm
Rq	0,125 µm
Rz	0,976 µm
Rt	1,21 µm

Profile: R [LC ISO 13565: 0,80 mm]

Rk	0,20 µm
Rpk	0,05 µm
Rvk	0,25 µm



MarSurf XR 20
V1.40-3

STRECON A/S
Tool & Polish
RAP

Lars
P000_008.PCD

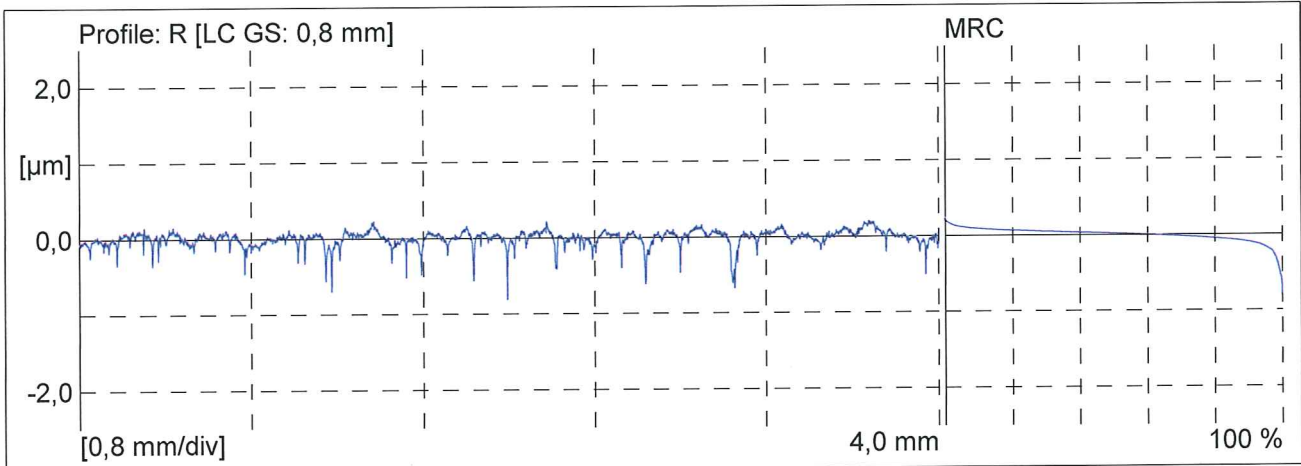


03/26/09

Object: D5701
Number: 01
Comment: 14µm 120 overløb.
Puls 0, spindel 300, tryk 2000, speed 6.

Meas. Instrum.: PS1
Drive Unit: PS1
Pick-up: PHT 350

Lt: 5,6 mm [N=5]
Ls: 2,5 µm
VB: ±200,0 µm
Vt: 0,50 mm/s
Points: 11200



Profile: R [LC GS: 0,8 mm]

Ra	0,068 µm
Rq	0,100 µm
Rz	0,823 µm
Rt	1,04 µm

Profile: R [LC ISO 13565: 0,80 mm]

Rk	0,16 µm
Rpk	0,07 µm
Rvk	0,20 µm



MarSurf XR 20
V1.40-3

STRECON A/S
Tool & Polish
RAP

Lars
P000_010.PCD

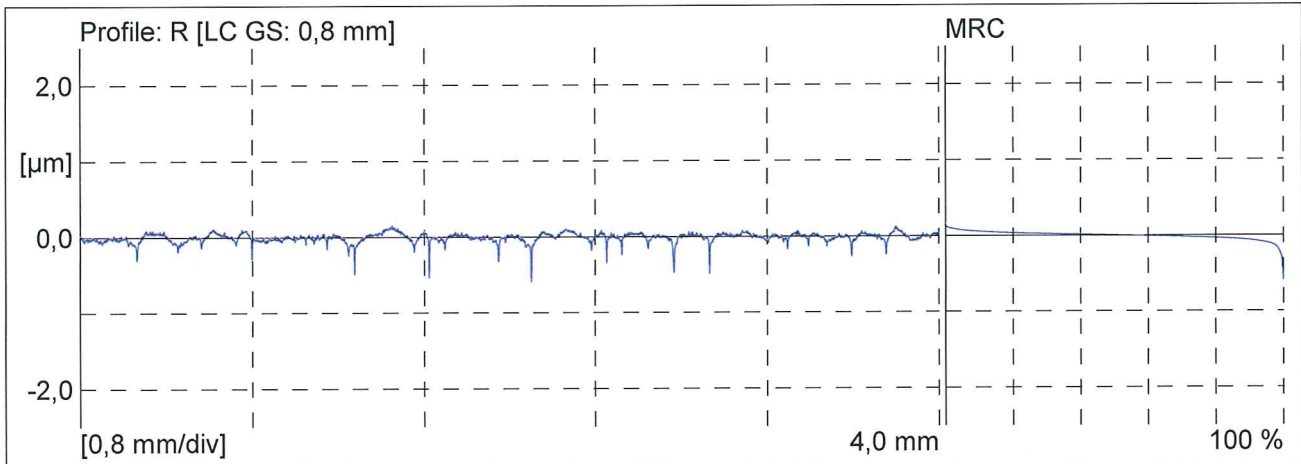


03/26/09

Object: D5701
Number: 01
Comment: 9µm 20 overløb.
Puls 0, spindel 800, tryk 2000, speed 6.

Meas. Instrum.: PS1
Drive Unit: PS1
Pick-up: PHT 350

Lt: 5,6 mm [N=5]
Ls: 2,5 µm
VB: ±200,0 µm
Vt: 0,50 mm/s
Points: 11200



Profile: R [LC GS: 0,8 mm]

Ra	0,040 µm
Rq	0,060 µm
Rz	0,545 µm
Rt	0,75 µm

Profile: R [LC ISO 13565: 0,80 mm]

Rk (9!)	0,11 µm
Rpk (9!)	0,05 µm
Rvk (9!)	0,12 µm

Appendix D

RAP polishing procedure - functional finish



MarSurf XR 20
V1.40-3

STRECON A/S
Tool & Polish
RAP

Lars
P000_013.PCD

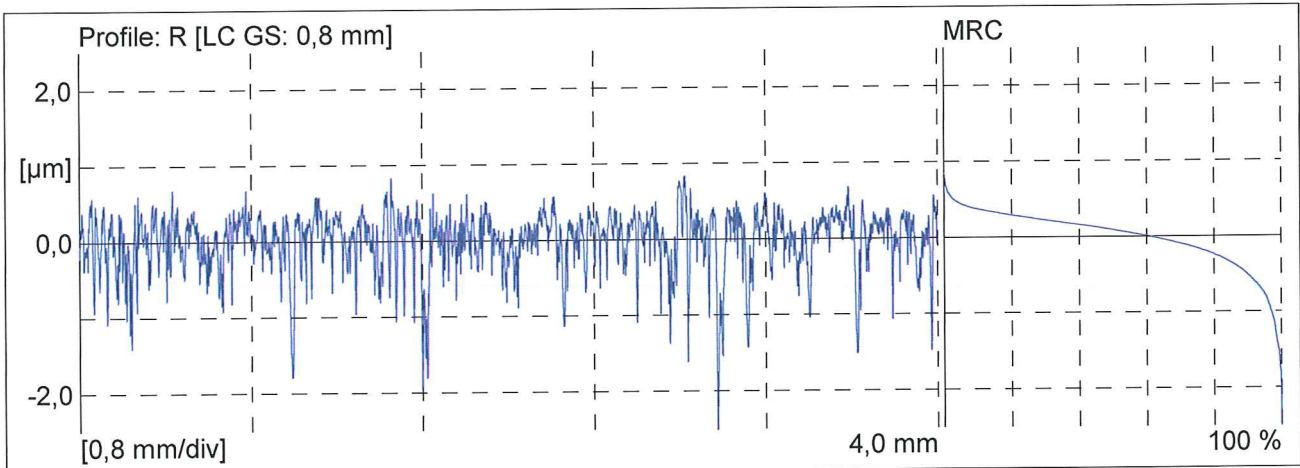


03/27/09

Object: D5701
Number: 02
Comment: Startoverflade. Slebet.

Meas. Instrum.: PS1
Drive Unit: PS1
Pick-up: PHT 350

Lt: 5,6 mm [N=5]
Ls: 2,5 μm
VB: $\pm 200,0 \mu\text{m}$
Vt: 0,50 mm/s
Points: 11200



Profile: R [LC GS: 0,8 mm]	
Ra	0,290 μm
Rq	0,398 μm
Rz	2,602 μm
Rt	3,47 μm
Profile: R [LC ISO 13565: 0,80 mm]	
Rk	0,67 μm
Rpk	0,18 μm
Rvk	0,81 μm
Profile: W [LC GS: 0,8 mm]	
Wa	0,136 μm



MarSurf XR 20
V1.40-3

STRECON A/S
Tool & Polish
RAP

Lars
P000_014.PCD

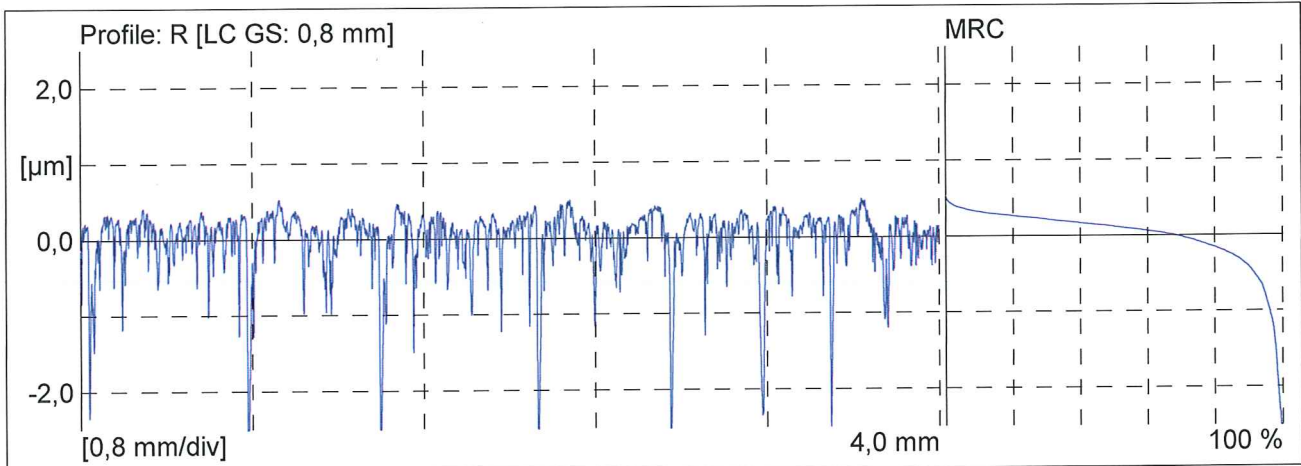


03/27/09

Object: D5701
Number: 02
Comment: MF600 10 overløb.
Puls 2000, spindel150, tryk 1000, speed 3.

Meas. Instrum.: PS1
Drive Unit: PS1
Pick-up: PHT 350

Lt: 5,6 mm [N=5]
Ls: 2,5 μm
VB: $\pm 200,0 \mu\text{m}$
Vt: 0,50 mm/s
Points: 11200



Profile: R [LC GS: 0,8 mm]

Ra	0,279 μm
Rq	0,451 μm
Rz	3,427 μm
Rt	3,70 μm

Profile: R [LC ISO 13565: 0,80 mm]

Rk	0,48 μm
Rpk	0,11 μm
Rvk	0,99 μm

Profile: W [LC GS: 0,8 mm]

Wa	0,077 μm
----	---------------------



MarSurf XR 20
V1.40-3

STRECON A/S
Tool & Polish
RAP

Lars
P000_015.PCD

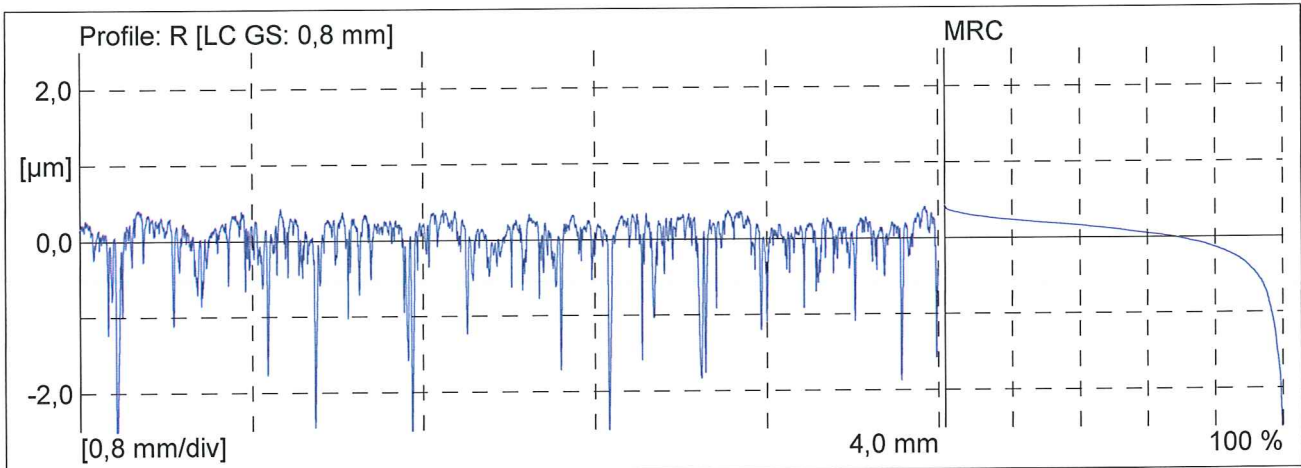


03/27/09

Object: D5701
Number: 02
Comment: MF600 20 overløb.
Puls 2000, spindel150, tryk 1000, speed 5.

Meas. Instrum.: PS1
Drive Unit: PS1
Pick-up: PHT 350

Lt: 5,6 mm [N=5]
Ls: 2,5 μm
VB: $\pm 200,0 \mu\text{m}$
Vt: 0,50 mm/s
Points: 11200



Profile: R [LC GS: 0,8 mm]

Ra	0,248 μm
Rq	0,393 μm
Rz	2,817 μm
Rt	3,63 μm

Profile: R [LC ISO 13565: 0,80 mm]

Rk	0,39 μm
Rpk	0,06 μm
Rvk	0,86 μm

Profile: W [LC GS: 0,8 mm]

Wa	0,043 μm
----	---------------------



MarSurf XR 20
V1.40-3

STRECON A/S
Tool & Polish
RAP

Lars
P000_001.PCD

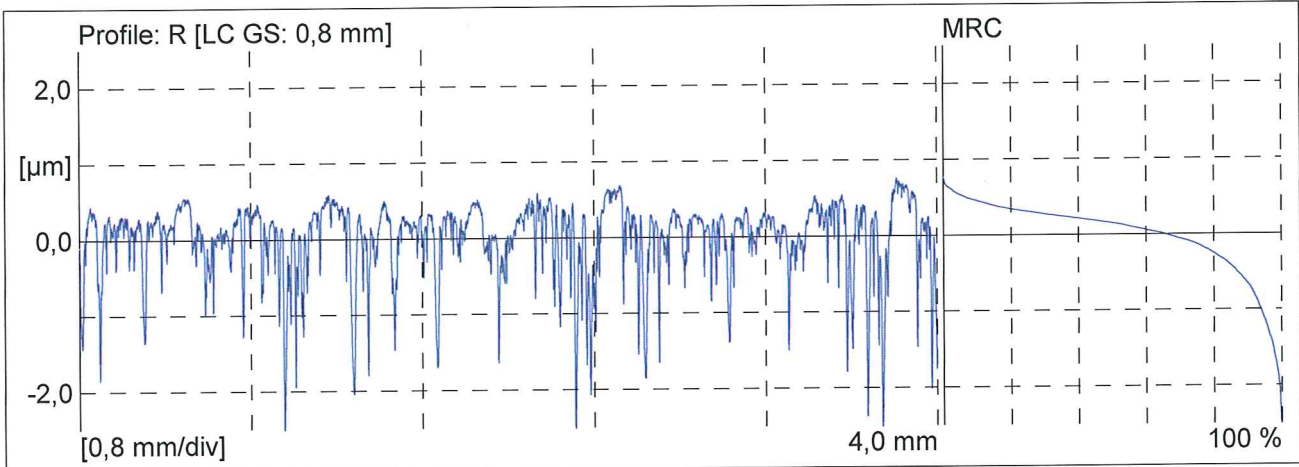


03/27/09

Object: D5701
Number: 02
Comment: DF900 20 overløb.
Puls 0, spindel 300, tryk 2000, speed 5.

Meas. Instrum.: PS1
Drive Unit: PS1
Pick-up: PHT 350

Lt: 5,6 mm [N=5]
Ls: 2,5 μm
VB: $\pm 200,0 \mu\text{m}$
Vt: 0,50 mm/s
Points: 11200



Profile: R [LC GS: 0,8 mm]

Ra	0,360 μm
Rq	0,506 μm
Rz	2,951 μm
Rt	3,43 μm

Profile: R [LC ISO 13565: 0,80 mm]

Rk	0,65 μm
Rpk	0,12 μm
Rvk	1,20 μm

Profile: W [LC GS: 0,8 mm]

Wa	0,186 μm
----	---------------------



MarSurf XR 20
V1.40-3

STRECON A/S
Tool & Polish
RAP

Lars
P000_002.PCD

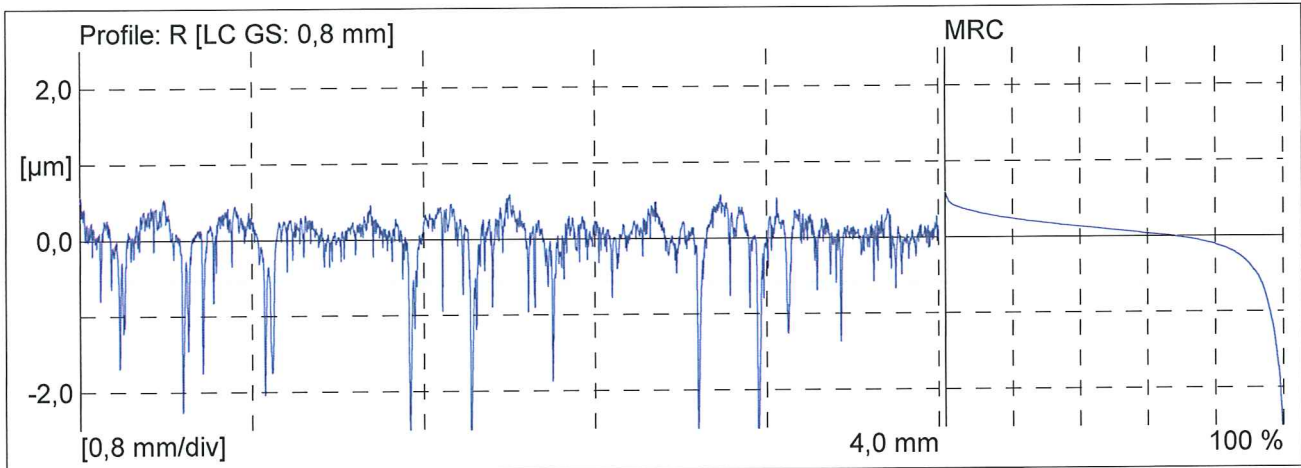


03/27/09

Object: D5701
Number: 02
Comment: 15µm 10 overløb.
Puls 3000, spindel 300, tryk 2000, speed 5.

Meas. Instrum.: PS1
Drive Unit: PS1
Pick-up: PHT 350

Lt: 5,6 mm [N=5]
Ls: 2,5 µm
VB: ±200,0 µm
Vt: 0,50 mm/s
Points: 11200



Profile: R [LC GS: 0,8 mm]

Ra	0,249 µm
Rq	0,416 µm
Rz	2,979 µm
Rt	3,66 µm

Profile: R [LC ISO 13565: 0,80 mm]

Rk	0,44 µm
Rpk	0,14 µm
Rvk	1,03 µm

Profile: W [LC GS: 0,8 mm]

Wa	0,111 µm
----	----------



MarSurf XR 20
V1.40-3

STRECON A/S
Tool & Polish
RAP

Lars
P000_003.PCD

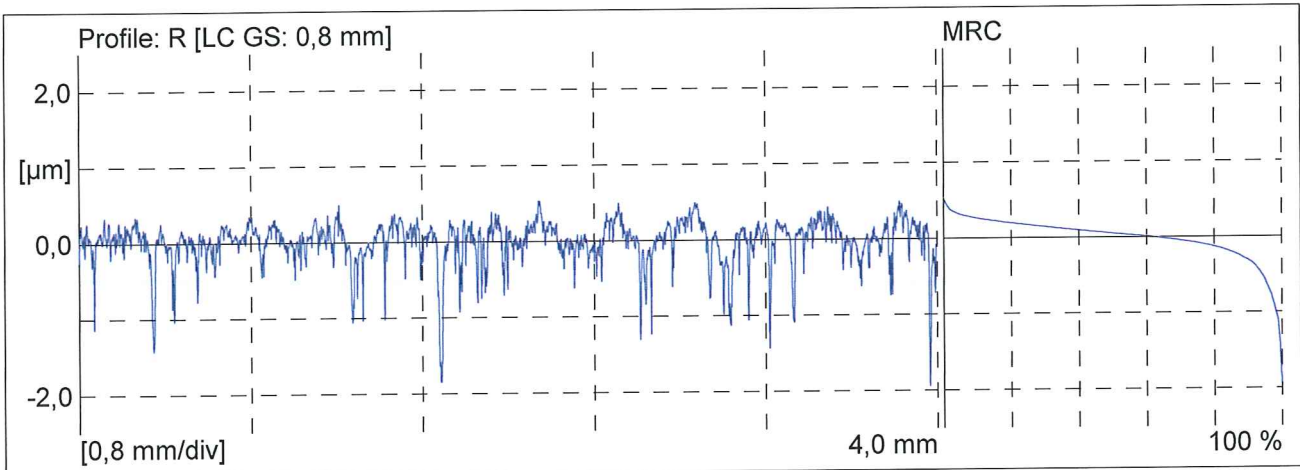


03/27/09

Object: D5701
Number: 02
Comment: 15µm 20 overløb.
Puls 3000, spindel 150, tryk 1000, speed 3.

Meas. Instrum.: PS1
Drive Unit: PS1
Pick-up: PHT 350

Lt: 5,6 mm [N=5]
Ls: 2,5 µm
VB: ±200,0 µm
Vt: 0,50 mm/s
Points: 11200



Profile: R [LC GS: 0,8 mm]

Ra	0,195 µm
Rq	0,292 µm
Rz	1,992 µm
Rt	2,48 µm

Profile: R [LC ISO 13565: 0,80 mm]

Rk	0,45 µm
Rpk	0,14 µm
Rvk	0,67 µm

Profile: W [LC GS: 0,8 mm]

Wa	0,122 µm
----	----------



MarSurf XR 20
V1.40-3

STRECON A/S
Tool & Polish
RAP

Lars
P000_004.PCD

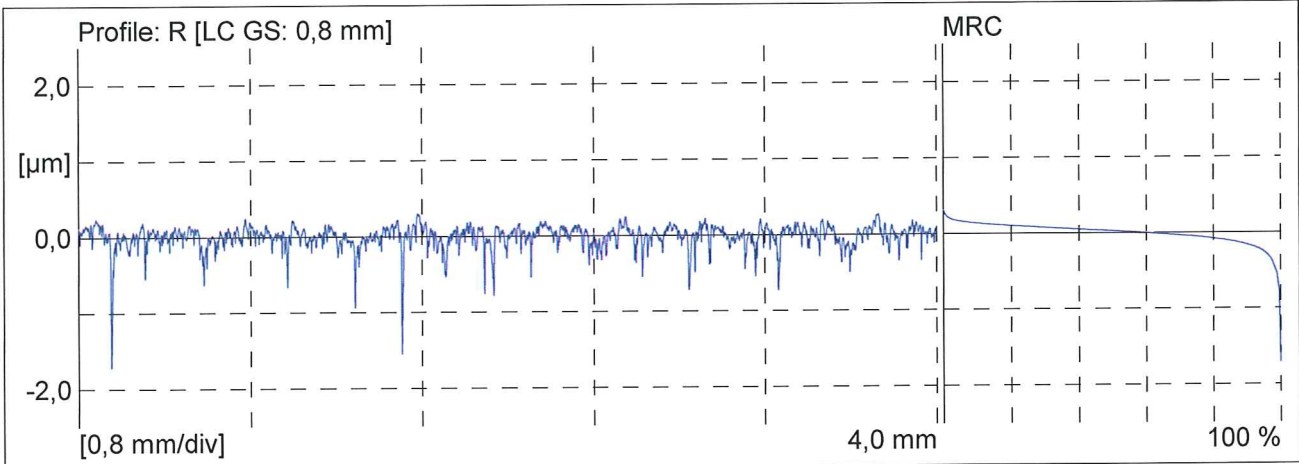


03/27/09

Object: D5701
Number: 02
Comment: 15µm 50 overløb.
Puls 0, spindel 120, tryk 1000, speed 3.

Meas. Instrum.: PS1
Drive Unit: PS1
Pick-up: PHT 350

Lt: 5,6 mm [N=5]
Ls: 2,5 µm
VB: ±200,0 µm
Vt: 0,50 mm/s
Points: 11200



Profile: R [LC GS: 0,8 mm]

Ra	0,102 µm
Rq	0,155 µm
Rz	1,351 µm
Rt	2,02 µm

Profile: R [LC ISO 13565: 0,80 mm]

Rk	0,26 µm
Rpk	0,07 µm
Rvk	0,31 µm

Profile: W [LC GS: 0,8 mm]

Wa	0,054 µm
----	----------



MarSurf XR 20
V1.40-3

STRECON A/S
Tool & Polish
RAP

Lars
P000_005.PCD

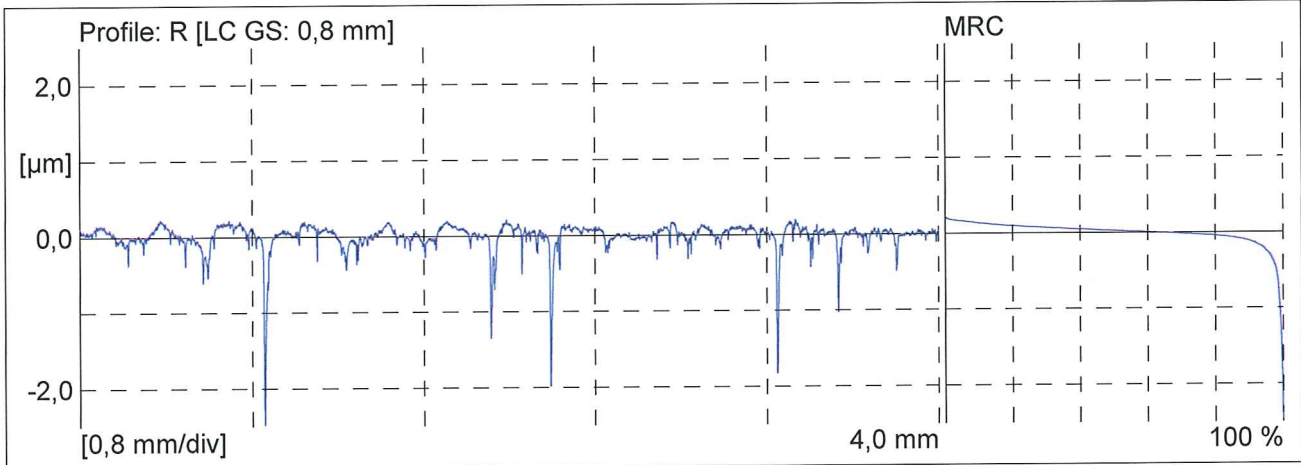


03/27/09

Object: D5701
Number: 02
Comment: 3µm 20 overløb.
Puls 0, spindel 800, tryk 2000, speed 6.

Meas. Instrum.: PS1
Drive Unit: PS1
Pick-up: PHT 350

Lt: 5,6 mm [N=5]
Ls: 2,5 µm
VB: ±200,0 µm
Vt: 0,50 mm/s
Points: 11200



Profile: R [LC GS: 0,8 mm]

Ra	0,098 µm
Rq	0,196 µm
Rz	1,647 µm
Rt	2,70 µm

Profile: R [LC ISO 13565: 0,80 mm]

Rk	0,20 µm
Rpk	0,06 µm
Rvk	0,48 µm

Profile: W [LC GS: 0,8 mm]

Wa	0,071 µm
----	----------



MarSurf XR 20
V1.40-3

STRECON A/S
Tool & Polish
RAP

Lars
P000_007.PCD

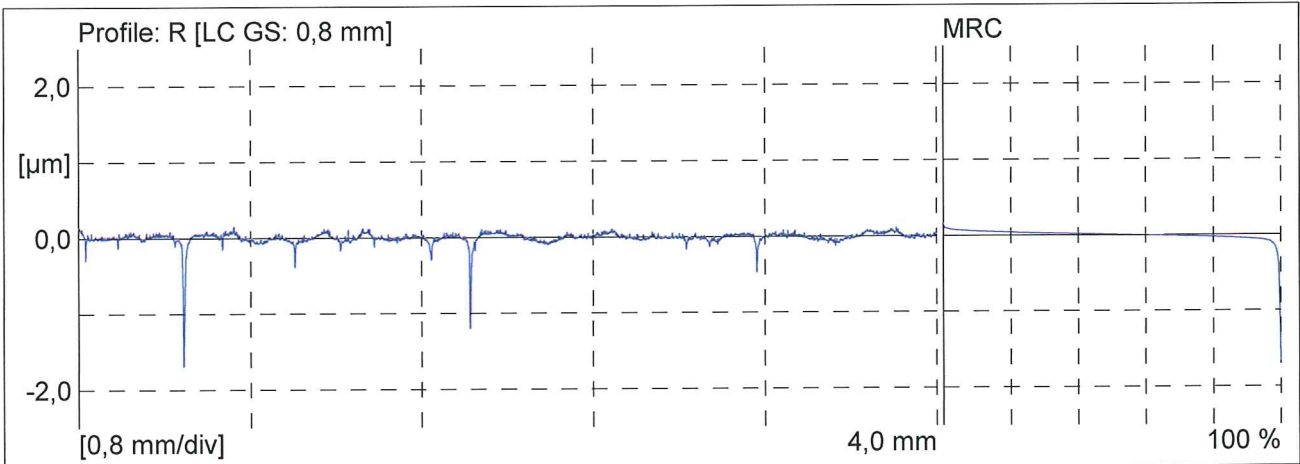


03/27/09

Object: D5701
Number: 02
Comment: 3µm 30 overløb.
Puls 3000, spindel 800, tryk 2000, speed 6.

Meas. Instrum.: PS1
Drive Unit: PS1
Pick-up: PHT 350

Lt: 5,6 mm [N=5]
Ls: 2,5 µm
VB: ±200,0 µm
Vt: 0,50 mm/s
Points: 11200



Profile: R [LC GS: 0,8 mm]	
Ra	0,042 µm
Rq	0,091 µm
Rz	0,895 µm
Rt	1,84 µm
Profile: R [LC ISO 13565: 0,80 mm]	
Rk (8!)	0,09 µm
Rpk (8!)	0,04 µm
Rvk (8!)	0,15 µm
Profile: W [LC GS: 0,8 mm]	
Wa	0,031 µm

Appendix E

Tiesler Size chapter

Verhalten erwartet werden, da die Gleitwege beim VVFP wesentlich höher sind als im kombinierten Napffließpreßversuch. Die hohe Reibung der kleinen Proben im Reibtest wurde jedoch gerade auf die zu geringen Gleitwege zurückgeführt, die nicht ausreichen, um die Oberfläche genügend einzuglätten und statische Schmiertaschen zu bilden.

6.1.4.1 Einfluß der Oberflächenrauheit

Die mit den aufgerauhten Proben erzielten Ergebnisse (**Bild 6.10**) zeigen keinen Miniaturisierungseffekt, obwohl dieser bei den Reibversuchen vorhanden ist. Die aufgerauhten D4-Proben weisen eine etwas höhere bezogene Stempelkraft als unbehandelte Proben desselben Durchmessers auf. Diese Beobachtung steht im Einklang mit den Ergebnissen des Reibtests, bei denen die D4-Proben mit rauher Oberfläche eine geringfügig höhere Reibung zeigen als die Proben im Ausgangszustand. Die D2- und D1-Proben weisen im Reibtest eine stark erhöhte Reibung auf, beim VVFP jedoch fallende bezogene Stempelkräfte. D05-Proben wurden aufgrund der Probleme bei der Aufrauung nicht verpreßt.

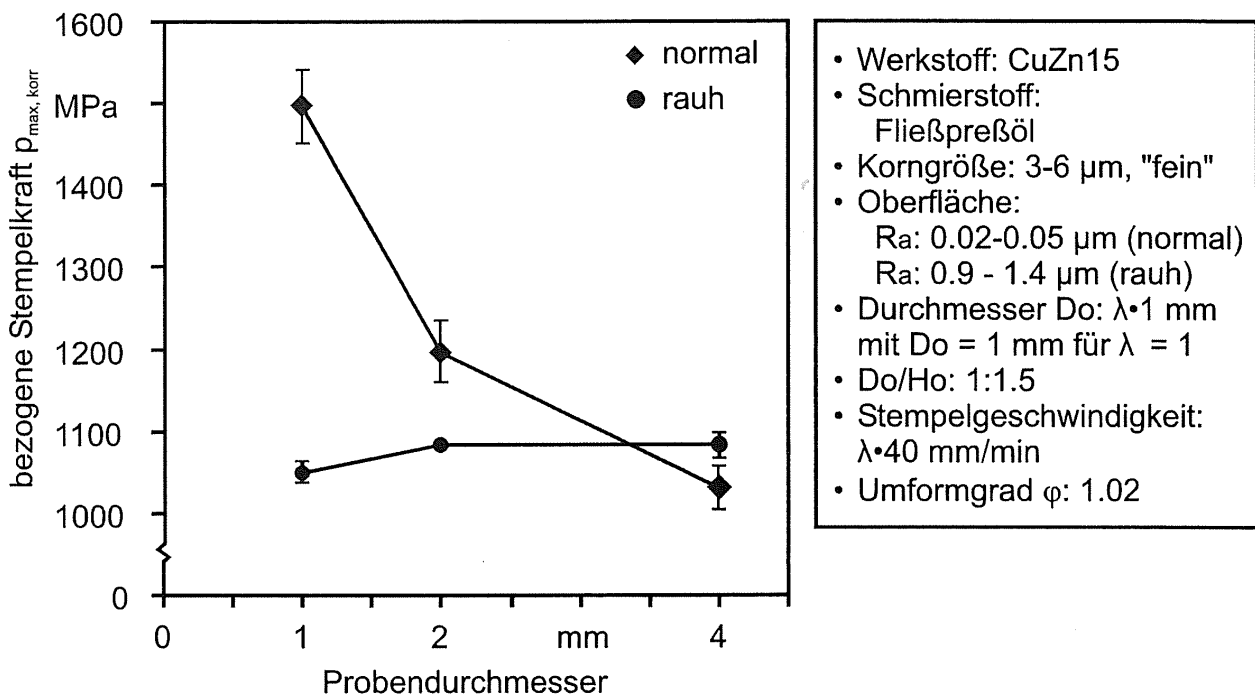


Bild 6.10: Maximale bezogene Stempelkraft $p_{max, korr}$ und Standardabweichung für die Zustände "normal" und "rauh"

Für den fehlenden Miniaturisierungseffekt kann keine eindeutige Erklärung gefunden werden. Die Proben für den Reibtest und die Vollvorwärtsfließpreßversuche stammen aus der selben Charge. Die Versuchsreihen für einen Durchmesser wurden unabhängig vom betrachteten Zustand (unbehandelt, rauh, feines oder grobes Gefüge, ...) hintereinander durchgeführt, so daß ein systematischer Fehler im Versuchsaufbau sich nicht durch die Versuche eines gleichen Zustands, sondern eines gleichen Durchmessers ziehen müßte. Daher können die Ergebnisse nur auf grundlegende Unterschiede zwischen den Prozessen VVFP und kombiniertes NRFP zurückgeführt werden.

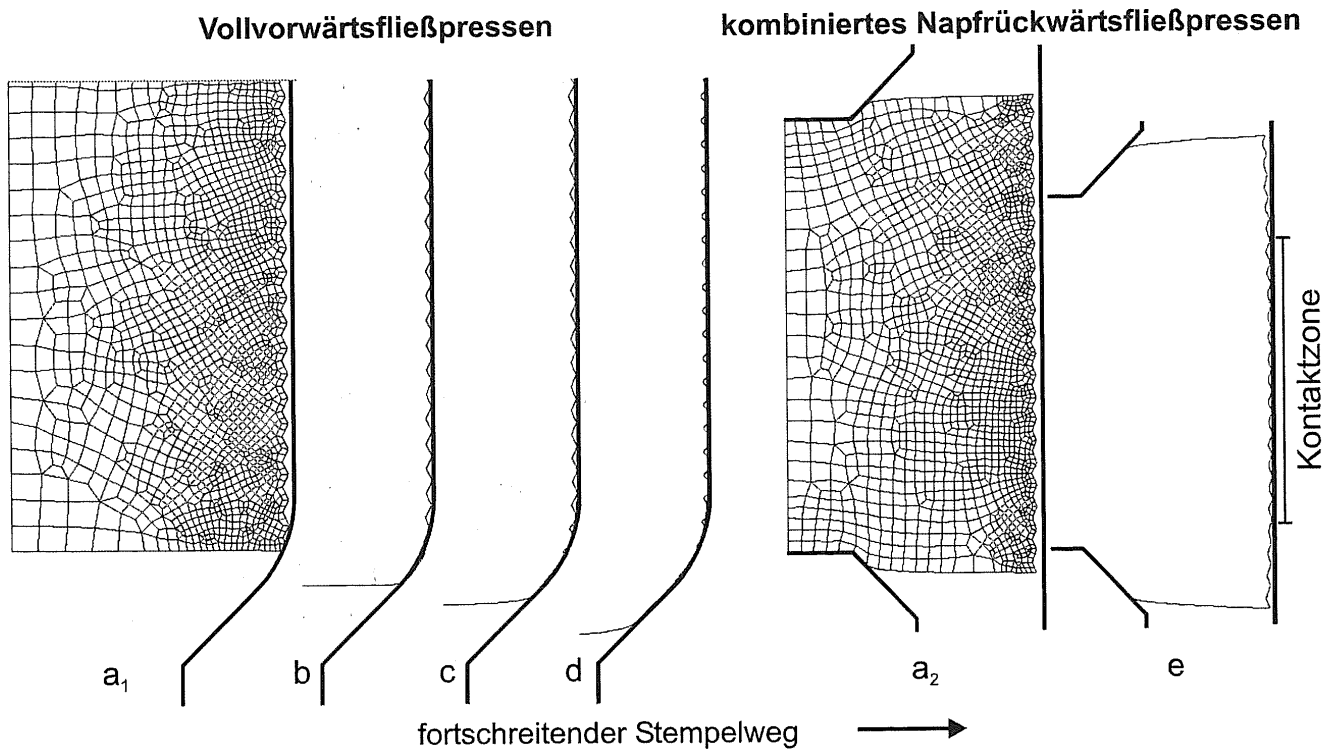


Bild 6.11: FE-Simulation der Oberflächeneinglättung beim VV- und kombinierten NRFP bei rauher Oberfläche

Das Verhalten der rauhen Oberfläche bei beiden Prozessen wurde modellhaft mit einer FE-Simulation untersucht (**Bild 6.11**). Ein Unterschied ist im Werkstofffluß, d.h. im Ausfüllen der Matrize zu sehen. Zu Beginn beider Prozesse herrscht zunächst ein gewisses Spiel zwischen Probe und Matrize (**Bild 6.11 a₁, a₂**). Mit Anstieg der Stempelkraft beginnt sich beim kombinierten Napffließpressen die Probe zunächst wie im Zylinderstauchversuch auszubauchen und legt sich zuerst in der Mitte zwischen oberem und unterem Stempel an die Matrizenwand an (**Bild 6.11 e**), bis sich mit fortschreitendem Stempelweg immer mehr Material an die Matrizenwand anlegt. Es ist vorstellbar, daß dadurch in gewissem Maße der Schmierstoff von der Probenmitte nach außen zum Probenrand verdrängt wird, wobei dies natürlich nicht nur für die Proben mit rauher Oberfläche gilt. Beim VVFP hingegen tritt der erste Kontakt am unteren Probenende auf, so daß der Schmierstoff hier nicht mehr entweichen kann (**Bild 6.11 b**). Mit fortschreitendem Stempelweg wird die Probe gleichmäßig aufgestaucht, bis sie die Matrizenwand berührt und anschließend eine Einebnung der Rauheitsspitzen beginnen kann (**Bild 6.11 c,d**). Zu diesem Zeitpunkt bilden sich in den Rauheitstälern Schmierstoffreservoirs, in denen der Schmierstoff bis in den Bereich der Fließpreßschulter transportiert werden kann. Der Einebnungsvorgang der Rauheitsspitzen, der Anfangs zu höherer Reibung und damit höheren Kräften führt (siehe Reibtest), und der damit verbundene Schmierstoffdruckaufbau in den Schmiertaschen, der schließlich zur Reibungsminderung beiträgt, findet großteils bereits im zylindrischen Bereich der Matrize statt. Die in die Fließpreßschulter einlaufende Probenoberfläche weist also bereits ein besseres Reibverhalten auf. Da aber der Reibanteil an der Fließpreßschulter nach Gleichung 6.5 einen wesentlich stärkeren Beitrag zur Gesamtließpreßkraft als der Reibanteil im zylindrischen Teil der Matrize liefert (etwa Faktor 2), fällt der Einebnungsvorgang im zylindrischen Bereich weniger stark bzw. die bzgl. der Reibung vorteilhafte Probenoberfläche im Schulterbereich um so stärker ins Gewicht. Im kombinierten Napffließpreßversuch hingegen beeinflusst der Einebnungsvorgang ganz wesentlich den Werkstofffluß und die resultierende Napfhöhe, die

zur Bewertung der Reibung herangezogen wird. Hier wird die hohe Reibung der kleineren Proben auf eine ungenügende Einebnung der Oberfläche durch die nicht ausreichenden Gleitwege zurückgeführt. Diese Unterschiede im Werkstofffluß könnten als Ursache für die beobachteten Widersprüche zwischen Reibtest und VVFP gesehen werden. Die beschriebenen Effekte treten natürlich auch bei glatter Probenoberfläche, aber nur stark abgeschwächt auf, da aufgrund des geringeren Schmierfahnen volumens wesentlich mehr Schmierstoff nach oben herausgedrückt werden kann.

6.1.4.2 Einfluß des Gefüges

Der Einfluß der Korngröße auf die beim Fließpressen beobachteten Miniaturisierungseffekte wurde mit den gleichen wärmebehandelten Proben untersucht, die auch für die Reibversuche verwendet wurden (siehe Abschnitt 5.4). **Bild 6.12** zeigt die Ergebnisse für feines, mittleres und grobes Gefüge bei Schmierung mit Fließpreßöl. Die Werte der D05-Proben wurden aufgrund der Matrizengeometrie um 8% korrigiert. Die dargestellten Ergebnisse wurden wie üblich mit der Vickershärte korrigiert, um eine Vergleichbarkeit zu schaffen. Als Bezugsbasis wurde die D4-Probe des jeweiligen Zustands gewählt, d.h. für die D1-Proben ist

$$p_{\max, \text{kor}} = p_{\max} \cdot \frac{HV_{D4}}{HV_{D1}} \quad (6.12)$$

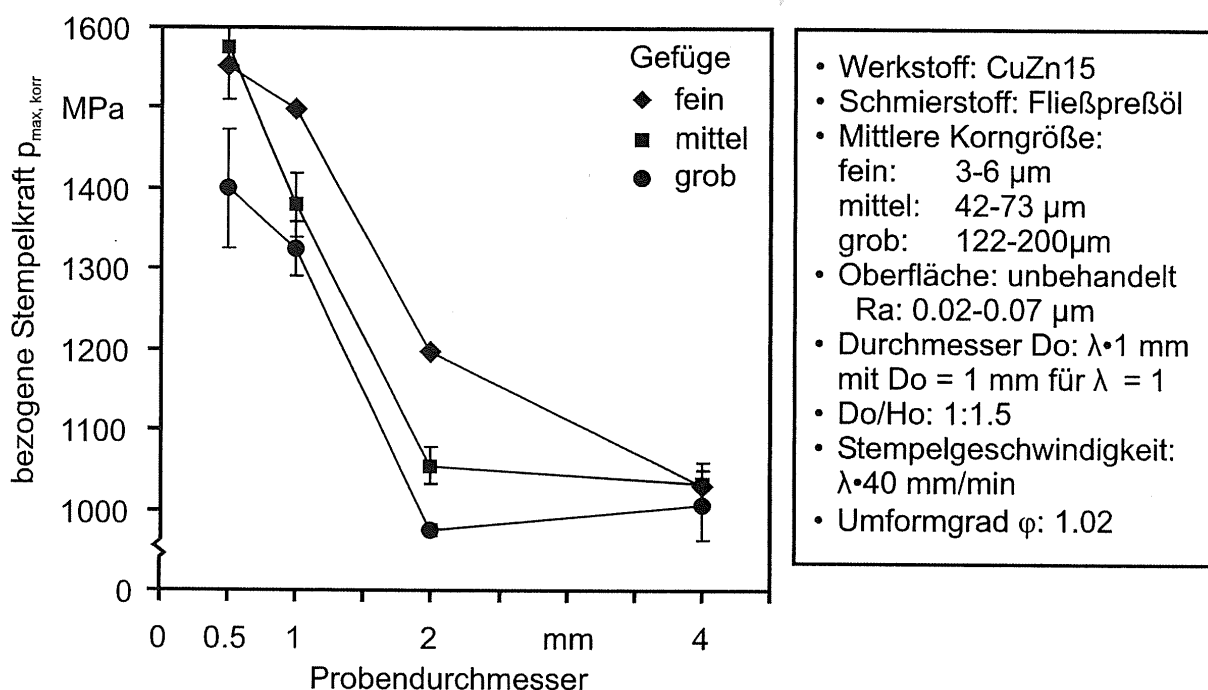


Bild 6.12: Maximale bezogene Stempelkraft $p_{\max, \text{kor}}$ und Standardabweichung für die Gefügestände "fein", "mittel" und "grob"

Der bekannte Miniaturisierungseffekt ist auch hier unabhängig vom Gefüge klar zu erkennen. Die höchsten Ergebnisstreuungen treten erwartungsgemäß bei den D05-Proben auf. Es fällt allerdings auf, daß die bezogene maximale Stempelkraft $p_{\max, \text{kor}}$ im Vergleich zum feinen Gefüge zunächst kaum ansteigt, bzw. bei grobem Gefüge leicht zu fallen scheint, wobei die Werte der D2-Proben im sehr hohen Streubereich der D4-Proben liegen. Bedingt durch die Korrektur können die Ergebnisse in **Bild 6.12** der Zustände "fein", "mittel" und "grob" nicht

Appendix F

Mechanical properties of common BMG materials

Thermal properties

Properties	Mg ₆₀ Cu ₃₀ Y ₁₀	Zr ₅₅ Cu ₂₀ Ni ₁₀ Al ₁₅	Zr ₄₄ Cu ₄₀ Al ₈ Ag ₈	Zr _{41,2} Be _{22,5} Ti _{13,8} Cu _{12,5} Ni ₁₀ Vitireloy1	Zr ₄₄ Ti ₁₁ Cu ₁₀ Ni ₁₀ Be ₂₅ Vitireloy 1B	Zr _{56,5} Cu _{15,6} Ni _{12,8} Al _{10,3} Nb _{2,8} Vitireloy 106	Pt _{57,5} Cu _{14,7} Ni _{5,3} P _{22,5}	Fe ₄₈ Cr ₁₅ Mo ₁₄ Er ₂ C ₁₅ B ₆
Density, g/cm ³	3.54	6.51	7.0	6.125	6.1	6.8	15.3	
Glass Transition, °C	146	465	423	349	350	400	236	570
Onset Crystallization Temperature, °C (Heating rate = 0.033 K s ⁻¹)	193	520	470	426	470	479	325	620
Crystalline phase	Mg ₂ Cu	Zr ₂ Cu, Zr ₂ Ni						
Melting temperature of crystalline phase, °C	460	810	903	730		830	522	1170
Glass thermal conductivity, W m ⁻¹ K ⁻¹		4.5 ¹		5.29 (0°C) 6.92 (100°C)	Similar to Vit1			
Glass heat capacity, J g ⁻¹ K ⁻¹		0.38 ¹		0.538 (0°C) 0.551 (100°C)	Similar to Vit1			

Thermal properties, references

Properties	Mg ₆₀ Cu ₃₀ Y ₁₀	Zr ₅₅ Cu ₂₀ Ni ₁₀ Al ₁₅	Zr ₄₄ Cu ₄₀ Al ₆ Ag ₈	Zr _{41,2} Be _{22,5} Ti _{13,8} Cu _{12,5} Ni ₁₀ Vitreyloy1	Zr ₄₄ Ti ₁₁ Cu ₁₀ Ni ₁₀ Be ₂₅ Vitreyloy 1B	Zr _{58,5} Cu _{15,6} Ni _{12,8} Al _{10,3} Nb _{2,8} Vitreyloy 106	Pt _{57,5} Cu _{14,7} Ni _{5,3} P _{22,5}	Fe ₄₈ Cr ₁₉ Mo ₁₄ Er ₂ C ₁₅ B ₆
Density, g/cm³	Risø measurement	Bobrov et al., J. Non-Cryst. Solids 342 (2004) 152.	Risø				Schroers and Johnson, Phys. Rev. Lett., 255506 , (2004)	
Glass Transition, °C	Linderoth et al., Mat. Sci. Eng. A304-306 (2001) 656.	Zhang et al., Materials Trans. 41 (2000) 1410.	Risø					Gu et al, JMR, 22, 2, 2007
Onset Crystallization Temperature, °C (Heating rate = 0.033 °C/s)	Linderoth et al., Mat. Sci. Eng. A304-306 (2001) 656.	Zhang et al., Materials Trans. 41 (2000) 1410.	Zhang and Inoue, Scripta Mat., 516, 55, 711-713 (2006)					
Crystalline phase	Risø measurement	Eckert et al., Materials Trans. 39 (1998) 623.						
Melting temperature of crystalline phase, °C	Eldrup et al., Mat. Sci. Forum 343- 346 (2000) 123.	Zhang et al., Materials Trans. 41 (2000) 1410.	Zhang et al. Mat Sci. Eng. B, 148, 1-3, 92-96 (2008)	Lee et al. Mat Sci. Eng. A, 390, 1, 427- 436 (2005)				
Glass thermal conductivity, W m⁻¹ K⁻¹		Yamasaki et al., Applied Phys Letters 84 (2004) 4653.		Demetriou and Johnson, Acta Mat., 52,12, 3403- 3412 , (2004)				
Glass heat capacity, J g⁻¹ K⁻¹		Yamasaki et al., Applied Phys Letters 84 (2004) 4653.						

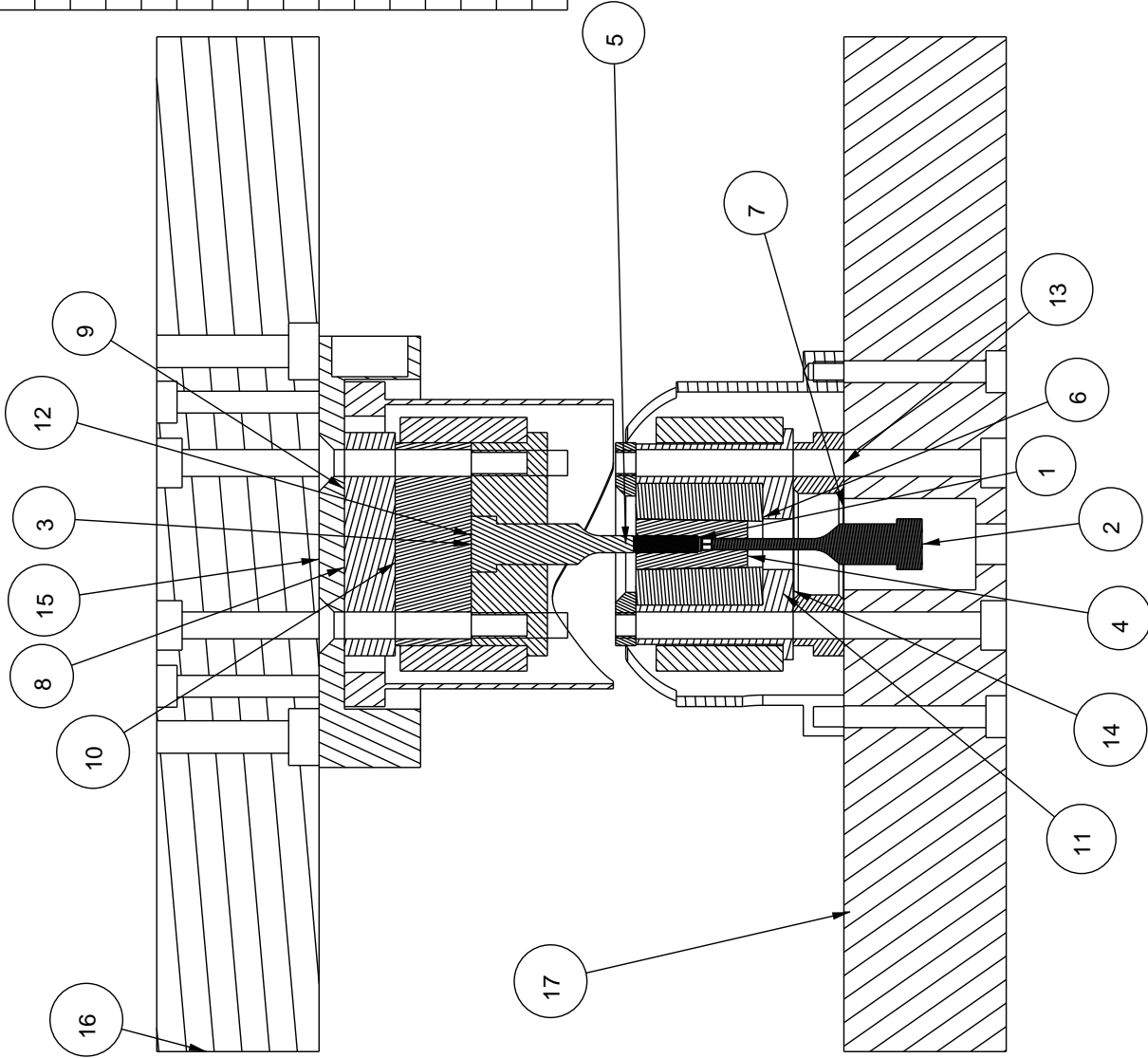
Mechanical properties at room temperature



Properties	Mg ₅₀ Cu ₃₀ Y ₁₀	Zr ₅₅ Cu ₂₀ Ni ₁₀ Al ₁₅	Zr ₄₄ Cu ₄₀ Al ₈ Ag ₈	Zr _{41.2} Be _{22.5} Ti _{13.8} Cu _{12.5} Ni ₁₀ Vitreloy1	Zr ₄₄ Ti ₁₁ Cu ₁₀ Ni ₁₀ Be _{2.5} Vitreloy 1B	Zr _{58.5} Cu _{15.6} Ni _{12.8} Al _{10.3} Nb _{2.8} Vitreloy 106	Pt _{57.5} Cu _{14.7} Ni _{15.3} P _{2.5}	Fe ₄₈ Cr ₁₅ Mo ₁₄ Er ₂ C ₁ ₅ B ₆
E, GPa	70	90	115 ⁷	96	96.7	87.3 ⁶	94.8	213
G, GPa	(25)	32		37.4	35.6	31.9 ⁶	33.3	81 ⁴
Yield strength, compression, MPa	850	1810 ²	1900	1900	1860	1820	1470	3750 ⁴
Plastic strain at fracture, compression	0.007%	0.2% ²	0.17	0	0	0.5%	~20%	0
Fracture strength tension, MPa	ca. 600	1760 ¹		1800	1800	1200		
Plastic strain at fracture, tension	0%	0% ¹				0%		
Vickers hardness, GPa	4.3	5.5		5.4	5	5.9 ⁶	4.02	13 ⁵
Fracture toughness, MPa m ^{1/2}		43 ³	177	55			80	12.7 ± 4.1

Appendix G

Tool system for forming of Dental implant

Pos	Beskrivelse/mål	Antal	Type	Komponent	Materiale	Stk. vægt
1	Billet	1	PART	BILLET10	Ti-C4	0,000 kg.
2	Ejector	1	PART	EJECTOR_STEP1_FC	Vanadis 23 (66HRC)	0,001 kg.
3	Punch	1	PART	PUNCH_STEP1_FC	Vanadis 23 (66HRC)	0,001 kg.
4	Die	1	PART	DIE_SINK_SPARK	Vanadis 23 (66HRC)	0,001 kg.
5	Lower Plate Holding	1	PART	DIEPLATE_FC	Stainless steel	0,004 kg.
6	Stress Ring	1	PART	STRESSRING_STEP1_FC	Vanadis 60 (54HRC)	0,010 kg.
7	Low Ceramic Isolation	1	PART	CERMICPLATE_FC	Duratec	0,010 kg.
8	Top Ceramic Isolation	1	PART	CERMICTOPPLATE_FC	Duratec	0,014 kg.
9	Top Reflection Ring	1	PART	TOPREFLECTORRING_FC	Stainless steel	0,016 kg.
10	Punch Holding Plate	1	PART	TOPPLATE_TOWARDSPISTON_NEW	Stainless steel	0,018 kg.
11	Heater Ring	2	PART	HEATERDIE_FC		0,018 kg.
12	Punch Holder	1	PART	UPSETTINGPISTONHOLDER_FC	Impax	0,018 kg.
13	Low Reflection Ring	1	PART	REFLECTORRING_FC	Stainless steel	0,025 kg.
14	Stress Ring Holder	1	PART	TOOLHOLDERSTEP1_FC	Impax	0,034 kg.
15	Position Plate	1	PART	POSITIONERINGSPLADE_FC	Rustfrit Stål	0,069 kg.
16	Top Palte	1	PART	TOPPLATE_FC	Tool steel	0,974 kg.
17	Low Palte	1	PART	STANDPLATE_FC	Tool steel	1,116kg.



	INSTITUTTET FOR PRODUKTUDVIKLING Sektionen for Produktion og Ledelse Produktionsstorvet, Bygning 425 2800 Lyngby Tlf.: 45254600 Telefax 45930190		Skala: 1:1	* * * * * *
	Rekvirent: Rasmus S. Eriksen			* * * * * *
Beskrivelse: FORGING_STEP_1		Projekt nr.:	Dato: 12-Mar-09	Navn: Andrea Vian
Materiale:		Titel:	Teg. nr./antal	

Appendix H

Macro DCE-results

	Test number	h_u [mm]	h_l [mm]
RAP 1 40%	1	11,796	4,644
RAP 1 40%	2	12,283	4,34
RAP 1 40%	3	10,039	6,793
RAP 1 60%	1	20,459	8,86
RAP 1 60%	2	20,366	8,763
RAP 1 60%	3	20,567	8,594
RAP 2 40%	1	11,876	4,29
RAP 2 40%	2	11,856	4,302
RAP 2 40%	3	11,918	4,236
RAP 2 60%	1	20,543	8,137
RAP 2 60%	2	20,771	8,219
RAP 2 60%	3	19,802	9,473
EDM 3 40%	1	11,902	4,375
EDM 3 40%	2	10,969	6,058
EDM 3 40%	3	11,933	4,451
EDM 3 60%	1	16,621	12,901
EDM 3 60%	2	20,425	8,848
EDM 3 60%	3	20,499	8,233

Table H.1: Measurement results of the Macro size DCE-test

